



**University Library**

Author/Filing Title ..... MILLS, CHRIS .....

Class Mark ..... T .....

Please note that fines are charged on ALL  
overdue items.

**FOR REFERENCE ONLY**

040317709X



# COMPUTER SIMULATION OF GYMNASTICS VAULT LANDINGS

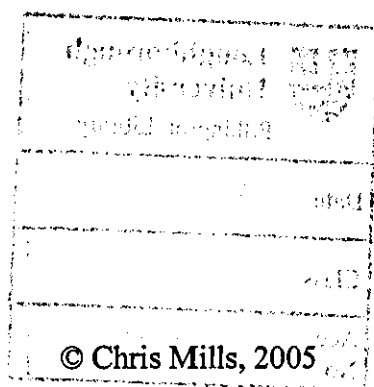
by


Chris Mills

A Doctoral Thesis

Submitted in partial fulfilment of the requirements for the award of Doctor of  
Philosophy of Loughborough University

October 2005



	<b>Loughborough University Pilkington Library</b>
Date	JAN 2006
Class	T
Acc No.	040317709X

## ABSTRACT

### Computer simulation of gymnastics vault landings

Chris Mills, Loughborough University, 2005

A computer simulation model of an International Gymnastics Federation (F.I.G.) landing mat and a gymnast was developed to investigate the mechanics of landing from the gymnastics vault. The landing mat model incorporated the multi-layer design of the landing mat and its deformation characteristics were based upon experimental data. The gymnast model was based upon an elite level gymnast and contained subject-specific parameters. The gymnast was modelled as a seven-segment link system with 'lumped' muscles producing joint rotation at the hip, knee and ankle. Wobbling masses were included within the trunk, thigh and shank segments to represent soft tissue movement. A two segment bone within the shank and thigh provided estimates of bone bending moments and bone deformations. Joint torques were based upon the torque / angle / angular velocity relationship established during isokinetic dynamometry testing of the subject. The muscle forces were calculated from the joint torques and from moment arm data taken from the literature and scaled to the subject.

The gymnast-mat model was evaluated using the kinetic, kinematic and EMG data collected from actual vaults performed by the subject. Evaluation results showed good agreement between the simulations and the actual performances with difference scores between 10.1% and 23.6%. The landing strategy and landing mat were optimised to minimise the ground reaction forces and bone bending moments. Optimised landing strategy results suggest that modifications to the gymnast's landing strategy could reduce the peak ground reaction forces but this may not decrease the peak internal joint forces. Optimised landing mat parameter results suggest that a landing mat with 20% more damping could reduce the peak ground reaction forces and internal joint forces but this may increase the initial impact force between the foot and the mat's surface.

Key words: landing mat, gymnastics, simulation, impact, muscle, optimisation

## PUBLICATIONS

### Abstracts:

Pain, M. T., Mills, C., and Yeadon M. R., "Determining shock transmission times and variable effective mass of gymnastics landing mats under loading conditions produced by male gymnasts." *Proceedings of the 27<sup>th</sup> Annual Meeting of the American Society of Biomechanics*, Toledo, USA, September 2003, 25-27.

Mills, C., Pain, M. T., and Yeadon, M. R., "A simple computer simulation model of the deformation characteristics of gymnastics landing mats." *Proceedings of the 27<sup>th</sup> Annual Meeting of the American Society of Biomechanics*, Toledo, USA, September 2003, 25-27.

Yeadon, M. R., Mills, C., and Pain, M. T., "Area deformation characteristics of gymnastics landing mats." *Proceedings of the 27<sup>th</sup> Annual Meeting of the American Society of Biomechanics*, Toledo, USA, September 2003, 25-27.

Matthew Pain, Chris Mills and David Jessop. Determining subject specific torque-velocity relationships with the inclusion of high velocity torque data. *Proceedings of the XXth Congress of the International Society of Biomechanics and 29th Annual Meeting of the American Society of Biomechanics*, Cleveland, Ohio, USA, August 2005, 1-3.

Chris Mills, Matthew Pain and Fred Yeadon. Modeling the gymnast-mat interaction during vault landings. *Proceedings of the XXth Congress of the International Society of Biomechanics and 29th Annual Meeting of the American Society of Biomechanics*, Cleveland, Ohio, USA, August 2005, 1-3.

### Papers:

Pain, M., Mills, C. and Yeadon, M.R. (2005). Video analysis of the deformation and effective mass of gymnastics landing mats. *Medicine and Science in Sports and Exercise* (in press).

Mills, C., Pain, M. and Yeadon, M.R. (2005). Modeling a viscoelastic gymnastics landing mat during impact. *Journal of Applied Biomechanics* (submitted).

## ACKNOWLEDGEMENTS

I wish to express my thanks to my supervisors Dr. Matt Pain and Prof. Fred Yeadon for all their support and guidance throughout this study.

I would like to thank the past and present members of the Biomechanics research group at Loughborough University and the British Gymnastics team for their friendship and encouragement.

Thanks to Sam Buck for participating in this study and for all his time and effort during the data collection sessions.

I would also like to thank my housemates and all my friends in my pole vault training group who have encouraged me throughout my time at Loughborough.

I would like to acknowledge the help from Continental Sports Ltd. for their help in constructing the sample landing mat used in this study and the financial support from British Gymnastics and the School of Sport and Exercise Sciences at Loughborough University.

A special thanks to my family for all their encouragement and support throughout my time in education. Last but not least, a special thanks to Molly who has always supported and encouraged me throughout my time at Loughborough.

## TABLE OF CONTENTS

ABSTRACT	i
PUBLICATIONS	ii
ACKNOWLEDGEMENTS	iii
TABLE OF CONTENTS	iv
LIST OF FIGURES	xi
LIST OF TABLES	xvii
<b>CHAPTER 1. INTRODUCTION</b>	<b>1</b>
1.1 Area of study	1
1.2 Statement of purpose	3
1.3 Research questions	4
1.4 Chapter organisation	6
<b>CHAPTER 2. LITERATURE REVIEW</b>	<b>8</b>
2.1 Introduction	8
2.1.1 Overview of the vault and development of the vault apparatus	8
2.1.2 The equipment	8
2.1.3 Types of vaults	11
2.1.4 Landing	14
2.2 Experimental and theoretical research	15
2.3 Experimentally based literature	16
2.3.1 Landing strategy	17
2.3.2 Foot position	17
2.3.3 Muscle pre-activation	18
2.3.4 Joint configuration and body orientation prior to landing	18
2.3.5 Landing mats	19
2.3.6 Injury	20
2.4 Simulation	21
2.5 Optimisation	22
2.6 Theoretical based literature	24
2.6.1 Rigid body models	24

2.6.2 Wobbling mass models	25
2.6.3 Heel pad properties	27
2.6.4 The rigid bone	27
2.6.5 The foot	27
2.6.6 Generating joint motion	28
2.6.7 Landing surface	28
2.7 Summary	29
<b>CHAPTER 3. MODELLING THE LANDING MAT</b>	<b>30</b>
3.1 An introduction to springs and dampers	30
3.1.1 Harmonic motion	30
3.1.2 Spring-dampers	32
3.2 The landing mat models	33
3.2.1 Landing mat model one	34
3.2.2 Landing mat model two	35
3.2.3 Landing mat model three	36
3.2.4 Landing mat model four	37
3.2.5 Landing mat model five	39
3.2.6 Landing mat horizontal model	40
3.3 Techniques used to collect data on landing mats	41
3.3.1 Image based motion analysis	42
3.3.2 Image and force synchronisation	42
3.3.3 Two and three-dimensional reconstruction	43
3.3.4 Force plate	45
3.3.5 Accelerometers	46
3.3.6 Filtering and curve fitting techniques	47
3.4 Gymnastic landing mat data collection	49
3.4.1 The equipment	49
3.4.2 High-speed camera calibration procedure	50
3.4.3 Determination of a gymnast's 'effective mass'	53
3.4.4 Impact testing	54
3.4.5 Image reconstruction and analysis	55
3.5 Vertical testing results	56
3.5.1 Determining the impact velocity	56



3.5.2	Ground reaction forces during impact	59
3.5.3	Compression wave propagation times	60
3.5.4	Vertical mat deformation	62
3.5.5	Landing mat area deformation	63
3.5.6	The mat's effective mass during impact	66
3.6	Oblique testing results	70
3.6.1	Oblique impact velocities	70
3.6.2	Ground reaction forces during impact	71
3.6.3	Oblique impact compression wave propagation times	73
3.6.4	Vertical and horizontal mat deformation	74
3.6.5	Landing mat area deformation (oblique)	74
3.7	Modelling the landing mat vertically	75
3.7.1	Landing mat model one parameter values	76
3.7.2	Landing mat model one evaluation	76
3.7.3	Landing mat model two parameter values	77
3.7.4	Landing mat model two evaluation	78
3.7.5	Landing mat model three parameter values	78
3.7.6	Landing mat model three evaluation	78
3.7.7	Landing mat model four parameter values	80
3.7.8	Landing mat model four evaluation	80
3.7.9	The development of landing mat model five	81
3.7.10	Landing mat model five parameter values	82
3.7.11	Landing mat model five evaluation	83
3.8	Modelling the landing mat horizontally	83
3.8.1	Landing mat horizontal model parameter values	84
3.8.2	Landing mat horizontal model evaluation	85
3.9	A Computer Model of Oblique Impacts onto Landing Mats	85
3.10	Sensitivity Analysis	87
3.11	Summary	88
<b>CHAPTER 4. MODELLING THE GYMNAST</b>		<b>90</b>
4.1	The structure of the gymnast models	90
4.1.1	Gymnast model one	90
4.1.2	Gymnast model two	95

4.1.3	Gymnast model three	96
4.1.4	Gymnast model four	98
4.1.5	Model structure summary	99
4.2	Data collection and parameter determination	99
4.2.1	Anthropometric measurement of subjects	99
4.2.2	Anthropometric data collection	103
4.2.3	Anthropometric parameter determination	104
4.2.4	Anthropometric measurement – summary	106
4.2.5	Strength measurement of subjects	106
4.2.6	Strength measurement data collection	109
4.2.7	Strength measurement data analysis & parameter determination	112
4.2.8	Strength measurement – summary	135
4.2.9	Wobbling mass	135
4.2.10	Wobbling mass parameter determination	136
4.2.11	Wobbling mass parameter evaluation	137
4.2.12	The bending bone	137
4.2.13	The bending bone parameter determination	138
4.2.14	The bending bone parameter evaluation	138
4.2.15	The two segment foot	139
4.2.16	The two segment foot parameter determination	139
4.2.17	The two segment foot parameter evaluation	140
4.2.18	The heel pad	140
4.2.19	The heel pad parameter determination	140
4.2.20	The heel pad parameter refinement	141
4.2.21	Kinematic and kinetic analysis of landing	142
4.2.22	Kinematic and kinetic data collection	143
4.2.23	Kinematic and kinetic data analysis & parameter determination	146
4.2.24	Kinematic and kinetic data analysis – summary	153
4.3	Modelling the Gymnast – Summary	153
<b>CHAPTER 5. MODEL EVALUATION</b>		<b>154</b>
5.1	Description of the models	154
5.2	Model refinement	155
5.2.1	Horizontal mat component	155

5.2.2 Ankle strength	157
5.2.3 The angle fit range of knee extension, ankle dorsi and plantar flexion	157
5.3 Evaluating the models by optimising muscle activation profiles	157
5.3.1 Criteria for evaluating the models	161
5.3.2 Objective function and weightings	161
5.3.3 Penalties	164
5.3.4 Results	164
5.3.5 Analysis and discussion of selected results	178
5.3.6 Summary	182
5.4 Analysis of joint reaction forces	182
5.5 Analysis of bone torques and deformation	184
5.5.1 Bone torque and deformation results	184
5.5.2 Analysis of bone torque and deformation results	186
5.5.3 The FEM of bone	187
5.6 Summary	188
<b>CHAPTER 6. MODEL OPTMISATION AND APPLICATION</b>	189
6.1 Optimising the landing strategy	189
6.2 Optimising the landing mat	193
6.3 Optimisation results	195
6.3.1 Optimisation of the landing strategy -- front somersault	195
6.3.2 Optimisation of the landing strategy -- back somersault	201
6.3.3 Optimising the landing mat -- front somersault	208
6.3.4 Optimising the landing mat -- back somersault	211
6.3.5 Optimising the landing mat -- front somersault (increased upper bound)	213
6.4 Discussion	216
6.5 Summary	219
<b>CHAPTER 7. SUMMARY AND CONCLUSIONS</b>	220
7.1 Summary of main findings	220
7.2 Answering the research questions	220
7.3 Discussion	224

7.3.1 Landing mat data collection	224
7.3.2 Gymnast data collection	225
7.3.3 Landing mat model	225
7.3.4 Gymnast models	227
7.3.5 Strength parameters and data collection	238
7.3.6 Segmental inertia parameters	239
7.3.7 Model limitations	239
7.3.8 Optimisation algorithm	230
7.3.9 Optimisation score and penalties	231
7.4 Future research	231
7.4.1 The landing mat	231
7.4.2 Initial conditions	232
7.4.3 Inertial parameters	232
7.4.4 Strength parameters	232
7.4.5 Sensitivity analysis	232
7.5 Conclusion	233
REFERENCES	234
APPENDICES	249
Appendix A: Raw anthropometric data for gymnast	249
Appendix B: Gymnast inertia data	251
Appendix C: Wobbling mass parameter determination	254
Appendix D: Segment moment of inertia and radius calculation	257
Appendix E: Informed consent form (Cybex testing)	260
Appendix F: SEC stiffness calculation	262
Appendix G: Isokinetic Dynamometry Raw data and 9 parameter muscle function 3D surface plots using muscle angle – all joints	269
Appendix H: Informed consent form (Vault testing)	279
Appendix I: Processed force, EMG and Vicon data during the four landing skills	281

Appendix J: Linear SEC Stiffness Calculations	292
Appendix K: Evaluation of all four skills using models 1, 2 and 3	294
Appendix L: Joint reaction forces and bone bending moments for all four skills	334

## LIST OF FIGURES

Figure 1.1.	Proposed model diagram.	4
Figure 2.1	Vaulting equipment layout.	9
Figure 2.2	Vault specifications. (F.I.G. Apparatus Norms, 2000/2001).	9
Figure 2.3	The new vaulting table dimensions (F.I.G. Apparatus Norms, 2000/2001).	10
Figure 2.4	Test impact sites (not too scale).	11
Figure 2.5	Direct vaults – example: Stoop (F.I.G., 2001).	12
Figure 2.6	Vaults with a full twist in the first flight phase – example: full twist on, handspring off (F.I.G., 2001).	12
Figure 2.7	Handspring and Yamashita style vaults – example: handspring tuck front (F.I.G., 2001).	12
Figure 2.8	Vaults with $\frac{1}{4}$ or $\frac{1}{2}$ turn in first flight phase – example: Tsukahara (F.I.G., 2001).	13
Figure 2.9	Round off entry vaults – example: Yurchenko (F.I.G., 2001).	13
Figure 2.10	The theory-experiment cycle of scientific method (Yeadon & Challis, 1994).	16
Figure 3.1	A mass spring system.	31
Figure 3.2	Force time history of a mass spring system in SHM.	32
Figure 3.3	A spring-damper system.	32
Figure 3.4	Critically, lightly and heavily damped displacement for a single mass spring-damper system.	33
Figure 3.5	Structure of landing mat model one.	35
Figure 3.6	Structure of landing mat model two.	36
Figure 3.7	Structure of landing mat model three.	37
Figure 3.8	Structure of landing mat model four.	38
Figure 3.9	Structure of landing mat model five using VN4D.	40
Figure 3.10	Field of view (left camera and right camera).	50
Figure 3.11	The calibration poles.	50
Figure 3.12	Dimensions of the calibration poles.	51
Figure 3.13	Custom built impactor – no added mass.	51
Figure 3.14	The landing mat set-up.	53
Figure 3.15	The landing mat marker locations (not to scale).	53
Figure 3.16	The custom-built drop rig.	55
Figure 3.17	Vertical velocity of the two points on the impactor (trial 2151).	57

Figure 3.18	Vertical force from force plate during trial 1541 (trigger at 7 ms).	59
Figure 3.19	Compression of mat layers to produce ground reaction force.	59
Figure 3.20	5 ms prior to force plate trigger in trial 1541.	60
Figure 3.21	Accelerometer data for trial 1541 (dashed line = trigger, solid line = accelerometer output).	61
Figure 3.22	Vertical displacement of the impactor prior to and during contact with the mat in trial 1541, the vertical line on the graph corresponds to 7 ms prior to force plate trigger (initial mat contact).	62
Figure 3.23	The surface of the mat during maximum vertical mat deformation during trial 1541 assuming deformation symmetry over the entire mat's surface. (Dots represent approximate location of actual mat markers).	63
Figure 3.24	Estimates of mat deformation volume using two methods of calculation: (a) Method 1, (b) Method 2.	65
Figure 3.25	Impact velocities at 45.7° (contact at 46 ms), (+ and * vertical; ... and – horizontal velocities).	71
Figure 3.26	Vertical force from force plate during trial 60lb (force plate triggered at 10ms).	72
Figure 3.27	4ms prior to force plate trigger (trial 60lb).	73
Figure 3.28	Mat surface deformation of trial 60lb assuming deformation symmetry over the entire mat's surface. (Dots represent approximate location of actual mat markers).	75
Figure 3.29	Single spring-damper model (model 1) of the landing mat during trial 1541 (RMS difference = 965.8 N).	76
Figure 3.30	Third spring-damper model of landing in trial 1541 (RMS difference = 894.5 N).	79
Figure 3.31	Fourth spring-damper model of landing in trial 1541 (RMS difference = 940.7 N).	80
Figure 3.32	Vertical ground reaction force (Model Five ) using point mass spring parameters from Model Four (RMS difference = 967.9N).	82
Figure 3.33	Vertical ground reaction force using re-optimised spring parameters (Nastran) (RMS difference = 1014.2 N).	83
Figure 3.34	Force time history for the mat's horizontal spring-damper using trial 60lb (RMS difference = 363.2 N).	85
Figure 3.35	Simulation of trial 60lb (RMS difference vertically = 1327.5 N).	86
Figure 3.36	Re-optimisation of vertical mat spring parameters using trial 60lb.	87

Figure 4.1	Seven-segment model of a gymnast.	91
Figure 4.2	The two segment foot modelled in VN4D.	93
Figure 4.3	The contractile component and SEC of the muscle-tendon complex.	95
Figure 4.4	The 'lumped' muscle model – knee extensors.	98
Figure 4.5	Finite element model of long bone.	99
Figure 4.6	Moment table used to determine centre of gravity.	100
Figure 4.7	Foot measurements.	106
Figure 4.8	Linear regression of Cybex torque against voltage output (RMS = 1.9 Nm).	110
Figure 4.9	Subject strapped to Cybex Norm dynamometer.	111
Figure 4.10	Identification of isometric period.	113
Figure 4.11	Isometric corrected torque data for KNEE flexion and extension.	114
Figure 4.12	Isometric corrected torque data for ANKLE plantar flexion and dorsi flexion.	114
Figure 4.13	Linear regression of crank angle against voltage output (RMS = 0.72°).	115
Figure 4.14	Identification of concentric and eccentric torque during constant angular velocity (knee extension at (a) 50°/s and (b) 450°/s).	116
Figure 4.15	Maximum and average torque versus joint angular velocity (knee flexion).	117
Figure 4.16	Concentric (Hill hyperbola) and eccentric torque / angular velocity relationship.	118
Figure 4.17	Differential activation function.	120
Figure 4.18	7-parameter fit for knee extension.	123
Figure 4.19	7-parameter fit for shoulder flexion.	123
Figure 4.20	Surface fit using 7 + 2 parameters (Knee Extension).	125
Figure 4.21	Knee extension using the 9-parameter optimisation method.	127
Figure 4.22	The contractile component and SEC of the muscle-tendon complex.	128
Figure 4.23	Surface fit using MUSCLE angle (Knee Extension).	134
Figure 4.24	Finite element bone model.	138
Figure 4.25	Marker placement on subject.	144
Figure 4.26	EMG electrode placement.	145
Figure 4.27	Vault landing equipment set-up.	146
Figure 4.28	Subject joint angles.	148
Figure 4.29	Joint angle time histories (backward somersault).	149



Figure 4.30	Force time history of landing during trial 1.	150
Figure 4.31	EMG time history for the landing of a backward somersault (Trial 1).	151
Figure 4.32	EMG time history (filtered) for a backward somersault (Trial 1).	152
Figure 4.33	Landing strategy during trial 1.	152
Figure 5.1	The 'folding' of the landing mat.	155
Figure 5.2	Horizontal ground reaction force using re-optimised spring parameters.	156
Figure 5.3	Extensor activation history.	158
Figure 5.4	Flexor activation history.	160
Figure 5.5	Horizontal force time history illustrating problem with objective function.	163
Figure 5.6	Vertical force time history illustrating the problem with the modified weighting of the objective function.	163
Figure 5.7	Comparison of Model Three simulation and performance for the front somersault in terms of (a) VGRF (b) HGRF (c) trunk orientation (d) ankle angle (e) knee angle (f) hip angle (g) shoulder angle.	167
Figure 5.8	Activation time histories for model Three front somersault simulation.	168
Figure 5.9	Comparison of Model Three simulation and performance for the back somersault in terms of (a) VGRF (b) HGRF (c) trunk orientation (d) ankle angle (e) knee angle (f) hip angle (g) shoulder angle.	170
Figure 5.10	Activation time histories for model Three back somersault simulation.	171
Figure 5.11	Comparison of Model Three simulation and performance for the handspring in terms of (a) VGRF (b) HGRF (c) trunk orientation (d) ankle angle (e) knee angle (f) hip angle (g) shoulder angle.	173
Figure 5.12	Activation time histories for model Three handspring simulation.	174
Figure 5.13	Comparison of Model Three simulation and performance for the Tsukahara in terms of (a) VGRF (b) HGRF (c) trunk orientation (d) ankle angle (e) knee angle (f) hip angle (g) shoulder angle.	176
Figure 5.14	Activation time histories for model Three Tsukahara simulation.	177
Figure 5.15	HGRF from Tsukahara vault and model One.	178
Figure 5.16	Model Three activation history during Tsukahara vault.	180

Figure 5.17	Joint angle time history for the ankle joint during a Tsukahara vault (model Three).	180
Figure 5.18	Joint angle (a) and activation histories (b) for the ankle joint during a Tsukahara vault.	181
Figure 5.19	Joint reaction forces for the front somersault skill (models One and Three).	183
Figure 5.20	Bone torques during the landing of a backward somersault skill (Model Three).	185
Figure 6.1	Optimisation of landing strategies for the front somersault skill (a) VGRF (b) HGRF (c) trunk orientation (d) ankle angle (e) knee angle (f) hip angle (g) shoulder angle.	196
Figure 6.2	Comparison of the muscle activation histories for the front somersault skill: model evaluation and optimisation results.	197
Figure 6.3	Joint reaction forces during the optimised landing strategies for the front somersault (a) Ankle, (b) Knee, (c) Hip.	198
Figure 6.4	Lower extremity bone bending torques during the front somersault skill (a) shank, (b) thigh.	199
Figure 6.5	Extensor muscle forces and shoulder torque during the front somersault skill (a) Ankle, (b) Knee, (c) Hip, (d) Shoulder.	200
Figure 6.6	Optimisation of landing strategies for the back somersault skill (a) VGRF (b) HGRF (c) trunk orientation (d) ankle angle (e) knee angle (f) hip angle (g) shoulder angle.	203
Figure 6.7	Comparison of the muscle activation histories for the back somersault skill: model evaluation and optimisation results.	204
Figure 6.8	Joint reaction forces during the optimised landing strategies for the back somersault (a) Ankle, (b) Knee, (c) Hip.	205
Figure 6.9	Lower extremity bone bending torques during the back somersault skill (a) shank, (b) thigh.	206
Figure 6.10	Extensor muscle forces and shoulder torque during the back somersault skill (a) Ankle, (b) Knee, (c) Hip, (d) Shoulder.	207
Figure 6.11	Optimisation of landing mat properties for the front somersault skill (a) VGRF (b) HGRF.	209
Figure 6.12	Lower extremity bone bending torques during the front somersault skill (a) shank, (b) thigh.	209
Figure 6.13	Toe to top mat layer force during the front somersault skill.	210
Figure 6.14	Optimisation of landing mat properties for the back somersault skill (a) VGRF (b) HGRF.	211
Figure 6.15	Lower extremity bone bending torques during the back somersault skill (a) shank, (b) thigh.	211

Figure 6.16	Toe to top mat layer force during the back somersault skill.	212
Figure 6.17	Optimisation of landing mat properties for the front somersault skill (a) VGRF (b) HGRF.	214
Figure 6.18	Lower extremity bone bending torques during the front somersault skill (a) shank, (b) thigh.	214
Figure 6.19	Toe to top mat layer force during the front somersault skill.	215
Figure 7.1	Mat model four with redistributed mat mass.	226

## LIST OF TABLES

Table 3.1	Vertical impact velocities	58
Table 3.2	Peak vertical force during impact	60
Table 3.3	Impact detection times from accelerometer and video in ms. (Force plate trigger = time zero)	61
Table 3.4	Maximum vertical mat deformation	63
Table 3.5	Estimate of mat volume at maximum deformation	65
Table 3.6	Filtered peak acceleration data	68
Table 3.7	Effective mass of mat at peak deformation calculated using four methods	68
Table 3.8	Percentage difference between calculated peak forces and actual peak forces	69
Table 3.9	Oblique impact velocities	71
Table 3.10	Peak vertical and horizontal force during an oblique impact	72
Table 3.11	Oblique compression wave propagation times (using high-speed video & force data)	73
Table 3.12	Vertical and horizontal mat deformation	74
Table 3.13	Estimate of mat volume at maximum deformation (oblique)	75
Table 3.14	Impact characteristics of the single spring damper model	77
Table 3.15	Impact characteristics of the single spring damper model (+ inertia term)	77
Table 3.16	Impact characteristics of the model three	79
Table 3.17	Impact characteristics of model four	81
Table 3.18	Horizontal velocity and recalculated force	84
Table 3.19	Sensitivity analysis of landing mat parameters	88
Table 4.1	Amount of bone and soft tissue mass in each segment	105
Table 4.2	Segmental inertia parameters for gymnast model	105
Table 4.3	Comparison of the calculated torque and Cybex machine torque on the monitor	110
Table 4.4	Isometric knee extension torques at different angles within the ROM	113
Table 4.5	Isometric torques obtained from isovelocity and isometric data	117
Table 4.6	Upper and lower limits for the seven parameters	121
Table 4.7	Optimisation results for the seven-parameter function	122
Table 4.8	Seven parameters for the ankle joint	124
Table 4.9	Nine parameters obtained for the 7 + 2 parameter optimisation (Joint angle)	125

Table 4.10	Ankle joint 7 + 2 parameters determined from isometric data	126
Table 4.11	Nine parameters determined via 9-parameter optimisation	127
Table 4.12	Subject SEC lengths	130
Table 4.13	Summary of moment arm lengths	132
Table 4.14	Subject SEC stiffness	133
Table 4.15	The 7 + 2 parameters for muscle angle	134
Table 4.16	Ankle joint 7 + 2 parameters determined using MUSCLE angle	135
Table 4.17	Spring-damper parameters for wobbling masses (Pain & Challis, 2004)	137
Table 4.18	Initial impact velocities	147
Table 4.19	Initial joint angles	147
Table 4.20	Initial joint angular velocities	148
Table 4.21	Key characteristics of the landing phase	150
Table 5.1	Lower and upper limits for the extensor activation parameters	158
Table 5.2	Lower and upper bounds for the flexor activation histories	160
Table 5.3	Objective function scores for models One to Three and all four skills	164
Table 5.4	Estimated maximum landing mat deformations during all four skills	165
Table 5.5	Model Three overall score breakdown	166
Table 5.6	Estimated peak joint reaction force during all four vault landings	184
Table 5.7	Maximum bone torques during each skill using models One and Three	185
Table 5.8	Maximum bone deformations during each skill using models One and Three	186
Table 6.1.	Comparison of peak forces and torques during model evaluation and optimisation for the front somersault skill	201
Table 6.2.	Comparison of peak forces and torques during model evaluation and optimisation for the back somersault skill	208
Table 6.3.	Optimised landing mat parameters for the front somersault skill	210
Table 6.4.	Optimised landing mat parameters for the back somersault skill	213
Table 6.5.	Optimised landing mat parameters for the front somersault skill (increased upper bounds)	215

## CHAPTER 1

### INTRODUCTION

This chapter provides a brief overview of the area of interest and a statement of purpose for this investigation. Questions that will be addressed in this study are identified. Finally a summary of organisation for the remainder of the chapters is outlined.

#### *1.1 Area of Study*

In Artistic Gymnastics the men compete on six pieces of apparatus: the floor, pommel horse, rings, vault, parallel bars and high bar. Of the six pieces the vault is the only one for which a routine is not performed. Instead the gymnast must execute a single vault in competition except in the apparatus finals where the gymnast must perform two vaults from different vault groups. The five vault groups are direct vaults (without somersaults), vaults with full turns in pre-flight, front handspring and Yamashita style vaults, vaults with a quarter turn in pre-flight, and round off entry vaults. (Federation Internationale de Gymnastique (F.I.G.), 2001).

Each vault consists of a run up (maximum 25m), pre-flight (from springboard to horse contact), support phase (hands in contact with horse), post-flight (from horse to initial contact with landing surface) and finally the landing. Evaluation of the vault starts the moment the gymnast touches the springboard. The landing of a vault as well as the landing from the other five pieces of apparatus can mean the difference between winning and losing. The F.I.G. (2001) Code of Points states that the gymnast must land with both feet within 50 cm of the extended centre line of the horse. Failure to do so leads to deductions from 0.1 to 0.2. Any loss of balance during landing (a hop or step) can also lead to a deduction from 0.1 to 0.3. Finally a fall during landing is a deduction of 0.5, if the gymnast lands on his feet and falls afterwards the element is recognised.

In order to gain the highest scores in a competition the gymnasts must comply with the judging criteria stipulated by the F.I.G. Each vault is given a start value and deductions due to errors are taken from the start value to get the final score. Since landing is key to the vault and other apparatus dismounts it is important

to understand the mechanics of landing and how the body absorbs impact during landing to ensure minimum risk of injury.

The landing of gymnastic skills performed in competition presents a significant challenge to the neuromuscular system. Gymnasts encounter a wide range of velocities; segmental configurations and visual conditions prior to contact that influence their ability to bring total body momentum to zero with a single foot placement (McNitt-Gray et al., 2000). A model of landing may help the understanding of how some of these factors affect the landing strategy, since each could be altered independently in a model.

Previous research on vault landings has been limited to articles describing how the landing strategy changes during different vaults and its influence on the final score (McNitt-Gray et al., 2000; Takei, 1998). Most of the literature is based upon drop landings and most studies are experimental as opposed to theoretical. Experimental drop landing research has provided valuable insights into the kinematics and kinetics of landings (Dufek & Bates, 1990; Ozguven & Berme, 1988; McNitt-Gray et al., 1993). This literature provides data on ground reaction forces (GRF) and joint kinematics of subjects when dropping from various heights onto different landing surfaces. These studies highlight how landing strategies change depending upon height and landing surface. A greater drop height or stiffer landing surface results in greater knee and hip flexion.

Theoretical modelling of whole body landing is limited. Denoth (1985) modelled the whole body as three linked rigid segments with four muscles. Most of the literature on modelling is restricted to smaller regions of the human body: for example a viscoelastic foot model by Gilchrist & Winter (1996), the foot as a shock absorber by Salathe et al., (1990) and the role of the heel pad and shank soft tissue during impact by Pain & Challis (2001b). The advantage of a simulation model is the ability to answer questions of the type "what if?". For example the same landing strategy may be used to investigate how different landing surfaces affect forces in and on the body.

Landing is a key area for investigation as many studies have reported injuries associated with landings in gymnastics (Andrish, 1985; Jensen, 1998; Meeusen & Borms, 1992). A model could be used to help to understand the mechanisms of injury and possibly offer solutions for reducing the injury potential associated with landings.

It has been highlighted that landing is a fundamental element of a successful vault. In the vault competitions of the Sydney 2000 Olympic Games the landings success rates of male gymnasts was nearly twice that of female gymnasts. Even so male gymnasts landed only 36% of backward rotating vaults successfully and only 16% of the forward rotation vaults successfully. A landing was deemed successful when the gymnast landed using a single foot placement and no additional steps (McNitt-Gray et al., 2000). Since the landing is critical from all apparatus during a gymnastic competition, it is the intention of this research project to explain the mechanics of a successful landing. To facilitate this a computer simulation model of a gymnast landing will be developed. The model will be used to provide explanations of the mechanics of landings and suggest possible improvements to landing surfaces.

### *1.2 Statement of Purpose*

To increase the scientific knowledge and understanding of mechanical factors that influence landing in Men's Artistic Gymnastics.

In order to provide a focus for the study the landings from vaults will be used. Factors that influence landing performance include the landing strategy adopted by the gymnast and the type of landing surface. The criterion for a successful landing in gymnastics is to bring the total body momentum to zero with a single foot placement, and also to minimize the magnitude of the internal forces experienced by the body to reduce the chances of injury. A model could be used to optimise the landing strategy and mat properties to ensure the lowest internal forces possible within the performance and equipment constraints set out by the F.I.G.

The proposed model shown in Figure 1.1 comprises seven segments (including three segments with wobbling masses) and two spring-damper systems, one at the foot representing the elastic properties of the foot / heel pad and one representing the landing surface. The model will be subject-specific and will use personalised inertia data, muscle models will produce the torques at the joints that will be used to drive the model, and the general torque / angle / angular velocity muscle properties will be determined via isokinetic dynamometer measurements on the subject. In addition a simple model of bone will be used in the lower extremities to represent any bending of the bones. It is anticipated that this may help to



determine when any fracture injuries may occur as a result of acute or chronic trauma.

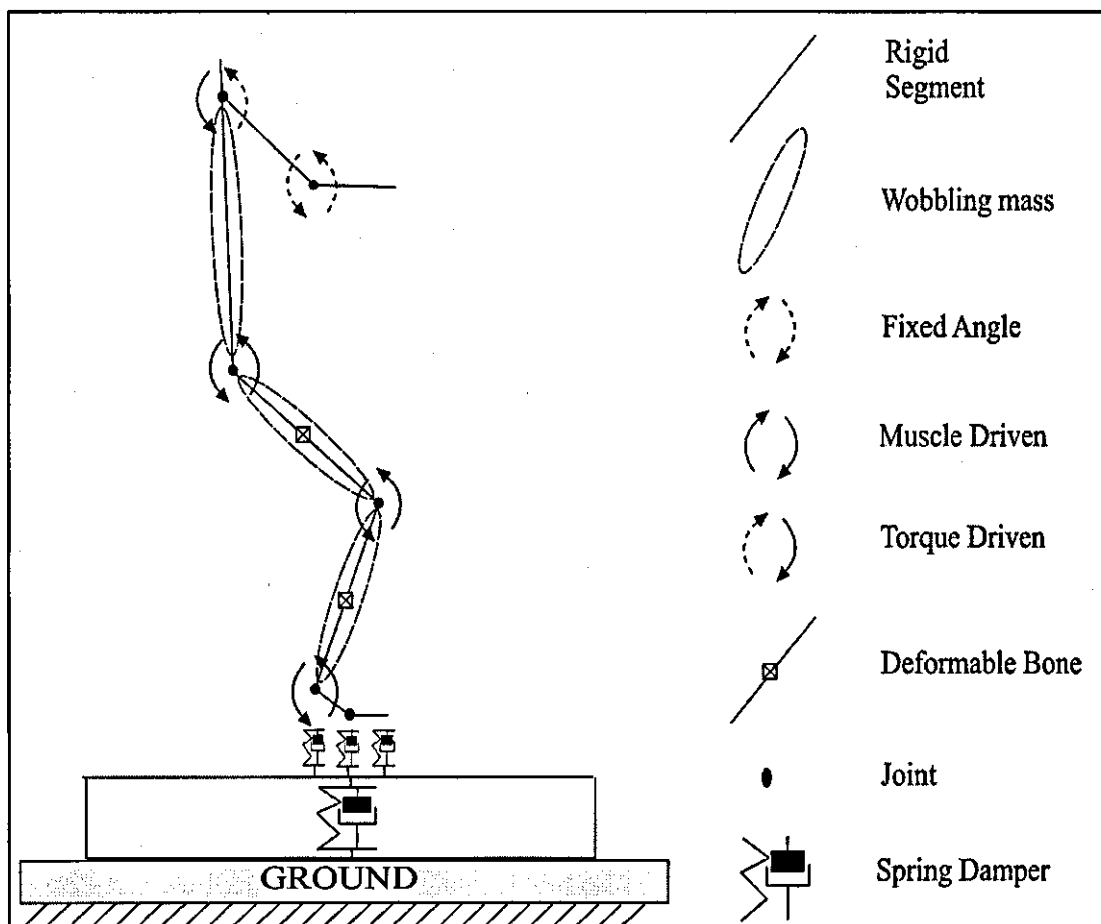


Figure 1.1 Proposed model diagram.

### 1.3 Research Questions

By addressing specific questions it is intended that the statement of purpose will be answered.

As a gymnast progresses through his career the vault complexity increases and as the vault gets more difficult the height required to perform the skills successfully may also increase. For example the peak height of the mass centre during post-flight in a handspring vault is lower than the peak height required for a handspring double front somersault vault.

Q.1. How do ground reaction forces and internal forces acting on a gymnast change in response to different impact velocities?

The landing must be controlled in order to ensure minimal deductions but this could lead to increases in GRF's and internal forces and therefore to chronic or even acute injuries. Are there any modifications that can be made to reduce GRF's and internal forces but still ensure minimum deductions and keep the landing surface within the acceptable limits for the F.I.G.? Devita & Skelly (1992) have highlighted the significance of joint stiffness and configuration on ground reaction forces, a stiffer landing (less than 90° knee flexion) resulted in a larger GRF.

Q.2. What adjustments can be made to the landing strategy to reduce GRF's, internal forces and minimize the chances of injury?

From learning a new skill to competing it means changing the landing mat from a soft thick mat to a thinner stiffer mat. When learning a new skill the chance of error is greater and therefore thicker and softer landing mats are used. As the chances of error decrease the landing mats are replaced with thinner stiffer mats, similar to these used in competition (McNitt-Gray et al, 1993).

Although competition mats are constructed to the same specification the mats will probably have different cushioning characteristics due to the number of impacts the mat has sustained (Wieners et al., 1995).

To facilitate performance and effective load distribution within the musculoskeletal system, the landing mats used by gymnasts during competition need to be predictable and complement the physiological capabilities of the gymnast to control momentum and absorb energy during landing. The ability of the gymnast to control the reaction force experienced during landing may be compromised by an inability of the gymnast to anticipate the task specific load, coordinate muscle forces, and withstand the load experienced during interaction with the landing mat. If the neuromuscular and skeletal systems experience an unexpected change in load, detrimental loading patterns may result. Repetitive application of these forces over time may lead to bone, ligaments, tendons and other soft tissues experiencing undesirable tissue adaptation and acute / overuse injuries (McNitt-Gray et al., 2000). The incidence of injury to the lower extremities of gymnasts reflects the mechanical demand imposed during landing. Practice and repetition are key in gymnastics to ensure that skills can be executed repeatedly. Research has shown that repetitive impacts below the fracture threshold (for a single impact) can lead to stress

fractures. This is a result of the skeleton failing to respond quickly enough to the stresses and strains imposed upon it (Burr, 1997). Through training, vault landings are repeated and this repetitive impact during landing could lead to injury. Gymnastic injuries are of two main types: one is due to direct trauma as a result of a fall or dismount, the other due to extreme stresses caused by excessive, repetitive sub-threshold injuries (Snook, 1979).

Q.3. What adjustments can be made to the landing mat to reduce GRF's and internal forces to minimize the chances of injury?

Pain & Challis (2001c) reported that the body is normally considered as a series of linked rigid segments connected by simple rotational joints. However people are not made up of rigid segments and there can be times when this assumption is valid and times when it is not. Lafortune et al. (1992) reported that during controlled impacts such as landing from a drop, segments showed intra-segmental motion of up to 70 mm relative to the underlying bone and this affected the joint forces and moments. But how much bone deformation occurs during landing and is the modelling of bone deformation important when investigating the forces acting on a body during landing?

Q.4. How much bone deformation occurs during landing?

Optimum technique (minimal GRF's and internal forces and minimal deductions) may depend upon strength characteristics of the individual. Similarly the optimal solution may be sensitive to differences in these strength characteristics and inertia parameters of the gymnast. Such considerations must be evaluated before generalisations can be made regarding optimum techniques or landing mat properties.

#### *1.4 Chapter Organization*

Chapter 2 reviews the experimental and theoretical research literature concerned with vault landings. Drop landings research is also reviewed, as actual research on vault landings is limited. Literature regarding wobbling masses, muscle

force production, inertia parameters, landing surfaces and injury mechanisms are reviewed as they play a major role in the proposed gymnast-mat model.

Chapter 3 presents the development of the landing mat model. The methodology for the landing mat data collection session together with its rationale are reviewed. Specific literature related to the equipment and techniques used to collect the data are discussed. The results and analysis are reported in detail and are used to evaluate the model of the landing mat.

Chapter 4 describes the development of the gymnast model. The methodology used for the subject related data collection is described. Specific literature related to each data collection session is discussed. The results are analysed and reported in detail.

Chapter 5 describes how each gymnast-mat model was evaluated. The development of the objective score is reported and the results of the evaluations are discussed in detail.

Chapter 6 presents the results of the optimisations that were run to answer some of the research questions. The results are presented and discussed in detail.

Chapter 7 summarises the results of the optimisations and attempts to answer the research questions. The problems encountered during modelling are discussed and future research that could be conducted following the present study is reported.

## CHAPTER 2

### LITERATURE REVIEW

#### *2.1 Introduction*

This review of literature has been divided into two sections. The first section comprises an overview of the vault apparatus together with an introduction to landing. The second section focuses upon the published research on landings and impacts and on associated key elements such as landing surfaces.

##### 2.1.1 Overview of the Vault and Development of the Vault Apparatus

Men's Artistic Gymnastics consists of exercises on six pieces of apparatus, namely the floor, pommel horse, rings, vault, parallel bars and high bar. Although this thesis focuses on the vault the research may have relevance for all six events as landing from a dismount occurs at the end of all routines except for the floor exercise which has several landings. Unlike the other apparatus the vault exercise comprises a single movement rather than a routine. King et al. (1999) described how vaulting technique could be broken down into four phases. Firstly the pre-flight phase was defined from springboard takeoff to initial contact of the hands on the horse. The second phase was defined as the period the hands were in contact with the horse. The third phase was the post flight phase: this was the second airborne phase, from horse takeoff to the instant of touchdown. Finally the fourth phase was the landing: this was from the instant of touchdown to the point at which the mass centre of the gymnast stopped moving.

##### 2.1.2 The Equipment

In modern gymnastics the vaulting equipment consists of a 25 metre run-up, a springboard, vaulting horse / table and a landing mat. The layout of the vaulting equipment is shown in Figure 2.1.

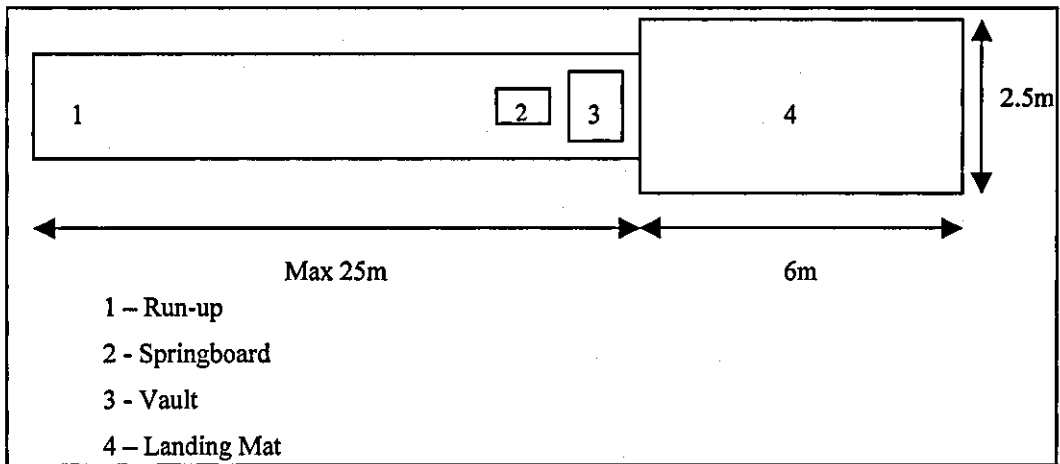


**Figure 2.1** Vaulting equipment layout.

Up until the start of 2001 the vaulting horse apparatus consisted of a prismoid body, supported by a base structure. The body consisted of a solid core and a connected surface. The base had to provide a stable support for the body and assure its levelled position. The body had a length 160 cm ( $\pm 1$ cm), width at top 35 cm ( $\pm 1$ cm), width at bottom 30 cm ( $\pm 1$ cm). The base had a height of 135 cm ( $\pm 1$ cm). A diagram of the vault specifications is shown in Figure 2.2.

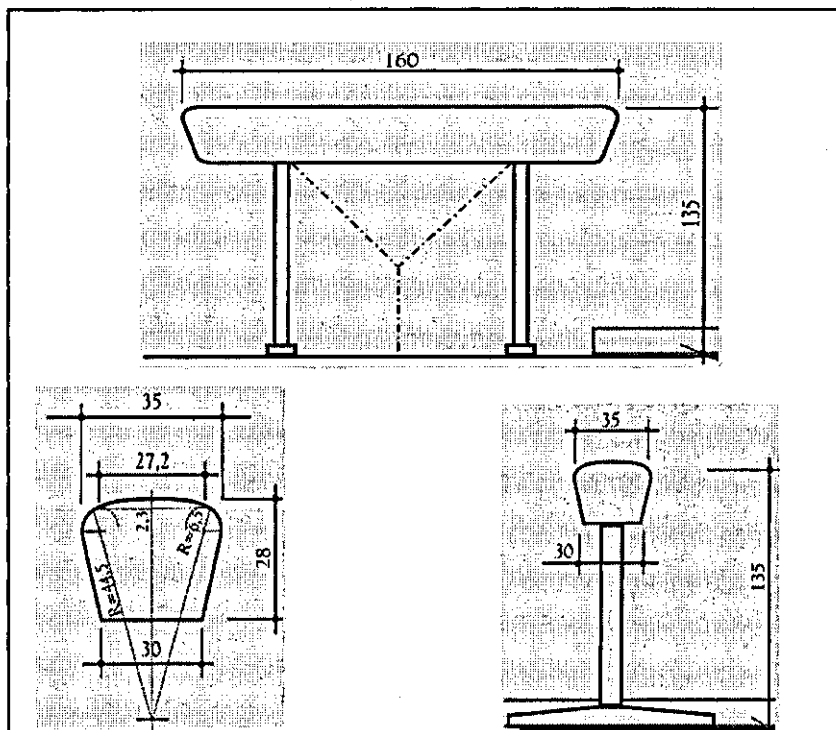


**Figure 2.2** Vault specifications. (F.I.G. Apparatus Norms, 2000/2001).

Since the 1<sup>st</sup> January 2001 the new vaulting table has been used in competition. The new vaulting table offers greater safety and is advantageous to the push-off during vaults (Knoll & Krug, 2000).

The new vaulting table is the same for men and women: the length is 120 cms, width 95 cms. In the men's vault the total height of the vault is 135 cms (women 125 cms). Again the vaulting table must be securely anchored to the floor to ensure no swaying or shifting (F.I.G. Apparatus Norms, 2000/2001). The dimensions of the new vaulting table are shown in Figure 2.3.

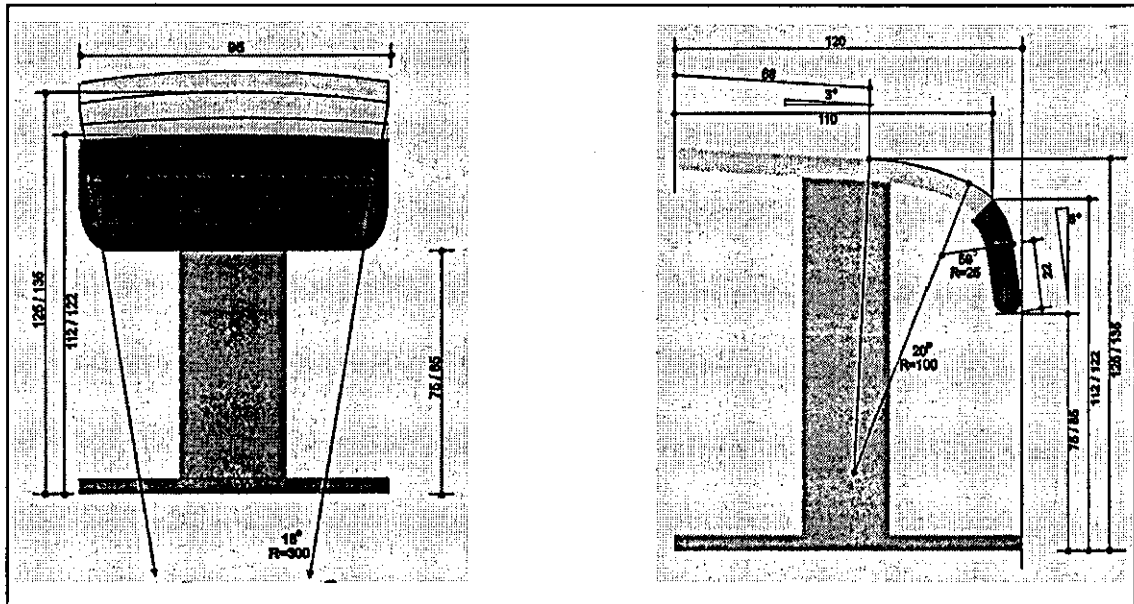


**Figure 2.3** The new vaulting table dimensions (F.I.G. Apparatus Norms, 2000/2001).

Since this thesis will focus on the vault landing it is pertinent to investigate the dimensions and cushioning characteristics of the competition landing mat. The vault landing mat is 600 cm in length and 250 cm in width. The depth (thickness) of the landing mat is 20 cm. The objective of the F.I.G. standard is to provide equal opportunities for all athletes in F.I.G. competitions by controlling the functional properties of landing mats and to minimize any differences between competition and training equipment (F.I.G. Apparatus Norms, 2000/2001). The F.I.G. test procedure is designed to test the cushioning properties of the mat and it involves dropping a mass of 20 kg ( $\pm 0.2$  kg) with a flat impact face of 10 cm ( $\pm 0.5$  cm) diameter. A total of nine impact sites are tested (Figure 2.4).

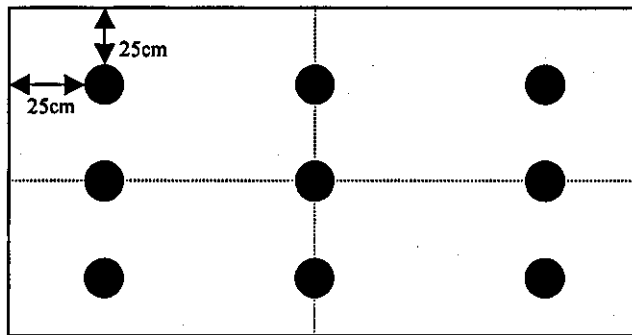


**Figure 2.4** Test impact sites (not too scale).

The mat is placed on a rigid floor and the mass is raised to a drop height of approximately 0.8 m corresponding to an impact velocity of 3.96 m/s ( $\pm 3\%$ ) and the acceleration time-history is recorded from an accelerometer mounted on the mass. One impact is performed, then less than 120 seconds later, the next impact is performed. A total of 90 impact trials are carried out for each impact site. The peak force (from the product of the impactor's mass and the maximum acceleration), deflection of the mat's surface and height of rebound are calculated for the last eight impacts from each site and an average is taken. The performance requirements are a deflection of 110 mm or less; a height of rebound of 90 mm or less and a peak force of 3000 N or less (F.I.G. Apparatus Norms, 2000). These values for mass and especially for velocity seem rather low as landing velocities reported by Takei (1988) were in the region of 5.5 m/s. Since a landing mat's behaviour is a function of stiffness and damping the impact velocity will affect the behaviour of the mat.

### 2.1.3 Types of Vaults

When competing in the vault event the gymnast can select from five vault groups. Each vault is given a start value based upon technical difficulty. The five vault groups are:



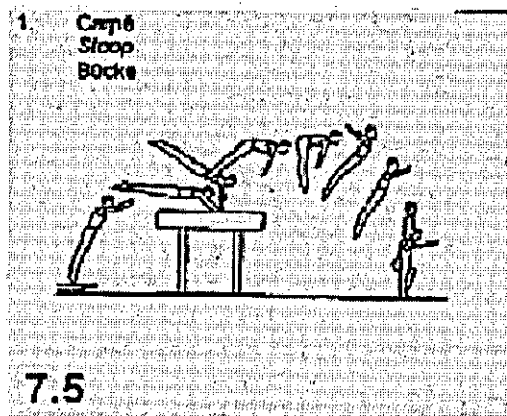


Figure 2.5 Direct vaults – example: Stoop (F.I.G., 2001).

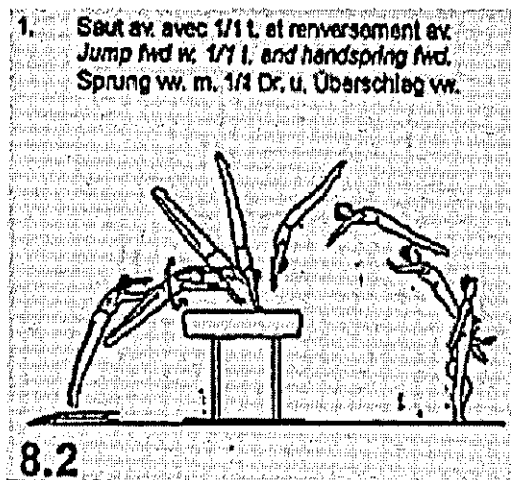


Figure 2.6 Vaults with a full twist in the first flight phase – example: full twist on, handspring off (F.I.G., 2001).

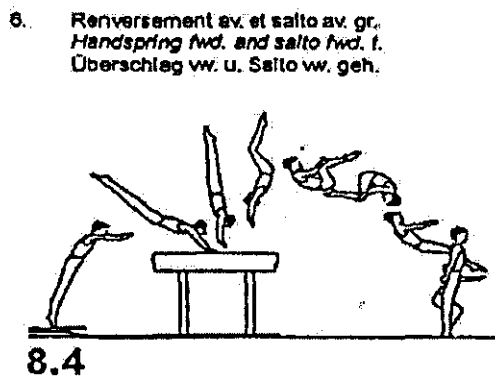
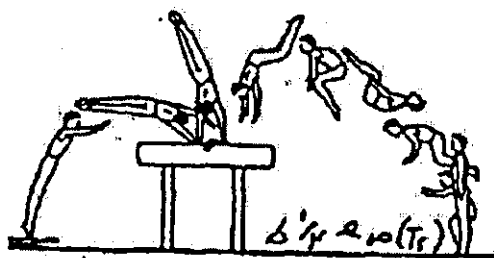


Figure 2.7 Handspring and Yamashita style vaults – example: handspring tuck front (F.I.G., 2001).

6. Renversement lat. avec  $\frac{1}{4}$  t. et salto arr. gr.  
*Handspring sw. w.  $\frac{1}{4}$  t. a. salto bwd. t.*  
 Überschlag sw. m.  $\frac{1}{4}$  Dr. u. Salto rw. geh

(Tsukahara)

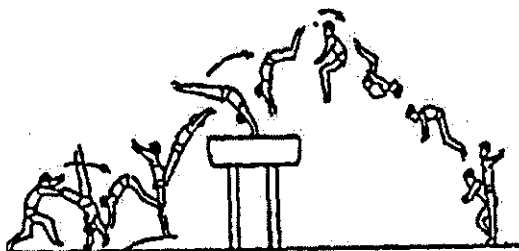


8.4

Figure 2.8 Vaults with  $\frac{1}{4}$  or  $\frac{1}{2}$  turn in first flight phase – example: Tsukahara (F.I.G., 2001).

6. Rondade, renversement arr. et salto arr. gr.  
*Round off, hdspr. bwd. and salto bwd. t*  
 Rondat und Überschlag rw. u. Salto rw. geh.

(Yurchenko)



8.4

Figure 2.9 Round off entry vaults – example: Yurchenko (F.I.G., 2001).

Deductions from the start value for landing include deviation of axis on landing (0.1 - 0.2); legs apart on landing (0.1 - 0.2); unsteadiness, minor feet adjustment or excessive swings of arms (0.1). Loss of balance, a step, a hop or hand down results in a deduction of 0.1 - 0.3 and a fall is a deduction of 0.5 (F.I.G., 2001).

#### 2.1.4 Landing

In the vault during the Sidney 2000 Olympic Games the landing success rates of male gymnasts was nearly twice that of female gymnasts. Even so male gymnasts landed only 36% of backward rotating vaults and only 16% of the forward rotation vaults successfully without any additional steps (McNitt-Gray et al., 2000). A small point deduction in landing is an important determinant in achieving high overall scores in the vault (Takei, 1998). The landing from the vault (or dismount from other apparatus) poses a problem for each gymnast. The gymnast must trade off technical difficulty with the probability of a successful landing. Increased technical difficulty may decrease the chances of a successful landing and increase the risk of injury. However decreased technical difficulty may mean a successful injury free landing but also limits the potential high score required to win.

Hume (2001) compared the number of injuries during practice with the number during competition. It was found that between 79% and 97% of injuries occurred during practice. However when time spent competing compared with practising was accounted for it was found that the injury rate was three times greater in competition than in practice. This was supported by Meeusen & Borms (1992) who initially reported 85% of injuries occurred in practice. However when athlete hours were accounted for the conclusion was that the relative rate of injuries per hour was 13 times greater in competition.

A possible reason for this is that during training as drop height increases the thickness of the landing surface tends to increase. However in gymnastic competitions thinner mats replace the thicker mats used in training. A thinner stiffer mat increases the peak vertical force upon landing. However the gymnast tends to increase joint flexion to accommodate the thinner mat. If a simple skill is executed, less joint flexion is required to execute a desired landing on a mat; therefore there is more range of motion available to the gymnast to accommodate unexpected events. If a more complex skill is not executed effectively the gymnast may land with greater knee and hip flexion and therefore has less range of motion available to accommodate the landing (McNitt-Gray et al., 1993). This may lead to a greater chance of injury especially on a thinner and stiffer landing mat.

## *2.2 Experimental and Theoretical Research*

Within sports biomechanics two main areas exist. The study of sports related injuries and the understanding of performance in sport. A researcher needs to ask the questions 'what?' 'how?' and 'why?' For example, what magnitude of force causes bones to break? How are these forces produced or reduced in the human body? Why do different landing techniques change the ground reaction forces?

One method of answering these questions is the experimental approach. Yeadon & Challis (1994) said that this might take the form of direct intervention in the activity or, alternatively, the experiment may be invisible to the athlete and coach. By obtaining movement and force data on an individual athlete it may be possible to answer the question "do different landing techniques influence ground reaction forces?" Taking a bone and bending it to failure may help to answer the question "what forces cause bone to break?" However this approach requires access to many bones and testing equipment with the added problem that bones may behave differently in vivo due to the surrounding muscles and other tissues.

Another method of investigation is the theoretical approach that takes the form of an idealisation of the activity. Hypothetical data are generated by using the model in specific situations (Yeadon & Challis, 1994). Winter (1990) describes the ultimate goal, once a valid model has been developed, is to ask the question – "what would happen if?". The theoretical approach allows the researcher to alter one variable without altering any others and determine its effect on performance. Movements of both the model of the subject and the equipment obey Newton's Laws of motion. This makes the theoretical models mathematical formulations of Newtonian systems (Yeadon & Challis, 1994).

Experimental and theoretical approaches are different yet both are important when conducting research. Yeadon & Challis (1994) showed how both theoretical and experimental research are linked (Figure 2.10).

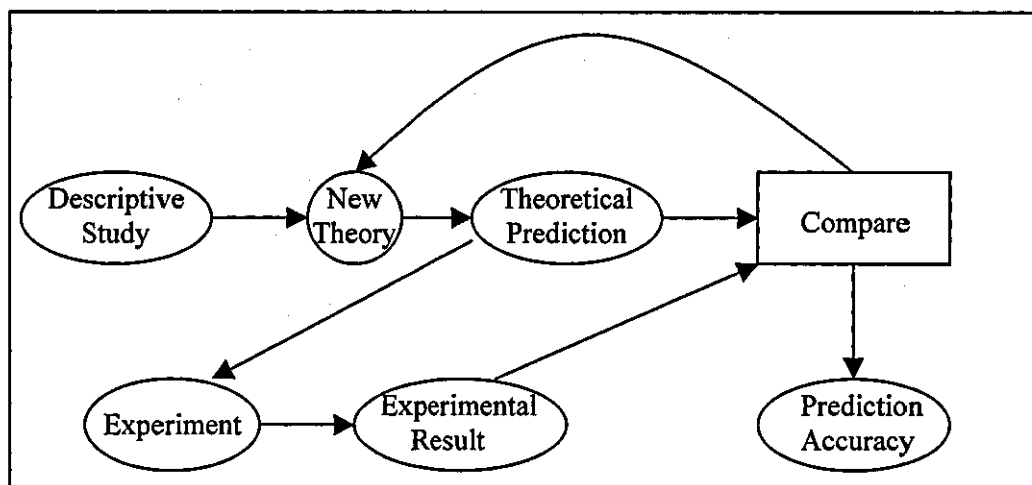


**Figure 2.10** The theory-experiment cycle of scientific method (Yeadon & Challis, 1994).

The majority of experimental landing research has involved observation of landings and manipulation of an independent variable such as drop height to determine its effects on ground reaction force (dependent variable). However researchers have found it difficult to constrain the landing strategy of the subjects so that each landing is the same from different drop heights. This is an aspect where theoretical modelling has the advantage.

### *2.3 Experimentally Based Literature*

Many studies have investigated the landing phase of a skill. These include impact force attenuation mechanisms during volleyball landing activities (Dufek & Zhang, 1996) and ground reaction forces during forward running somersaults (Miller & Nissinen, 1987). However the majority of published literature has focused on skills such as drop landings (Dufek & Bates, 1990; Ozguven & Berme, 1988; McNitt-Gray et al., 1993,1994; Devita & Skelly, 1992). Investigations into drop landings are split into two main areas: these are kinematics of drop landings where the joint angles, velocities and accelerations are reported with varying drop conditions, and the kinetics of drop landings that focuses upon impact forces during the landing activity.

The general consensus of the work focusing on the kinematics of landing was summarized by McNitt-Gray et al. (1993) who concluded that as drop height

increased the degree of joint flexion, rate of joint flexion and landing phase time increased.

Impact forces are the other area of focus for published experimental literature. The research investigates the effect of different landing strategies on ground reaction forces. Landing strategy refers to the multi-joint coordination plan an individual executes to satisfy the objectives of the landing task (McNitt-Gray et al., 1993). Vertical ground reaction forces generally increased with greater height (Dufek & Bates, 1990). This was also supported by McNitt-Gray et al. (1993) who reported a vertical ground reaction force of 8 BW from a height of 1.82 m, 6.8 BW from a height of 1.25 m, and 5 BW from a height of 0.69 m onto the same mat.

### 2.3.1 Landing Strategy

The landing strategy itself can influence the peak vertical ground reaction force even when drop height remains constant. From a drop height of 0.59 m stiffer landings (characterised by less than 90° knee flexion during landing) resulted in larger peak vertical ground reaction forces when compared to soft landings (more than 90° knee flexion). The muscular system absorbed 19% more of the body's kinetic energy in the soft landing compared to the stiff landing, reducing the impact stresses on other body tissues. The ankle plantar flexors provided the major energy absorption function in both conditions, averaging 44% of the total muscular work done followed by the knee (34%) and the hip (22%) extensors (Devita & Skelly, 1992). 75% of the total mechanical energy of the body (2 to 93 J) was dissipated passively in the musculoskeletal system during a stiff landing. The rest of the total mechanical energy was dissipated actively by negative work of the muscles (calculated from the integral of the joint power) (Zatsiorsky & Prilutsky, 1987). The passively dissipated energy possibly included soft tissue movement and the compression of some visco-elastic structures of the body.

### 2.3.2 Foot Position

Toe to heel landings versus flat foot landings reduce vertical impact forces (Dufek & Bates, 1990). These results were also supported by Gross & Nelson (1988) who found that forefoot landings significantly reduced maximum vertical ground reaction force by 22%. Subjects were found to dorsi-flex at the ankle approximately 15° from maximum plantar flexion during the final stages of the

flight phase. However if too much dorsi-flexion occurred at the ankle, a heel to toe landing could result in a large and rapid (20 – 25 ms) vertical impact force. The impact peak was 3.4 to 3.8 times greater in heel to toe landings than in forefoot landings (Kovacs et al., 1999).

### 2.3.3 Muscle Pre-activation

During landing impact absorption can last 150 – 200 ms. After this time the downward momentum of the body has been substantially reduced and the landing movements are concerned with balance. The important features of impact occur in a time period that is shorter than the conscious voluntary human reaction time (Lees, 1981; Ozguven & Berme, 1988). Winter & Brookes (1991) reported a reaction time of 0.123 s from light stimulus to change in electrical activity in the muscle. However, the human body can react faster than this: an involuntary response (mono-synaptic) involves transmission of information from a sensory neurone to the appropriate motor neurone across a single synapse in the spinal cord and can occur in approximately 30 ms (e.g. stretch reflex). This cannot be altered or trained. A polysynaptic reflex involves an electrical impulse being transferred from a sensory neurone to a motor neurone with one connecting neurone (interneurone) in the spinal cord (e.g. pain withdrawal reflex, 50 – 70 ms). This suggests that the human body can react faster depending upon the stimulus. The neuromuscular system prepares for the impending load after foot contact by activating muscles prior to contact. After contact muscle tendon units must generate sufficient force to stabilise the joint, control joint flexion and reduce total body momentum (McNitt-Gray et al. 2001). This notion of pre-activation is supported by Fukuda et al. (1987) who reported that EMG of the gastrocnemius muscle starts to increase about 120ms before foot contact. Pre-activation of co-contracting muscle groups allows the system to stiffen in preparation for controlling a relatively large reaction force and reduces the potential for quick fluctuations in net joint moments, during a short period of time (40 ms) with limited opportunity for neural feedback.

### 2.3.4 Joint Configuration and Body Orientation Prior to Landing

Not only do pre-activation of muscles, co-contraction and muscle recruitment patterns affect the landing strategy and impact forces but so does the amount of joint flexion prior to impact. Knee angle at touchdown affects the

maximum force: greater knee extension results in greater maximum impact forces (Dufek & Bates, 1990).

The trunk orientation and joint kinematics prior to landing have been shown to influence the ground reaction force of a gymnast landing from the same height but performing different aerial skills and hence a different body configuration prior to landing (McNitt-Gray et al., 2001). The musculoskeletal system experiences large loads immediately following touchdown and so ensuring the correct joint orientation prior to landing is important for the gymnast when attempting to minimise these forces (Requejo et al., 2004).

### 2.3.5 Landing Mats

Experimental research has investigated the effects of landing mats on landing strategies and impact forces. The effect of different mat thickness, density and composition has been reported for walking and running. A thicker mat of the same material or a less stiff mat of the same thickness reduced the impact forces experienced by the subjects, providing the mat was not 'bottomed out'. Results suggest that human subjects maintain similar peak impact forces by adjusting their running kinematics. The mats with least impact absorption resulted in an increased amount of knee flexion during contact (Dixon et al., 2000). This is also supported by Skelly et al. (2003) who found no significant differences between the impact forces for thin and thick mats of the same composition during step aerobics. Again subjects tended to adjust their joint kinematics to accommodate the change in landing mat.

McNitt-Gray et al. (1994) investigated the effects of different landing mats on impact forces during drop landings. Mats classified as soft, stiff and no mat were used when dropping from a height of 0.69 m. Results showed that mats enable gymnasts to use less joint flexion when landing.

When landing from heights attained with an aid of mechanical apparatus (pole vaulting, gymnastics) humans can use landing mats as a means of protection against injury. When an object impacts a deformable surface, the acceleration it experiences is inversely proportional to its mass (Martin et al., 1994) providing the mat is not 'bottomed out'.

Nigg (1990) described six methods for testing landing mats ranging from dropping a mass onto the surface of interest and using accelerometers attached to the mass to calculate the impact force, to using subjects performing typical movements



onto the surface where deformation of the surface is quantified and ground reaction force recorded.

The majority of research uses material tests. Within the Federation Internationale Gymnastique (F.I.G.) the landing mats are standardised according to F.I.G. guidelines. A 20 kg mass with diameter 10 cm is released from a height of approximately 0.8 m to achieve 3.96 m/s touchdown velocity. Peak force, deformation and rebound height characteristics must fall within F.I.G. guidelines for the mat to be used in competition.

McNitt-Gray et al. (1993) used a similar drop test in which the mass was only 5.5 kg and was dropped from 3 heights (0.69 m, 1.25 m, 1.28 m). Neither the F.I.G. test nor the test by McNitt-Gray seems suitable for testing the mat under realistic loading conditions associated with landing from vaults or other apparatus. Gymnasts land from vaults with vertical impact velocities of approximately 5.5 m/s (Takei, 1988).

This suggests that although the F.I.G. has a standardised test for the mats insufficient thought has gone into developing mats to reduce the forces experienced by the gymnast and minimise injuries associated with landing. Subject tests provide information on actual deformations to be expected during typical activities performed by subjects on the surface of interest (Nigg, 1990). The currently available material tests for area-elastic surfaces are not appropriate for assessing area-elastic surface characteristics for vault landings.

### 2.3.6 Injury

Injuries are unfortunately a part of all sports and gymnastics has its fair share. One question is "how can injuries be reduced in gymnastics?" To answer this question evidence of injury types and occurrence must be gathered and analysed. An injury will be defined as any gymnastic related incident that prevented participation by the gymnast in any part of a workout or competition (Pettrone & Ricciardelli, 1987). To avoid injury, load experienced by the body needs to be kept in balance with the ability of the musculoskeletal structures to respond to stress induced loading. Absence of stress results in degeneration or muscle atrophy, whereas a single excessive load may result in acute injury or may lead to chronic injury (McNitt-Gray, 2000).

Impact injury to the human body is caused by deformation of biological tissues beyond their elastic limit. Chronic injuries include stress fractures, jumper's knee, anterior compartment syndrome and tendonitis. Jensen (1998) reported that stress fractures typically occur in normal bone that has been subjected to repeated loading with loads less than those that cause spontaneous fracture. Dismounts in gymnastics are identified as possible activities that could cause stress fractures (Jensen, 1998). Body landing positions, performance execution and landing surfaces are critical factors that might contribute to the frequency and severity of injuries (Dufek & Bates, 1991). Acute injuries include sprains, strains, dislocations, fractures, tendon and meniscus tears. Meeusen & Borms (1992) reported that the majority of sprains occurred during dismounts.

Many studies have investigated injuries in gymnastics (Snook, 1979; Jensen, 1998; Andrish, 1985; McAuley et al., 1987; Meeusen & Borms, 1992). It was reported that between 57% and 82% of injuries in gymnastics are acute. The lower extremity was the most injured, comprising 54% to 70% of all injuries. Injuries ranged from strains and sprains to fractures and dislocations.

Pettrone & Ricciardelli (1987) reported 62 injuries, 51 acute and 11 chronic of which 9 occurred on vault. Acute injuries included 21 sprains and 16 fractures. A significant finding was the high frequency of acute injury from dismounts. Landing surface standards established by the F.I.G. are based on the need to establish uniformity of equipment and are not based on musculoskeletal loading issues (McNitt-Gray et al., 2000).

Through experimental studies important areas have been identified. These include the landing strategy adjustments, muscle preactivation, joint angle prior to contact, toe to heel landing, the landing surface and how all affect the impact forces during landing.

#### *2.4 Simulation*

Simulation as defined by van den Bogert & Nigg (1999) is the process of performing experiments on a numerical model. Research on human movement does not always use human subjects. It is not usually ethically acceptable to use an invasive technique such as putting a strain gauge in a muscle on human subjects although implanted strain gauges into tibial bone seems rather invasive (Rolf et al., 1997). Nigg & Herzog (1999) provide an example to illustrate the usefulness of

simulation and modelling. They state that the study of knee injuries in distance runners has a basic biology component and a mechanical component. Basic biology could be the reaction of the cartilage to mechanical loads; this could be studied in animal models. However it is impossible to use animal models to learn how to reduce forces at the knee with mechanical interventions such as orthotics. The force in the knee cannot be measured and other factors contributing to injury cannot be controlled. In this example of human movement, one possible option is to build a model of the system and perform experiments on the model. Computer models are used almost exclusively for this purpose.

It is important that a model replicates the features of the system of interest and that the model can answer the question being studied. Careful design of the model and appropriate validation tests once the model is finished are essential. The simulation of the dynamics of movement allows the researcher to apply controlled conditions to the anatomy. Determining the stress and strains on bone during impacts increases the complexity of the model and increases the number of 'what if?' questions asked of the model.

The mathematical model must replicate the actual movement as closely as possible. The choice of variable parameters such as knee extensor torques has to be realistic. Errors need to be minimised: van den Bogert & Nigg (1999) refer to a simple error that can effect the results greatly. The choice of step size has an effect on the accuracy. For example, assume a mass on a spring where no energy is lost or gained. The mass is given an acceleration and begins to oscillate at a fixed frequency and amplitude, this remains constant and the displacement time curve resembles a sine wave. If the simulation model has too large an integration step size the amplitude of the oscillation may increase due to errors in numerical integration (assuming constant acceleration over the time step) and so the model will no-longer reproduce the experimental results. The step size has caused the model to become unstable.

### *2.5 Optimisation*

Since a simulation model may be used to determine the outcome of a given set of conditions, it is possible to investigate the conditions that will result in the best performance (Yeadon & Challis, 1994).

A research question example could be “what is the optimal approach velocity and plant angle to maximise the height jumped in high jump?” An optimisation may vary the plant angle and approach velocity and find the combination of both that produces the greatest height jumped (Alexander, 1990). Another example may be taken from longswings on high bar where the goal is to maximise the size of the release window and the optimisation parameters could be the hip and shoulder joint angle time histories. By altering both an optimal configuration can be found to maximise the release window (Hiley et al., 2005).

A problem is that most optimisation methods tend to converge on a local optimum rather than a global optimum. This may be prevented by solving the optimisation problem many times with different initial guesses. However some situations have many local optima and the global solution may never be found (van den Bogert & Nigg, 1999).

The Simulated Annealing algorithm (Corana et al., 1987) is a method of global optimisation based on the analogy of minimisation of potential energy in a crystal lattice, which is a function of the positional coordinates of all nuclei. At high temperature, large random changes in position occur. Lattice configurations with low energy will be encountered from time to time and the system is likely to stay longer in such a state. As the temperature decreases, the system will ‘freeze’ in the state of lowest energy. It has been proved analytically that with a sufficiently slow decrease in temperature and suitable input and simulation parameters, the simulated annealing method will converge to a global optimum. The performance of the simulated annealing method for human movement optimisation has been shown to be faster as well as to result in a better solution than other methods in a practical application (van den Bogert & Nigg, 1999).

The Simplex optimisation algorithm is a method of local optimisation. It works by creating a number of initial trials that is equal to the number of control variables plus one. These initial trials form the first simplex. The simplex has a few simple rules, these include; the rejection of the trial with the least favourable response value in the current simplex. Never return to control variable levels that have just been rejected. Trials retained in the simplex for a specified number of steps are re-evaluated. Calculated trials outside the bounds are not made. Find the minimum and gradient towards the minimum then re-evaluate. After the initial trials the simplex process is sequential, with the addition and evaluation of one new trial

at a time. The simplex searches systematically for the best levels of the control variables. The optimisation process ends when the optimisation objective is reached or when the responses cannot be improved further (Walters et al., 1991).

When simulation is used, experiments are performed on a numerical model. Direct validation of a numerical model is usually difficult because the same experiment cannot be performed on human subjects. This could be because of injury risks, or the inability of humans to exactly reproduce a movement. When optimisation of performance is carried out care should be taken to ensure that variables such as approach velocity or parameters such as muscle strength are not optimised beyond the range of human capabilities.

## *2.6 Theoretical Based Literature*

Theoretical models of landing and impact situations range from very simple models such as masses with springs and dampers (Ozguven & Berme, 1988; Mizrahi & Susak, 1982) to multi-segment, wobbling mass, torque-driven simulation models (Pain and Challis, 2004; Yeadon et al., 2005; Peikenkamp et al., 2002; Gruber et al., 1998; Cole et al., 1996).

Little simulation modelling of the gymnastic vault event currently exists. King et al. (1999) determined the optimum pre-flight characteristics of the Hecht and handspring somersault vaults using a two segment model. The landing was modelled as an instantaneous impact followed by a contact phase where the model was treated as a single rigid body rotating about a contact point on the mat.

### **2.6.1 Rigid Body Models**

In biomechanical calculations of internal kinetics the human body is normally considered to be a series of rigid links connected by simple rotational joints. This approach is used in various levels of complexity and applied to a wide range of sporting activities. For example, Alexander (1990) used two rigid linked segments to represent the body when simulating high and long jump take offs. King et al. (1999) used two rigid linked segments to represent the whole body during a gymnastic vault. Denoth (1985) used three rigid links to simulate a drop landing of the whole body. This approach allows the development of simulation models based on mathematical principles such as taking moments about a point and generating equations of motion to solve for angular accelerations.

Although this approach is commonly used the assumption that a human may be represented as a series of rigid links must be questioned. Humans are not made of rigid links and there can be times when this assumption is valid and times when it is not. During low acceleration movements such as gentle arm swinging no measurable intra-segmental motion occurs (Luchetti et al., 1998). However during high acceleration activities involving large muscle groups and impacts, 70mm of segmental motion may occur relative to the underlying bone (Lafortune et al., 1992). Along this continuum there comes a point where modelling the human body as a series of rigid linked segments is not appropriate.

### 2.6.2 Wobbling Mass Models

Developing a highly complex wobbling mass model consisting of mostly unknown parameter values is pointless. A balance between the number of rigid segments and wobbling masses must be achieved to ensure sufficient complexity to solve the proposed problem with a limited number of unknowns. The first step could be to separate bone from all other tissues and calculate the relative mass contributions of each component. The bone component could represent the 'rigid body skeleton' and the wobbling mass components could represent the soft tissue. Each must be connected to the other, via a spring so that movement with respect to each other is possible. This gives two rigid structures for each body segment that interact in a way that is dependent upon the viscoelastic properties of the soft tissue.

Including the soft tissue motion means that a real set of forces are used in the analysis. Forces can be absorbed and produced in a way that cannot be accounted for using a rigid body model alone. One major problem that arises is that of determining how much of the total segment is rigid (bone) and how much is wobbling (soft tissue). Clarys & Marfell-Jones (1986) reported the result of a dissection of three males and three females in terms of the percentage of bone, muscle, adipose tissue and skin. This data can be used as a guideline to determine the relative percentages of mass of bone and soft tissue in a subject-specific model. However the subjects in the Clarys & Marfell-Jones (1986) study were reported to have percentage body fat of around 28% and therefore care must be taken when applying the ratios to athletes with considerably less percentage body fat.

Gruber et al. (1998) used a three rigid linked segment skeleton combined with a wobbling trunk, thigh and shank when simulating a drop landing. Half the

mass of the trunk segment was bone, one third of the mass of the thigh was bone and half the mass of the shank was bone. These values are much higher than reported in Clarys & Marfell-Jones (1986) and no justification could be found for them. Cole et al. (1996) reported using percentages based on Clarys & Marfell-Jones (1986) to determine rigid and wobbling segment percentages.

Once the relevant percentages of rigid to wobbling mass of each segment have been determined the next stage is to develop a method of modelling the motion of the soft tissue relative to the rigid skeleton. Both Gruber et al. (1998) and Cole et al. (1996) split the body segment into bone or soft tissue. Gruber et al. (1998) represented the soft tissue as a rigid body attached to the rigid skeleton of the segment via each body's centre of mass. The soft tissue body could translate and rotate in two dimensions. Cole et al. (1996) represented the soft tissue as a point mass with no moment of inertia and its movement was restricted to translation. No attempt was made to compare the magnitude and frequency of soft tissue motion to actual empirical data.

Pain & Challis (2001b) used a rigid skeletal structure with a surrounding wobbling mass body, comprising a hollow cylinder with the bone in the centre. The two bodies were connected via two translational spring dampers allowing the bodies to rotate and translate with respect to each other in two dimensions. Using rigid bodies to represent soft tissue motion ensures that some of the important kinetics of the system are incorporated into the model as a whole. Pain & Challis (2001b) compared experimental data and the model's wobbling mass displacements to ensure the simulation model produced realistic soft tissue motion.

A further assumption during the modelling of soft tissue incorporates the assumption that each segment's moment of inertia is fixed and cannot alter during the simulation. However the motion of muscles associated with the generation of muscle tension changes the mass distribution and stiffness of the muscles. This may have an influence on the forces and moments acting on a joint (Pain & Challis, 2005).

Although Hatze (1998) reported the modelling of soft tissue motion as 'doomed to failure' current research papers (Gruber et al. 1998; Pain & Challis, 2001b) have managed to reproduce soft tissue motion and ground reaction forces similar to empirical data during impact situations.

### 2.6.3 Heel Pad Properties

During impact situations the heel pad plays an important role in force attenuation by deforming. The viscoelastic properties of it allow the heel pad to adapt to different impact velocities. Heel pad properties have been measured using various techniques, both in vivo and in vitro, yielding different values for the heel pad. Pain & Challis (2001b) have shown through computer modelling of the lower limb and heel pad that both in vivo and in vitro tests yield similar heel pad properties once the effect of the lower leg wobbling mass has been removed. Models that replicate the in vivo results do not include soft tissue movement (Gilchrist & Winter, 1996; Scott & Winter, 1993). Models that have used a wobbling mass approach such as Pain & Challis (2001b) have showed that in vitro heel pad properties are appropriate parameters to use when the model of the body includes wobbling masses.

### 2.6.4 The Rigid Bone

So far the rigid body models and wobbling mass models have used rigid segments representing either the whole segment or the bone. This assumption may be valid in a wide range of situations but how rigid are bones? McNitt-Gray et al. (1993) have reported that humans rely on the lengthening of active muscles during joint flexion and bone deformation to attenuate forces experienced during landing from self-propelled jump heights. Martin et al. (1986) have reported that human femoral bones can bend up to 3.6% of their unit length before failure. The bending is measured as the vertical displacement of the bone centre perpendicular to its longitudinal axis. Bone deformation during impact absorbs energy from the system so that modelling this deformation may be important during impacts at high velocities.

### 2.6.5 The Foot

Empirical studies (Gross & Nelson, 1988) have reported that forefoot landings reduce maximum impact force by 22%. To represent this movement at the foot an additional joint in the model of the foot is required. Gilchrist & Winter (1996) developed a two segment model of the foot with a joint representing the metatarsal – phalangeal joint. Results for the two segment foot showed an



improvement (model results similar to experimental results) when modelling the impact phase during gait simulations.

#### 2.6.6 Generating Joint Motion

Human joint motion consists of mainly rotation although small amounts of translation are present in most joints (e.g. as the knee flexes and extends the joint centre moves back and forth). The small amount of joint translation is usually ignored in whole body models (Gruber et al., 1998; Pain & Challis, 2004; Denoth, 1985; Alexander, 1990). In modelling terms active joint motion can occur via muscles applying torques around joints (Denoth, 1985; Cole et al. 1996; Spagale et al., 1999). This approach requires knowledge of the line of action of the muscle, the effective moment arm and all its mechanical properties together with the estimation of muscle mass whilst moving and the muscle's activation profile. Muscle models tend not to be used for whole body simulations. Pain & Challis (2004) and Gruber et al. (1998) used rotational spring damper actuators to control joint motion. This approach gives the net muscle forces driving the kinematics. A different approach is that of a joint torque generator with 'muscle-like' parameters (Wilson et al., 2001; Alexander, 1990; King & Yeadon, 2002). This approach has the advantage of allowing subject joint torque parameters to be measured via isokinetic dynamometry and used in the whole body model. However one disadvantage is that the effect of bi-articular muscles cannot be represented in a joint torque model. Another disadvantage of the torque driven model is that realistic joint reaction forces are not produced as there are no muscles to compress the joint as they cross it during co-contraction.

Gruber et al. (1998) used joint torque actuators with no activation until 5ms after contact. During drop jumps subjects might keep their joint angles the same but co-contract their muscles prior to contact (Bobbert et al., 1992). Both Wilson et al. (2005) and Alexander (1990) pre-activated the muscles prior to contact in their models of high and long jumping.

#### 2.6.7 Landing Surface

During landing situations the feet impact the floor or mat, tissue deformation and changes in joint kinematics helps to attenuate the shock at impact. If a subject lands onto a mat, as opposed to a rigid surface, the mat also helps to absorb the

shock at impact (McNitt-Gray et al., 1994). Most whole body models of impact incorporate the cushioning effects of the foot, shoe, surface into one spring damper (Wilson et al., 2005; King et al., 1999; Nigg & Anton, 1995). However other attempts have been made to model a landing surface. Finite element modelling has been used by Lyn & Mills (2002) yet the most common approach is the parallel spring damper (Peikenkamp et al., 2002; Nigg & Lui, 1999; Nigg & Anton, 1995). Careful experimental testing of the landing surface and determination of its material properties can help to reduce the unknowns in a whole body model of a landing onto a mat.

### *2.7 Summary*

This literature review has discussed the modelling of impacts and has highlighted the need for the body segments to consist of both rigid and wobbling bodies. Construction of a model must also consider the foot's interaction with any landing surface and the model as a whole must be sufficiently complex as to answer the research questions.

## CHAPTER 3

### MODELLING THE LANDING MAT

In order to investigate the effects of different landing mats on the gymnast a simulation model of the F.I.G. competition landing mat was developed. This chapter begins by describing the structure of the landing mat models, then the methodology and the equipment used to collect data on the sample landing mat. The results are presented and discussed in detail and are used to determine the parameter values for each model in turn. Each model was evaluated by comparing the simulation to the actual experimental data. Problems with the models are identified and solutions offered. The chapter concludes with the final model of the landing that is to be combined with a model of the gymnast to investigate landings in gymnastics.

#### *3.1 An Introduction to Springs and Dampers*

The spring-damper system is the most commonly used approach in modelling a landing mat or foot-ground interface (Wilson et al., 2005; King et al., 1999; Nigg & Anton, 1995). A brief description of the underlying mechanics of springs and dampers is presented prior to describing how spring-damper systems can be used to model the landing mat.

##### 3.1.1 Harmonic Motion

Simple harmonic motion (SHM) is a fundamental form of movement that occurs when an object is subjected to a restoring force. As a spring can provide this restoring force to a mass it seems relevant to start to investigate harmonic motion using a mass-spring system. Figure 3.1 shows the system set-up – a fixed mass (single rigid body) attached directly to the massless spring that is in turn fixed to a solid immovable object. Gravity is ignored in this example, as weight effects are constant.

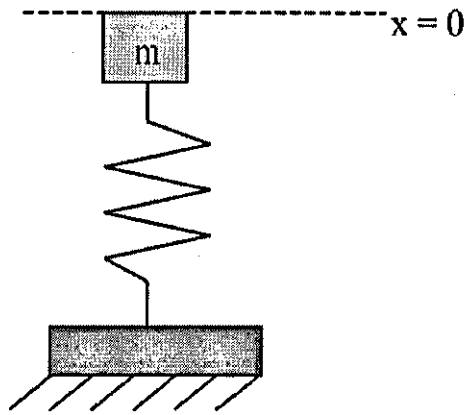


**Figure 3.1** A mass spring system.

Hooke's Law states that the restoring force (pushing the spring back to its original position) is dependent upon the stiffness of the spring and the displacement of the spring. The restoring force is exerted in the opposite direction to the displacement.

Force in a linear spring:	$F = -kx$	$m = \text{mass}$
		$k = \text{spring stiffness}$
		$x = \text{displacement of spring}$
Newton's Second Law:	$F = ma$	
Therefore:	$ma = -kx$	

Assuming no energy is lost in the system the mass will oscillates back and forth at a given amplitude and frequency once the spring is displaced from its natural or resting length (Figure 3.2).

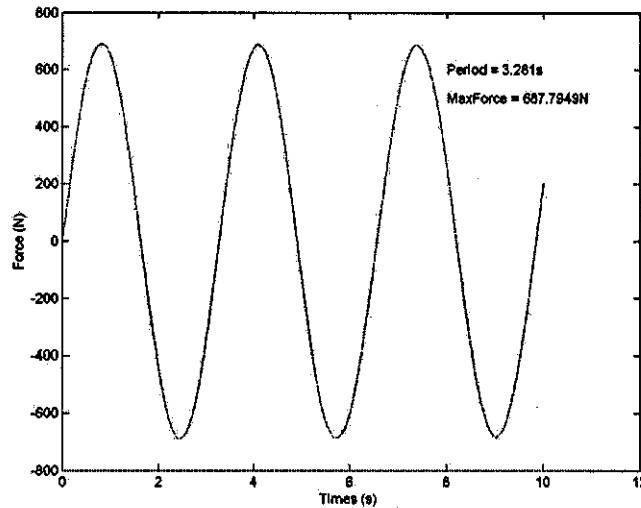


**Figure 3.2** Force time history of a mass spring system in SHM.

### 3.1.2 Spring-dampers

The spring-damper model is often referred to as the viscoelastic model (Figure 3.3). If a material is subjected to a constant force or deformation and its response varies over time, its mechanical behaviour is said to be viscoelastic (Nigg & Herzog, 1999). Many passive materials deform as an elastic material with a linear stress strain curve over small ranges (Fung, 1981). However the linear spring does not allow for energy loss and is independent of rates of change. Both elastic and energy loss components are present in real physical systems.

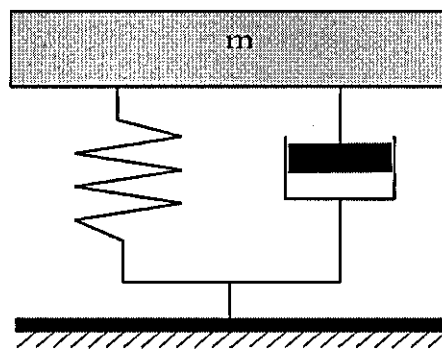


**Figure 3.3** A spring-damper system.

$$\text{Force} = F(t) = F_{\text{spring}} + F_{\text{damper}}$$

Equation of motion for the spring damper:

$$F(t) = -kx(t) - r \dot{x}(t)$$

$k$  = spring stiffness  
 $x$  = spring deformation  
 $r$  = damping coefficient

A spring-damper system can be lightly damped, critically damped or heavily damped. Lightly damped means the mass oscillates around an equilibrium position with diminishing amplitude. Heavily damped means the mass returns to its equilibrium position without any oscillations. In a critically damped situation the mass regains its equilibrium position in the shortest possible time without any oscillations (Figure 3.4).

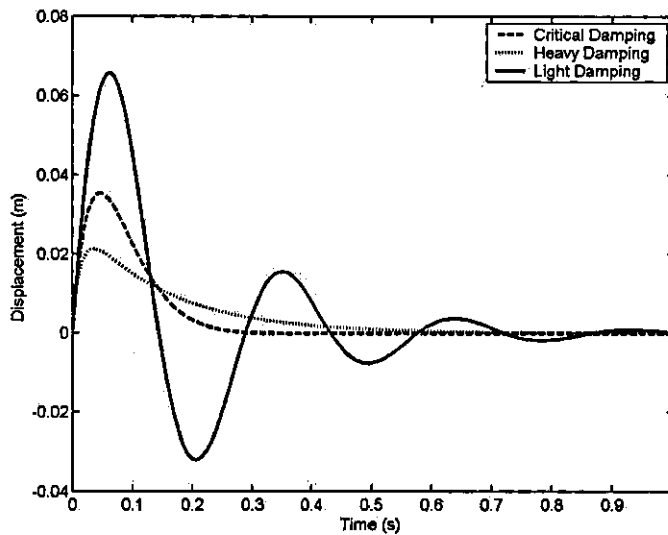


**Figure 3.4** Critically, lightly and heavily damped displacement for a single mass spring-damper system.

### 3.2 The Landing Mat Models

A total of five models were developed to reproduce the vertical component of the landing mat's behaviour during impacts. The sample landing mat comprised three layers: a thin carpet layer (0.5 cm) of negligible mass, a thicker stiff layer (5 cm) of mass 2.44 kg and an even thicker softer layer (15 cm) of mass 3.67 kg. The landing mat models increased in complexity based upon the construction of the landing mat. The aim was to have the simplest model construction possible that could successfully match the force and deformation behaviour of the landing mat during impacts and could also be combined with a model of the gymnast (Figure 4.1). The first four models were developed using MatLab software and one model

was integrated into visual Nastran 4D (VN4D). However problems with simulation time resulted in a fifth model being developed within VN4D based upon the principles identified in model four. VN4D is software that can be used to construct a mechanical system using a GUI. Bodies are classified by their geometries. In VN4D there are boxes, cylinders, spheres, extruded polygons, and polymesh bodies. In addition, each body has parameters, which define how it behaves when run in a simulation, such as inertia characteristics of the body. When a VN4D simulation is run, bodies behave according to the properties and constraints specified during the design. For example, bodies fall under gravity, collide with (or penetrate) other bodies, and/or freely slide along a slot. Bodies in VN4D are rigid. Rigid bodies do not deform or break apart during simulation, even though a physical object (the subject of simulation) may actually do so. However, the finite element modelling software does allow 'rigid' bodies to deform, for example a bone bending under loading. VN4D was chosen as it could interface with MatLab and a basic FEM toolbox. Other software within the department such as Autolev could not interface with the MatLab software whereas the GUI in VN4D made the actual modelling procedure easier by being able to visualise the model as it was being constructed. Software such as ADAMS may have been more advantageous as it has a similar GUI and also allows the user to alter the body inertia parameters whilst maintaining the constraints of any joints. VN4D does not allow this and therefore the bodies have to be reconnected by hand, however VN4D is much cheaper than ADAMS and hence was the only realistic option.

One model was developed to reproduce the horizontal component of the landing mat's behaviour. The final vertical model and the horizontal model were combined to replicate the behaviour of the sample landing mat during oblique impacts.

### 3.2.1 Landing Mat Model One

The landing mat in model one was modelled as single spring-damper system (Figure 3.5). The massless spring-damper system was attached at one end to the ground and at the other end to a point mass. The mass ( $m$ ) used in this model only represented the mass of the impactor used during the experimental testing. The vertical behaviour of the landing mat was defined by Newtons's Second Law of motion and the spring-damper equations:

$$F - mg = ma$$

$$F = -kz - rv$$

- where  $F$  = vertical reaction force  
 $k$  = vertical spring stiffness  
 $r$  = vertical damping  
 $z$  = vertical spring displacement  
 $v$  = vertical spring velocity  
 $a$  = acceleration of mass ( $m$ )

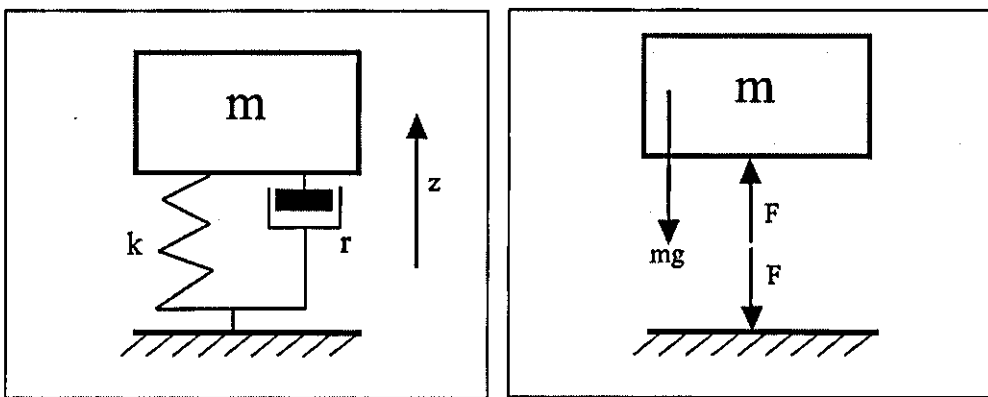


Figure 3.5 Structure of landing mat model one.

The spring stiffness and damping coefficient were optimised using Simulated Annealing (Corana et al., 1987) to minimise the RMS difference between the force time histories of the simulation and the results obtained from the experimental data.

### 3.2.2 Landing Mat Model Two

The second model of the landing mat used a single mass spring-damper system similar to that in model one (Figure 3.6). The landing mat was assumed to be constructed of a single layer. In addition to the point mass (representing the impactor) an effective mat mass was added to the model that represented the mass of the mat being accelerated during the impact (an inertia term). This additional effective mass was accounted for within the equations defining the behaviour of the landing mat. Newton's Second Law of motion and the spring-damper equations:



$$m = m_i + m_e$$

$$F - mg = ma$$

$$F = -kz - rv$$

where  $m_e$  = effective mat mass

$m_i$  = impactor mass

$a$  = acceleration of mass

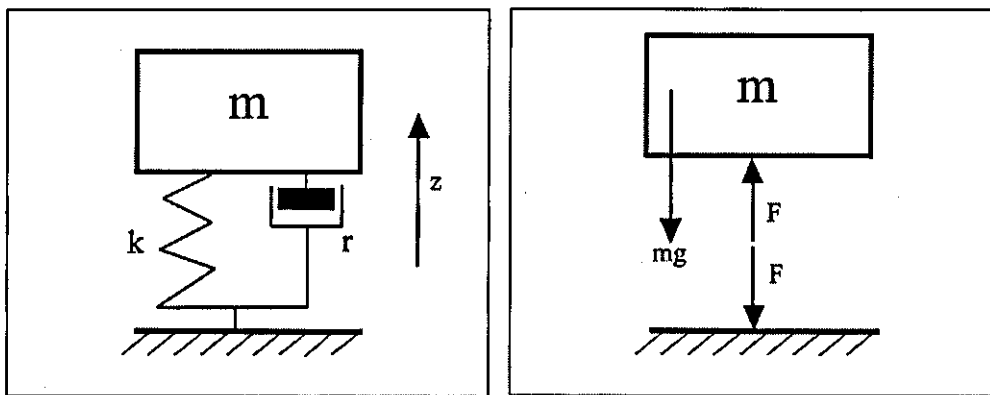


Figure 3.6 Structure of landing mat model two.

The spring stiffness and damping coefficient were optimised to minimise the RMS difference between the force time histories of the simulation and the results obtained from the experimental data. The effective mat mass was determined from force and acceleration measurements taken during impact on the sample landing mat.

### 3.2.3 Landing Mat Model Three

The landing mat in model three used a mass spring-damper, mass spring-damper system (Figure 3.7). This model assumed that the landing mat was constructed of two main layers. The bottom massless spring-damper system was attached to the ground and a point mass ( $m_1$ ). The second massless spring-damper system was connected to the first point mass ( $m_1$ ) and to a second point mass ( $m_2$ ). The actual mass of the bottom point mass ( $m_1$ ) was estimated from the actual mass of the mat (discussed later in this chapter), the other point mass ( $m_2$ ) was also estimated from the actual mass of the mat plus the mass of the impactor. The vertical

behaviour of the landing mat was defined by Newton's Second Law of motion and the spring-damper equations:

$$F_2 - m_2g = m_2(\ddot{z}_2 + \dot{z}_1)$$

$$F_1 - F_2 - m_1g = m_1\ddot{z}_1$$

$$F_2 = k_2z_2 - r_2\dot{z}_2$$

$$F_1 = k_1z_1 - r_1\dot{z}_1$$

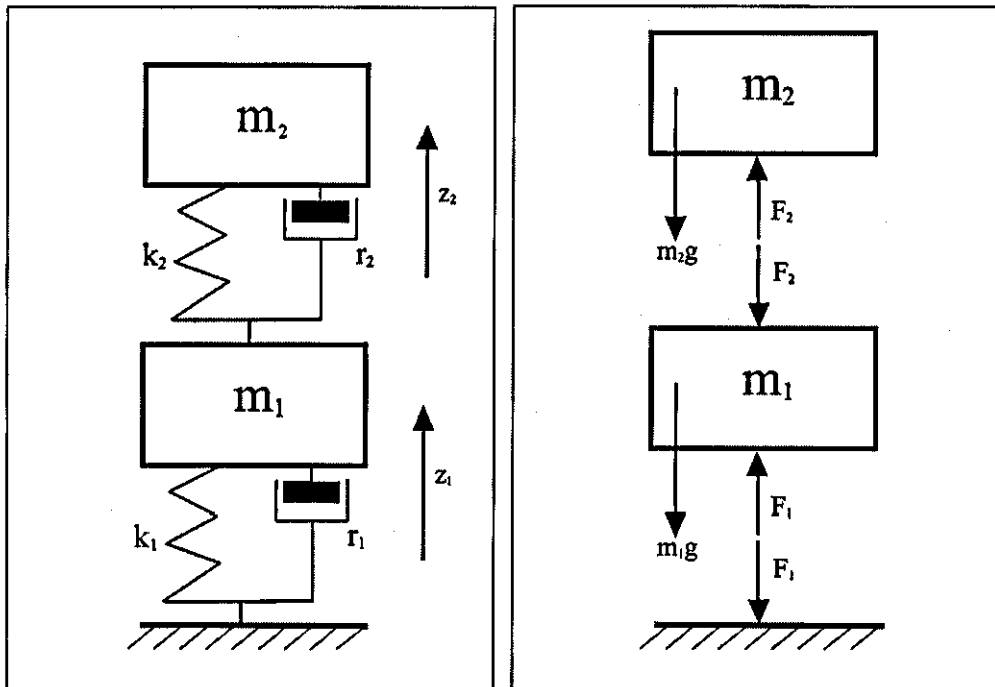


Figure 3.7 Structure of landing mat model three.

The spring stiffness and damping coefficients were optimised to minimise the RMS difference between the force-time histories of the simulation and the experimental trial 1541.

### 3.2.4 Landing Mat Model Four

Model four increased the complexity of model three by adding an additional mass spring-damper system (Figure 3.8). This means model four consisted of a massless spring-damper system connected to the ground and the first point mass ( $m_1$ ). The second massless spring-damper system was connected to the first point mass and the second point mass ( $m_2$ ). The third massless spring-damper system was connected to the second point mass and the third point mass ( $m_3$ ). All point masses

were determined from the actual mass of each layer (density and area) of the sample landing mat and the mass of the impactor, the mass of the carpet layer was very low and hence neglected. The vertical behaviour of the landing mat was defined by Newtons's Second Law of motion and the spring-damper equations:

$$F_3 - m_3g = m_3(\ddot{z}_3 + \ddot{z}_2 + \ddot{z}_1)$$

$$F_2 - F_3 - m_2g = m_2(\ddot{z}_1 + \ddot{z}_2)$$

$$F_1 - F_2 - m_1g = m_1\ddot{z}_1$$

$$F_3 = k_3z_3 - r_3\dot{z}_3$$

$$F_2 = k_2z_2 - r_2\dot{z}_2$$

$$F_1 = k_1z_1 - r_1\dot{z}_1$$

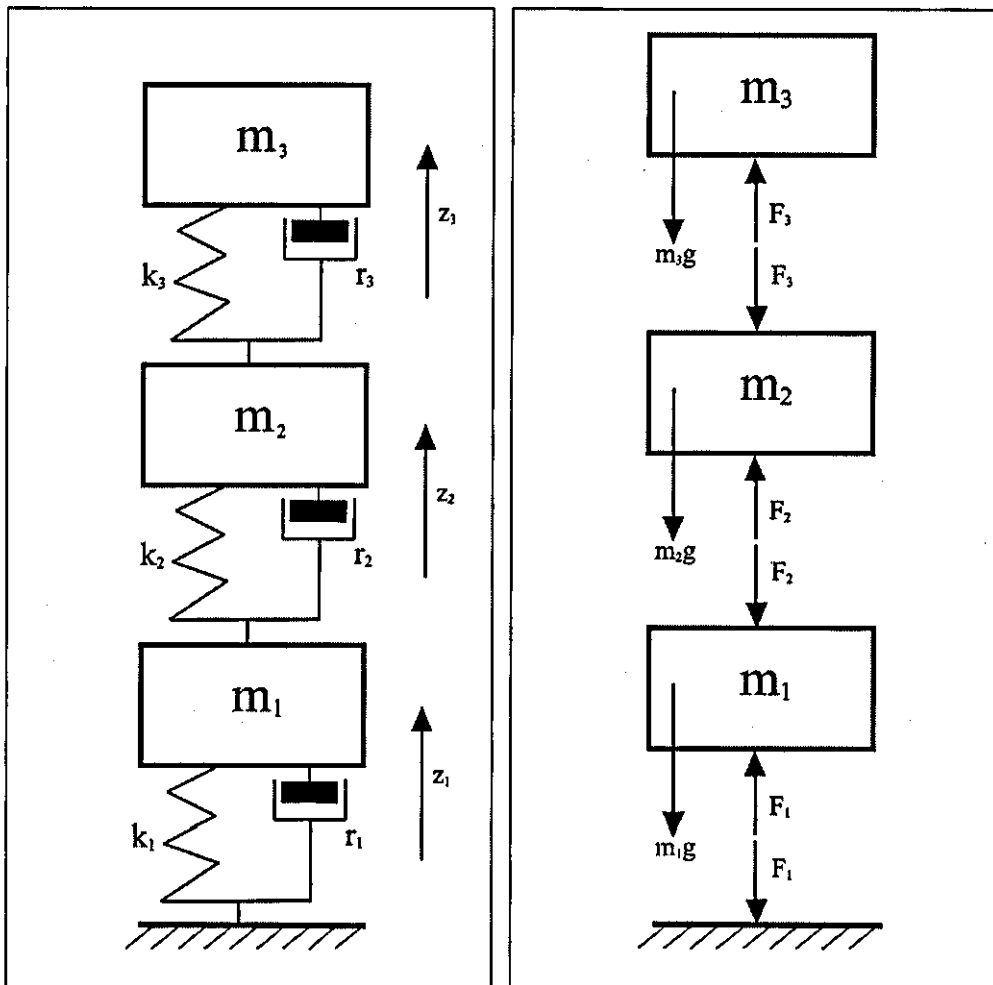


Figure 3.8 Structure of landing mat model four.

Again the spring stiffness and damping coefficients were optimised to minimise the RMS difference between the force-time histories of the simulation and the experimental trial 1541.

### 3.2.5 Landing Mat Model Five

This additional model was developed because integrating the MatLab mat model four with VN4D caused an increase in simulation time. This was identified as a potential problem as the introduction of a gymnast model would also slow the simulation time. The multi-layer approach developed in model four was recreated using VN4D (Figure 3.9). Since the software easily allows the creation of rigid bodies, the multi-layer landing mat incorporated the physical dimensions and the individual component layers of the sample landing mat. Spring-damper systems connected the layers together and defined how the layers interacted. The spring-damper systems that constrained the layer of the mat were modelled in a similar way to that in model four, the vertical behaviour of the landing mat was defined by the equations:

$$F_3 - m_3g = m_3(\ddot{z}_3 + \ddot{z}_2 + \ddot{z}_1)$$

$$F_2 - F_3 - m_2g = m_2(\ddot{z}_1 + \ddot{z}_2)$$

$$F_1 - F_2 - m_1g = m_1\ddot{z}_1$$

$$F_3 = k_3z_3 - r_3\dot{z}_3$$

$$F_2 = k_2z_2 - r_2\dot{z}_2$$

$$F_1 = k_1z_1 - r_1\dot{z}_1$$

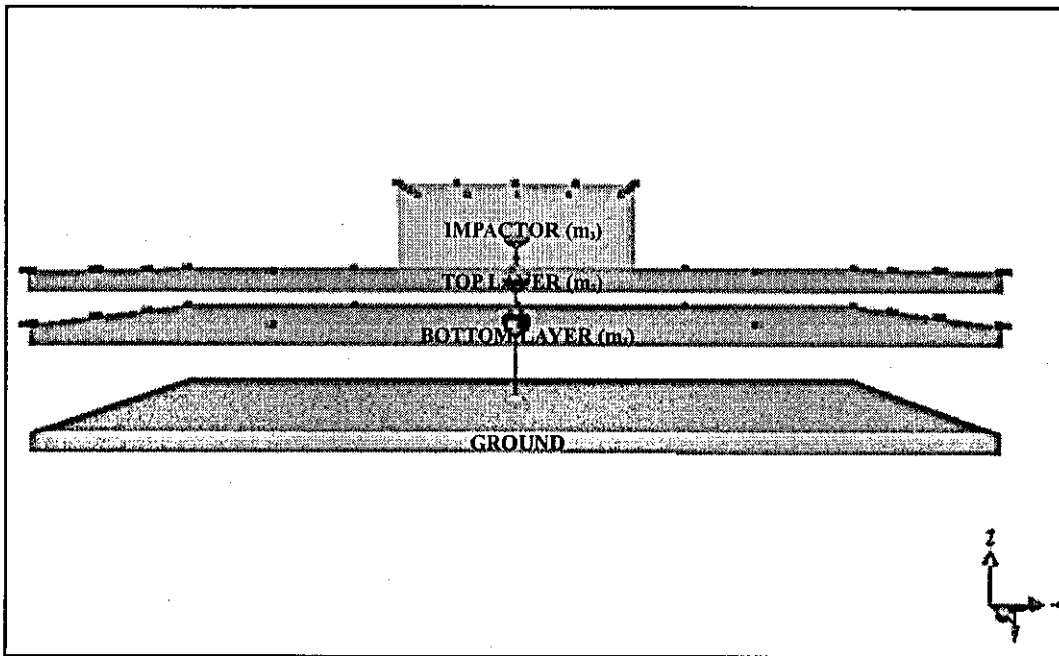


**Figure 3.9** Structure of landing mat model five using VN4D.

Again the spring stiffness and damping coefficients were optimised to minimise the RMS difference between the force time histories of the simulation and the experimental trial 1541.

### 3.2.6 Landing Mat Horizontal Model

Several different spring-damper equations were used to attempt to model the horizontal behaviour of the landing mat. These ranged from a linear system to the more complex non-linear system. The experimental data suggested a linear spring-damper would not be sufficient to model the horizontal behaviour of the mat since horizontal force did not increase linearly with horizontal mat deformation. Therefore horizontally the landing mat was constrained using a non-linear spring-damper system. The form of the equation was similar to the non-linear response seen in foot / heel pad responses to impact. One end was attached to the ground and the other was attached to a rigid body that was in turn attached to each layer of the mat via three rigid rods. Each rigid rod was allowed to pivot at its point of attachment therefore allowing the necessary vertical deformation of the mat as well as the horizontal deformation. The non-linear spring-damper system used to model the force of the mat was defined by the equation:

$$F = -k_1x^2 - k_2x^3 - k_3x^4 - r \dot{v}x$$

where  $x$  = horizontal spring displacement

The spring stiffness and damping coefficients were optimised to minimise the RMS difference between the force time histories of the simulation and the experimental trial 60lb.

### *3.3 Techniques Used to Collect Data On Landing Mats*

There are six common methods of testing landing surfaces. Firstly, there are drop tests in which the dropping mass falls into a test foot (containing force sensors) that lies on the surface of interest (Artificial Athlete Stuttgart). Secondly, the dropping mass has accelerometers attached to it and falls onto the surface of interest. Thirdly, the mass is dropped onto the surface and a force sensor (force plate) is located under the mat. Fourthly, stress-strain characteristics are measured using a mass and accelerometer dropped directly onto the surface of interest. Fifthly, subjects land on the surface of interest where force is measured underneath surface (force plate). Lastly, subjects perform typical movements on the surface and the deformation of the surface is quantified and force recorded (Nigg, 1990).

The majority of the research has used material tests. Within the Federation Internationale Gymnastique (F.I.G.) the landing mats are standardised according to the F.I.G. guidelines. A 20 kg spherical mass with diameter 10 cm is released from a height of approximately 0.8 m to achieve a velocity of 3.96 m/s at touchdown. Accelerometers are firmly attached to the impactor and are used to determine peak force, deformation and rebound height. All results must fall within F.I.G. guidelines for the mat to be used in competition.

Filming has been used to determine landing surface deformation through a secure film marker being firmly attached to the landing surface. The film marker was digitised during the impact to measure the surface deformation. Results showed that surface deformation could be accurately digitised to within 0.12 mm (Yeadon & Nigg, 1988).

Finite element modelling has been used by Lyn & Mills (2002) to model a landing surface: this approach requires a great deal of time to run one simulation and hence the most common approach is the multiple parallel spring-damper system

(Peikenkamp et al., 2002; Nigg & Liu, 1999; Nigg & Anton, 1995). However a single spring-damper system has been used by (Wilson et al., 2005; King et al., 1999; Nigg & Anton, 1995) to represent the foot-shoe-ground interface. This is a far simpler model of the foot-ground interface than the finite element model and requires less time to run one simulation and therefore could be incorporated into a larger model. A more complex model of a landing surface has used nine parallel spring dampers to represent the deformation characteristics of the surface (Fritz & Peikenkamp, 2003).

### 3.3.1 Image Based Motion Analysis

Video images are extremely useful for coaching, diagnostics or qualitative biomechanical analysis. In quantitative studies, measurements are made from sequential video images of the sport being analysed.

Moving from two-dimensional to three-dimensional analysis involves a significant increase in complexity to derive positional data. Three-dimensional analysis is now becoming the standard approach for image-based analysis (Yeadon & Challis, 1994). Three-dimensional analysis techniques require at least two video cameras: the points of interest should be visible in two or more simultaneously recorded images before they can be located in three-dimensional space. After the two cameras are set up to record the movement the cameras are calibrated, this transforms the two-dimensional digitised image coordinates into three-dimensional coordinates in the movement space.

The Phantom (v4) camera and software developed by Vision Research Inc. can record at 20 Hz to 1000 Hz at a pixel resolution of 512 x 512. The exposure time can be adjusted to correspond to the amount of light available. At a maximum frame rate of 1000 Hz the maximum exposure time is 990  $\mu$ s. This type of camera records images in volatile memory in the camera that can be downloaded after capture by the user to a computer.

### 3.3.2 Image and Force Synchronisation

The ability to locate a point in three dimensions generally requires that the image coordinates of that point are measured simultaneously from at least two camera views (Yeadon & Challis, 1994). Recording the same event simultaneously

with two cameras can be achieved by gen-locking the cameras. However this requires a physical connection between all the cameras being used and this is sometimes not feasible in the experimental environment. If the exposures made with two cameras are not simultaneous, synchronisation may be effected by interpolating the separately recorded data sets over the same time base (Yeadon & Challis, 1994).

A general method of synchronising that makes use of the direct linear transformation (DLT) reconstruction uses digitised data for all body landmarks to synchronise digitised data sets of a sporting movement. The mean (absolute) synchronisation error over the sports analysed was 0.0005 s (Yeadon & King (1999).

The Phantom (v4) high-speed cameras and software allow a digital trigger from a force plate (or other source) to be used to trigger the cameras and therefore synchronise the force plate with the cameras. The cameras can also be gen-locked to ensure each camera is synchronised with the others.

### 3.3.3 Two and Three-Dimensional Reconstruction

The common method of two-dimensional reconstruction is to define a plane, at right angles to the optical axis of the camera, in which horizontal and vertical references are provided. Once a common origin has been defined a simple transformation from image to object coordinates can be made (Bartlett, 1997). Dainty & Norman (1987) reported a scaling error of less than 0.5% if the procedure was followed correctly. However this procedure requires that the image plane is parallel to the object plane. This is sometimes difficult to achieve in competition situations and therefore a more complex technique of two-dimensional direct linear transformation (DLT) is used where the inclination of the image plane to the object plane is not restricted.

From two or more sets of image coordinates a method is required to reconstruct the three-dimensional movement space coordinates. Several algorithms can be used for this purpose and the choice of the algorithm may have procedural implications. The simplest algorithm requires two cameras to be aligned with their optical axes perpendicular to each other. The alignment of the cameras in this technique is difficult although the reconstruction equations are relatively simple. This camera set-up is also usually too restrictive for use in sports competitions (Bartlett, 1997).



The most common reconstruction technique used in sports biomechanics is the direct linear transformation, which permits arbitrary camera placement but requires that control points with known locations are distributed throughout the activity space. This is usually achieved using a calibration frame that contains a number of control points that fill or surround the volume within which the activity will take place (Yeadon & Challis, 1994).

Direct linear transformation involves transforming the image to movement space coordinates by camera / digitiser calibration involving 11 (or more) independently treated transformation parameters ( $C_1$ -  $C_{11}$ ) for each camera (Abel-Aziz & Karara, 1971). The simplest forms of the pair of transformation equations for each camera are:

$$C_1 + C_2X + C_3Y + C_4Z + C_5xX + C_6xY + C_7xZ + x = r_x$$

$$C_8 + C_9X + C_{10}Y + C_{11}Z + C_5yX + C_6yY + C_7yZ + y = r_y$$

The algorithm requires a minimum of six calibration points with known three dimensional coordinates  $X$ ,  $Y$ ,  $Z$  and measured image coordinates  $x$ ,  $y$  to establish the direct linear transformation parameters for each camera independently (12 equations for 11 unknowns). The direct linear transformation parameters incorporate the optical parameters of the camera. The direct linear transformation equations also contain residual error terms ( $r_x$ ,  $r_y$ ). Once the direct linear transformation parameters have been established for each camera, the unknown movement space coordinates ( $X$ ,  $Y$ ,  $Z$ ) of other points such as body landmarks, can then be reconstructed. The direct linear transformation parameters and the image coordinates ( $x$ ,  $y$ ) from both cameras are used with a least squares solution to determine the  $X$ ,  $Y$ ,  $Z$  coordinates.

Accurate coordinate reconstruction can only be guaranteed within the space spanned by the control points, which must, therefore fill the volume within which the movement takes place. Extrapolation outside of the volume increases the possibility of reconstruction errors. Small calibration structures necessitate for extrapolation outside the calibration volume. Also it is necessary that the control points are distributed evenly throughout the volume. If a dis-proportionally large number of points are clustered in a particular region, the corresponding direct linear

transformation parameters will produce an increased reconstruction accuracy in this region and poorer reconstruction elsewhere (Yeadon & Challis, 1994).

Dropping a ball and calculating the acceleration due to gravity from reconstructed vertical displacement data produced an error between 1% and 4% (Shapiro, 1978). Shapiro (1978) had used a calibration volume containing 48 control points. However only 20 were used to calculate the 11 parameters, the others were used to determine reconstruction accuracy. For a three-metre field of view the average reconstruction error was 5 mm.

The direct linear transformation approach to three-dimensional reconstruction allows flexible camera set-ups. Ensuring six or more control points distributed evenly throughout the entire movement space reduces any errors associated with extrapolation.

#### 3.3.4 Force Plate

The force platform is the most commonly used device to measure contact forces between a subject and the surroundings. Force-time data can be combined with video and inertia data to provide an analysis of a sporting movement. However force platforms alone only provide measurements of resultant whole body centre of mass external kinetics with no information on segmental dynamics. Newton's Third Law of Motion states that the reaction force has the same magnitude as, but is opposite in direction to, the force exerted by the subject on the platform.

The most common force studied is the ground reaction force (GRF). This 3D force vector is normally described by a vertical component and two horizontal components. The most commonly used force platforms have a relatively small contact area, for example, 600 mm by 400 mm (Kistler 9281B) but recently larger platforms have become available: for example, 600 mm by 1200 mm (AMTI). Four triaxial force transducers are located at the four corners of the force platform, the transducers are typically either piezoelectric cells (e.g. Kistler) or strain gauges (e.g. AMTI, Bertec) (Yeadon & Challis, 1994).

No matter which type of force sensor is used in the force plate construction, the force platform's mounting should be set in a concrete block that is mechanically isolated from the foundations in order to reduce extraneous vibration. Mounting angle is important as it affects the pre-stress on the transducers and the tension on the plate. Accurate and reliable force platform measurements depend on adequate

system sensitivity, a low force detection threshold, high linearity, low hysteresis, low-cross talk and the elimination of cable interference, electrical induction and temperature and humidity variations (Bartlett et al., 1997).

Force platforms have been used in many studies. The most common applications are walking and running (Nigg & Herzog, 1999). McNitt-Gray et al. (1993, 1994) used force platforms to collect GRF data from drop landings. Force platforms are often covered by a landing mat to establish the effects of the landing mat on the ground reaction forces (McNitt-Gray et al., 1993, 1994). However if the landing mat is larger than the force plate there is a risk that the mats could dissipate the impact force over a larger area than that detected by the force plate or that the mass of the mat is accelerated due to the impact. Ozguven & Berme (1988) used a six-component load transducer mounted beneath an 18 kg mass that had a ground contact surface area of approximately 175 cm<sup>2</sup> (to simulate the area under the feet). The mass was dropped onto regulation thickness landing matting from various heights. The impact forces developed by the weight were monitored simultaneously, above the matting by the load transducer and below the matting by the force platform. No detectable differences were observed between the two measurements. This implies that the landing mat was rigid and unable to dissipate any force during the impact which is not the case. If the landing mat dissipates little force outside the area of the force plate the impulse during the impacts should be similar for the sample mat and a larger mat. The peak forces above and below the mat may be the same, but a phase delay of the force time history of the impact would be expected in the transmission of force above the mat to below the mat.

### 3.3.5 Accelerometers

An accelerometer is a device that measures acceleration. Accelerometers are nothing more than force transducers designed to measure reaction forces associated with a given acceleration. Accelerometers normally consist of a mass attached to a fixed base, the acceleration of which is detected and measured by extension and compression of a distortion-sensitive element (Miller & Bartlett, 1997).

PCB<sup>tm</sup> sensors incorporate built-in, signal-conditioning electronics (Integrated Circuit – Piezoelectric (ICP)). The built-in electronics convert a high impedance charge signal that is generated by the piezoelectric sensing element into a usable low impedance voltage signal that can be transmitted over ordinary coaxial

cables to any voltage readout device. Accelerometers can be used in temperatures from  $-65^{\circ}\text{F}$  to  $+250^{\circ}\text{F}$ , depending on make and model (PCB Piezotronics Inc.). The range can vary greatly: examples include 500g and 10000g with resolution from 0.005g to 0.04g respectively.

The acceleration can be toward or away from the face of the transducer and this is indicated by a reversal in the sign of the signal. In most movements there is no guarantee that the acceleration vector will act at right angles to the face of the force transducer. Thus the transducer measures one component without knowing anything about any other component. However triaxial accelerometers can be used. These comprise three individual transducers mounted at right angles to each other and are therefore capable of three-dimensional data collection (Winter, 1990).

### 3.3.6 Filtering and Curve Fitting Techniques

Measurements made using an image-based motion analysis system are contaminated with noise generated during the recording and digitising process (Yeadon & Challis, 1994). The data consists of three parts: the true signal together with systematic and random noise. Sources of systematic noise include lens distortion, incorrect marker placement, errors in locating calibration objects and skin and marker movement (Yeadon & Challis, 1994). This noise needs to be reduced in order to reveal the true signal. However care must be taken to reduce the noise in the data without removing much of the true signal. It can be difficult to distinguish between noise and signal and a number of techniques can be used to help reduce noise: these include filtering and curve fitting techniques.

Low-pass digital filters are often used to remove noise from sampled data. To apply a digital filter the data must be sampled at equal intervals. The desired filter cut-off frequency must normally be specified (Challis et al., 1997). Digital filters can be categorised as recursive or non-recursive. The output of a recursive filter is determined from the weighted sums of past output values as well as past or present input values. The output of a non-recursive filter is determined only from the sum of weighted past and present input values. The most commonly used recursive low-pass filter is the Butterworth filter. Recursion introduces phase lag. To cancel this, recursive filters are normally applied in forward and then reverse directions (Challis et al., 1997).

There are several ways to choose the best cut-off frequency. The first is to carry out a harmonic analysis. By analysing the power in each of the components a decision can be made as to how much power to accept and how much to reject. However a better method is to do a residual analysis of the difference between filtered and unfiltered signals over a wide range of cut-off frequencies (Winter, 1990). Examination of the transition region helps to determine the best cut-off frequency. The compromise is always a balance between the amount of signal distortion versus the amount of noise allowed through.

Using a curve fitting technique assumes that the trajectory signal has a predetermined shape and that by fitting the assumed shape to a 'best fit' with the raw data, a smooth signal will result (Winter, 1990). Fourier series truncation replaces the familiar representation of displacement as a function of time by a series of sinusoidal waves of different frequencies. The data are then filtered to remove high frequency noise. This is done by reconstituting the data up to a chosen cut-off frequency and truncating the series beyond this frequency.

Many techniques used for the smoothing and differentiation of data in sports biomechanics involves the use of spline functions (Challis et al., 1997). These are a series of polynomial curves through multiple points joined together at points called knots. The smoothing technique, which is performed in the time domain, can be considered to be the numerical equivalent of drawing a smooth curve near the data points. Challis & Kerwin (1987) reported that splines are a particular technique suited to the removal of noise from film-derived data. It was found that the quintic spline technique was superior to the truncated Fourier series and Butterworth filter techniques. The Butterworth filter does not produce good results due to the use of the central difference differentiating formula as this technique amplifies any noise remaining in the signal. Subsequent investigation by Challis (1999) has found that the Butterworth 2<sup>nd</sup> order filtering technique can perform very similarly to the quintic spline technique for the removal of noise in biomechanical data.

Baker (1994) used data from digitisation of a cine film sequence of a flic flac and direct measurement with a force plate to evaluate different smoothing techniques. The selected smoothing techniques were Smith's (1975) manual method, the Hanning method and the Butterworth 2<sup>nd</sup> order digital filter. The conclusion was that the Butterworth 2<sup>nd</sup> order digital filter produced the closest approximation to the criterion curve.

A poor choice of smoothing parameter may corrupt data, treating vibrations as noise may lead to errors. Consideration (when selecting a filtering technique) must be given to the nature of the technique used, as well as the degree of smoothing selected (Yeadon & Challis, 1994).

An overlap of true signal and noise means a poor choice in cut-off frequency can result in some noise being retained or some of the true signal being rejected. The cut-off frequency should be chosen to include the highest frequency of interest in the movement. It is recommended that a technique should be used that involves a justifiable procedure taking into account the peculiarities of each new data set. Using previously published filter cut-off frequencies or manual adjustments of the smoothing parameter is not recommended (Bartlett, 1997).

Elastic surfaces on force plates during impacts introduce a 'rippling effect' between the force plate and the elastic surface. This is a surface interaction and does not represent the dynamic response of the whole mat. This effect introduced 20 Hz or higher oscillations into the force data; therefore a low pass filter is required to minimise the noise in the system (Fritz & Peikenkamp, 2003).

### *3.4 Gymnastic Landing Mat Data Collection*

The aim of the landing mat testing was to determine the material properties of the mat so that the mat can be modelled in a computer simulation of an impact.

#### *3.4.1 The Equipment*

The main pieces of equipment used were:

1. Two high-speed cameras
2. Two accelerometers
3. A force plate
4. The impactor
5. The sample landing mat

1. Two Phantom (v4) high-speed video cameras (Vision Research Inc.) were used to record the impact testing. The camera capture rates were both set at 1000 Hz, allowing one second of recording time. The post trigger setting was 763 ms and the exposure time was set to 594  $\mu$ s and two additional lights were used. The left camera

was placed at a height of 2.07m and at a horizontal distance of 3.32m from the centre line of the mat at an angle of  $31.1^\circ$  to the A-P centre line of the force plate. The right camera was placed at a height of 2.12m and at a horizontal distance of 3.48m from the centre line of the mat at an angle of  $47.7^\circ$  to the centre line of the force plate (Figure 3.10).

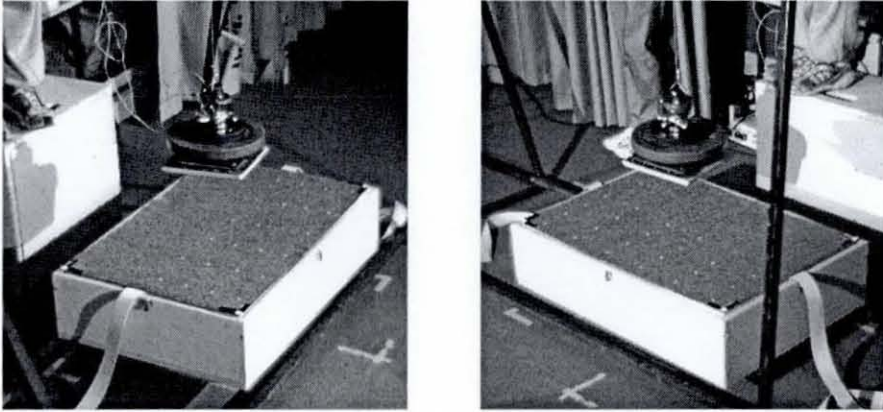


**Figure 3.10** Field of view (left camera and right camera).

#### 3.4.2 High-Speed Camera Calibration Procedure

The cameras recorded the calibration poles, (Figure 3.11) the dimensions of which are shown in Figure 3.12 with a measurement accuracy of 0.5 mm. These dimensions were used later in order to determine the camera DLT parameters and reconstruct the marker positions.

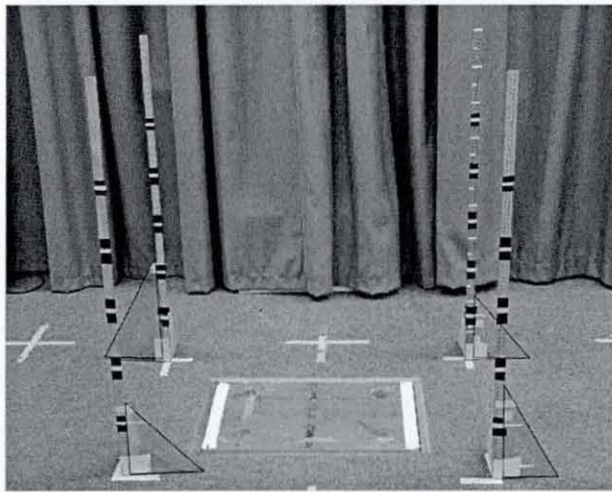


**Figure 3.11** The calibration poles.

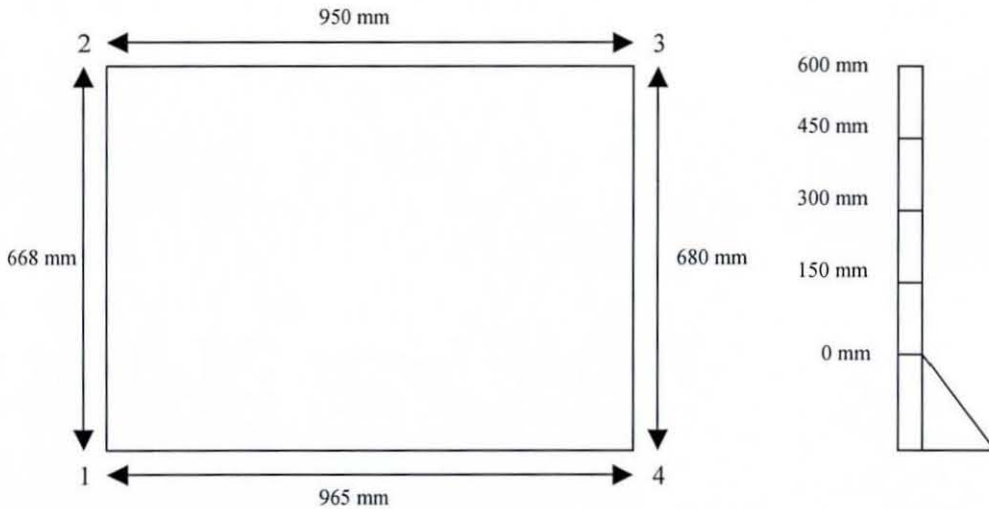


**Figure 3.12** Dimensions of the calibration poles.

2. Two accelerometers (PCB Piezotronics) were firmly attached to the impactor. One accelerometer was aligned vertically (Model 353B18) and the other was aligned perpendicular to the first (Model 350B08). The sampling frequency was set to 1000 Hz.

3. A Kistler (90281B) force plate (600 mm by 400 mm) sampling at 1000 Hz was located under the metal spacer holding the mat's wooden frame. The force plate was set to trigger on a level of 25 N with a 10% pre-trigger and a collection time of five seconds. When the force plate was triggered a signal was sent to the cameras and accelerometers.

4. A custom-built impactor of mass 24 kg and contact area 0.25 m by 0.25 m was used to represent the effective mass and surface contact area of the gymnast during impact (Figure 3.13).

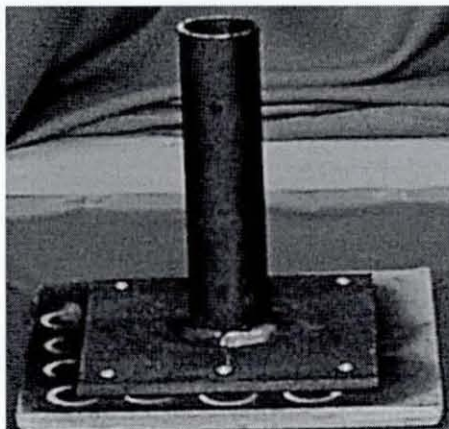


**Figure 3.13** Custom built impactor – no added mass.



The impactor contact area was determined via the analysis of anthropometric data collected on six elite male gymnasts. The average length of the six gymnast's feet (posterior calcaneus to toe nails) was used to determine the length of the impactor's contact surface. The average length was 227.7 mm. The width calculation was based upon the idea that the feet should land in line with the hip joints to ensure minimal risk of injury as minimal moments are produced except in the sagittal plane where the joints are designed to take the loading. It was assumed that the ankle joint should line up vertically with the hip joint. The average distance between hip joint centres of the six gymnasts was added to two times half the width of a foot. This calculation gave a total width of 252.7 mm. Qualitative analysis of vault landing revealed that the area of the landing mat between the feet also deformed to the depth of the feet. Therefore the flat impactor's contact area was built to be similar to that of the contact area of the gymnast's feet.

5. The sample-landing mat (Figure 3.14) construction was based on an official F.I.G. competition-landing mat and was custom-built by the manufacturer 'Continental Sports Ltd.' for the purpose of this experiment. The mat had mass 6.1 kg, measured 0.90 m long by 0.60 m wide by 0.20 m deep and was surrounded by a custom-built wooden frame, which was designed to constrain the landing mat so that it behaved more like a full size landing mat. Restraining the mat horizontally also prevented any slipping of the mat on the force plate. The sample landing mat was designed to be the size of the landing mat that was to be used during actual vault landings (the size of the gymnastics centre force plate). The wooden frame was bolted to a metal spacer that was in turn bolted to the force plate to ensure all forces were transferred directly to the force plate during the impact. To assess the area deformation of the mat, the mat's surface was covered by 28 (5 mm diameter) markers arranged in four rows of six with an additional four markers located at the corners of the mat (Figure 3.14 & 3.15). When the impactor landed in the centre of the landing mat the mat's deformation behaviour was assumed to be symmetrical therefore only half the mat's surface had markers.

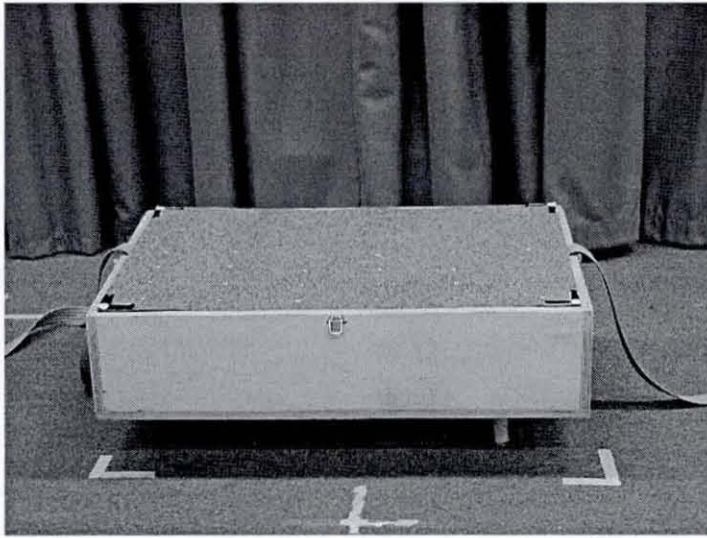


**Figure 3.14** The landing mat set-up.

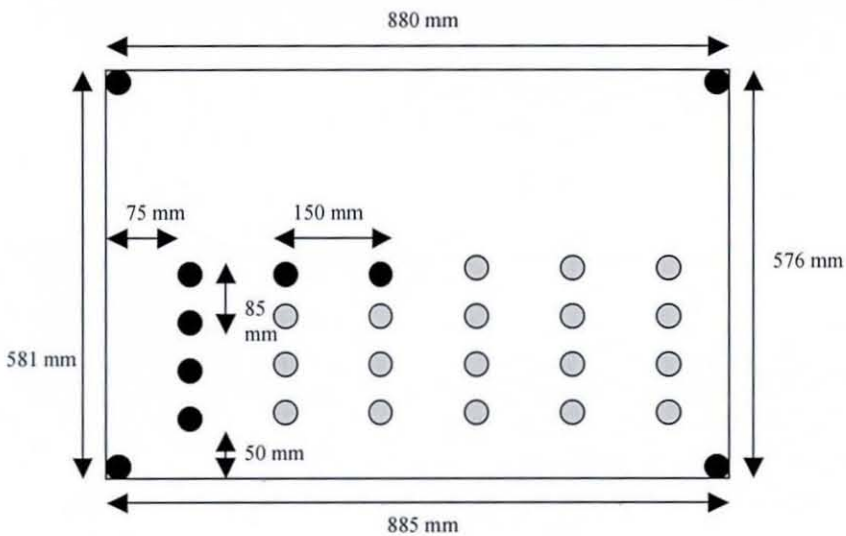


**Figure 3.15** The landing mat marker locations (not to scale).

It may have been useful to have a larger sample mat as the width of the impactor and the width of the mat may cause the deformation region of the mat to reach the edges of the mat. However the sample landing mat size was equivalent to the landing mat size used to cover the plate in the vault testing area.

### 3.4.3 Determination of a Gymnast's 'Effective Mass'

A male gymnast (mass 72 kg) performed a competition style landing (minimal deductions as scored by F.I.G.) onto the sample-landing mat from a height of approximately 1.56 m. (5.5 m/s vertical impact velocity). The gymnast landed with feet approximately hip width apart (legs vertical). The entire surface of the

landing mat was seen to deform during the impact. During this trial the peak force was 5638 N and the time to peak was 0.0417s. The vertical GRF time trace was used to determine the impactor mass.

To determine an 'effective mass' of a gymnast the custom built impactor was loaded with additional mass and dropped from the same height as the subject test. In order to correctly select the appropriate mass of the impactor, key characteristics of the subject impact were compared to those of the impactor tests. During the subject test the subject's upper body was actively becoming involved at 0.03 s during landing (from the high-speed video). After this point the force and acceleration characteristics were not of interest as lower accelerations were present indicating that the subject was controlling the impact and also indicating the end of the passive landing phase. The mass of the impactor increased with each test until the impulse, vertical force and rate of force production for the impactor matched the subject test. The effective mass of the gymnast determined in this way was 24 kg. This impactor mass was used for the material mat testing.

#### 3.4.4 Impact Testing

The impact testing had three main aims.

1. To assess the deformation characteristics of the landing mat during impacts at different velocities.
2. To assess the amount of mat mass accelerated during an impact.
3. To determine the material properties of the mat that could be used as an initial estimate in a computer model of the impact.

Vertical impact testing consisted of the impactor being released vertically from five different heights corresponding to impact velocities between 4.3 m/s and 6.5 m/s (Figure 3.16). Two trials at each height were recorded.

Oblique impact testing used the same equipment as the vertical testing but was adapted for the oblique trials. No accelerometers were used, as they would have easily been damaged. The custom-built drop rig was also designed to drop the impactor at a pre-set angle and velocity (Figure 3.16). The impactor (I) slid down the angled guide rail (G) and impacted with the landing mat at the bottom.

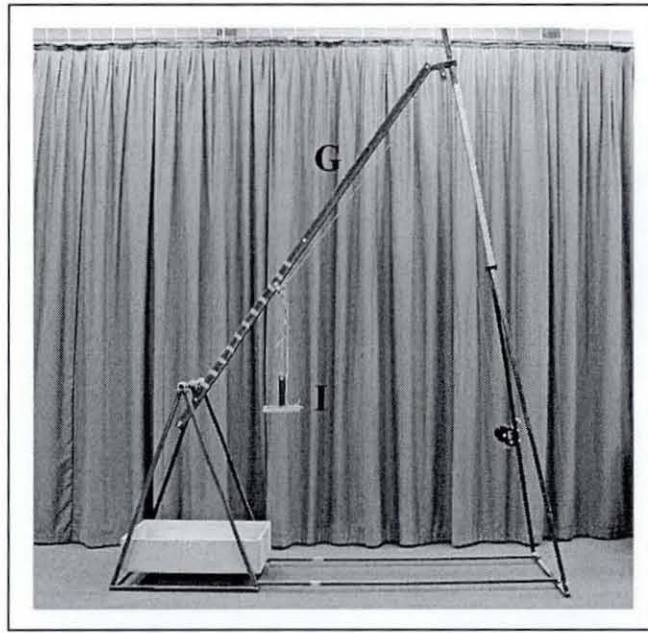


**Figure 3.16** The custom-built drop rig.

A total of five angles (between  $46^\circ$  and  $71^\circ$ ) with two different drop heights at each angle were recorded. Pre-setting the guide rail angle for a particular impact angle provided insufficient control due to the pendulum motion of the impactor as it slid down the guide rail. Only impacts that landed flat were used for further analysis. Visual inspection of the high-speed film allowed a trial to be selected or rejected.

### 3.4.5 Image Reconstruction and Analysis

All markers on the landing mat were digitised manually to obtain displacement data. Two additional markers on the impactor were also digitised manually to determine the impact velocity for each trial and maximum vertical displacement of the impactor. The KineMat DLT reconstruction MatLab program file was used to reconstruct the three-dimensional coordinates of the markers throughout the impact tests (Reinschmitt & Van den Bogert, 1997). Prior to the impact trials the calibration structure comprising 20 markers that spanned the volume of the mat was video recorded and digitised. Ten calibration points were used to determine the 11 DLT parameters and the remaining 10 points were reconstructed to within 1 mm of their measured locations in all axes.

### 3.5 Vertical Testing Results

The following sub-sections report and discuss the results of the vertical drop testing.

#### 3.5.1 Determining the Impact Velocity

The two points on the impactor were digitised from approximately 50 ms prior to impact to 150 ms after impact. Positional data were low pass filtered then differentiated to determine the impactor's velocity prior to contact and throughout the contact phase.

##### Method 1

Visual inspection of the velocity graph (looking at last few frames prior to touchdown) showed the velocity of the two points on the impactor throughout the pre-impact and impact phase of the drop test. The positional data was filtered using a low pass Butterworth 2<sup>nd</sup> order filter (filtering both forwards and backwards) at a frequency of 20 Hz with a padding in the filter to reduce end-point problems. Filtering impacts can reduce the high frequency components that are necessary to describe them fully. This means careful attention must be made to the cut off frequency chosen. The Butterworth filter proved adequate at estimating the impact velocity as Figure 3.17 shows a downward gradient around  $10 \text{ ms}^{-2}$  and the results of the quadratic fit to the data (Method 3) also produces a comparable impact velocity. This suggests that any loss in velocity due to the filter at impact was less than 0.1 m/s. The cut off frequency was selected via a residual analysis that showed a cut off frequency between 18 Hz and 24 Hz was appropriate for the data. 20 Hz was chosen as this also represented the cut off frequency used for the force plate data. This allowed the force and video data to be compared once the effect of filtering on the peak values were adjusted for. Time of impact was approximately one quarter of the way through the data and any endpoint problems should have effected the result. The data were then differentiated to determine velocity. Filtering at a higher frequency (60 Hz) did not greatly alter the impact velocity (less than 0.05 m/s). The example trial (Figure 3.17) used for this was 2151 and the impact velocity was 6.5 m/s. Impact occurred at 42 ms.

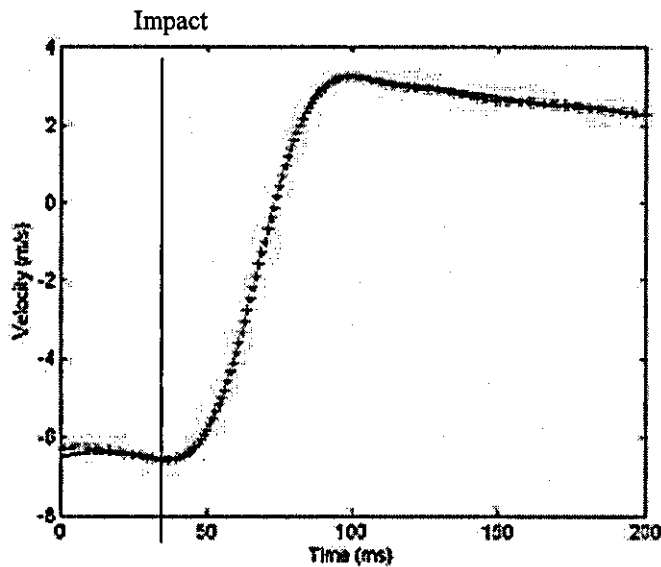


Figure 3.17 Vertical velocity of the two points on the impactor (trial 2151).

#### Method 2

This involved using the constant acceleration equations and determining the initial velocity via visual inspection of the velocity graph (point 1 on the impactor). Initial velocity was 6.05 m/s and the change in start position to that of the frame prior to impact was  $(0.7 - 0.44 = 0.26 \text{ m})$ .

Using the equation ( $V = \text{impact velocity}$ ,  $U = \text{initial velocity}$ ,  $s = \text{displacement}$ )

$$\begin{aligned} V^2 &= U^2 + 2as \\ &= (6.05)^2 + 2 \times 9.81 \times 0.26 \\ &= 36.6025 + 19.62 \times 0.26 \\ &= 41.7037 \end{aligned}$$

$$V = 6.46 \text{ m/s}$$

#### Method 3

A quadratic was also used to fit to the data (assumes that impactor is in free fall). Using point 1 on the impactor and frames 1 to 42 (impact at 42 ms) the quadratic equation was:

$$Y = -1 \times 10^{-6} x^2 - 0.0063x + 0.7089$$

with an  $R^2$  value of 0.9999

( $x = \text{time in seconds}$ )

The quadratic was differentiated to obtain velocity.

$$\dot{Y} = (2x - 1 * 10^{-6}) - 0.0063$$

$x = 42$  s at impact so replacing  $x$  in the above equation with 42 produces an impact velocity of 6.4 m/s.

The same method was applied to point 2 on the impactor.

The quadratic was:

$$Y = -5 * 10^{-6} x^2 - 0.0062x + 0.6177$$

with an  $R^2$  value of 0.9999

The quadratic was differentiated to obtain velocity.

$$\dot{Y} = (2x - 5 * 10^{-6}) - 0.0062$$

$x = 42$  seconds at impact so replacing  $x$  in the above equation with 42 produces an impact velocity of 6.6 m/s.

Results from all methods produce a similar result therefore method 1 was used to obtain the impact velocities of the remaining trials (Table 3.1).

**Table 3.1** Vertical Impact Velocities

<b>Trial Number</b>	<b>Vertical impact velocity (m/s)</b>
1031	4.30
1272	4.80
1541	5.25
1841	5.75
2151	6.50

Only the selected trials reported in Table 3.1 were used for further analysis. Other trials not included in Table 3.1 were disregarded on the grounds of either a problem with the dropping mechanism during testing or a non-flat landing by the impactor, or the impactor landing off centre of the landing mat.

### 3.5.2 Ground Reaction Forces During Impact

Vertical ground reaction force was recorded via the force plate under the mat. Results showed the characteristic double peak (Figure 3.18).

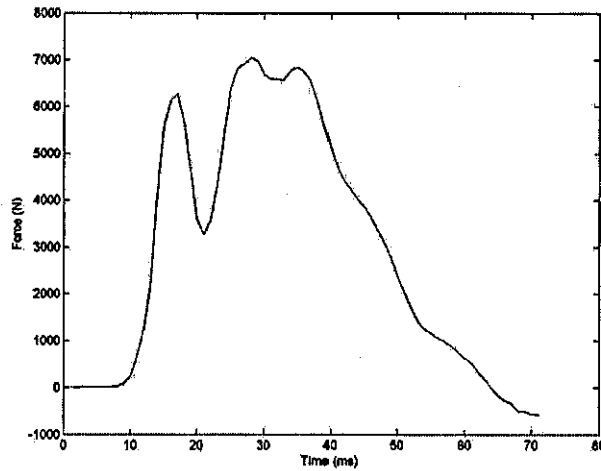


Figure 3.18 Vertical force from force plate during trial 1541 (trigger at 7 ms).

This double peak during the first 10 to 30 ms was too quick for any bouncing of the whole mat or impactor to occur and this was supported by the high-speed video. The double peak may also be caused by the impactor landing unevenly however the high-speed video has shown that this was not the case. The most likely reason for the double peak was the shock wave moving ahead of the upper layer mass. The top layer ( $m_2$ ) initially compressed sending a compression wave through the mat compressing the bottom layer ( $m_1$ ) causing the first impact peak. Then  $m_1$  can rebound slightly as the force above it is low. Next the top layer compresses producing a high force on the top of  $m_1$  causing the bottom layer to compress further (Figure 3.19). Table 3.2 shows the peak forces associated with each trial.

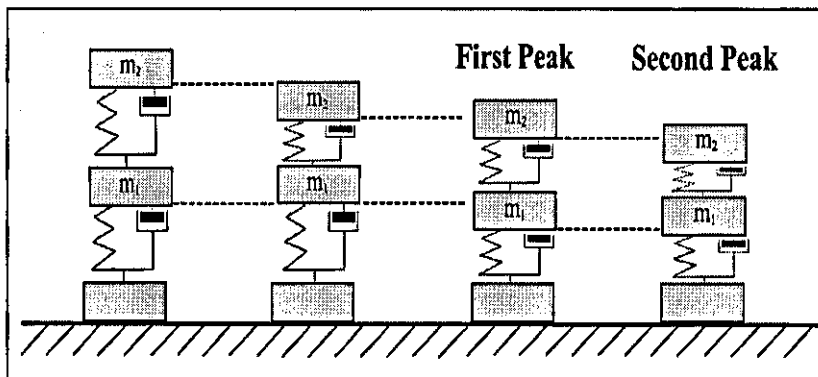


Figure 3.19 Compression of mat layers to produce ground reaction force.



**Table 3.2 Peak Vertical Force During Impact**

Trial Number	Peak Vertical Force (N)	Time to Peak (s)
1031	5593	0.018
1272	6341	0.019
1541	7054	0.020
1841	8398	0.021
2151	9597	0.019

### 3.5.3 Compression Wave Propagation Times

Further investigation of the high-speed video recordings revealed that the impactor contacted the surface of the mat prior to the force plate being triggered (Figure 3.20).

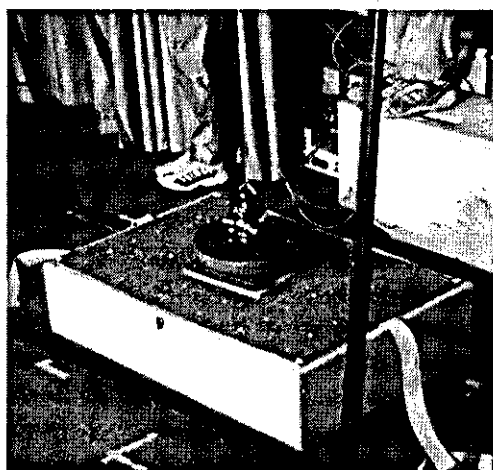


**Figure 3.20** 5 ms prior to force plate trigger in trial 1541.

This suggests that time is required for the compression wave to propagate through the mat to the force plate during impact. This was confirmed by striking the wooden box. Results showed no time delay between striking the box and the force detected via the force plate. Therefore any time delay was due to the landing mat.

Results from the accelerometers also support a time delay for the compression wave to propagate through the mat (Figure 3.21).

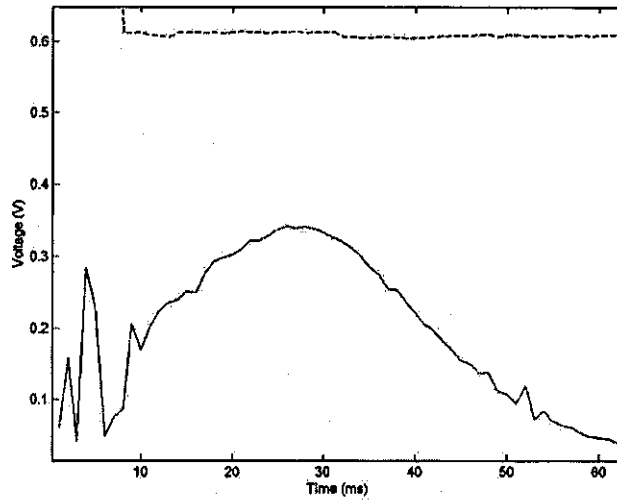


**Figure 3.21** Accelerometer data for trial 1541 (dashed line = trigger, solid line = accelerometer output).

The vertical accelerometer had detected changes in acceleration prior to the trigger signal being sent by the force plate. This time difference corresponded to 7 ms (Figure 3.21). The high-speed video recording indicated that this value was lower (5 ms). However, shock transmission times are a little harder to determine from high-speed video due to the difficulty in determining initial mat contact in a single frame but the shock transmission times were within 4 ms of the times determined from the accelerometer and force plate. The accelerometer data will be used to identify the time delay during impact (Table 3.3).

**Table 3.3** Impact Detection Times from Accelerometer and Video in ms. (Force plate trigger = time zero)

Trial	Impact detection time (ms)	
	Accelerometer	Video
1031	-7	-4
1272	-8	-4
1541	-7	-5
1841	-7	-5
2151	-8	-6

This transmission time is important when attempting to compare force and accelerometer data as the loading at the surface of the mat at time  $t$  has not propagated to the bottom of the mat until time  $t+\Delta t$ . During the initial impact large forces can be produced at the surface of the mat and within the mat but not be registered at the force plate.

### 3.5.4 Vertical Mat Deformation

Results from point 1 on the impactor showed that the maximum vertical deformation of the mat was 0.107 m in trial 1541. Figure 3.22 shows that from 43 ms (initial impact with mat) until time of maximum deformation (71 ms) the total deformation was 0.107 m and Table 3.4 shows the amount of mat deformation for each trial.

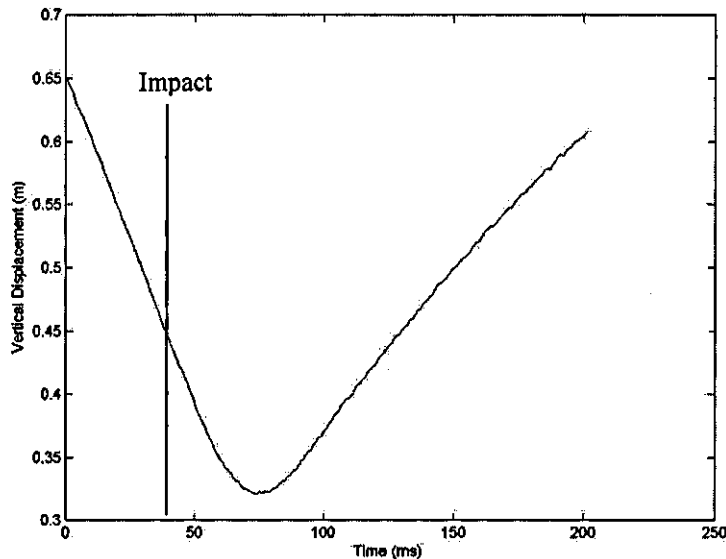


**Figure 3.22** Vertical displacement of the impactor prior to and during contact with the mat in trial 1541, the vertical line on the graph corresponds to 7 ms prior to force plate trigger (initial mat contact).

**Table 3.4** Maximum Vertical Mat Deformation

Trial Number	Vertical Deformation (m)
1031	0.092
1272	0.108
1541	0.107
1841	0.115
2151	0.127

### 3.5.5 Landing Mat Area Deformation

The 28 markers on the mat's surface were digitised over 200 frames for all trials. The data were reconstructed to provide the three-dimensional coordinates of each point. The area of deformation (trial 1541) of the mat at maximum vertical displacement is shown in Figure 3.23. It should be noted that the whole of the surface of the mat is deformed at maximum vertical mat deformation during all trials.

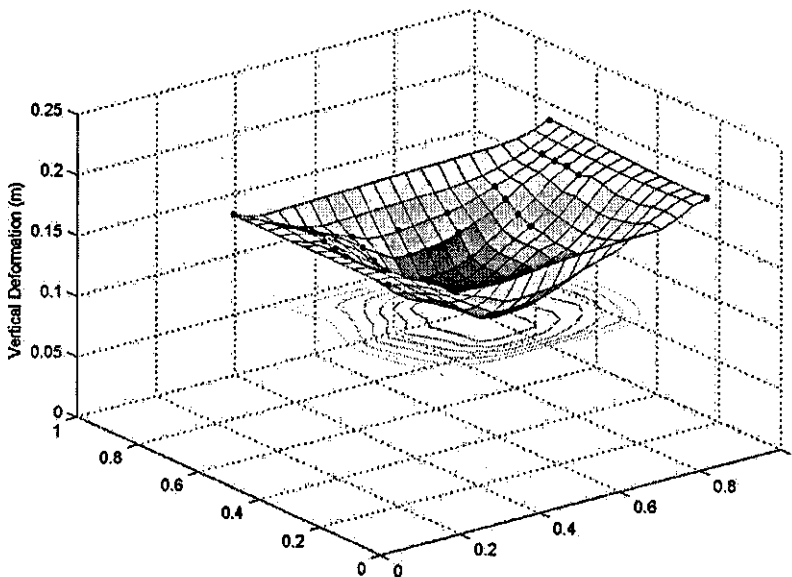


**Figure 3.23** The surface of the mat during maximum vertical mat deformation during trial 1541 assuming deformation symmetry over the entire mat's surface. (Dots represent approximate location of actual mat markers).

The volume of the mat deformed by the impact can be estimated using two methods. The mat's deformation volume (Method 1) was estimated at maximum mat

deformation by assuming that a rectangular prism the length of the impactor and width of the mat depressed the mat to its maximum deformation. Either side of the rectangular prism two triangular prisms represented the deformation volume from the rectangular prism to the edge of the mat (Figure 3.24a).

$$V = L_I W D + 0.5(L_M - L_I) W D$$

where:

V = volume estimate

$L_I$  = impactor length / width (0.25m)

W = mat width (0.60m)

D = vertical depression

$L_M$  = mat length (0.90m)

The mat's deformation volume was also estimated (Method 2) at maximum mat deformation by assuming that a cuboid the length and width of the impactor depressed the mat to its maximum deformation. Surrounding the impactor four triangular prisms represented the deformation volume from the cuboid to the edge of the mat (Figure 3.24b). The total mat volume was 0.102 m<sup>3</sup>. Both methods are used to estimate deformation volume and the results for all trials are shown in Table 3.5.

$$V = 8/3bcD + 2L_I bD + L_I^2 D$$

where:

$b = (L_M - L_I)/2$

$c = (W - L_I)/2$

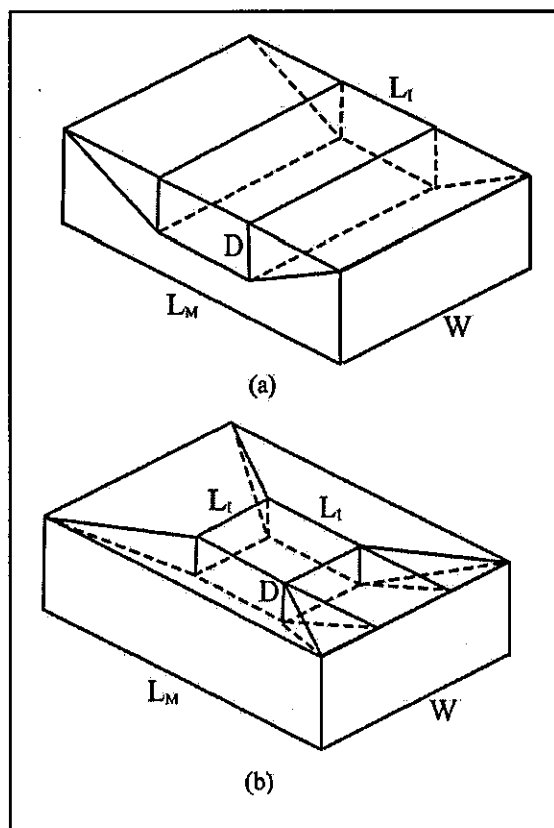


**Figure 3.24** Estimates of mat deformation volume using two methods of calculation: (a) Method 1, (b) Method 2.

**Table 3.5** Estimate of Mat Volume at Maximum Deformation

Trial Number	Volume Estimate (m <sup>3</sup> ) (Method 1)	Volume Estimate (m <sup>3</sup> ) (Method 2)
1031	0.030	0.033
1272	0.034	0.037
1541	0.034	0.038
1841	0.038	0.043
2151	0.040	0.044

Method 1 maybe a more accurate method of accessing the deformation volume of the sample mat as in some trials the mat appeared to 'fold' during deformation. However it is thought that Method 2 maybe more suitable when attempting to estimate the deformation volume of larger landing mats as the deformation area is unlikely to reach the sides of the mat and hence the mat will not 'fold'.

### 3.5.6 The Mat's Effective Mass During Impact

The effective mass represents the mass that would have to be accelerating at the measured acceleration to give the measured force. In the limiting case of a translating rigid body the effective mass and the real mass are equivalent, as the acceleration measured at any point equals the acceleration of the centre of mass. For a uniform body undergoing uniform compression the effective mass would equal half the real mass of the body, as the centre of mass acceleration is half the top surface acceleration. The landing mat is neither a uniform body nor does it undergo uniform compression when it deforms. Until the shock transmission includes all of the mat volume the effective mass can change. After this the effective mass should remain constant.

Video data were used to calculate the effective mass. The area of deformation of the mat, the mass of the mat layers and the shape of the deformation were used. These calculations accounted for the fact that the acceleration at the surface was not uniform and was only measured at the point of impact. Two different assumptions of how the different density layers of the mat deformed were employed with the measurements for volume calculation Method 1. Assuming that both layers compressed equally gave equation 3.1 while assuming that the top layer remained uncompressed and compressed the softer layer below gave equation 3.3. These simplify leading to expressions for the effective mass (equations 3.2 and 3.4). In both cases the mat surface immediately below the impactor was accelerating at the same rate as the impactor and the average acceleration of the mat surface making up a triangular prism was assumed to be half that of the impactor.

$$ma = A_c M(a/2) + A_s M(a/4) \quad (3.1)$$

giving  $m = (A_c/2 + A_s/4)M \quad (3.2)$

$$ma = A_c M_u a + A_s M_u (a/2) + A_c M_b (a/2) + A_s M_b (a/4) \quad (3.3)$$

giving  $m = (A_c + A_s/2)M_u + (A_c/2 + A_s/4)M_b \quad (3.4)$

where

$A_c$  = area of rectangular prism as a percentage of mat area

$A_s$  = area of triangular prism as a percentage of mat area

$M$  = total mat mass

$M_u$  = mass of upper dense layer of mat

$M_b$  = mass of bottom soft layer of mat

$a$  = acceleration measured at impactor

The force at the top of the mat was estimated using the acceleration from the video and the impactor mass. The effective mass of the mat estimated using video combined with the video acceleration produced an estimate of the force due to the acceleration of mat mass. These two forces added gave an estimate of the force beneath the landing mat and could be compared to that recorded via the force plate.

$$R_2 - M_i g = M_i a \quad (3.5)$$

$$R_1 - (M_i + m)g = (M_i + m)a \quad (3.6)$$

where

$M_i$  = mass of the impactor

$g$  = acceleration due to gravity

$a$  = acceleration of mat's surface

$m$  = effective mass of mat

$R_1$  = force at bottom of mat

$R_2$  = force at top of mat

The peak filtered accelerations from the accelerometer and video were similar. The difference between the two accelerations ranged from 2 to 11  $\text{ms}^{-2}$  (Table 3.6). The accelerometer data proves that the acceleration determined from video data was accurate. This accuracy was essential if this methodology was to be used in a competition environment where only video could be used to determine the landing mat's behaviour during impacts.



**Table 3.6** Filtered Peak Acceleration Data

<b>Trial Number</b>	<b>Accelerometer (ms<sup>-2</sup>)</b>	<b>Video (ms<sup>-2</sup>)</b>
1031	192	185
1272	226	224
1541	241	238
1841	280	274
2151	289	300

The effect of filtering on the effective mass calculation is shown in Table 3.7. The average percentage drop in peak force from unfiltered to filtered data was 14.5%. The average percentage drop in peak acceleration from unfiltered to filtered data was 11.7%. The difference in percentage drop between the force and acceleration data was corrected for when determining effective mass (Table 3.7).

**Table 3.7** Effective Mass of Mat at Peak Deformation Calculated Using Four Methods

<b>Trial</b>	<b>Filtered (kg)</b>		<b>Corrected (kg)</b>		<b>Unfiltered (kg) Acc</b>
	<b>Acc</b>	<b>Video</b>	<b>Acc</b>	<b>Video</b>	
1031	2.0	3.0	2.7	3.7	2.9
1272	1.6	1.8	2.3	2.5	2.0
1541	2.0	2.3	2.7	3.0	2.7
1841	1.6	2.1	2.3	2.8	3.4
2151	3.4	2.4	4.1	3.1	2.8
<b>Mean</b>	2.1	2.3	2.8	3.0	2.8

The effective mass from video data calculated with equal compression between layers (equation 3.2) was 2.0 kg. For unequal compression (equation 3.4) the effective mass was 2.8 kg. Half the mat mass was 3.05 kg. Using the peak acceleration from the video and these effective masses the forces beneath the landing mat for the five trials were calculated and were compared to the force plate peak forces (Table 3.8).

**Table 3.8** Percentage Difference Between Calculated Peak Forces and Actual Peak Forces

Trial	2.0 kg effective mat mass	2.8 kg effective mat mass	3.05 kg effective mat mass
1031	- 4.0%	-1.1 %	+ 0.1%
1272	- 0.5%	+ 3.7%	+ 4.8%
1541	- 1.3%	+ 1.6%	+ 2.8%
1841	- 0.7%	+ 2.3%	+ 3.5%
2151	- 1.6%	+ 1.3%	+ 2.6%

For the 2.0 kg effective mass, peak vertical ground reaction force was underestimated within a  $-0.5\%$  to  $-4.0\%$  range. The 2.8 kg forces were within a  $-1.1\%$  to  $+3.7\%$  range. For the 3.05 kg effective mass, peak vertical ground reaction forces were overestimated within a  $+0.1\%$  to  $+4.8\%$  range.

The effective mass of the mat was required to calculate the difference in force at the top and bottom of the mat. The effective mass of the mat being accelerated produced a force that ranged from 480 N to 930 N and this cannot be ignored as it accounted for up to 12% of the peak force in the trials.

The high-speed video peak acceleration was on average within 2.5% of the accelerometer peak acceleration. High-speed video can also be used to describe the mat deformation. In this experiment the complex mat deformation may be characterised as a 3D rectangular depression near the mat centre with a triangular prism on either side (Method 1). Method 2 resulted in greater estimates of deformation volume than Method 1. It is likely that with a larger mat a more symmetrical deformation pattern will be present and therefore Method 2 may be more appropriate for determining deformation volume for a full size landing mat. In this case the effective mass calculations should use the deformation area and relative accelerations for the deformation described by Method 2.

Determining the effective mass from video data relied on assumptions and approximations. Despite this, using equation 3.1 along with the deformation as described in Method 1, gave an effective mass of 2.8 kg. This compares well with values for the effective mass calculated from force and acceleration measurements from Table 3.7 and indicates that the video method could determine a reasonable

effective mass. These calculated mass values have only been reported to one decimal place and it is unlikely that the different effective mass methods truly give an identical result. Nonetheless, using the effective mass and the acceleration obtained by double differentiating positional data, the peak force measured at the bottom of the plate could be estimated to within 3.7%. With displacement, velocity, acceleration, extent of deformation and material composition of the mat known, the dynamic response of the mat can be calculated from video data alone. This could allow the magnitude and direction of forces on a gymnast during landing to be calculated during competition or it could allow the comparison of different mats when not all mats are available for testing in a laboratory.

### *3.6 Oblique Testing Results*

The following sub-sections report and discuss the results of the oblique drop testing. A number of off centre impacts occurred during oblique testing however only centre impacts where appropriate markers were visible were used for further analysis.

#### *3.6.1 Oblique Impact Velocities*

The two digitised points on the impactor were used to obtain the vertical and horizontal components of velocity at the instant of impact via 'determining the impact velocity Method One' in the vertical testing sub-section. Although the drop angle on the custom-rig could be set, during testing it was found that the actual impact angle was different to the angle set by the drop rig. This difference was due to the swinging of the impactor prior to impact and this caused a slight change in the impact angle. Table 3.9 reports the impact velocities from the oblique tests and the actual angles of impact calculated from the velocity data. The velocity of the two points on the impactor in trial 45max are shown in Figure 3.25.

**Table 3.9 Oblique Impact Velocities**

Trial	Horizontal Velocity (m/s)	Vertical Velocity (m/s)	Angle at Impact (°)
45max	4.30	4.40	45.7
50nb	3.80	4.30	48.5
50b	3.30	4.60	54.3
60lb	2.60	5.60	65.1
65b	2.25	6.60	71.2

(Note: 45max refers to the maximum velocity at the drop angle, 'b' refers to the bungee used to increase the impact velocity of the impactor.)

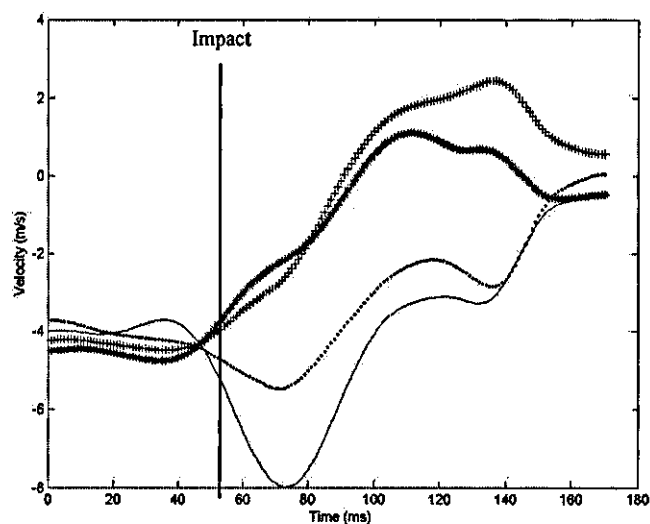


**Figure 3.25** Impact velocities at 45.7° (contact at 46 ms). (+ and \* vertical; ... and -- horizontal velocities).

### 3.6.2 Ground Reaction Forces During Impact

Vertical and horizontal ground reaction forces were recorded via the force plate under the surface of the mat. The forces associated with trial 60lb are shown in Figure 3.26.

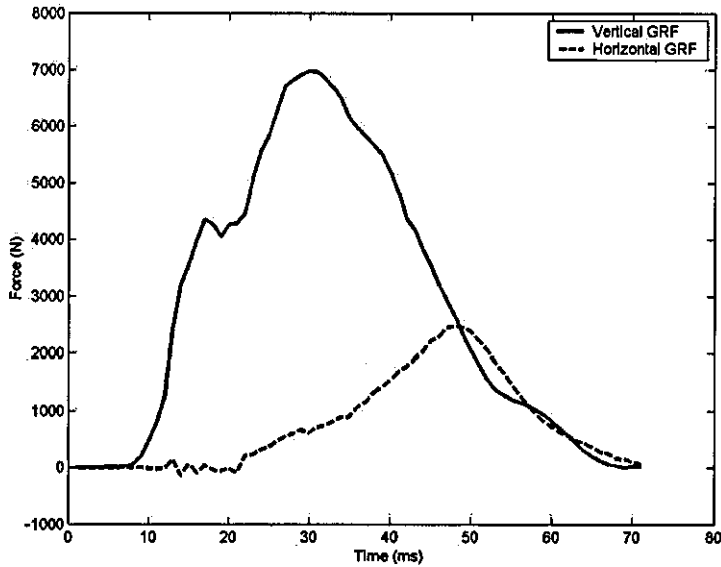


**Figure 3.26** Vertical force from force plate during trial 60lb (force plate triggered at 10ms).

**Table 3.10** Peak Vertical and Horizontal Force During an Oblique Impact

Trial Number	Peak Vertical Force (N)	Time to Peak (s)	Peak Horizontal Force (N)	Time to Peak (s)
45max	5250	40	2590	27
50nb	3808	29	3565	28
50b	5515	29	4024	28
60lb	6977	27	2467	45
65b	9280	21	2902	42

The varying vertical and horizontal times to peak (Table 3.10) may be explained by viewing the high-speed video. The video showed that during the first trial (45max) the impactor did not land flat but rather front edge, first producing a peak horizontal force earlier than a peak vertical force. Video of trials 50nb and 50b showed that the impactor landed flat and therefore the peak horizontal and vertical forces occurred at approximately the same instance in time. The video of trials 60lb and 65b showed that the impactor landed back edge first producing a peak vertical force before the horizontal. As the impactor rotated on the mat surface horizontal force increased until its peak.

### 3.6.3 Oblique Impact Compression Wave Propagation Times

Further investigation of the oblique impact high-speed video also revealed that the impactor contacted the surface of the mat prior to the force plate being triggered (Figure 3.27).

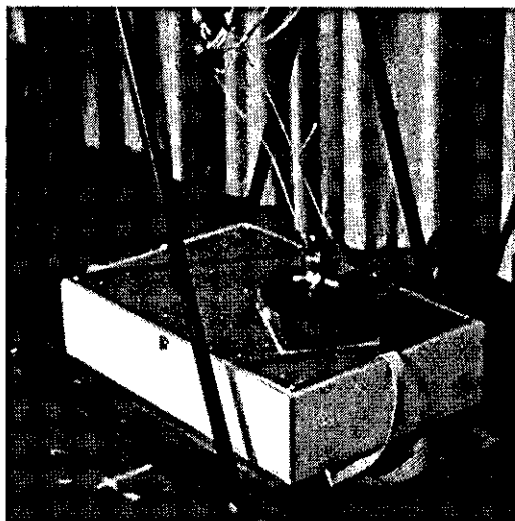


Figure 3.27 4 ms prior to force plate trigger (trial 60lb).

Table 3.11 Oblique Compression Wave Propagation Times (using high-speed video & force data)

Trial Number	Propagation time (ms)
45max	-4
50nb	-3
50b	-5
60lb	-4
65b	-5

A combination of high-speed video and force data was required to determine the compression wave propagation times (Table 3.11). The force plate data was required as no accelerometers were used during oblique testing. The force plate had a pre-trigger of 20% which corresponded to 200 ms. In trial 50b the high-speed video showed that the impactor contacted the mat 17 ms prior to trigger. However the force data showed that force was present 12 ms before the trigger and therefore the difference between them was 5 ms. The reason for this discrepancy could be that the trigger sensor on the force plate was located in one corner and the other transducers recorded a force before the trigger sensor had.

### 3.6.4 Vertical and Horizontal Mat Deformation

The six markers at the centre of the mat were used to determine the maximum horizontal deformation. An average of all six points was used to determine the horizontal deformation. Three markers at the centre of the mat were used to determine the maximum vertical deformation. The maximum deformation of either marker was used as the maximum vertical deformation. All results were similar to those seen when using the markers on the impactor to determine the deformations. Table 3.12 shows the deformation of the mat during each trial.

**Table 3.12** Vertical and Horizontal Mat Deformation

<b>Trial</b>	<b>Max Horizontal Displacement (m)</b>	<b>Max Vertical Displacement (m)</b>
45max	0.03	0.06
50nb	0.05	0.07
50b	0.05	0.09
60lb	0.03	0.08
65b	0.03	0.09

### 3.6.5 Landing Mat Area Deformation (Oblique)

The 28 markers on the mat's surface were digitised over all the frames of each oblique trial. The data were reconstructed to provide the three-dimensional coordinates of each point. The area of deformation of the mat at maximum vertical displacement in trial 60lb is shown in Figure 3.28. It should be noted that the whole of the surface of the mat is deformed during maximum deformation, also that the landing mat appears to 'fold' at maximum deformation.

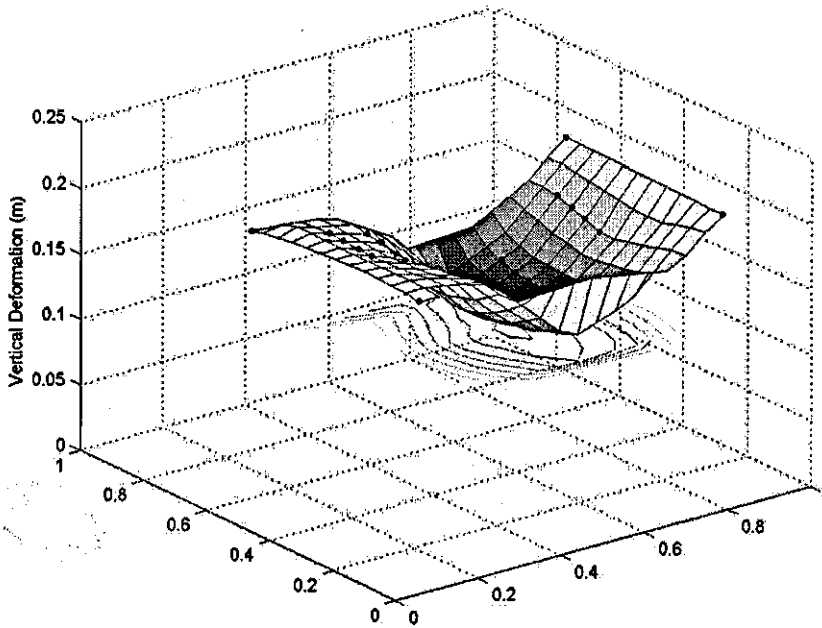


**Figure 3.28** Mat surface deformation of trial 60lb assuming deformation symmetry over the entire mat's surface. (Dots represent approximate location of actual mat markers).

The sample landing mat deformation volume was estimated using Method 1 from the vertical trials as the mat can be seen to 'fold' (Table 3.13).

**Table 3.13** Estimate of Mat Volume at Maximum Deformation (oblique)

Trial Number	Volume Estimate (m <sup>3</sup> )
45max	0.023
50nb	0.026
50b	0.030
60lb	0.028
65b	0.031

### 3.7 Modelling the Landing Mat Vertically

The first model, a simple spring-damper system computer model of the mat, was developed using the initial inputs from trial 1541. Trial 1541 was used as it represented the middle velocity trial. The Simulated Annealing optimisation



algorithm (Corana et al., 1987) was used to minimise the difference between the experimental and simulated peak force, time to peak and vertical deformation using the data from the vertical drop tests.

### 3.7.1 Landing Mat Model One Parameter Values

The optimised spring stiffness was 84183.6 N/m and the damping coefficient was 5700 Ns/m.

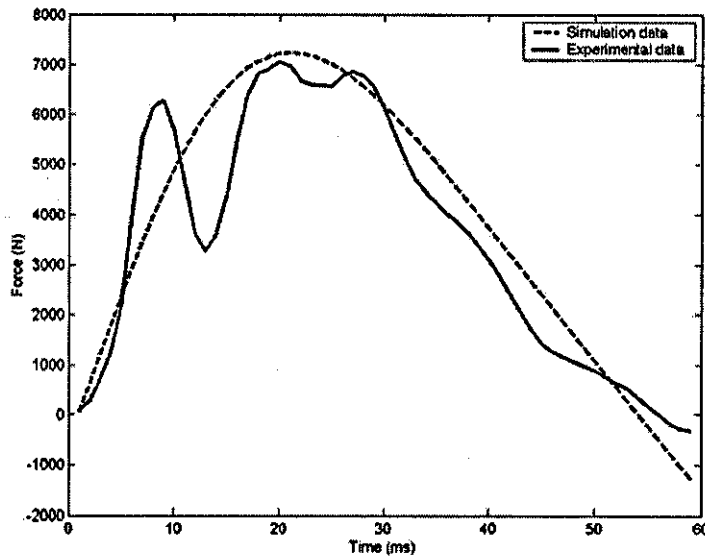


**Figure 3.29** Single spring-damper model (model 1) of the landing mat during trial 1541 (RMS difference = 965.8 N).

### 3.7.2 Landing Mat Model One Evaluation

The first model produced a peak force of 7085 N at a time of 0.020 s (Figure 3.29). The deformation at this time was 0.0799 m. This compares to the actual experimental data of a peak force of 7054 N at 0.20 s with a deformation of 0.107 m. The first model has been applied to the remaining trials (Table 3.14).

**Table 3.14** Impact Characteristics of the Single Spring Damper Model

<b>Trial</b>	<b>Peak Force (N)</b>	<b>Time to Peak (s)</b>	<b>Maximum Deformation (m)</b>
1031	5797	0.0200	0.067
1272	6458	0.0201	0.074
1541	7085	0.0200	0.078
1841	7721	0.0196	0.087
2151	8726	0.0189	0.097

The first model overestimated the peak force in trial 1031 by 3.5% and underestimated the peak force in trial 2151 by 9.1%.

Although the model matched the peak force, time to peak and vertical deformation very well, the complexity of the model was increased in an attempt to match the peak forces during all trials. The second model included the effective mass of the mat being accelerated during impact. This adds an additional force to that being calculated by the spring-damper model.

### 3.7.3 Landing Mat Model Two Parameter Values

The spring stiffness and damper coefficient parameters were re-optimised with the extra inertia term. The optimised parameter values were 101725.5 N/m for the spring stiffness and 4400 Ns/m for the damping coefficient. The force due to the extra inertia term (section 3.2.2) was 769 N. Table 3.15 shows the peak force, time to peak and maximum deformation for each trial after re-optimisation.

**Table 3.15** Impact Characteristics of the Single Spring Damper Model (+ inertia term)

<b>Trial</b>	<b>Peak Force (N)</b>	<b>Time to Peak (s)</b>	<b>Maximum Deformation (m)</b>
1031	5671	0.0207	0.062
1272	6400	0.0200	0.069
1541	7054	0.0200	0.075
1841	7780	0.0197	0.082
2151	8870	0.0192	0.092

### 3.7.4 Landing Mat Model Two Evaluation

Using an equation containing an 'ma' (inertia) term in Model Two produced an overestimation of the peak force in trial 1031 of 1.4% and an underestimation of the peak force in trial 2151 of 7.6%. The RMS difference between the experimental and simulation force-time data in trial 1541 was 947.3 N. The second model was more accurate than the first and could be used in subsequent analysis of gymnastic landings to assess the forces experienced by the gymnast's body due to the landing mat.

The second model was able to reproduce some elements of the impacts such as the peak force and time to peak. However, since the landing mat is actually constructed of two layers and the force-time history of the impact has not been reproduced very well the third model of the mat was developed. Trial 1541 was used to develop the model.

### 3.7.5 Landing Mat Model Three Parameter Values

Multiple simulations and optimisations were run to determine the lowest RMS difference between the actual force time history and the simulated force time history. A combination of MatLab's optimisation toolbox, Simulated Annealing and an adaptive neural network feedback procedure was used to determine the spring parameters. The optimised spring parameters were  $k_1 = 76700$  N/m,  $k_2 = 807380$  N/m,  $d_1 = 490$  Ns/m,  $d_2 = 980$  Ns/m. The top mass was 26.4 kg (impactor mass plus top layer of mat) and the bottom mass was 3.7 kg (mass of bottom layer of mat).

### 3.7.6 Landing Mat Model Three Evaluation

After optimisation of the spring parameters the timing of the first peak was 3 ms too early and the drop in force after the first peak was only half the drop of the actual force (Figure 3.30).

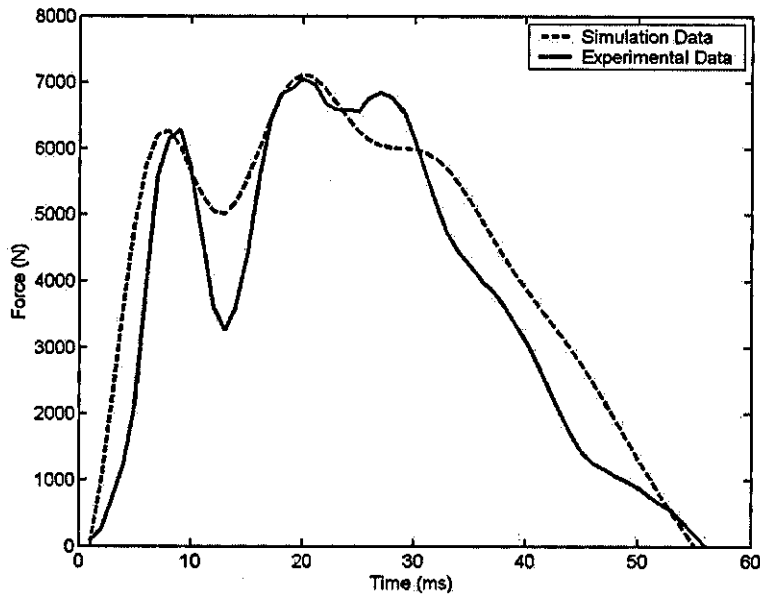


**Figure 3.30** Third spring-damper model of landing in trial 1541 (RMS difference = 894.5 N).

In the simulation the vertical deformation was 8.0 cm, which was similar to the actual deformation of 8.8 cm. However the third model started to match key elements of the impact such as the first and second impact peaks. The third model overestimated the peak force during trial 1031 by 5.0% and underestimated the peak force in trial 2151 by 8.7% (Table 3.16).

**Table 3.16** Impact Characteristics of the Model Three

Trial	Peak Force (N)	Maximum Deformation (m)
1031	5871	0.066
1272	6528	0.073
1541	7120	0.080
1841	7776	0.087
2151	8762	0.098

Although Model Three matched the force time profile better than the first two spring-damper models a fourth model consisting of three spring-dampers was developed to represent the surface (carpet)( $m_3$ ), middle (stiff)( $m_2$ ) and bottom (soft) ( $m_1$ ) layers of the mat. Each spring damper was separated by a mass.

### 3.7.7 Landing Mat Model Four Parameter Values

Again Simulated Annealing was used to determine the parameters of the springs and dampers. The optimised spring parameters were  $k_1 = 72075 \text{ N/m}$ ,  $k_2 = 1061532 \text{ N/m}$ ,  $k_3 = 748625 \text{ N/m}$ ,  $d_1 = 263 \text{ Ns/m}$ ,  $d_2 = 761 \text{ Ns/m}$ ,  $d_3 = 1007 \text{ Ns/m}$ . The first mass represented the mass of the impactor (24 kg), the second mass represented the mass of the top layer of the mat (2.4 kg) and the third mass was 3.7 kg (mass of bottom layer of mat).

### 3.7.8 Landing Mat Model Four Evaluation

These parameters produced a close match between the actual force time profile and the simulated force time profile during the first half of the simulation. The experimental force time history and the simulated force time history for the three spring-damper system are shown in Figure 3.31.

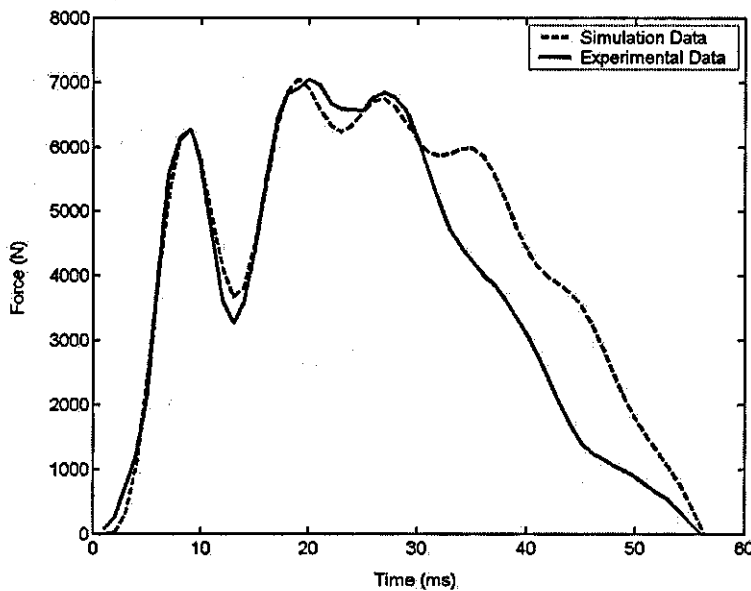


**Figure 3.31** Fourth spring-damper model of landing in trial 1541 (RMS difference = 940.7 N).

Vertical mat deformation was 10.1 cm compared to the actual 8.8 cm. The fourth model overestimated the peak force during trial 1031 by 4.0% and underestimated the peak force in trial 2151 by 9.6% (Table 3.17). The unloading phase of the impact during the simulation suggests that there is more momentum in the model than actually present due to the additional impulse towards the end of the simulation.

**Table 3.17** Impact Characteristics of Model Four

<b>Trial</b>	<b>Peak Force (N)</b>	<b>Maximum Deformation (m)</b>
1031	5814	0.083
1272	6465	0.093
1541	7052	0.101
1841	7703	0.111
2151	8680	0.125

All four models produced a similar RMS score. Models One and Two closely matched the peak force but the key characteristics of the impact were not reproduced. The first two models generally matched the loading and unloading phases of the impact giving a reasonable RMS score. The fourth model accurately matched the loading phase of the impact but was unable to match the unloading phase; this produced a RMS score similar to the other models although the match appeared to be better. The passive loading phase of a gymnast landing is important when assessing injury risk as elastic surfaces with low stiffness can lead to a reduction in the injury risk (Fritz & Peikenkamp, 2003). Future simulations of a gymnast landing on a mat will focus on technique used during the loading phase rather than the unloading phase. As a consequence matching the unloading phase of the impact during the material tests was thought to be less important than matching the loading phase. The fourth model and parameters could be used in future combined gymnast and mat models to accurately represent the behaviour of an F.I.G. landing mat.

### 3.7.9 The Development of Landing Mat Model Five

When Model Four was integrated into VN4D using MatLab it was found that the simulation time increased dramatically (30 s). This could have caused a problem as optimising a gymnast-mat model is critical to answering the research questions. Therefore Model Five was developed in VN4D to reduce the simulation time and was based upon the same principles as Model Four.

### 3.7.10 Landing Mat Model Five Parameter Values

Using the same spring parameters as Model Four produced a different result when implemented in VN4D (Figure 3.32). This suggests that VN4D was running the model in a different way to what was expected as the same spring parameters should have given the same result. However VN4D was to be used to construct the model of the gymnast and the VN4D technical representative could not give an answer to this problem. The decision was made to re-optimize the spring parameters to ensure a satisfactory force time history match.

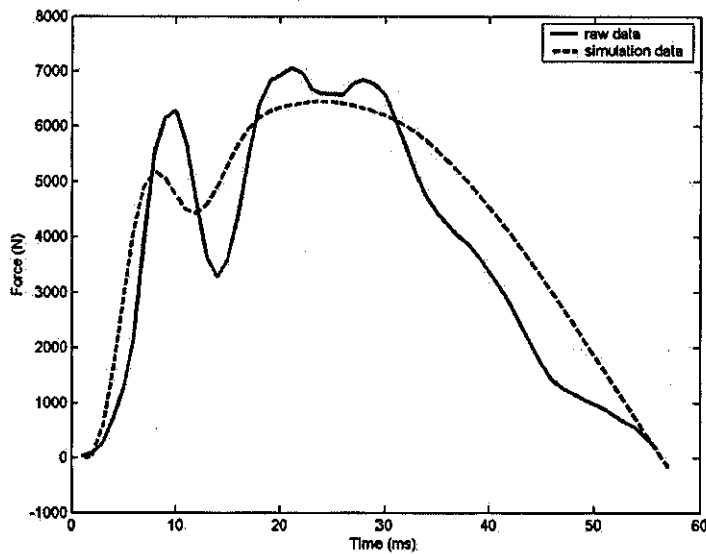


**Figure 3.32** Vertical ground reaction force (Model Five ) using point mass spring parameters from Model Four (RMS difference = 967.9N).

The spring parameters were re-optimized using the Nastran model. Again the simulation results were compared to the raw data in order to minimise the RMS difference. Re-optimisation produced a better match with the experimental results (Figure 3.33) in the first phase of the impact.

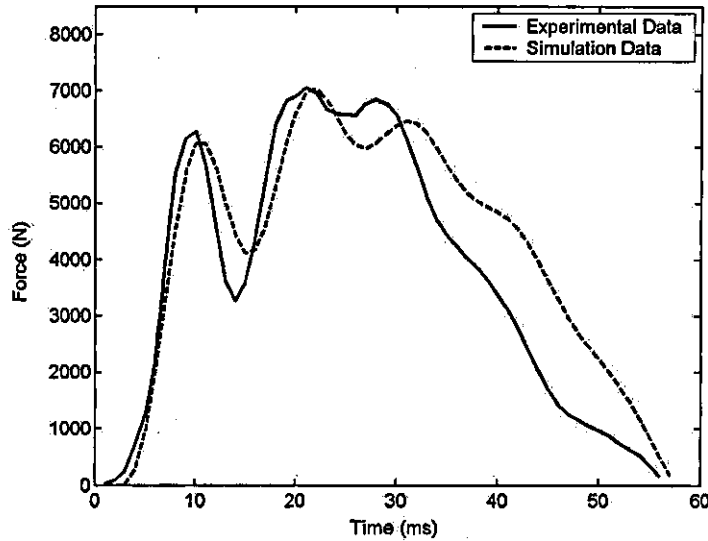


**Figure 3.33** Vertical ground reaction force using re-optimised spring parameters (Nastran) (RMS difference = 1014.2 N).

The result of the optimisation used the following spring parameters in the VN4D mat model:

Top layer spring stiffness (vk1)	= 70880 N/m
Middle layer spring stiffness (vk2)	= 787200 N/m
Bottom layer spring stiffness (vk3)	= 617120 N/m
Top layer damping (vdamp1)	= 260 Ns/m
Middle layer damping (vdamp2)	= 280 Ns/m
Bottom layer damping (vdamp3)	= 850 Ns/m

### 3.7.11 Landing Mat Model Five Evaluation

The RMS difference of 1014.2 N was similar to Model Four with the unloading phase giving most of the error. These new re-optimised parameters match the loading phase and are used in the gymnast-mat model as the risk of injury is higher during the passive phase of the landing and that it was more important to model this phase as accurately as possible.

### 3.8 Modelling the Landing Mat Horizontally

An attempt was made to match the horizontal velocity of the impactor and the horizontal force measured via the force plate. During the oblique impacts the



impactor did not always strike the mat's surface with its flat base. Therefore this introduced an inconsistency in to the force data. A line was fitted to the horizontal velocity and horizontal force data of each trial (not trial 45max as the video showed that the impactor slipped at impact) and the equation was  $y = 728.63x + 1062.7$ . Each force was recalculated using this equation for each of the impact velocities (Table 3.18).

**Table 3.18** Horizontal Velocity and Recalculated Force

<b>Trial Number</b>	<b>Horizontal Velocity at Impact (m/s)</b>	<b>Peak Horizontal Force (N)</b>
45max	4.30	4196
50nb	3.80	3831
50b	3.30	3467
60lb	2.60	2957
65b	2.25	2702

Vertically the mat behaved like a spring, the impactor compressed the mat and the mat produced a restoring force in the opposite direction pushing the impactor back up again. Horizontally this did not happen, the impactor struck the mat's surface and deformed the mat horizontally but the impactor continued in the same direction. This means that the mat did not absorb all the impactor's energy during the impact. In trial 60lb approximately 81 J of energy impacted the mat and 24 J continued in the same direction. Therefore the mat absorbed 57 J. The horizontal spring parameters were optimised and the horizontal mass of the mat was also optimised with bounds set between the mass of the mat and the mass of the impactor.

### 3.8.1 Landing Mat Horizontal Model Parameter Values

The Simulated Annealing optimisation algorithm was used to determine the spring parameters required to produce the minimum RMS difference between the horizontal experimental force time history and the simulated force time history. This produced a result that closely matched the actual trial (Figure 3.34). The parameters

determined via the optimisation were  $k_1 = 5820 \text{ N/m}$ ,  $k_2 = 12805000 \text{ N/m}$ ,  $k_3 = 82000000 \text{ N/m}$ ,  $r = 1462 \text{ Ns/m}$ ,  $\text{mass} = 12 \text{ kg}$ .

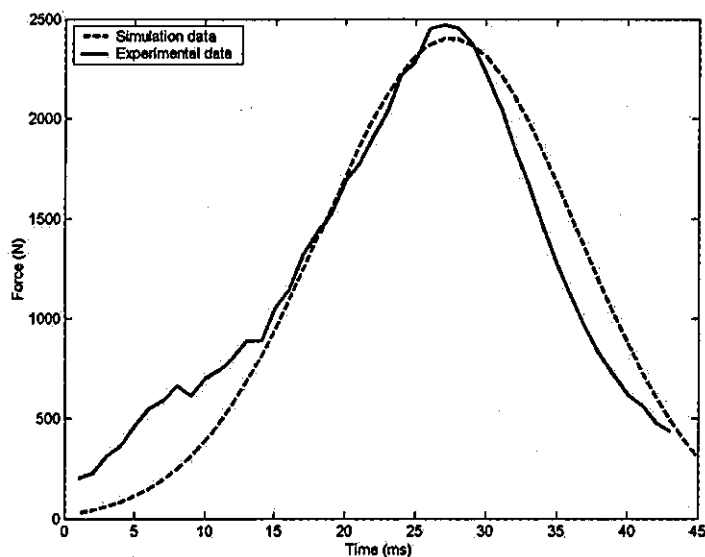


**Figure 3.34** Force time history for the mat's horizontal spring-damper using trial 60lb (RMS difference = 363.2 N).

### 3.8.2 Landing Mat Horizontal Model Evaluation

The model matched the time to peak force and the peak force. The horizontal mat deformation for this trial was 0.03 m, the simulation produced a deformation of 0.06 m. However this deformation was as close a match as possible whilst keeping the simulated force within 25% of the actual force. During testing the mat was seen to fold, this made it difficult for the model to match the force and deformation. The mat mass and spring parameters were optimised in an attempt to keep the horizontal mat deformation within twice that of the actual deformation whilst also keeping the simulated force within 25% of the actual force. The non-linear equation was required to ensure that the timing of the peak force matched the timing of the actual peak force. A linear model resulted in a simulated peak force earlier than the actual peak force as less deformation was required to produce a greater force, hence a greater RMS difference.

### 3.9 A Computer Model of Oblique Impacts onto Landing Mats

The aim of the mat testing was to develop a computer model of the mat that could represent oblique impacts. The vertical Model Five and the horizontal model

was able to produce a similar impact force and give reasonable mat deformations for the example oblique impact trial 60lb. The simulated deformations were 0.11m vertically and 0.06 m horizontally, this compared to the actual deformations of 0.08 m and 0.03 m. Both Model Five and the horizontal mat model are combined in Figure 3.35 together with the actual data from trial 60lb. When combining the horizontal and vertical models it was hoped that the vertical force time history would match closely to the experimental data but this was not the case as the model treats the two components of force separately. The landing mat may have interaction between the horizontal and vertical displacements therefore each component is not independent of the other: an example of this can be seen when the mat 'folds' during impact. Since a gymnast would land at an oblique angle with a component of both vertical and horizontal velocity it was felt that the vertical part of the model did not perform adequately. The initial impact peak was too great in the simulation compared to the actual vertical component of the oblique impact.

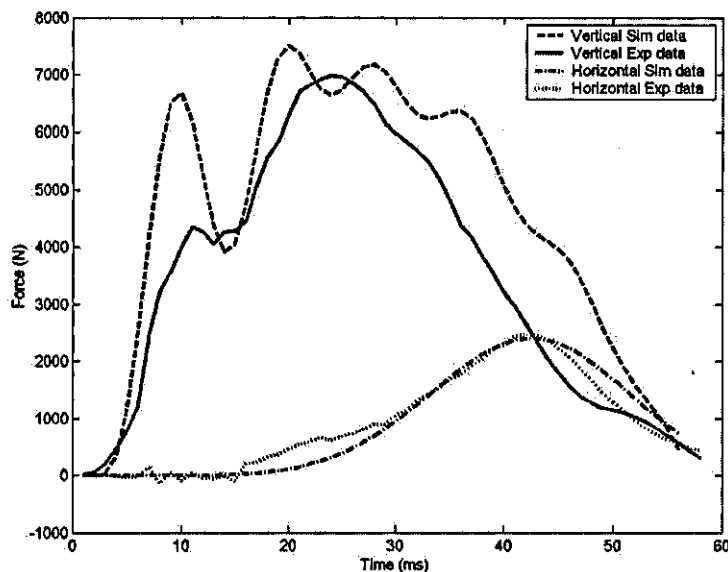


**Figure 3.35** Simulation of trial 60lb (RMS difference vertically = 1327.5 N).

This problem was because the vertical mat parameters were based upon vertical drop tests. A gymnast performing a vault would actually land at an oblique angle so the decision was made to re-optimize the vertical mat parameters again but this time matching the vertical component of an oblique drop test. Re-optimization resulted in an RMS difference score of 1008 N based on oblique trial 60lb (Figure 3.36). The re-optimized spring parameters were:

$$k1 = 61080 \text{ N/m}$$

$$d1 = 350 \text{ Ns/m}$$

$$k2 = 57530 \text{ N/m}$$

$$d2 = 430 \text{ Ns/m}$$

$$k3 = 928210 \text{ N/m}$$

$$d3 = 290 \text{ Ns/m}$$

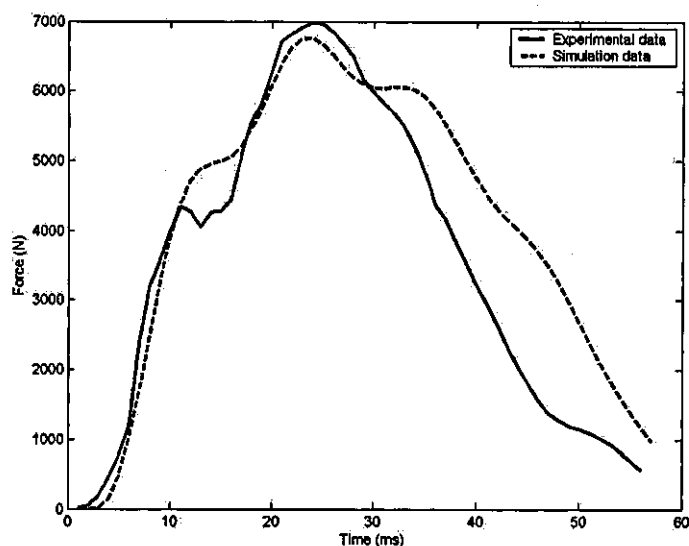


**Figure 3.36** Re-optimisation of vertical mat spring parameters using trial 60lb.

This approach works for oblique impacts within the test range however a poorly executed landing maybe outside the test range and therefore the model may not be as accurate. Yet for the gymnast to clear the vault horse some horizontal velocity must be present therefore the landing angle should always be oblique.

### 3.10 Sensitivity Analysis

A sensitivity analysis was performed on all five vertical mat models. The springs stiffness and damping coefficients were varied by  $\pm 10\%$  and the percentage difference in the peak vertical force was calculated. The results of the sensitivity analysis showed that the peak force varied  $+ 5.4\%$  and  $- 5.7\%$  for the  $\pm 10\%$  change in the landing mat spring parameters (Table 3.19).

**Table 3.19** Sensitivity Analysis of Landing Mat Parameters

Model Number	Percentage change in peak vertical force (+10%)	Percentage change in peak vertical force (-10%)
1	+ 5.0	- 5.3
2	+ 5.4	- 5.7
3	+ 4.6	- 4.5
4	+ 5.0	- 1.2
5	+ 4.0	- 4.3

### 3.11 Summary

Five vertical mat models were constructed and one horizontal mat model. Material testing of an F.I.G. landing mat has been performed and the results used to assess the deformation characteristics of the landing mat during vertical and oblique impacts. The testing protocol has revealed that the key deformation characteristics associated with an impact can be obtained by the use of high-speed cameras if required during a restrictive sporting environment.

The mat testing results and subsequent analysis has been used to develop a computer model of the mat that reproduces the material tests. Models One and Two lacked the complexity to accurately model the landing mat's behaviour under varied loading conditions. Model Three improved upon the first two but again was unable to match the complex landing mat behaviour during impacts. Model Four successfully matched the key characteristics of the landing mat's behaviour, however, once integrated into VN4D simulation time increased dramatically. Model Five was developed using a similar construction to Model Four; this again could match the key characteristics of the landing mat's behaviour and also reduced the simulation time within VN4D. The horizontal component of the mat model was implemented without any problems in VN4D. When the vertical and horizontal components of the mat model were combined and evaluated against an oblique trial the vertical component proved inadequate at matching the force time history of the impact. The vertical spring parameters were re-optimised and an improved match was obtained.

The final mat model that will be combined with a model of a gymnast consisted of the re-optimised parameter values for Model Five and the horizontal mat model. These parameters can be used in a subsequent model of the gymnast and mat to reproduce the F.I.G. landing mat's behaviour during impacts.

## CHAPTER 4

### MODELLING THE GYMNAST

A simulation model of a gymnast was developed in order to investigate the effects of different landing strategies used by a gymnast to land safely and within the F.I.G. performance guidelines. This chapter describes the structure of four models of the gymnast. Each model increased in complexity at a cost of simulation time so the simpler models were used to obtain starting points for the optimisations of the more complex models. The methodology and equipment used to collect data for the subject specific parameters. The results are presented and discussed in detail and are used to determine the subject-specific parameters values for each model.

#### *4.1 The Structure of the Gymnast Models*

Each of the four models were constructed using a combination of MatLab, Simulink and VN4D. The following sub-sections describe each model's structure in detail.

##### 4.1.1 Gymnast Model One

The gymnast in Model One was represented by a seven-segment planar link system comprising the head + trunk, upper arm, lower arm + hand, thigh, shank, and a two segment foot. The gymnast's orientation was specified by  $\theta_t$ , the angle between the trunk and the vertical. The six joint angles were the angles at the following joints: metatarsal-phalangeal ( $\theta_{mp}$ ), ankle ( $\theta_a$ ), knee ( $\theta_k$ ), hip ( $\theta_h$ ), shoulder ( $\theta_s$ ) and elbow ( $\theta_e$ ) (Figure 4.1).

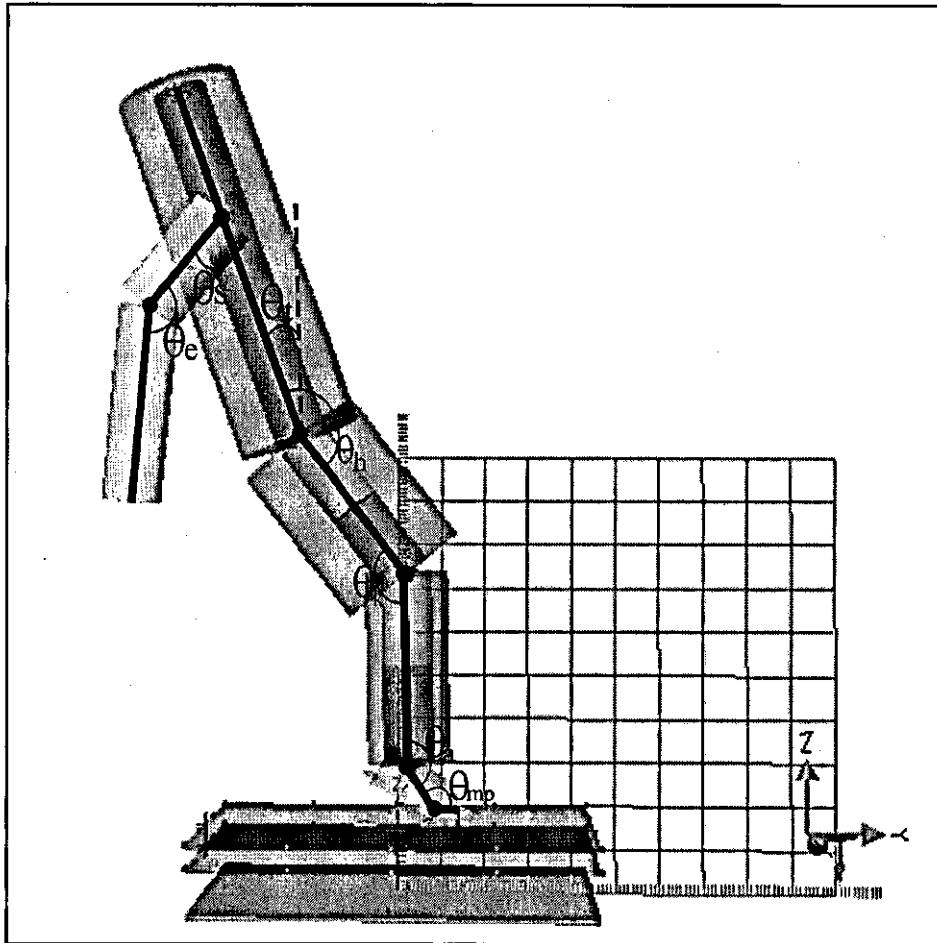


**Figure 4.1** Seven-segment model of a gymnast.

Each segment was subject-specific in terms of length, mass, location of mass centre and moment of inertia. The segments were linked via pin joints; this constrained the joints to rotate in the sagittal plane.

Wobbling masses were included within the trunk, thigh and shank body segments to represent soft tissue movement. Each segment was divided into a fixed mass and wobbling mass. The fixed mass, representing the bone, was a rigid body lying between adjacent joint centres. The wobbling mass, representing the soft tissue, was a rigid body connected to the fixed mass at the endpoints via non-linear spring-dampers. One spring-damper system was located at the proximal end of the segment and the other at the distal end of the segment. The behaviour of the wobbling masses were defined by the equation (Pain & Challis, 2004):



$$F = -kx^3 - cv \quad (4.1)$$

where  $F$  = spring force

$k$  = spring stiffness

$c$  = spring damping

$x$  = displacement

$v$  = velocity

The wobbling mass equation was developed so that results from a simulation matched the amplitude and frequency of soft tissue displacement from experimental data.

The thigh and shank fixed masses included a rigid joint in the centre of each element to determine the torque at the centre of the bone during simulations.

The M-P joint was modelled as a torsional spring-damper system and its behaviour was defined by the equation (Gilchrist & Winter, 1996):

$$T = -k\theta - r\omega \quad (4.2)$$

where  $T$  = spring torque

$k$  = spring stiffness

$r$  = spring damping

$\theta$  = angle

$\omega$  = angular velocity

The foot was divided into two segments, the upper foot and lower foot (toes). The upper foot had length from the rear of the subject's heel to the M-P joint and width of both of the subject's feet. The lower foot was the length of the subject's toes (from the M-P joint to the end of the toes) and the width of the subject's feet (Figure 4.2).

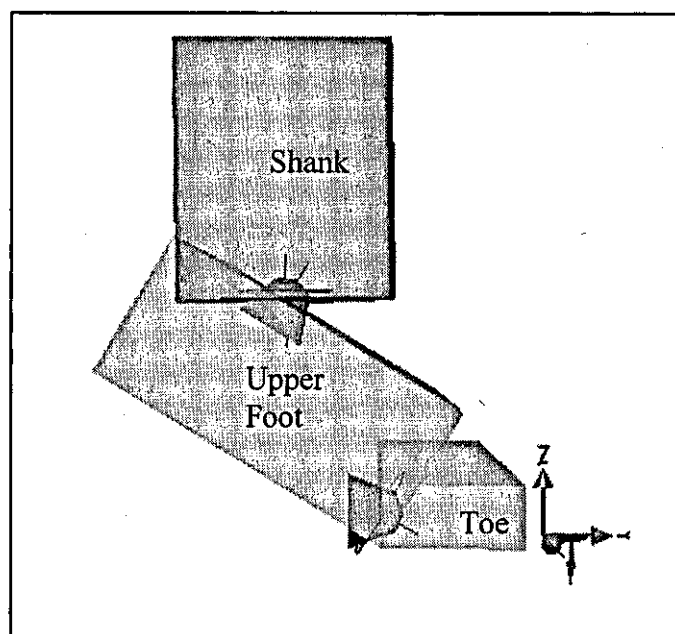


**Figure 4.2** The two segment foot modelled in VN4D.

During impacts heel pad deformation plays an important role in energy dissipation during impacts (Pain & Challis, 2001b). The foot / mat interface was modelled to represent the properties of the soft tissue of the heel pad. Three spring-damper systems, one at the rear of the heel, one at the M-P joint and one at the end of the toes connected the foot to the landing mat's surface. The behaviour of the heel pad was defined by the equation (Pain & Challis, 2001b):

$$F = K_1 \cdot X^7 + K_2 \cdot X^5 + K_3 \cdot X^3 + K_4 \cdot X - C \cdot \dot{X} \cdot X \quad (4.3)$$

where  $F$  = heel pad force

$k_i$  = spring stiffness

$c$  = damping coefficient

$x$  = displacement

The heel pad equation was constructed so that the mechanical properties of the element in terms of stiffness and energy loss were representative of those measured on isolated heel pads.

Flexor and extensor torque generators acted at the ankle, knee, hip and shoulder. The elbow angle remained fixed but the angle varied depending upon the

skill being simulated. These eight torque generators were responsible for ankle plantar flexion and dorsi flexion, knee extension and flexion, hip extension and flexion, shoulder extension and flexion. Each torque generator represented the musculo-tendon properties of the gymnast. Since Model One does not have a series elastic component (SEC) the torque generator in this model represents the contractile component (CC). In this model the CC force represents the series elastic force for isovelocity movements (King & Yeadon, 2002). The contractile component torque along with the given time was calculated from a nine parameter function which related torque, angle and angular velocity in a similar way to Yeadon et al. (2005). The parameter values were obtained from the gymnast using an isokinetic dynamometer (discussed in detail later in this chapter). The torque calculated from the nine parameter function was the maximum voluntary torque that could be produced at a given joint angle and angular velocity. The torque was then multiplied by the muscle activation level to give the final torque at time t:

$$\text{TOR}(t) = A(t) \cdot T(\theta\omega) \quad (4.3)$$

where: TOR(t) = torque at time t

A(t) = muscle activation level at time t

T( $\theta,\omega$ ) = maximum voluntary torque calculated from nine parameter function

When the muscle was relaxed the activation level was 0.0 and when the muscle was fully activated the activation level was 1.0. Two quintic functions were used to ramp the activation level up and down (Yeadon & Hiley, 2000). The function used to ramp up and down was:

$$q(x) = x^3 (6x^2 - 15x + 10) \quad (4.4)$$

The parameter x in equation 4.4 represents the x-axis and hence t in equation 4.3. The parameter q in equation 4.4 represents the activation level A in equation 4.3. This function increases from 0 to 1 (or decreases from 1 to 0). The function also has zero velocity and acceleration at the endpoints (2<sup>nd</sup> differentials are zero at endpoints). The function models a smooth change from low to high. The rate of

change is slower at the beginning and end phases of the function. This resembles the typical activation pattern recorded by EMG (see results later in this chapter).

#### 4.1.2 Gymnast Model Two

Model Two was the same as Model One except for the torque generators. The torque generators use a similar contractile component (CC) as model one but also include an additional series elastic component (SEC). The muscle angle is required because a sub-maximal torque at the joint will yield a different muscle and SEC angle to that of a maximal torque produced at the joint. Fitting the nine-parameter function to the experimental isovelocity joint torque/angle/angular velocity data meant that the surface will only behave well over the joint angular velocities and joint angles used to calculate the surface. The joint angle was converted into muscle angle and a new set of parameters determined. These can be used in a muscle-tendon model, which in turn can be incorporated into a whole body model of a gymnast. The muscle-tendon complex model was based upon Alexander (1990). A graphical representation of the muscle-tendon complex is shown in Figure 4.3.

where  $\theta$  = joint angle

$\theta_{con}$  = contractile component angle

$\theta_{sec}$  = series elastic component angle

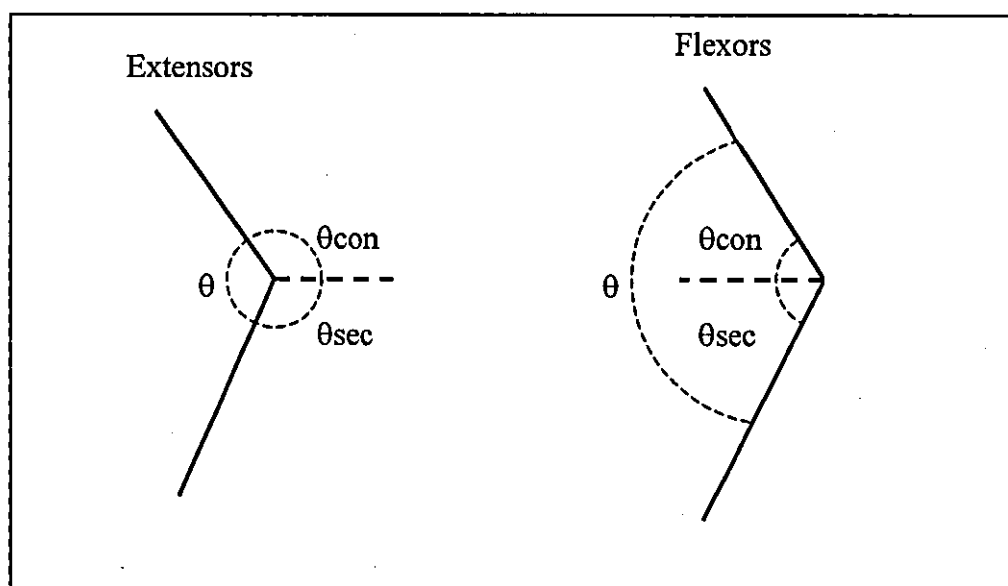


Figure 4.3 The contractile component and SEC of the muscle-tendon complex.

The geometrical relationships in Figure 4.3 can be represented by two equations:

$$\text{Extension} \quad 2\pi = \theta + \theta_{\text{con}} + \theta_{\text{sec}} \quad (4.5)$$

$$\text{Flexion} \quad \theta = \theta_{\text{con}} + \theta_{\text{sec}} \quad (4.6)$$

The CC torque was calculated using the nine parameter function (model one). The contractile component angular velocity at time zero was assumed to be the same as the joint angular velocity. The CC torque calculated from the nine parameter function was set to be equal to the SEC torque. The torque ( $T_{\text{sec}}$ ) in the SEC was defined by the equation:

$$T_{\text{sec}} = k \theta_{\text{sec}} \quad (4.7)$$

where  $k$  = SEC stiffness

Using the geometrical relationships in Figure 4.3 and the equation defining the torque in the SEC the initial contractile component angle was determined. Using this initial CC angle and the joint angular velocity the torque in the CC was calculated from the nine parameter function. The CC angle was updated every time step by assuming constant velocity:

$$\theta_{\text{con}} = \theta_{\text{con}} + \omega_{\text{con}} dt \quad (4.8)$$

where  $dt$  = integration time step

After time zero a new SEC angle was calculated from the new joint angle and the new CC angle. The new SEC torque was calculated. The new CC angular velocity was obtained from the CC torque and the SEC torque and substituting for the SEC angle. Using the new CC angle and angular velocity the new CC torque could be calculated using the nine parameter function. Then finally the CC angle was updated again.

#### 4.1.3 Gymnast Model Three

Model Three was similar to Models One and Two except some of the torque generators were replaced with linear muscle-tendon models. Model Three had six linear muscle-tendon models. They were: ankle plantar flexors, ankle dorsi flexors, knee extensors, knee flexors, hip extensors and hip flexors. The shoulder joint

remained torque driven as in Model Two. The linear muscle model was a 'lumped' muscle model meaning all muscles responsible for a particular joint's flexion were 'lumped' together and represented by one muscle model. All the muscle responsible for a particular joint's extension were 'lumped' together and also represented by one muscle. The linear muscle model represented the CC of Model Two. The torque at the joint was calculated from the joint angle and angular velocity and from the nine parameter function, then the torque was divided by the estimated moment arm for the muscle group to give the force in the linear muscle. The muscle was attached at the proximal attachment point of the muscle group it was representing. The distal end of the muscle was attached to a circular rigid body that had a radius equivalent to of the moment arm for that muscle group. The circular rigid body was attached to the joint centre and was free to rotate. This meant that as the CC shortened the force the muscle applied to the circular rigid body would rotate the rigid body. The SEC was represented by a linear spring-damper system and its behaviour was defined by the equation:

$$F = -kx - rv \quad (4.9)$$

The SEC was also attached to that circular rigid body and was attached to the distal segment at the insertion point. No bi-articular muscles were modelled. The knee extensors are modelled in Figure 4.4.

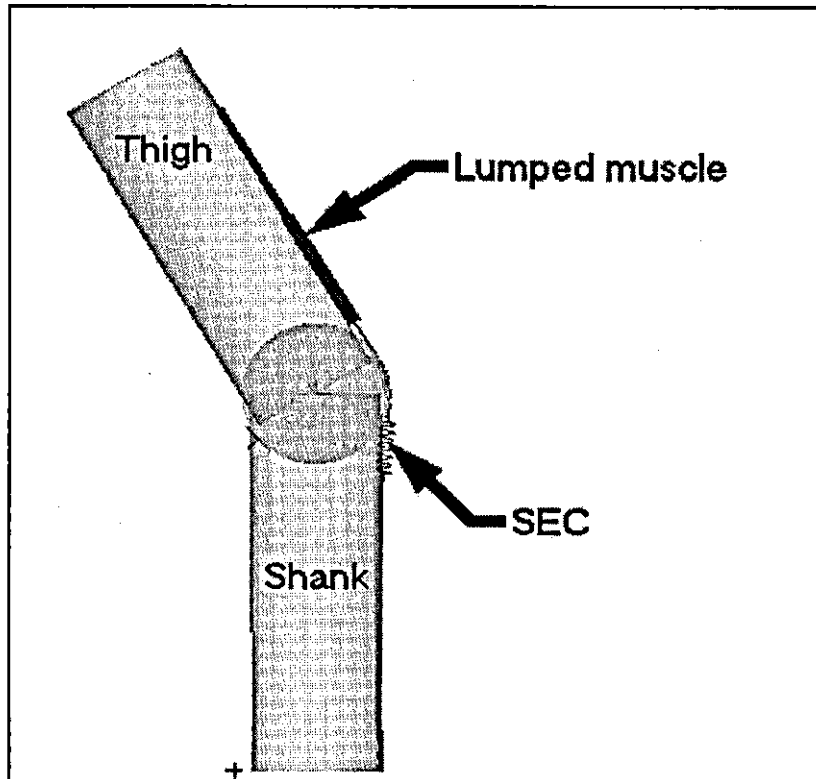


**Figure 4.4** The 'lumped' muscle model – knee extensors.

The proximal end of the knee extensor was attached to the thigh at the approximate attachment point of the muscle group. The distal end of the knee extensor was attached to the rigid circle. The distance between the attachment of the muscle to the attachment of the SEC represented the length of the patella. The SEC was attached to the rigid circle and the other end of the SEC was attached to the shank at the approximate attachment site of the patella tendon. As the leg extends and flexes the rigid circle is free to rotate maintaining the moment arm for the muscle group.

#### 4.1.4 Gymnast Model Four

Model Four was similar to Model Three except the rigid bones representing the lower extremity were replaced with linear FEM's of long bone that could deform during the simulation. The FEM of bone was the approximate length and mass of the subject's bone as in Models One, Two and Three, however the bone was a cylinder of uniform density. The FEM consisted of 961 nodes and 444 elements. The mesh size was 0.016 m with a mesh factor of 0.996. The maximum mesh angle was set at 45° (Figure 4.5).

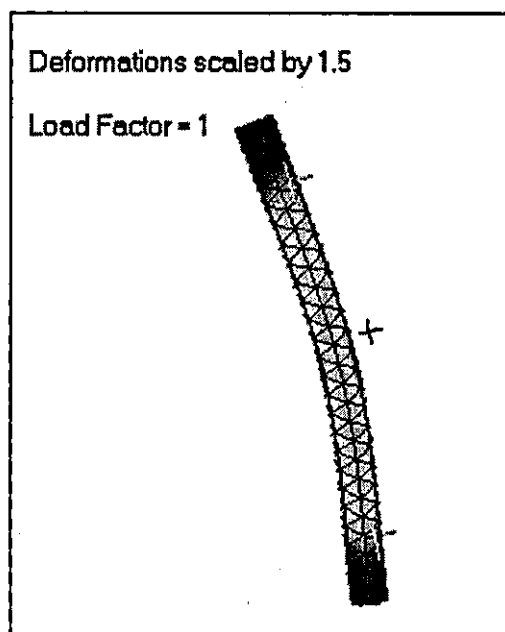


**Figure 4.5** Finite element model of long bone.

#### 4.1.5 Model Structure Summary

Four models of the gymnast were constructed using VN4D. All the models were similar in construction. Model One used torque generators to produce joint motion, the torque generators represented the CC of muscles. Model Two expanded Model One by including a SEC within the torque generator. Model Three replaced the torque generators with linear muscle-tendon models. Model Four included a simple FEM of the lower extremity bones.

#### 4.2 Data Collection and Parameter Determination

A brief review of the relevant techniques used to collect the subject data is presented and discussed. This includes the use of anthropometric models, isokinetic dynamometers, electromyography (EMG) and automatic tracking systems such as Vicon. Each section is followed by how the relevant model parameter values were determined and evaluated.

##### 4.2.1 Anthropometric Measurement of Subjects

The inertia properties of the human body, such as mass, centre of mass location and moments of inertia, are required for kinetic analysis of human motion.



Direct measures, surface measures, regression equations and geometric modelling are all used to determine segmental inertia parameters.

Measurements of whole body inertial properties can be performed directly on a subject. Two methods are commonly used to determine mass, density and volume. The first method involves weighing the object in the air and then lowering the object into water and weighing the displaced water. The volume of the object can then be determined. The mass and volume of the object are used to determine its density. The second method involves the object being weighed in air and then in water. Nigg (1999) reported that the volume displacement method proved less reliable for living people than for cadavers. Repeat measurements indicated that the variation was between 3 to 5% perhaps due to the residual air left in the lungs.

To determine the location of the centre of gravity of a segment the suspension method or the balance method can be used and the methods are similar in principle. The segment is either suspended from a cable or balanced on a knife-edge in three different planes to determine the centre of gravity. An indirect method of determining whole body centre of gravity is commonly performed using the balance method (Figure 4.6). The table is supported at one end by a knife-edge (O). The other end can be placed on weighing scales to determine force. If the weight of the object is known, the location of the centre of gravity can be determined by calculating moments about (O) and using the distance between the two knife edges.

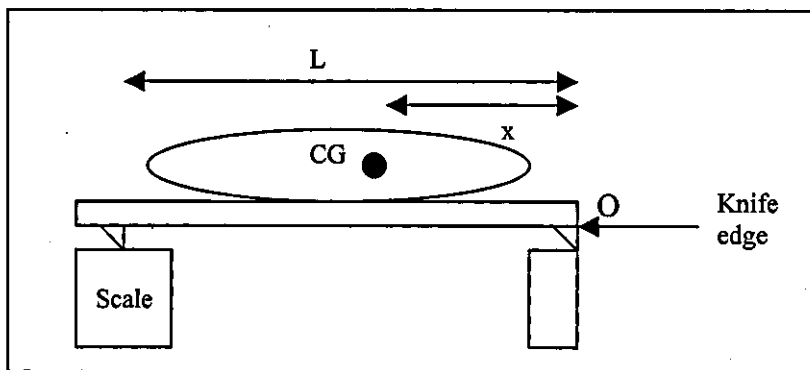


Figure 4.6 Moment table used to determine centre of gravity.

$$x = L \cdot W_{\text{scale}} / W_{\text{object}} \quad (4.10)$$

where  $L$  is the length of the board between the two knife-edges,  $W_{\text{scale}}$  is the weight reading on the scale,  $W_{\text{object}}$  is the weight of the object and  $x$  is the distance to the centre of gravity from the origin  $O$ .

Moments of inertia can be determined using the pendulum method. This consists of suspending the object of interest from a fixed point, setting it swinging a few degrees from its equilibrium position and measuring the time it takes to swing for one period of oscillation. Moment of inertia about the swinging axis can be calculated using the equation.

$$I_o = \frac{W.h.T^2}{4\pi^2} \quad (4.11)$$

where:

- $I_o$  = moment of inertia about an axis through the point of suspension
- $W$  = weight of the object
- $h$  = distance from the centre of gravity of the object to the point of suspension
- $T$  = period of one oscillation

So far the indirect methods described have provided data on whole body inertia properties. However additional data are required on individual segments. Attempts at obtaining segmental inertial data were first performed with cadavers. These studies involved dissecting the cadavers into body segments and measuring the parameters experimentally using a combination of balance plate and pendulum methods (Dempster et al., 1955; Chandler et al., 1969). These studies directly measured segmental inertial parameters although the sample groups were usually small in size and not representative of other populations.

Other methods of directly measuring segmental inertia parameters include computerised axial tomography (CAT). CAT scans take multiple x-rays of a thin section of the object of interest generating a series of cross-sections of the segment. The cross-sections can be used to determine various tissue areas such as bone, muscle and fat. The area data can be used to calculate some inertia properties of the segment. Magnetic Resonance Imaging (MRI) uses the change in orientation of the magnetic moment of hydrogen nuclei for a particular tissue that is generated when the tissue is placed in a magnetic field and stimulated with a radio frequency wave (Nigg, 1999). Gamma mass scanning is another method of obtaining inertia data on subjects and has been used by Zatsiorsky & Seluyanov (1983) to determine the

inertial parameters of 10 segments in the bodies of living subjects. The gamma radiation beam passes through the body and becomes attenuated as it passes through different substances. A Dual X-ray adsorpiometry (DEXA) scan involves the body being exposed to low doses of x-ray radiation and measuring the transmission of the x-rays through the different areas of the body. It can be used to determine the skeletal muscle mass and bone mass (Fuller et al., 1992).

Linear regression equations are a simple tool for estimating subject-specific inertial parameters. The equations are based on curve-fitting procedures using directly measured data which is limited by the populations used. The equations may require only a few inputs such as mass and height of subject or other anthropometric measurements (Zatsiorsky, 2002). However the linear regression equations developed by Hinrichs (1975) can produce a negative moment of inertia when used outside the subject range. A non-linear regression method was developed by Zatsiorsky et al. (1990) which used measured length and circumferences of segments to calculate subject specific inertia parameters. Yeadon & Morlock (1989) used the data from Chandler et al. (1975) to produce non-linear regression equations that were compared with the linear equivalents. It was concluded that non-linear equations are superior to linear equations and that non-linear regression equations can provide better estimates of segmental inertial parameters even when the anthropometric measurements are outside the sample range.

The method of geometric modelling is to model body segments or their parts as homogeneous solids with simple geometric shapes. Density data are taken from the literature, such as Chandler et al. (1975) or Dempster (1955). For the homogeneous solids the inertial parameters can be computed (Zatsiorsky, 2002).

The technique of geometric modelling to determine inertial parameters has been used by Jensen (1978), Hatze (1980) and Yeadon (1990). Jensen (1978) modelled the human body as elliptical zones using a photogrammetric method. The entire body was sectioned into 2 cm wide zones and represented as 16 segments. The segments were positioned parallel to the body axis and were photographed with the subject. The photographs were digitised and segmented. Segmental inertia parameters as well as whole body inertia parameters were calculated from the digitised records using the density values from Dempster (1955). The body mass calculated using the photogrammetric method was within 2% of the measured body mass.

Hatze (1980) developed a 17-segment model, which required 242 separate measurements as inputs to calculate the inertia parameters. This model included gender differences through the use of density functions and mass distributions. It modelled separate shoulder girdles and segments had neither simple shapes nor assumptions about symmetry. Each segment was assigned a separate density value estimated from the immersion method and a moment of inertia from the suspension method data collected by the author on similar subjects but a different study. The maximum total body mass error was 0.32% for three subjects. This approach seems accurate but can take around 80 minutes which is very time consuming.

Yeadon (1990) developed an 11-segment stadium shape based model requiring 95 anthropometric measurements taken on an individual and used to define the shape of the model. The model estimated the total body masses of three subjects to within 2-3%. If a correction is made for the air contained in the lungs (instead of uniform thoracic density) the total body mass error is reduced to approximately 1% (Nigg & Herzog, 1999). Yeadon (1990) explained that one problem is the effect of breathing when obtaining torso measurements. If the lungs contained an extra one litre of air the volume increase will cause the estimate of the total body mass to increase by 1.5% for a 70 kg subject. The 95 measurements can be performed in 30 minutes, which is a considerably shorter time than that for the Hatze model.

An accurate mass total may not mean an accurate segment moment of inertia because inertia refers to how the mass is distributed, so the mass total could be accurate but the distribution of mass (moment of inertia) not so accurate. Also a good mass total maybe not reflect an accurate distribution of mass between the segments. It is possible that total body mass is acceptable but individual masses of segments may be in error. This modelling approach still requires data from the limited number of cadavers, for example density values, to produce a result.

#### 4.2.2 Anthropometric Data Collection

A total of 95 anthropometric measurements were taken from the subject (an international gymnast with seven years experience) and used as an input to the inertia model of Yeadon (1990). Segmental density values from Chandler (1975) were used as initial estimates in the inertia model. These values were subsequently adjusted until there was an exact match between estimated whole body mass and actual whole body mass as measured during the collection of the anthropometric

measurements. The model splits the body into 13 segments and calculates the inertia parameters for each of the segments. For the purpose of the gymnast simulation model the inertia parameters for each arm or leg were combined to determine the inertia parameters for a 2-D model.

Each segment's inertia parameters were assumed to be values for the combined (trunk, thigh & shank) fixed and soft tissue masses. The gymnast model has seven segments, three of which are segments that comprise a wobbling mass and fixed mass. Using the Parallel Axis Theorem the inertia parameters of the wobbling and fixed masses were determined. One assumption was that the fixed mass of the segment was a uniform cylinder. Ratios of fixed mass to wobbling mass were based upon data from Clarys and Marfell-Jones (1986).

A new fat ratio was calculated using the gymnast's body fat and the subject's body fat in the Clarys & Marfell-Jones (1986) report. The new amount of fat in kilograms was used to re-calculate the percentage of bone to soft tissue for each limb. A full and complete methodology for the determination of the rigid bone to wobbling segments and associated calculation of the segment moment of inertias can be found in Appendix C.

#### 4.2.3 Anthropometric Parameter Determination

The segmental inertial parameters used as an input into the simulation models are presented in Tables 4.1 and 4.2. The distances for the mass centre location are taken from the proximal end of the segment.

**Table 4.1** Amount of Bone and Soft Tissue Mass in Each Segment

Segment	Total mass (kg)	Soft (kg)	Bone (kg)	% Bone	Comments
Lower Foot	0.28	-	-	-	
Upper Foot	2.27	-	-	-	
Lower Leg (shank)	9.54	6.63	2.91	30.5	Using Clarys & Marfell Jones (1986) (Accounting for fat)
Upper Leg (thigh)	19.07	16.08	2.99	15.7	
Trunk (and head)	37.42	30.41	7.01	18.7	
Upper Arm	5.52	-	-	-	
Lower Arm (and hand)	4.10	-	-	-	

**Table 4.2** Segmental Inertia Parameters for Gymnast Model

Segment		Length of Segment (m)	Distance to CofM from proximal end (m)	Moment of Inertia (kg/m <sup>2</sup> ) *
Lower foot	Bone	0.063	0.025	0.000077
	Soft	-	-	-
Upper foot	Bone	0.151	0.70	0.001
	Soft	-	-	-
Lower leg	Bone	0.442	0.221	0.002
	Soft	0.440	0.189	0.009
Upper leg	Bone	0.397	0.1985	0.002
	Soft	0.395	0.162	0.012
Trunk and head	Bone	0.871	0.436	0.03
	Soft	0.869	0.344	0.25
Upper arm	Bone	0.272	0.111	0.0045
	Soft	-	-	-
Lower arm	Bone	0.460	0.171	0.0015
	Soft	-	-	-

(\* = longitudinal axis)

Additional foot anthropometric values were required for the two-segment model of the foot (Figure 4.7). The foot was modelled as two rectangles, one representing the heel to the metatarsal-phlangeal (M-P) joint and the second from the M-P joint to the end of the toes.

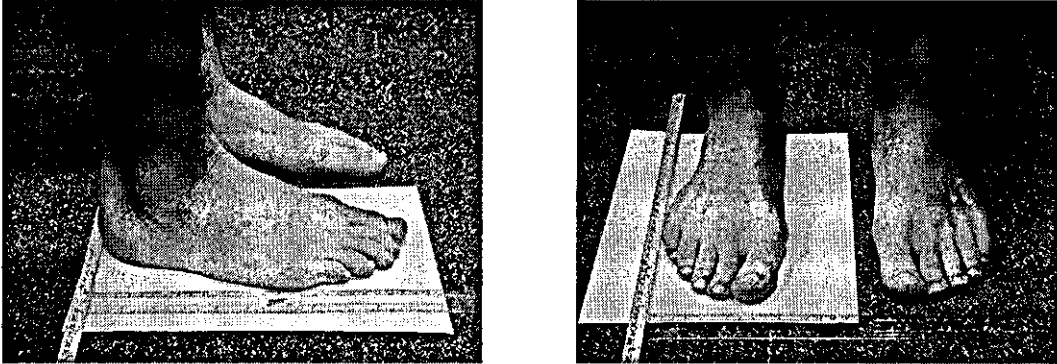


Figure 4.7 Foot measurements.

From the rear of the heel to the M-P joint was 0.151 m, the width at the M-P joint was 0.210 m and the height of the foot vertically from ground to ankle joint was 0.070 m. The ankle joint was located approximately 0.050 m from the rear of the heel.

#### 4.2.4 Anthropometric Measurement – Summary

The results from the anthropometric measurements can be used to develop a subject-specific whole body model of a gymnast. The gymnast model can incorporate the correct segment lengths, distances to centre of mass and moments of inertia. The distribution of mass between bone and soft tissue can be used in the model and the supplementary measurements of the foot can be used to represent the gymnast's foot in the model.

#### 4.2.5 Strength Measurement of Subjects

Human joint motion consists of mainly rotation, although small amounts of translation are present in most joints (e.g. as the knee flexes and extends the joint centre moves back and forth). The small amount of joint translation is usually ignored in whole body models (Gruber et al., 1998; Pain & Challis, 2004; Denoth, 1985; Alexander, 1990). In modelling terms active joint motion can occur via muscles applying moments around joints (Denoth, 1985; Cole et al. 1996; Spagale et

al., 1999). This approach requires knowledge of the line of action of the muscle, the effective moment arm and all its mechanical properties together with the estimation of muscle mass whilst moving and the muscle's activation profile.

An alternative method of active joint motion was used by Pain & Challis (2004) and Gruber et al. (1998) who used rotational spring-damper actuators to control joint motion. This approach gives the net muscle forces driving the kinematics. A common approach to the rotational actuators is that of a joint torque generator with 'muscle-like' parameters (King & Yeadon, 2002; Wilson et al., 2004; Alexander, 1990). The torque generator approach has the advantage of allowing subject joint torque parameters to be measured via isokinetic dynamometry and used in the whole body model. To determine these 'muscle-like' parameters the strength of the subject must be measured.

Isokinetic dynamometers have frequently been used to determine in vivo properties of human skeletal muscles (Herzog, 1988). Isokinetic dynamometry is the assessment of the dynamic function of a joint during movements at a controlled velocity (Baltzopoulos, 1997). Measurement of net joint torques can be recorded and used to provide an insight into muscle function and the muscle performance data can be used for various modelling purposes.

Constant angular velocity conditions require the application of a resistive dynamometer moment, equal to the resultant moment applied to the crank arm, over the range of movement. The resultant moment is the effect of the muscle groups and other forces such as gravitational forces. The maximum angular velocity available in most isokinetic dynamometers is around 5 to 7 rad/s concentric and 2.5 to 4.5 rad/s eccentric (Baltzopoulos, 1997). The manual for the Cybex Norm isokinetic dynamometer permits an angular velocity of 500°/s (8.7 rad/s) concentric and 300°/s (5.2 rad/s) eccentric. However the machine was successfully programmed to accept eccentric angular velocities up to 450°/s (7.85 rad/s).

Herzog (1998) reported differences between resultant moments at a joint and the moments measured by an isokinetic dynamometer. These differences were shown to be due to gravitational effects, inertia effects and non-rigidity of the Cybex arm / shank – foot system. Results showed 2.7% to 17% differences between actual resultant joint moment and Cybex dynamometer recorded moments. These differences cannot be neglected if basic muscle properties such as length-tension and force-velocity relationships are to be investigated.



Winter et al. (1981) said that far too often gravitational forces have not been taken into account and the error involved is significant. When gravitational errors are not corrected for the weight of the crank arm and human limb can be as much as 24% of the total torque produced (Herzog, 1988; Winter et al., 1981). Typically the error is greatest when the crank arm and limb reach a horizontal position. This is due to the geometry defining the biggest moment arm at this point and the muscles producing the least amount of torque, so the influence of weight is much larger than at other joint angles. Torque values are underestimated if the subject is working against gravity and is overestimated if the subject is working with gravity. Herzog (1988) used an equation to correct for crank arm and limb weight that is based on joint angle and dynamometer arm angle. An alternative is to perform the movement in the horizontal plane to eliminate the effects of gravity on the results.

Sapega et al. (1982) found that errors in torque values were due to the initial acceleration of the crank arm to the pre-set angular velocity. It was found that the crank arm accelerated beyond the pre-set velocity and then decelerated until the pre-set angular velocity was reached (Herzog, 1988). However Herzog (1988) also reported that errors were small at an angular velocity of 120 °/s and remained small up to 240 °/s. An error of 0.3% showed that the non-constant angular velocity of the input arm does not contribute much to the differences and thus the assumption of constant velocity is good, at least in the midsections of the exercise and up to an angular velocity of 240 °/s. If 240 °/s is exceeded errors increase and the range of the exercise containing accurate data is reduced. However it was not stated exactly how much the error increases as the angular velocity increases beyond 240 °/s but simply that it should be accounted for. Additional errors in determining limb velocity in the extremes of the movement may occur due to compression of the padding of the limb - crank interface.

The crank arm's axis of rotation and the subject's limb joint axis are assumed to be equivalent. Herzog (1988) acknowledged that if the axes are carefully aligned and the subject is strapped firmly to the dynamometer the differences can be kept small and may be neglected. Herzog (1988) reported an error of less than 2.2% between the angle of the crank arm and limb joint axes during knee extension trials. This value seems rather low as compression of the soft padding on the seat and straps during loading may increase the angle difference between crank and limb.

King & Yeadon (2002) reported a maximum difference of 35° between crank angle and knee joint angle during isovelocity trials.

Gravity corrections, pre-set angular velocities less than 240 °/s and correctly aligned joint and crank arm axis increases the reliability of isokinetic dynamometry testing but ultimately reliability is machine dependent.

#### 4.2.6 Strength Measurement Data Collection

An isovelocity dynamometer (Cybex Norm) was used to measure isometric and isovelocity joint torques. Four joints were tested in the following order: right knee, hip, shoulder and ankle. The subject performed isometric and isovelocity trials on the knee, hip and shoulder. The ankle was only measured isometrically.

The Cybex Norm was set-up according to the manufacturer's manual. A laptop was connected to the auxiliary output socket of the Cybex Norm via a custom built box. This provided a direct method of recording crank angle and crank torque via the voltage output. A spirit level was used to vertically align the crank arm prior to testing.

Four isometric peak torques with the crank arm horizontal were recorded. The first was with the mass of the crank arm and associated padding. The remainder were with three different weights attached to the crank arm. The crank arm length was 0.36 m. The actual torque ( $T_{\text{actual}}$ ) exerted on the crank can be calculated using the following equation:

$$T_{\text{actual}} = m.g.d \quad (4.12)$$

where:  $m$  = mass of load

$g$  = acceleration due to gravity ( $9.81 \text{ms}^{-2}$ )

$d$  = length of crank arm

$T_{\text{actual}}$  was corrected for the weight of the crank arm (Herzog, 1988; Winter et al., 1981) and compared to the torque displayed by the Cybex Norm software on the computer monitor ( $T_{\text{mon}}$ ). The average systematic difference between the two torque values was 0.9%. This difference may have been due to the a slight inaccuracy when measuring the test masses. Table 4.3 summarises the calibration results.

**Table 4.3** Comparison of the Calculated Torque and Cybex Machine Torque on the Monitor

Test Mass (kg)	T <sub>actual</sub> (Nm)	Corrected T <sub>actual</sub> (Nm)	T <sub>mon</sub> (Nm)	% difference
Crank Arm	-	-	8	-
89.0	314	322	321	0.3
77.3	273	281	283	0.7
68.7	243	251	255	1.6

For each of the three test mass trials a voltage history (1000Hz) was recorded via a laptop corresponding to the torque displayed on the Cybex monitor. The voltage output (V) was linearly regressed against T<sub>mon</sub> to obtain the following equation (Figure 4.8):

$$T_{\text{mon}} = 75.838 \cdot V \quad (4.13)$$

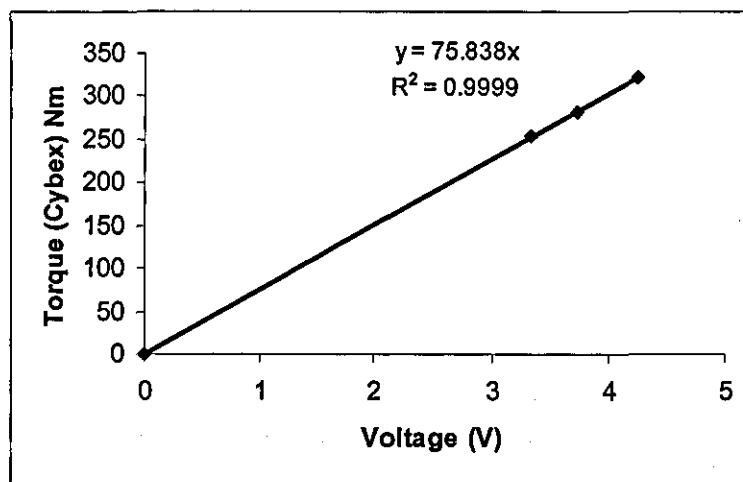


**Figure 4.8** Linear regression of Cybex torque against voltage output (RMS = 1.9 Nm).

The measurement procedures were explained to the subject in accordance with Loughborough University ethical guidelines and an informed consent form was signed (Appendix E). The dynamometer was adjusted to ensure that the segmental joint centre being measured was aligned with the crank joint centre (Herzog, 1988). This was achieved by measuring the offset of the crank arm centre and the joint centre during maximal effort because the soft padding compressed during testing. This offset was accounted for during rest to ensure during maximal effort the subject's joint centre and crank arm centre were correctly aligned. This proved more

difficult at the shoulder joint as it was harder to securely strap the subject in the correct position. However the subject was strapped as securely as possible to the dynamometer using the straps provided by the manufacturer (Figure 4.9).

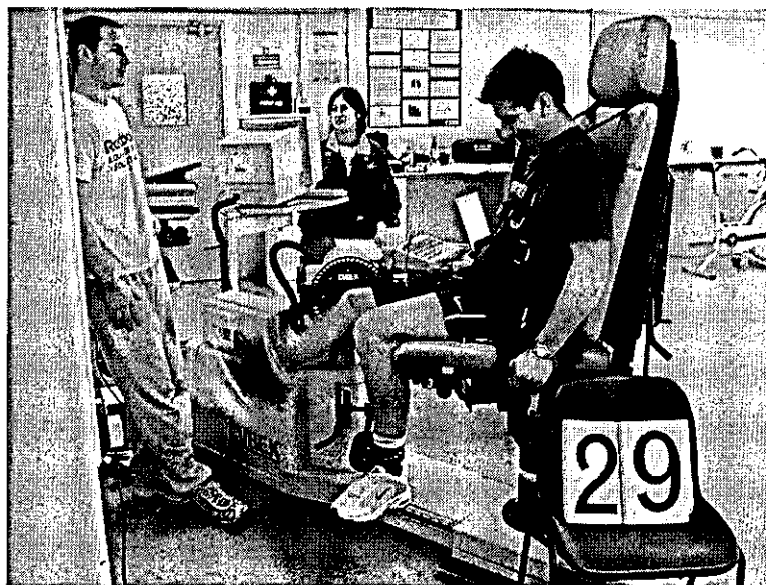


**Figure 4.9** Subject strapped to Cybex Norm dynamometer.

At each joint the maximum range of motion (ROM) was determined. A safety range was set according to the Cybex Norm software. The subject performed a few sub-maximal trials in order to become accustomed to the equipment. Six passive trials were performed throughout the joint range at the knee and two passive isometric trials were performed at the other joints, one with the crank arm at horizontal and the other approximately half way in the ROM. The subject was asked to relax and let the crank arm take the weight of the limb. The torque due to the crank arm weight and limb weight was recorded (Winter et al., 1981).

Both isometric flexion and extension were performed at six angles throughout the ROM at the knee and ankle joints. The angles were evenly distributed within the ROM. Isometric trials were also performed at the minimum and maximum ROM for the hip and shoulder joints. A goniometer was used to measure the joint angle during each trial to later determine the difference between the crank arm angle and the subject joint angle (Herzog, 1988). Following the isometric trials, isovelocitry trials were conducted at crank angular velocities of 50°/s, 100°, 150°/s, 200°/s, 250°/s, 300°/s, 350°/s and 400°/s (450°/s at the knee).

Two cycles of concentric-eccentric contractions were performed at each velocity at each joint. The subject was asked to exert maximum effort during each trial.

After the completion of the isometric and isovelocity trials using one muscle group the subject was allowed to take a break before continuing with the opposite muscle group. The testing sequence was knee extension, knee flexion, hip extension, hip flexion, shoulder flexion, shoulder extension, ankle plantar flexion and ankle dorsi flexion.

#### 4.2.7 Strength Measurement Data Analysis and Parameter Determination

For all isometric trials the torque time history was obtained via the voltage time history using the equation based upon the linear regression (Figure 4.8). A period of time was identified over which the isometric torque was the most stable closest to and including the maximum torque (Figure 4.10). The average torque over this period was used and was corrected for limb weight based on the passive trials. The data from the passive trials was angle dependent and the data suggested a linear relationship. This cannot be correct from a purely theoretical point of view since the torque is related to the perpendicular distance to the axis of rotation and as the angle increases ( $0^\circ$  was horizontal, and  $90^\circ$  was vertical) the torque should decrease as a sine wave. As a result of studying the video of the trials it was evident that small shifts in the subject's body position through the ROM due to seat padding deformation during the passive trials could have led to the linear results. The linear results were used as it was thought that this best represented the actual passive torque associated with small changes in body position during maximum isometric trials, since during maximal isovelocity measurements the subject may also make the same small body position movements. The data were used to fit a linear equation (passive torque versus joint angle); the fitted equation was used to calculate the passive torque at each isometric angle at each joint. Table 4.4 shows the isometric joint angles measured via the goniometer (maximum knee extension was  $180^\circ$ ), the maximum torque reported by the Cybex machine and the joint torques calculated from the output voltage with the passive correction. For knee extension the torque acting clockwise (passive) was added to the torque acting anti-clockwise to produce the corrected torque.

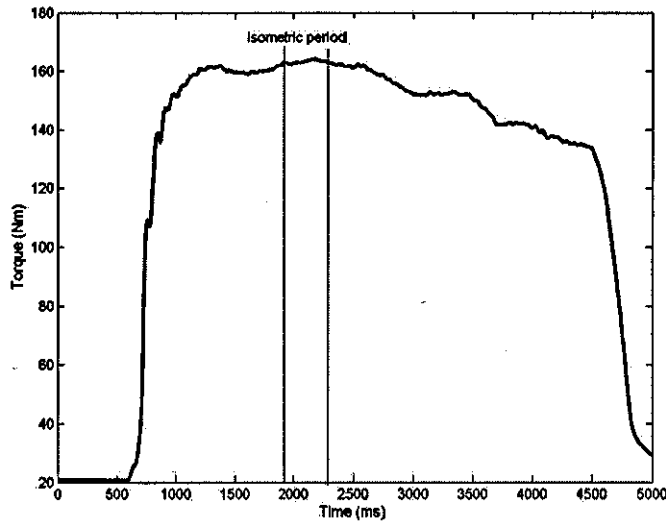


Figure 4.10 Identification of isometric period.

Table 4.4 Isometric Knee Extension Torques at Different Angles within the ROM

Joint Angle (°)	Max. Torque Cybex (Nm)	Max Torque (Voltage) (Nm)	Average Torque (Voltage) over isometric period (Nm)	Passive torque (Nm)	Corrected Torque (Nm)
172	63	66	65	25	90
162	147	152	151	20	171
148	208	215	210	16	226
139	247	254	251	13	264
122	256	263	261	8	269
92	203	209	208	0	208

Figures 4.11 and 4.12 show the relationship between isometric corrected joint torque and joint angle for both flexion and extension at the knee and ankle joint respectively. The isometric joint torques at the hip and shoulder were determined using the isovelocity trials and two isometric joint torques.

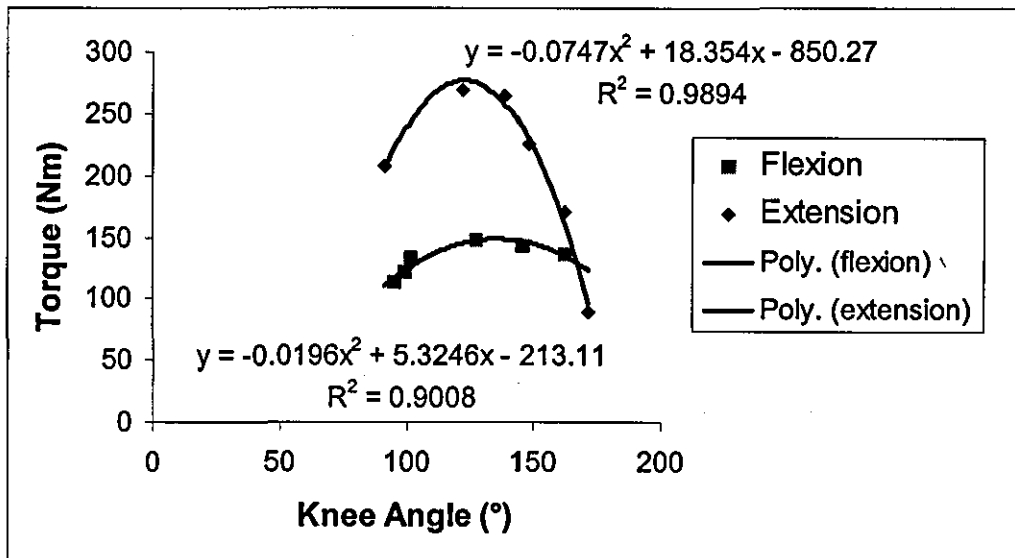


Figure 4.11 Isometric corrected torque data for KNEE flexion and extension.

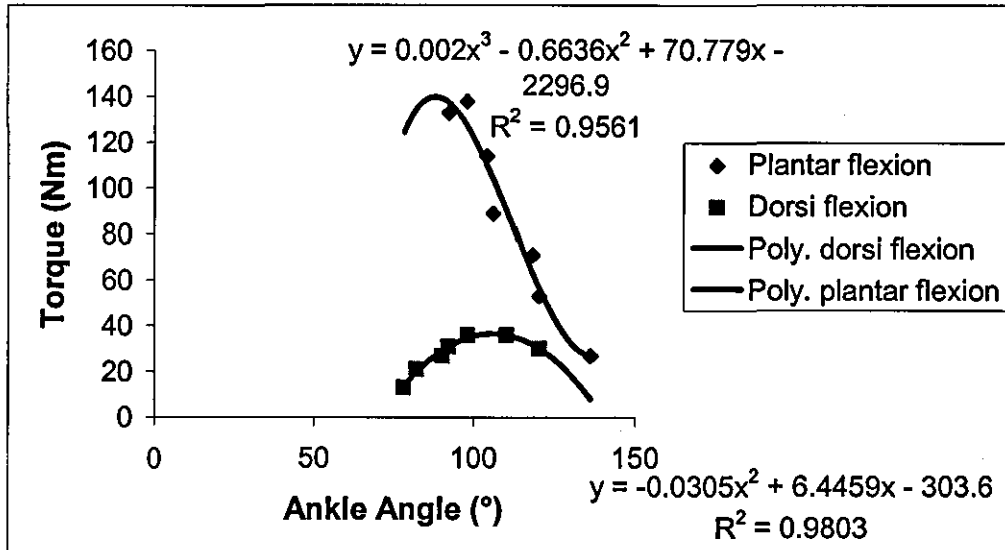


Figure 4.12 Isometric corrected torque data for ANKLE plantar flexion and dorsi flexion.

During isovelocitry trials an additional voltage output was required to determine crank angle. Crank angle was linearly regressed against voltage (Figure 4.13) and the equation for the relationship between crank angle and voltage was:

$$\theta_{\text{crank}} = 61.982 V - 259.99 \quad (4.14)$$

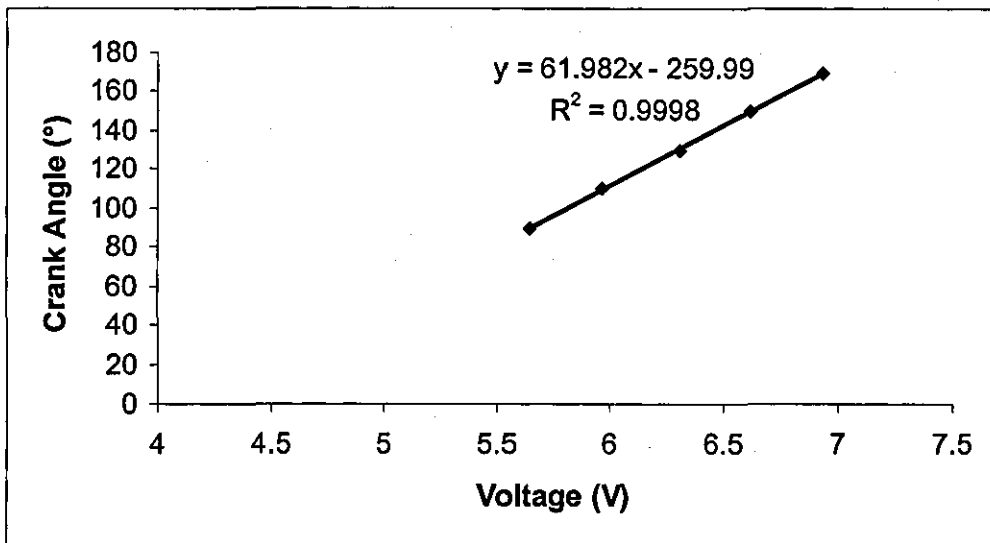


Figure 4.13 Linear regression of crank angle against voltage output (RMS = 0.72°).

The limb and crank arm weight correction procedure used in the isometric trials was applied to the isovelocity trials. During the isovelocity trials the segments adjacent to a joint moved from their resting positions during muscular contraction. Therefore the angle calculated from the voltage output was the crank angle and not the joint angle. The crank angular velocity was determined by the Cybex machine over the crank range. However the joint did not move through the same range in the same amount of time, reducing the joint angular velocity. The joint angular velocity was calculated by using the crank range and time and the joint range and time. For example:

$$\text{Crank range} = 102^\circ \text{ at } 50^\circ/\text{s} = 2.04\text{s}$$

$$\text{Joint range} = 80^\circ / 2.04\text{s} = 39^\circ/\text{s}$$

Although the crank angular velocity was 50 °/s the joint angular velocity was only 39 °/s. This approach was used for the knee, hip and shoulder. Using the angle data, periods of constant velocity were identified during which the peak eccentric and concentric torque occurred (Figure 4.14).



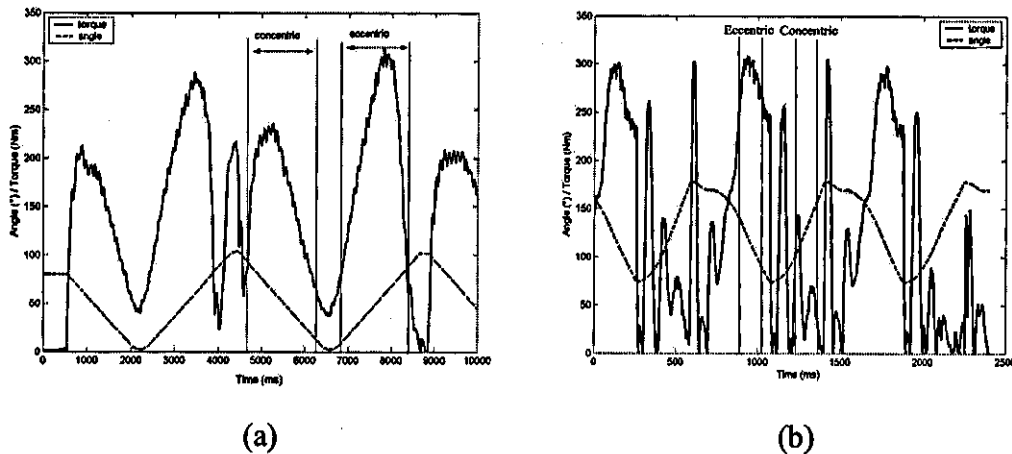


**Figure 4.14** Identification of concentric and eccentric torque during constant angular velocity (knee extension at (a) 50°/s and (b) 450°/s).

The MatLab software was used to correct the joint torque for the passive component, identify the maximum torque and the joint angle at which the torque occurred and calculate the average torque over the period of constant angular velocity.

Joint angle was calculated from Cybex crank angle using the following equation:

$$\theta_{joint} = \theta_{cybex} + (A_{max} * (1 - \frac{\theta_{cybex} - C_{min}}{C_{range}})) + (A_{min} * (1 - \frac{C_{max} - \theta_{cybex}}{C_{range}})) \quad (4.15)$$

$A_{max}$  = joint angle at maximum – Cybex angle at maximum

$A_{min}$  = joint angle at minimum – Cybex angle at minimum

$C_{min}$  = Cybex minimum range value

$C_{max}$  = Cybex maximum range value

$C_{range} = C_{max} - C_{min}$

Figure 4.15 shows the maximum torque and average torque versus joint angular velocity.

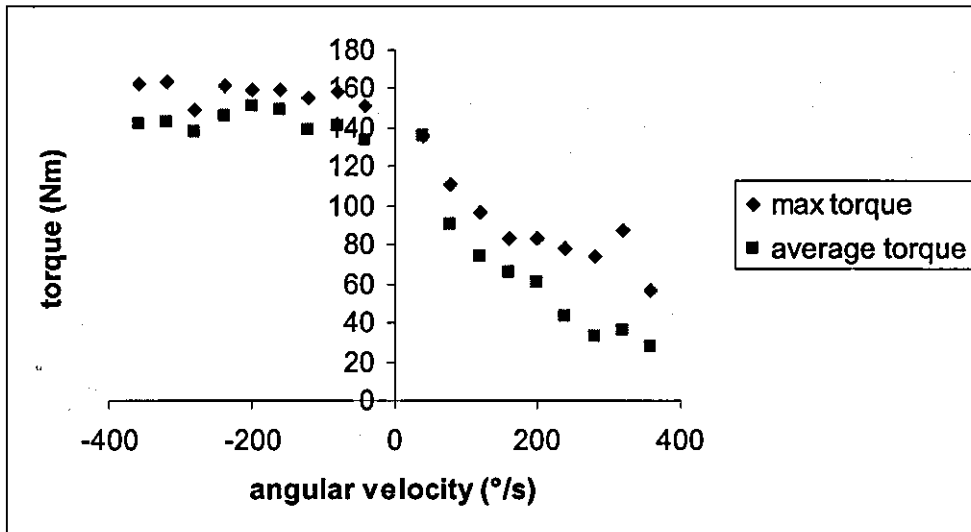


**Figure 4.15** Maximum and average torque versus joint angular velocity (knee flexion).

Using the data produced with the MatLab software, the torque value at zero angular velocity was calculated by taking the average of the lowest eccentric and concentric angular velocities. Table 4.5 compares the calculated  $T_0$  and joint angle to the torque and joint angle measured isometrically.

**Table 4.5** Isometric Torques Obtained from Isovelocity and Isometric Data

Joint & Movement	Torque - isovelocity (Nm)	Joint angle (°)	Torque - isometric (Nm)	Joint angle (°)
Knee extension	282.5	126	269	122
Knee Flexion	143.5	148	143	146
Hip Extension	239.0	49	-	-
Hip Flexion	88.0	68	-	-
Shoulder Extension	110	85	-	-
Shoulder Flexion	91.5	131	-	-

A function was required to fit the experimental data representing the behaviour of the muscles. The function comprised of a four-parameter function defining the eccentric and concentric phases of muscle contraction (two hyperbolic functions) and three parameters representing the differential activation of the

muscle. The maximum torque values were fitted to a rotational equivalent of Hill's hyperbolic function for the concentric phase and another rectangular hyperbola for the eccentric phase. This was achieved using the Simulated Annealing Optimisation algorithm (Corana et al., 1987) to minimise the RMS difference between the subject maximum torque values and the values obtained via the functions. The four-parameter function (Yeadon et al., 2005) used the equations 4.16 to 4.21.

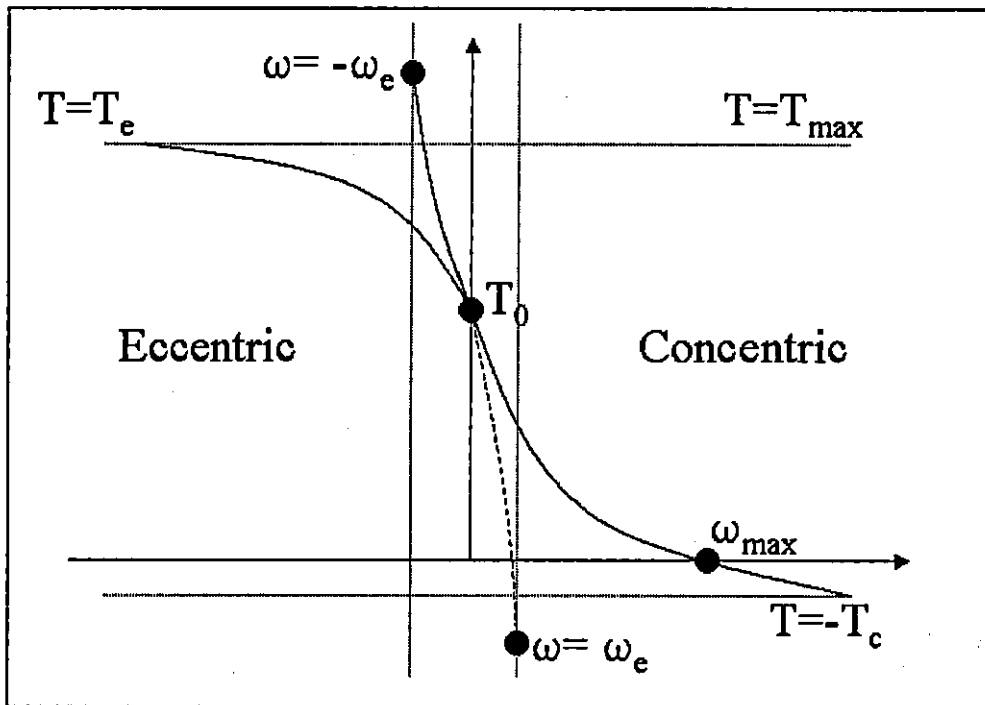


**Figure 4.16** Concentric (Hill hyperbola) and eccentric torque / angular velocity relationship.

Figure 4.16 shows the relationship between torque ( $T$ ) and angular velocity ( $\omega$ ) where:

$T_0$  = maximum isometric torque

$T_{\max}$  = maximum torque

$\omega_{\max}$  = maximum angular velocity when torque equals zero

$T/T_e$  = asymptote of torque in concentric/eccentric hyperbola

$\omega/\omega_e$  = asymptote of angular velocity in concentric/eccentric hyperbola

During the concentric phase the relationship between  $T$  and  $\omega$  is given by the equation:

$$T = \frac{C}{(\omega_c + \omega)} - T_c \quad (4.16)$$

which has asymptotes at  $T = -T_c$  and  $\omega = -\omega_c$ .

where:

$$T_c = \frac{T_0 \omega_c}{\omega_{\max}} \quad (4.17)$$

$$C = T_c(\omega_{\max} + \omega_c) \quad (4.18)$$

During the eccentric phase the relationship between  $T$  and  $\omega$  is given by the equation:

$$T = \frac{E}{(\omega_e + \omega)} + T_{\max} \quad (4.19)$$

where:

$$E = -(T_{\max} - T_0) \cdot \omega_e \quad (4.20)$$

$$\omega_e = \frac{(T_{\max} - T_0)}{kT_0} \cdot \frac{\omega_{\max} \cdot \omega_c}{(\omega_{\max} + \omega_c)} \quad (4.21)$$

$k$  = ratio of the slopes at  $\omega = 0$  for the concentric and eccentric phases (constant)

The two hyperbolas consist of four parameters:  $T_0$ ,  $T_{\max}$ ,  $\omega_c$  and  $\omega_{\max}$  and a  $k$  value for the slope at crossover. The value of  $k$  was set as 4.3, the theoretical value which Huxley (1957) predicted with his original model. A differential activation function (Yeadon et al., 2005) can be used to modify the maximum torque determined by the four-parameter function to better fit the experimental data. Differential activation is based on the fact that during the eccentric phase muscles are inhibited on the isovelocity dynamometer and cannot produce maximum torque. Therefore the muscles are not at maximum torque but some level below, i.e. they are not fully activated. The differential activation function (Figure 4.17) requires three parameters to define the activation level,  $a_{\min}$ ,  $m$  and  $\omega_1$ .

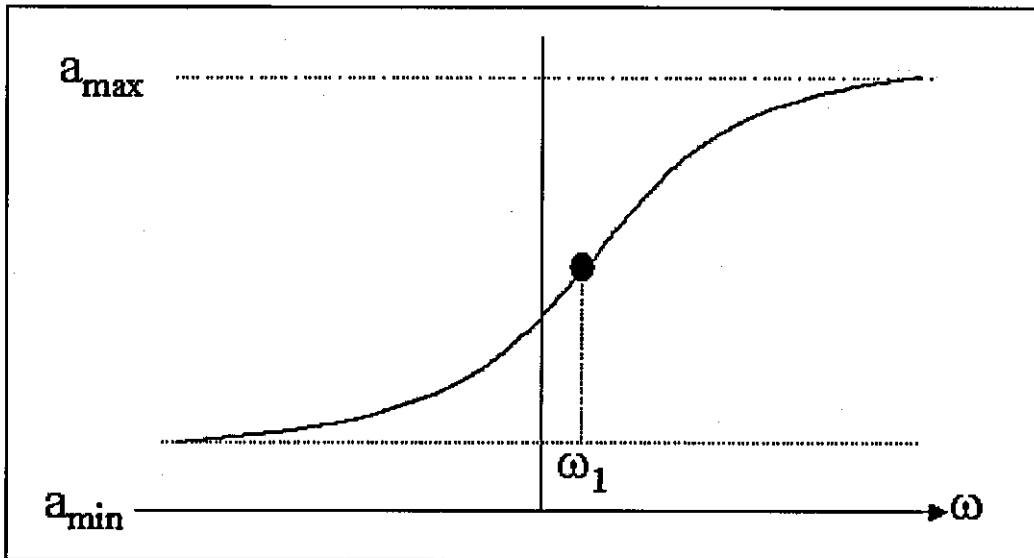


Figure 4.17 Differential activation function.

$$\omega - \omega_1 = \frac{m(a - 0.5(a_{\min} + a_{\max}))}{(a_{\max} - a)(a - a_{\min})} \quad (4.22)$$

$$T = a \cdot T \quad (4.23)$$

where:

$a_{\min}$  = minimum activation level in eccentric phase

$a_{\max}$  = maximum activation level in concentric phase

$m$  ~ the inverse of the slope of activation angular velocity function

$\omega_1$  = angular velocity at mid-point of the slope

To fit the experimental data using Simulated Annealing each parameter must have an upper and lower bound. The bound limits for the seven parameters can be found in Table 4.6.

**Table 4.6** Upper and Lower Limits for the Seven Parameters

Parameter	Lower Bound	Upper Bound
$T_0$ (Nm)	15% less than isovelocity trials	15% larger than isovelocity trials
$T_{max}$ (Nm)	1.5 times $T_0$	1.5 times $T_0$
$\omega_{max}$ ( $^{\circ}$ /s)	1000	2000 / 1600 *
$\omega_c$ ( $^{\circ}$ /s)	100	1000
$a_{min}$	0	0.995
$m$	0.1	25
$\omega_1$ ( $^{\circ}$ /s)	-300	300

\* 2000 $^{\circ}$ /s for the knee and shoulder, 1600 $^{\circ}$ /s for the hip and ankle.

Maximum isometric torques values were measured from isometric trials and calculated from isovelocity trials using the average of the lowest eccentric and concentric angular velocities. These values varied by approximately 5% during knee extension and flexion. In some cases results suggested unrealistically high eccentric torques at 50  $^{\circ}$ /s, this in turn produced an unrealistically high  $T_0$ . It may have been possible that at low angular velocities the subject could have moved his body position a little to increase the amount of body weight contributing to the measurement. It was decided to allow  $T_0$  to vary  $\pm 15\%$  at all joints from the  $T_0$  estimated from the isovelocity ( $\pm 50^{\circ}$ /s) trials. The ratio of eccentric torque  $T_{max}$  to isometric torque  $T_0$  was kept constant at 1.5 (Harry et al., 1990) as it is possible that many combinations of  $a_{min}$  and  $T_{max}$  could result in the correct eccentric torque level.

$\omega_{max}$  was set at either 2000 $^{\circ}$ /s or 1600 $^{\circ}$ /s based upon isolated limb angular velocities found by Jessop & Pain (2005). Jessop & Pain (2005) found that the maximum angular velocity during knee extension was 28 rad/s (1600 $^{\circ}$ /s). An upper limit of 2000 $^{\circ}$ /s was thought reasonable as during the study the knee joint was still producing a torque to overcome the weight of the lower limb and therefore was not at the asymptote required for the 7-parameter fit. It is possible that the upper bound may still be reached during the fitting of the data. However this bound was thought to be realistic and was not increased any higher. A similar rationale using the data from Jessop & Pain (2005) to obtain estimates of maximum limb angular velocities was used for the hip, shoulder and ankle joints.

$a_{\min}$  was constrained to be a positive number between 0 and 0.995; narrower bounds were not required as  $T_{\max}$  and  $T_0$  were fixed.  $m$  was also constrained to be positive to ensure that the gradient of the activation slope increased from  $a_{\min}$  to  $a_{\max}$ .  $\omega_1$  was limited to  $\pm 300$  °/s as maximum activation of the joint torque generators was expected to lie within these bounds. A certain amount of depressed activation was expected but the exact amount was unknown. Allowing  $\omega_1$  to be either positive or negative meant that the amount of torque suppression in the eccentric and concentric phases could be varied.

A score was developed to minimise the root mean square (RMS) difference between the known experimental maximum torques and the calculated torques at each angular velocity. Optimisation results for the seven parameters are shown in Table 4.7. Example curve fits for knee extension and shoulder flexion are shown in Figures 4.18 and 4.19.

**Table 4.7** Optimisation Results for the Seven-Parameter Function

Parameter	Knee Extension	Knee Flexion	Hip Extension	Hip Flexion	Shoulder Extension	Shoulder Flexion
$T_0$ (Nm)	242.2	146.3	239.9	131.9	116.2	85.3
$\omega_{\max}$ (°/s)	2000.0	2000.0	1600.0	1600.0	2000.0	2000.0
$\omega_c$ (°/s)	664.8	381.6	523.4	203.0	577.9	364.4
$a_{\min}$	0.9	0.8	0.8	0.8	0.8	0.9
$m$	15.5	3.6	15.8	5.1	18.4	7.3
$\omega_1$ (°/s)	-130.9	-25.9	-44.4	-17.3	-72.4	-114.0
$T_{\max}$ (Nm)	363.3	219.5	359.9	197.9	174.3	128.0
score (Nm)	19.8	7.9	18.9	20.8	7.4	3.6

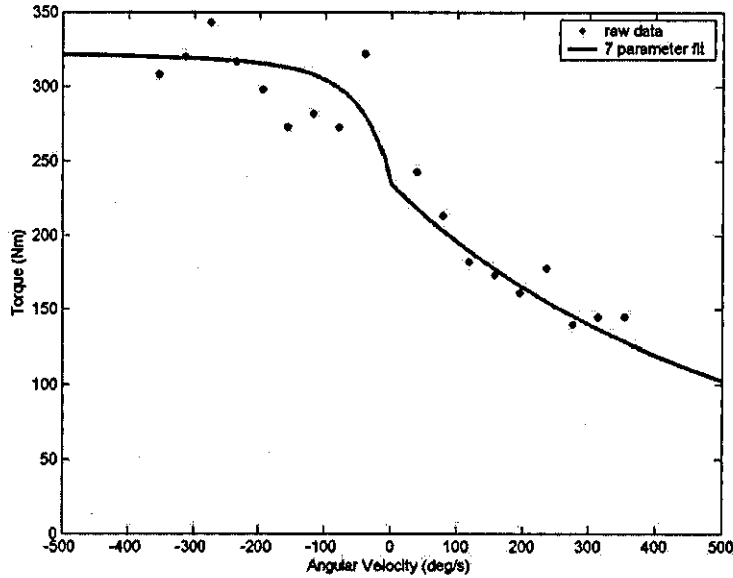


Figure 4.18 Seven parameter fit for knee extension.

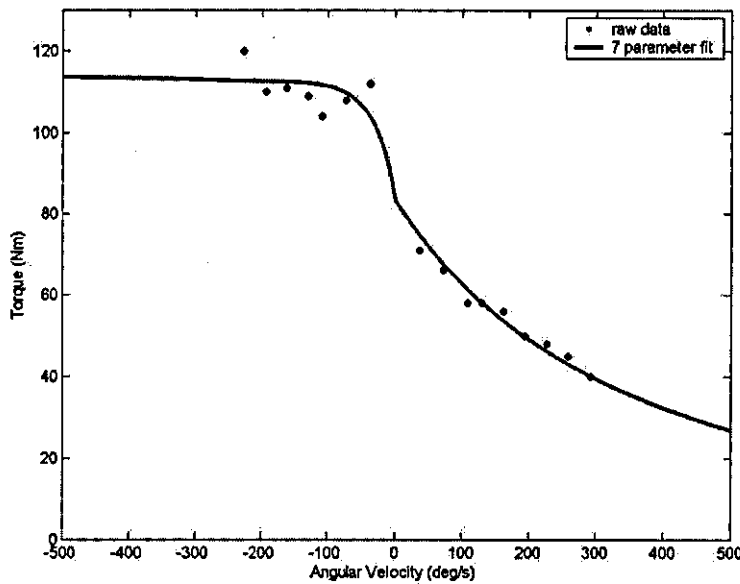


Figure 4.19 Seven parameter fit for shoulder flexion.

Due to the difficulty in collecting isovelocity data at the ankle joint the 7-parameter function at the ankle could not be fitted to the data using the same method as the other joints. The isometric trials at the ankle joint were used to determine  $T_0$ .  $T_{\max}$  was again set at 1.5 times that of  $T_0$ .  $\omega_{\max}$  was set at  $1600^\circ/\text{s}$  and the remaining parameters were calculated from the other joints. To obtain the remaining four parameters for the 7 parameter fit, the average of the parameter values for the other



joints was calculated. Table 4.8 shows the values of the seven parameters for the ankle.

**Table 4.8 Seven Parameters for the Ankle Joint**

Parameter	Ankle Plantar Flexion	Ankle Dorsi Flexion
$T_o$ (Nm)	138	36
$\omega_{max}$ ( $^{\circ}/s$ )	1600	1600
$\omega_c$ ( $^{\circ}/s$ )	588.7	316.3
$a_{min}$	0.83	0.83
$m$	16.6	5.3
$\omega_1$ ( $^{\circ}/s$ )	-82.6	-52.4
$T_{max}$ (Nm)	207	54

The 7-parameter function produces a torque-angular velocity relationship. The torque a human muscle can produce is also dependent upon the joint angle. Therefore a function is required that defines a torque for both a specific joint angle and angular velocity. The torque-angle relationship can be defined using a quadratic function. This function requires a further two parameters.

$$T_{\theta\omega} = T_{\omega} [1 - r(\theta - \theta_{opt})^2] \quad (4.24)$$

- $T_{\theta\omega}$  = angle and angular velocity dependent torque  
 $T_{\omega}$  = 7-parameter angular velocity dependent torque  
 $r$  = rate at which torque drops off from optimal angle  
 $\theta_{opt}$  = optimum angle at which maximum torque occurs

The seven parameters used to determine the torque-angular velocity were kept fixed and the extra two parameters defining the torque-angle relationship were optimised using the subject torque-angle-angular velocity data. The bounds for the parameter  $r$  were 0 to 0.01. The bounds for the parameter  $\theta_{opt}$  were set to the minimum and maximum range of the joint. For each joint a total of nine parameters were used to define the torque-angle-angular velocity relationship. The values for

the 7 + 2 parameters are in Table 4.9 and an example of the 3-D surface fit can be seen in Figure 4.20.

**Table 4.9** Nine Parameters Obtained for the 7 + 2 Parameter Optimisation (Joint angle)

Parameter	Knee Extension	Knee Flexion	Hip Extension	Hip Flexion	Shoulder Extension	Shoulder Flexion
$T_0$ (Nm)	242.2	146.3	239.9	131.9	116.2	85.3
$\omega_{\max}$ ( $^{\circ}/s$ )	2000.0	2000.0	1600.0	1600.0	2000.0	2000.0
$\omega_c$ ( $^{\circ}/s$ )	664.8	381.6	523.4	203.0	577.9	364.4
$a_{\min}$	0.9	0.8	0.8	0.8	0.8	0.9
$m$	15.5	3.6	15.8	5.1	18.4	7.3
$\omega_1$ ( $^{\circ}/s$ )	-130.9	-25.9	-44.4	-17.3	-72.4	-114.0
$T_{\max}$ (Nm)	363.3	219.5	359.9	197.9	174.3	128.0
score	19.8	7.9	18.9	20.8	7.4	3.6
$r$	0.00036	0.00015	0.000061	0.0000043	0.000027	0.000026
$\theta_{\text{opt}}$ ( $^{\circ}$ )	127.3	148.3	56.1	359.5	153.0	155.2
score (Nm)	37.8	14.7	21.8	18.7	11.0	8.3

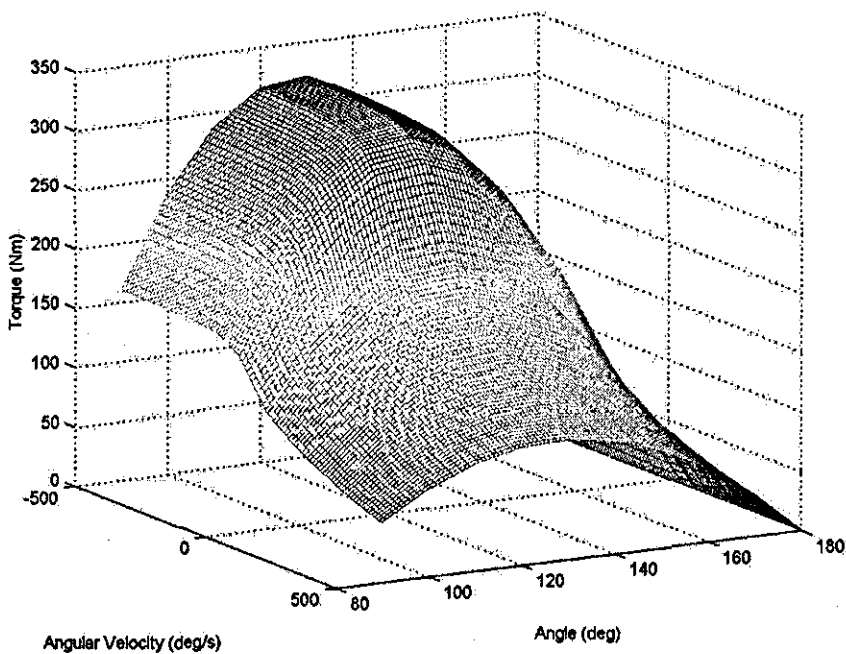


**Figure 4.20** Surface fit using 7 + 2 parameters (Knee Extension).

The extra two parameters for the torque-angle relationship at the ankle joint were determined via the isometric data. The results are in Table 4.10.

**Table 4.10 Ankle Joint 7 + 2 Parameters Determined From Isometric Data**

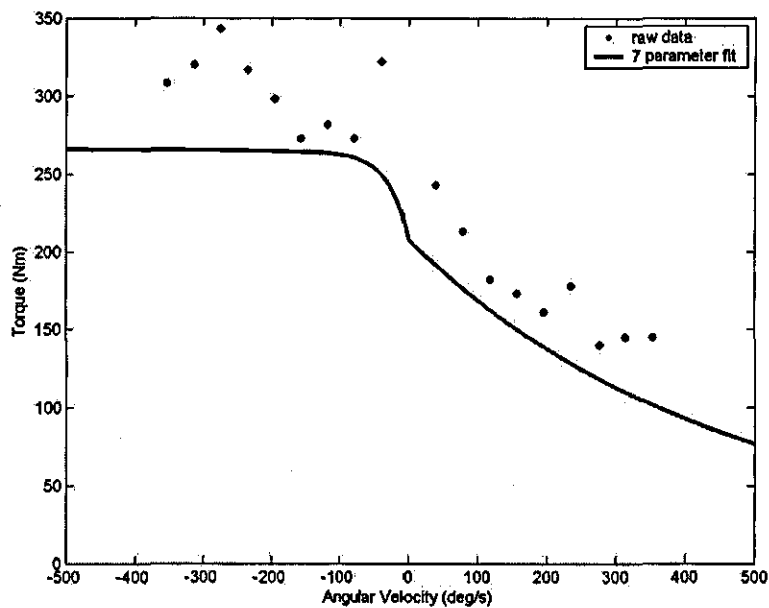
Parameter	Ankle Plantar Flexion	Ankle Dorsi Flexion
$T_o$ (Nm)	138	36
$\omega_{max}$ ( $^{\circ}/s$ )	1600	1600
$\omega_c$ ( $^{\circ}/s$ )	588.7	316.3
$a_{min}$	0.83	0.83
$m$	16.6	5.3
$\omega_1$ ( $^{\circ}/s$ )	-82.6	-52.4
$T_{max}$ (Nm)	207	54
$r$	0.00011	0.000095
$\theta_{opt}$ ( $^{\circ}$ )	98	104

Having determined the nine parameters by firstly optimising seven parameters to obtain the torque-angular velocity relationship, then optimising an additional two parameters to obtain a torque / angle / angular velocity relationship, an attempt was made to fit all nine parameters at one time. The Simulated Annealing algorithm was used to optimise all nine parameters and to minimise the RMS difference between the torque values given by the nine parameter function and the experimental values. It was found that using this method resulted in depressed maximum torques. The reason for this is that Simulated Annealing was attempting to fit the torque-angular velocity part of the surface to the average torque over the range rather than the maximum torque. This resulted in a better RMS score but the data fitted poorly to the maximum torques at each angular velocity. The nine parameters obtained by Simulated Annealing using this method are in Table 4.11.

**Table 4.11** Nine Parameters Determined via 9-Parameter Optimisation

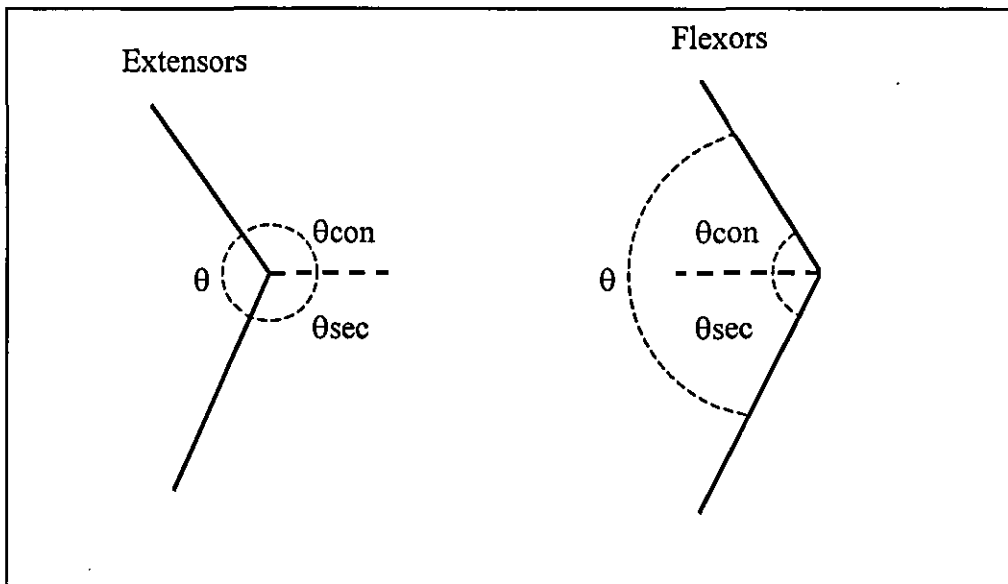
Parameter	Knee Extension	Knee Flexion	Hip Extension	Hip Flexion	Shoulder Extension	Shoulder Flexion
$T_o$ (Nm)	223.2	137.4	215.3	95.1	129.9	91.8
$\omega_{max}$ ( $^{\circ}/s$ )	1531.0	1643.1	1534.5	1132.2	2000.0	1841.8
$\omega_c$ ( $^{\circ}/s$ )	535.8	244.0	889.7	129.2	240.5	298.3
$a_{min}$	0.80	0.76	0.71	0.65	0.60	0.77
$m$	17.4	10.7	24.6	9.8	14.5	6.2
$\omega_1$ ( $^{\circ}/s$ )	-55.7	-24.2	54.3	-23.3	87.0	28.0
$T_{max}$ (Nm)	334.8	206.1	323.0	142.7	194.9	137.7
$r$	0.00035	0.000085	0.0000088	0.000076	0.000035	0.000042
$\theta_{opt}$ ( $^{\circ}$ )	127.7	146.3	134.3	72.8	95.4	132.7
score (Nm)	31.3	10.6	19.8	13.9	6.9	8.7

Figure 4.21 shows the torque-angular velocity fit for knee extension using the 9-parameter optimisation method and also clearly shows the fit being depressed from the maximum torques values.

**Figure 4.21** Knee extension using the 9-parameter optimisation method.

The 7 + 2 parameter method has been chosen for use in future optimisations as it better fits the maximum torque values obtained from the isovelocity dynamometer.

To model the contractile and elastic properties of muscle and tendon separately the torque / angle / angular velocity relationship for the joint angle and velocity must be converted into muscle angle and velocity. The muscle angle is required because a sub-maximal torque at the joint will yield a different muscle and SEC angle to that of a maximal torque produced at the joint. The muscle-tendon model can be incorporated into a whole body model of a gymnast. The muscle-tendon complex comprises a contractile component and a series elastic component (SEC). Figure 4.22 shows how the joint angle is converted into contractile component angle and SEC angle.



**Figure 4.22** The contractile component and SEC of the muscle-tendon complex.

Figure 4.22 can be represented by two equations:

$$\text{Extension} \quad 2\pi = \theta + \theta_{con} + \theta_{sec} \quad (4.25)$$

$$\text{Flexion} \quad \theta = \theta_{con} + \theta_{sec} \quad (4.26)$$

The isovelocity dynamometer measured joint torque produced by the contractile component acting via the SEC. The next stage was to convert joint angle and angular velocity into contractile component angle and angular velocity. King &

Yeadon (2002) showed that for realistic series elastic component extensions, joint angular velocity is approximately equal to the contractile component angular velocity under constant joint velocities. To obtain the contractile component angle from the joint angle the following procedure was used. The torque in the SEC is given by:

$$T_{\text{sec}} = k \theta_{\text{sec}} \quad (4.27)$$

where  $k$  is the stiffness of the SEC

If the torque in the contractile component and the SEC stiffness is known, the SEC angle can be determined by assuming the torque in the SEC is equal to the torque in the contractile component (CC). The CC angle can be calculated from the joint angle and SEC angle. The SEC has been used to represent tendon properties (Wilson et al., 2001). However it is not only the tendon that exhibits elastic properties but parts of the muscle as well (Finni & Komi, 2002; Muramatsu et al., 2001). The aponeuorsis and muscle fibres themselves also have elastic properties that must be included in the model of the SEC. The length of the SEC, the moment arm and the physiological cross-sectional area (pCSA) of the muscle was used to determine the stiffness ( $k$ ) of the SEC. The distance the aponeuorsis extends along the muscle belly was calculated using muscle fibre length ( $L_f$ ) and pennation angle ( $\alpha$ ) (Pierrynowski, 1995). The muscle belly length ( $L_b$ ) and the tendon length ( $L_t$ ) are also required for each muscle of interest to calculate SEC length.

$$\text{SEC length} = L_t + L_b - L_f \cos \alpha \quad (4.28)$$

Table 4.12 summaries the muscles of interest and the associated parameters required to calculate SEC length. The data was taken from Allard et al. (1995). The authors base their data on a male subject of height 178 cms. The subject in this study was male and 178.5 cms in height therefore little scaling was required.

**Table 4.12** Subject SEC Lengths

Joint	Muscles	Pennation angle (°)	Muscle belly length (mm)	Muscle fibre length (mm)	Tendon length (mm)	SEC length (mm)
<b>Ankle</b>	Anterior Tibialis	9	117	99	217	236
	Extensor Digitorum Longus	11	124	101	344	369
	Gastrocnemius	13	237	78	217	378
	Soleus	26	129	49	227	312
<b>Knee</b>	Rectus Femoris	10	302	88	186	401
	Vastus lateralis	11	273	110	138	303
	Vastus medialis	10	360	112	49	299
	Vastus intermedius	6	320	106	87	302
	Biceps femoris	18.5	213	123.5	127	223
	Other hamstrings	9.5	296	127	156	327
<b>Hip</b>	Psoas major	5	238	190	54	103
	Gluteus (all)	5	111	104	73	80
	Sartorius	0	430	538	430	322

To obtain the moment arm length of the corresponding muscle groups a number of different sources were used. Depending upon the measurement method and sample subjects the moment arms for the same muscle varied. Measurement methods included surgical procedures (Delp et al., 1994), MRI scans (Arnold et al., 2000) and calculations of the moment arms based upon various muscle measurements (Duda et al., 1996). Table 4.13 shows the scaled moment arm range for each muscle / tendon for each study and the average moment arm. Only data from male subjects was used due to gender differences related to moment arms. The moment arm was scaled to the subject using the following equations (Forwood et al., 1985):

$$r_{sub} = \sqrt{\frac{m}{L}} \quad (4.29)$$

where  $m$  = mass of the subject,  $L$  = length of subject

$$\text{scaled } d = d \cdot r_{\text{sub}}/r_{\text{lit}} \quad (4.30)$$

where  $d$  = moment arm,  $r_{\text{sub}}$  = subject in present study,  $r_{\text{lit}}$  = subject in literature

The mass of the subject is proportional to volume. The square root of (mass divided by length) is an indicator of depth and any increase in depth could be said to increase the moment arm of a subject.

Although the average moment arm can be calculated using Table 4.13, the moment arms in Jacobs et al. (1996) will be used as the subjects in the study best represent the gymnast in this present study.



**Table 4.13** Summary of Moment Arm Lengths

<b>Muscle / Tendon</b>	<b>Reference</b>	<b>Moment arm range (mm)</b>	<b>Scaled moment arm (mm)</b>	<b>Average scaled moment arm (mm)</b>
TA	Rugg et al. (1990)	34 - 51	34 - 50	42
Achillis Tendon	Rugg et al. (1990)	49 - 60	48 - 59	54
	Maganaris et al. (1998)	44 - 55	44 - 55	50
	Duda et al. (1996)	26	26	26
	Jacobs et al. (1996)	46	42	42
Patella Tendon	Jacobs et al. (1996)	42	39	39
	Duda et al. (1996)	42 - 46	42 - 46	44
Hamstrings	Jacobs et al. (1996)	17 - 26	15 - 24	20
	Duda et al. (1996)	20 - 43	20 - 43	32
Psoas	Duda et al. (1996)	11	11	11
Rectus femoris	Jacobs et al. (1996)	35	33	33
Glutes	Jacobs et al. (1996)	62	59	59
	Duda et al. (1990)	40	40	40

The SEC length was allowed to stretch up to 5% at maximum isometric torque (Finni & Komi, 2002). The calculated change in SEC length was converted into a change in SEC angle by dividing by the moment arm. The torque produced by the subject during maximum isometric contraction was divided by the angle to obtain the SEC stiffness in Newton metres per degree. An example of the calculation procedure can be found in Appendix F. Table 4.14 shows the results of the SEC stiffness calculations based upon a single leg or arm.

**Table 4.14** Subject SEC Stiffness

Joint movement	SEC stiffness (Nm/°)
Ankle plantar flexion	7.5
Ankle dorsi flexion	1.7
Knee extension	11.2
Knee flexion	4.3
Hip extension	66.3
Hip flexion	5.4
Shoulder flexion	26.2*
Shoulder extension	26.2*

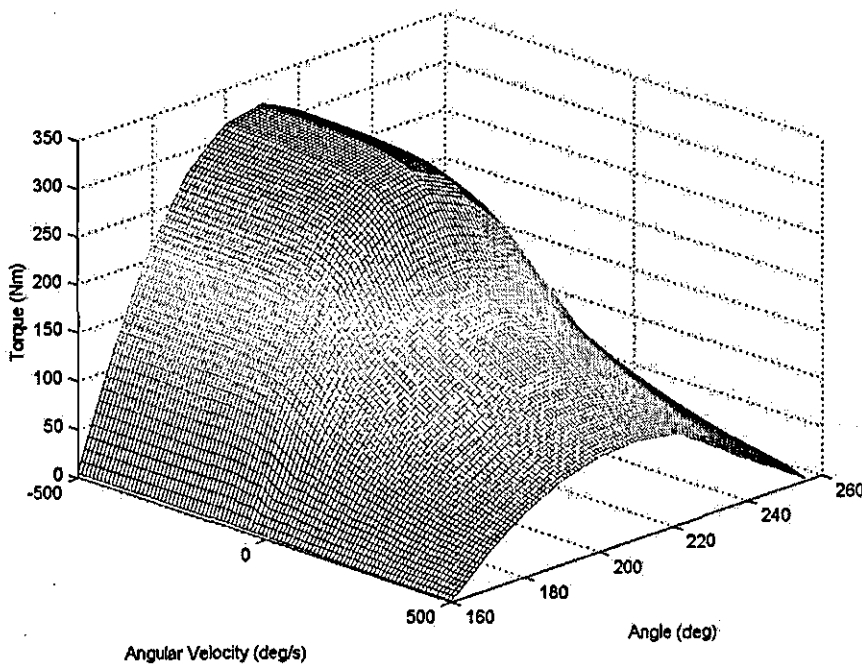
\* no data available for determination of SEC length so SEC stiffness taken from King et al. (1999).

The muscle and SEC angle (Figure 4.22) was used to determine the two angle-dependent parameters of the nine-parameter torque / angle / angular velocity relationship. The seven parameters associated with the torque / angular velocity relationship were kept the same as in Table 4.9. The remaining two parameters were re-optimised using muscle angle (7+2 method). The new values for the two parameters are reported in Table 4.15.

**Table 4.15** The 7 + 2 Parameters for MUSCLE Angle

Parameter	Knee Extension	Knee Flexion	Hip Extension	Hip Flexion	Shoulder Extension	Shoulder Flexion
$T_o$ (Nm)	242.2	146.3	239.9	131.9	116.2	85.3
$\omega_{max}$ ( $^{\circ}/s$ )	2000.0	2000.0	1600.0	1600.0	2000.0	2000.0
$\omega_c$ ( $^{\circ}/s$ )	664.8	381.6	523.4	203.0	577.9	364.4
$a_{min}$	0.9	0.8	0.8	0.8	0.8	0.9
$m$	15.5	3.6	15.8	5.1	18.4	7.3
$\omega_l$ ( $^{\circ}/s$ )	-130.9	-25.9	-44.4	-17.3	-72.4	-114.0
$T_{max}$ (Nm)	363.3	219.5	359.9	197.9	174.3	128.0
Score	19.8	7.9	18.9	20.8	7.4	3.6
$r$	0.00043	0.00066	0.000054	0.0000084	0.0000023	0.0000056
$\theta_{opt}$	207.9	139.0	300.2	260.5	360	117.2
score (Nm)	45.6	12.9	21.9	17.4	8.5	7.6

An example of the surface fit using muscle angle is shown in Figure 4.23. Raw data and 3D surface plots for all joints can be found in Appendix G.

**Figure 4.23** Surface fit using MUSCLE angle (Knee Extension).

The scores were all lower when muscle angle was used instead of joint angle except for knee extension. Knee extension always gave the highest score due to the torque measured at lower angular velocities causing problems with the curve fitting.

The same procedure was used for muscle angle at the ankle joint. The optimum joint angle was converted into muscle angle. Table 4.16 shows the all nine parameters used at the ankle joint after the re-calculating  $\theta_{opt}$  to muscle angle.

**Table 4.16** Ankle Joint 7 + 2 Parameters Determined using MUSCLE Angle

Parameter	Ankle Plantar Flexion	Ankle Dorsi Flexion
$T_o$ (Nm)	138	36
$\omega_{max}$ ( $^{\circ}/s$ )	1600	1600
$\omega_c$ ( $^{\circ}/s$ )	588.7	316.3
$a_{min}$	0.83	0.83
m	16.6	5.3
$\omega_1$ ( $^{\circ}/s$ )	-82.6	-52.4
$T_{max}$ (Nm)	207	54
r	0.00011	0.000095
$\theta_{opt}$	243.6	82.8

#### 4.2.8 Strength Measurement – Summary

Using the isometric and isovelocity data collected, a joint torque-angle-angular velocity relationship was established using a nine-parameter function. Fitting the nine-parameter function to the experimental isovelocity joint torque/angle/angular velocity data meant that the surface will only behave well over the joint angular velocities and joint angles used to calculate the surface. The joint angle was converted into muscle angle and a new set of parameters determined. These can be used in a muscle-tendon model, which in turn can be incorporated into a whole body model of a gymnast.

#### 4.2.9 Wobbling Mass

In biomechanical whole body model calculations of internal kinetics the human body is normally considered to be a series of rigid links connected by simple rotational joints. This approach is used in various levels of complexity and applied

to a wide range of sporting activities. For example, a rigid linked two segment model to represent the lower half of the body when simulating high and long jump take offs was used by Alexander (1990) and a rigid linked two segment model was also used to represent the whole body during a gymnastics vault (King et al., 1999). Three rigid links were used to simulate a drop landing of the whole body (Denoth, 1985). This approach allows the development of simulation models based upon determining the equations of motion from Newton's Second Law of motion.

Although this approach is commonly used, the assumption that humans are a series of rigid links must be questioned. Humans are not made of rigid links and there can be times when this assumption is legitimate and times when it is not. During low acceleration movements such as gentle arm swinging no measurable intra-segmental motion occurs (Luchetti et al., 1998). However during high acceleration activities involving large muscle groups and impacts, 70 mm of segmental motion may occur relative to the underlying bone (Lafortune et al., 1992). Along this continuum there comes a point where modelling the human body as a series of rigid linked segments is not appropriate.

Pain & Challis (2004) used a rigid skeletal structure with a surrounding wobbling mass body, a hollow cylinder with the bone in the centre. The two bodies were connected via two translational spring-dampers allowing the bodies to rotate and translate with respect to each other. Using rigid bodies to represent soft tissue motion ensures that some of the important kinetics of the system are incorporated into the model as a whole. Experimental data and the model's wobbling mass displacements were compared to ensure the simulation model produced realistic soft tissue motion.

#### 4.2.10 Wobbling Mass Parameter Determination

The parameter values from Pain & Challis (2004) were used to ensure realistic soft tissue movement during impact situations (Table 4.17). Using set values was necessary since optimisation of wobbling masses would have increased the total optimisation time. This was not practical with the VN4D model of the gymnast and mat.

**Table 4.17** Spring-damper Parameters for Wobbling Masses (Pain & Challis, 2004)

Model Parameter	Stiffness ( $10^8\text{N}$ )	Damping (Ns/m)
Shank	0.9	280
Thigh	1.8	560
Torso	2.3	700

#### 4.2.11 Wobbling Mass Parameter Evaluation

Subsequent analysis of the wobbling mass displacements during impacts within the whole body model one showed soft tissue displacements similar to that reported by Pain & Challis (2005). This mean soft tissue displacement of the shank was 2.8 cms from all four skills, this compared to 1.8 cms reported by Pain & Challis (2005). The mean thigh soft tissue displacement was 4.4 cm compared to 3.2 cm. Although the simulation soft tissue displacements were higher than those reported by Pain & Challis (2005) it was thought that this may have been due to the greater impact force at landing and therefore these parameters were acceptable for further use in the whole body models.

#### 4.2.12 The Bending Bone

In previous research the rigid body models and wobbling mass models have used rigid segments representing either the whole segment or the bone and wobbling mass. This assumption may be valid in a wide range of situations but how rigid are bones? McNitt-Gray et al. (1993) have reported that humans rely on the lengthening of active muscles and bone deformation during joint flexion to attenuate forces experienced during landing from self-propelled jump heights. The human femoral bones can bend up to 3.6% (lateral displacement) of their unit length before failure with a maximum bending load of 6410 N and a maximum bending moment of 373 Nm using a four point bending test (Martens et al., 1986). Bone deformation during impact absorbs energy from the system and therefore modelling this deformation may be important during impacts at high velocities.

#### 4.2.13 The Bending Bone Parameter Determination

Data were entered into the VN4D FEM of bone to define the bone's behaviour during loading. The parameters used to define the FEM bone were based upon the data from Martin et al. (1998) and were:

Elastic modulus	= $2.5 \times 10^9$ Pa
Poisson's Ratio	= 0.39
Yield Stress	= $5.4 \times 10^7$ Pa
Ultimate Tensile Stress	= $1.7 \times 10^6$ Pa

These parameter values represent the best data available that closely matches the anthropometric characteristics of the subject in this study.

#### 4.2.14 The Bending Bone Parameter Evaluation

The behaviour of the FEM of bone was compared to experimental data on the bending of human (femur) bones. Data from Martens et al., (1986) were used to compare the applied force with the bone deformation. The applied force (6410 N) resulted in a bone deformation (1.70 cm) of the FEM, similar to the experimental data (1.69 cm) (Figure 4.24). Results for the FEM were within 95% of the experimental data.

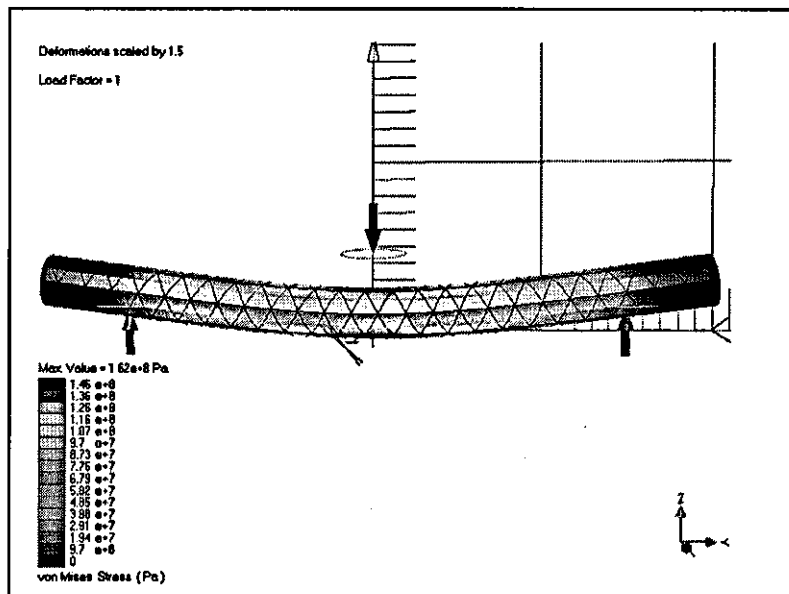


**Figure 4.24** Finite element bone model.

When applying the maximum bending load of 6410 N (Martens et al., 1986) the FEM also reached its ultimate bending limit indicating that the FEM of the bone

would have also fractured. This FEM of bone is suitable for use in a whole body model of a gymnast landing.

#### 4.2.15 The Two Segment Foot

Empirical studies (Gross & Nelson, 1988) have reported that forefoot landings significantly reduce maximum impact force, by up to 22%. If the foot were modelled as a single rigid segment the ground reaction force would be of greater magnitude and shorter duration (Salathe et al., 1990). The foot is actually restrained by flexible tendons, and flexible ligaments holding its many bones together. As the foot deforms during impact the ligaments and tendons stretch to absorb some of the shock. The foot has been modelled using three segments in abnormal foot deformity gait analysis (Henley et al., 2002) and in 3D by seven rigid segments (Arampatzis et al., 2002).

The use of the 3D seven-segment foot (Arampatzis et al., 2002) was thought to be too complex since a planar model of the foot was required for the gymnast model. A three-segment foot was sufficient when investigating dorsiflexion and eversion angles during gait analysis. However the primary focus of the foot in the Henley et al. (2002) model was to represent abnormal feet therefore an extra segment was required to represent the foot deformities.

Gilchrist & Winter (1996) developed a two-segment model of the foot with a joint representing the metatarsal-phalangeal joint. Results for the two-segment foot model were similar to experimental results when modelling the impact phase during gait simulations (Gilchrist & Winter, 1996). A linear torsional spring-damper at the joint was used to represent the viscoelastic effects of the tendons and ligaments in the foot. The torsional spring had a stiffness of 12 Nm/rad and a damping of 0.5 Nms/rad. Sensitivity tests revealed the importance of the parameters values as slight changes  $\pm 10\%$  brought about large errors.

#### 4.2.16 The Two Segment Foot Parameter Determination

The parameter values from Gilchrist & Winter (1996) were used at the torsional spring-damper in the two segment foot. The parameter values were:

Spring stiffness = 12 Nm/rad

Damping Coefficient = 0.5 Nms/rad



These parameters were selected for the foot as optimising the parameters would have increased the total optimisation time. This was not practical with the VN4D model of the gymnast and mat.

#### 4.2.17 The Two Segment Foot Parameter Evaluation

The maximum change in forefoot angle during the simulation of landing for four gymnastic skills was 19°. This compares well with the actual angular displacements (maximum 16°) collected during the subject vault landing data collection. The foot parameters did not appear to be overly sensitive as varying the spring stiffness by 10% only altered the maximum forefoot range by 2° (approx. 10%). These parameters were acceptable for further use in the gymnast-mat models.

#### 4.2.18 The Heel Pad

During impact situations the heel pad plays an important role in force attenuation by deforming. The viscoelastic properties of the heel pad allow it to adapt to different impact velocities. Heel pad properties have been measured using various techniques both in vivo and in vitro, yielding different properties for the heel pad. Computer modelling of the lower limb and heel pad has shown that both in vivo and in vitro tests yield similar heel pad properties once the effect of the lower leg wobbling mass has been removed (Pain & Challis, 2001b). Heel pad models that reproduce the in vivo results of Gilchrist & Winter (1996) and Scott & Winter (1993) have used the rigid segment modelling approach. Heel pad models such as Pain & Challis (2001b) have showed that in vitro heel pad properties are appropriate when the model of the body includes wobbling masses.

#### 4.2.19 The Heel Pad Parameter Determination

The parameter values used to represent the heel pad in the gymnast-mat model were taken from Pain & Challis (2001b) because the gymnast-mat model included wobbling masses in vivo heel pad properties were required. The parameter values used in the gymnast-mat models were:

$$K_1 = 3 \times 10^{15} \text{ N/m}^7$$

$$K_2 = 6 \times 10^{13} \text{ N/m}^5$$

$$K_3 = 3 \times 10^9 \text{ N/m}^3$$

$$K_4 = 3 \times 10^4 \text{ N/m}$$

$$C = 75000 \text{ Ns/m}^2$$

#### 4.2.20 The Heel Pad Parameter Refinement

During the design stage of the gymnast-mat models it was intended that the gymnast model would have a heel pad. Early model testing showed that this would cause a vibration problem at the foot whilst running simulations using a landing mat. The heel pad behaved correctly on a rigid floor in terms of forces and deformations. The landing mat behaved correctly with no heel pad in terms of mat forces, deformations and surface accelerations. When the heel pad is put in series with the mat the heel pad is not dominant and can be removed from the model. A displacement must be used to compare how stiff the heel pad and mat are. If the heel pad deforms 1 cm the force in the heel pad can be calculated. This force can be used to calculate the heel pad stiffness for the amount of heel pad deformation ( $F = kx$ ). This new stiffness ( $k$ ) represents the heel pad stiffness for the given displacement and can be used in the equation below. The total stiffness of the mat and heel pad is given by:

$$k_{total} = \frac{1}{\left(\frac{1}{k_{mat}} + \frac{1}{k_{heelpad}}\right)}$$

$$k_{mat} = 67060 \text{ (from material testing results)}$$

$$k_{total} = 66567 \text{ (assuming heel pad deforms 1cm)}$$

$$\% \text{ difference} = 0.7\%$$

$$k_{total} = 62563 \text{ (assuming heel pad deforms 1mm)}$$

$$\% \text{ difference} = 6.7\% \text{ (4\% peak force using trial 1541)}$$

$$k_{total} = 65537 \text{ (assuming heel pad deforms 5mm)}$$

$$\% \text{ difference} = 2.3\% \text{ (1\% peak force using trial 1541)}$$

The differences reported are differences in total stiffness of the mat compared to the mat and heel pad. These results suggest that because the gymnast is landing on a soft mat the effect of the heel pad is minimal. The risk of injury to the foot and heel pad is low as the heel pad undergoes little deformation, as the mat is much softer. A difference of 0.7% was thought to be acceptable in order to stop the vibration problem within the model. Therefore the heel pad was removed from the gymnast-mat models.

#### 4.2.21 Kinematic and Kinetic Analysis of Landing

Automatic motion tracking systems use 2D data to obtain 3D coordinates that define the position and orientation of a body, typically using a version of the DLT method. The two categories of image-based automatic tracking systems are the active marker system and the passive marker system. Coda (an active marker system) requires an energy supply to the light source, a light-emitting diode (LED). The LED's flash in a given sequence that can be tracked by the cameras allowing for automatic identification of the markers. Each marker requires power and is therefore connected to a power supply via wires which can restrict the subject performing a skill (Allard et al., 1995). Vicon (a passive marker system) uses markers made of a retro-reflective material that reflects light back to the camera. No wires or power supplies are required. However the resolution range can be limited making automatic identification of markers difficult (Yeadon & Challis, 1994). All automatic systems allow faster access to processed data than manually digitising joint centres but the systems are restricted to markers being placed on the subject.

Electromyography (EMG) can provide a method of monitoring the electrical activity associated with muscles generating force. It is possible to use EMG systems, such as Biovision, to estimate activation timings of muscles, the force/EMG signal relationship and the use of the signal as a fatigue index (De Luca, 1997). However many factors can influence the EMG signal. Intrinsic factors include the physiological firing rates of motor units, the type of fibre and the conduction velocity of the muscle fibres. Extrinsic factors include the location of the sensors with respect to the motor end plates and the electrical characteristics of the recording device (Burden & Bartlett, 1997). The placement of the EMG sensors / electrodes is an essential part of reducing noise. The electrodes should be placed over the visual midpoint of the contracted muscle. The muscles do not remain in the same place

during their isometric and dynamic state, the movement of these muscles may introduce crosstalk into the recorded signal by new muscles moving near to or under the electrodes. It is also possible that surrounding muscles may contribute to the EMG signal. The orientation of the electrodes on the muscle belly is also important and should be placed parallel to that of the underlying muscle fibres.

Temporal processing (time domain analysis) can be used to investigate the amount of activity in relation to time. The signal is usually half wave rectified (removal of negative voltages) or full wave rectified (inverting the negative voltages). Following rectification of the signal a method must be chosen to analyse the data. Different methods included average rectified, moving average, root mean square and integrated EMG. The most commonly used method is integrated EMG although data have been widely miscalculated and results misinterpreted (Burden & Bartlett, 1997). Due to this the average EMG is becoming more popular (Burden & Bartlett, 1997). The RMS method gives the power of the signal and is also common in signal processing.

#### 4.2.22 Kinematic and Kinetic Data Collection

The main pieces of equipment used during data collection were:

1. Vicon motion tracking system
2. AMTI force plate
3. Biovision EMG system

1. The kinematic data were collected using the Vicon 624 motion tracking system. Twelve M2 cameras, set at a sampling frequency of 250 Hz, were used to calibrate the volume and record the skills performed by the gymnast. Twenty-five millimetre retro-reflective markers placed on the joint centres recorded positional data of each marker. The markers were placed on the left and right sides of the body at the head, shoulder, elbow, wrist, hip, knee, ankle, metatarsal – phalangeal joint and the toe (Figure 4.25). After the markers were placed on the subject a measurement was taken from the marker centre to the joint centre. This measurement would be used later to calculate the location of the joint centre from the marker placement location using the measured offset. The offset for the shoulder was implemented by using the shoulder and hip makers to define a trunk reference plane then the measured offsets were used to determine the shoulder joint centres.

Static and dynamic calibration of the volume yielded a mean reconstruction error of 1.5 mm. An analogue channel was set up in the Vicon software to receive the external remote signal that was also used to start the force plate recording. This allowed the Vicon and force plate data to be synchronised.

2. An AMTI force plate (1200 mm by 600 mm) located underneath the landing mat was used to collect kinetic data during the skills. The force plate was connected to a DSA-6 DigiAmp that was connected to a Dell laptop computer. The computer used the BioAnalysis software provided by AMTI to record the output from the DigiAmp. The sampling frequency was set at 1000 Hz with a 10% pre-trigger and a sampling time of five seconds. The force plate was triggered via an external remote signal. Upon receiving the external signal the BioAnalysis software began to record the output from the DigiAmp.

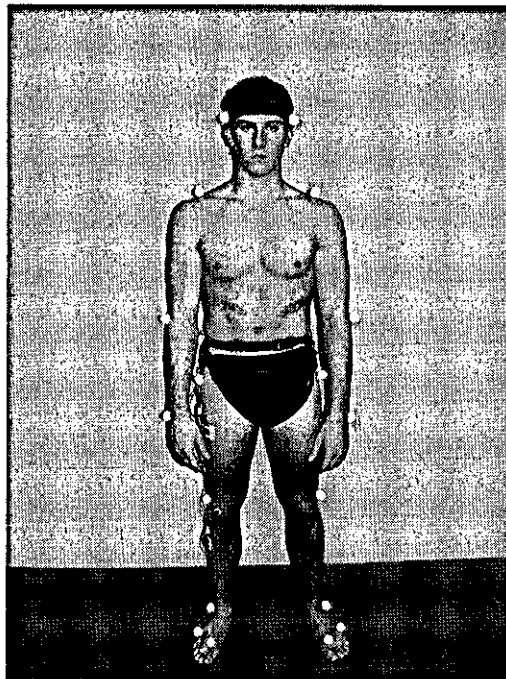


**Figure 4.25** Marker placement on subject.

3. A portable Biovision EMG system with built in amplifiers was used to collect the electrical signals produced by selected muscles during contraction. The selected muscles on the right side of the subject's body were the medial head of the gastrocnemius, tibialis anterior, biceps femoris, vastus lateralis, rectus femoris and gluteus maximus. This allowed the electrical signals of the muscles to be recorded

during each skill. The associated wires and amplifiers were taped to the subject's skin to minimise any movement and hence reduce noise (Figure 4.26). The sampling frequency was set to 1000 Hz and the gain to 3000. An additional channel was set to accept an analogue signal from the external remote trigger used for both the force plate and the Vicon system.

The external remote trigger was used to synchronise all three pieces of equipment. The remote trigger would activate the force plate and simultaneously send a signal to the EMG system and the Vicon system. The trigger would appear as a square pulse on the respective analogue channel.

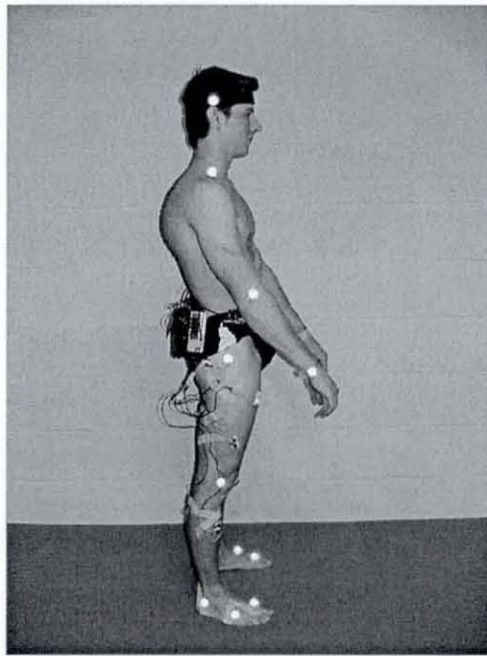


**Figure 4.26** EMG electrode placement.

The testing procedures were explained to the subject in accordance with the Loughborough University ethical guidelines and an informed consent form was signed (Appendix H). The subject was asked to warm up as if in a competition. Following warm up markers and EMG electrodes were placed on the subject. The vault apparatus was set at the men's height (135 cms) and the competition F.I.G. modified landing mat placed correctly (Figure 4.27). The subject was asked to perform four different skills a total of five times each. The first skill was a standing backward somersault starting on the vault table and landing on the landing mat. The

second skill was a standing forward somersault starting from the vault table and landing on the landing mat. Thirdly, the subject was asked to perform any forward rotating vault. Fourthly, the subject was asked to perform any backward rotating vault. Kinematic and kinetic data were collected during the testing of the gymnast whilst performing the different skills.

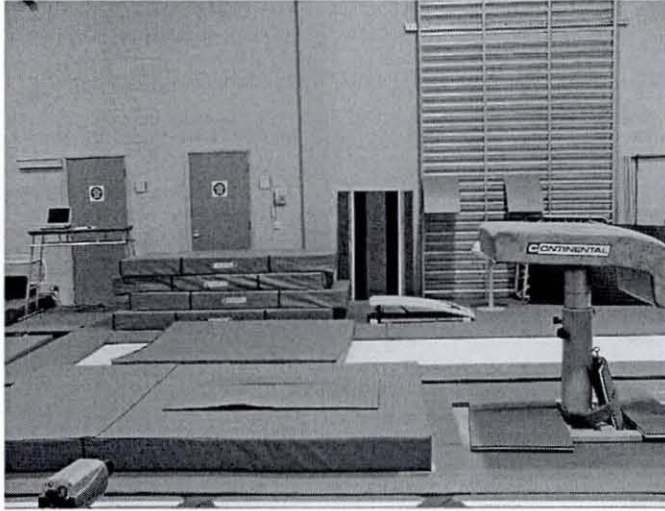


**Figure 4.27** Vault landing equipment set-up.

#### 4.2.23 Kinematic and Kinetic Data Analysis and Parameter Determination

The Vicon software was used to analyse the kinematic data. Within the Vicon Bodybuilder software the marker (landing.mkr) and model (landing.mod) code was developed specifically for this analysis. The markers were assigned labels and joint angles identified. The raw positional data was smoothed using Woltring's generalised cross-validated quintic spline method. The smoothed position data was used to calculate initial impact velocities of the mass centre and joint angle time histories. Tables 4.18, 4.19 and 4.20 show the initial impact velocities during each skill and the initial joint angles and joint angular velocities.

**Table 4.18 Initial Impact Velocities**

<b>Trial Number</b>	<b>Description</b>	<b>Vertical Velocity at Impact (m/s)</b>	<b>Horizontal Velocity at Impact (m/s)</b>
1	Standing back somersault	6.4	1.1
2	Standing front somersault	5.2	0.4
3	Handspring	6.2	2.6
4	Tsukahara	7.5	3.6

**Table 4.19 Initial Joint Angles**

<b>Trial</b>	<b>Shoulder Angle (°)</b>	<b>Hip Angle (°)</b>	<b>Knee Angle (°)</b>	<b>Ankle Angle (°)</b>	<b>MP Angle (°)</b>	<b>Elbow Angle (°)</b>
1	+60	130	165	118	156	180
2	-60	162	143	122	164	165
3	-80	169	154	126	164	176
4	+91	122	157	99	160	156

A graphic representation of the joint angles is shown in Figure 4.28. During the landing of a backward rotating skill the gymnast exhibits a greater amount of knee extension at initial mat contact than that of the forward rotating skills. However greater hip extension is present at initial contact during forward rotating skills than during backward rotating skills.



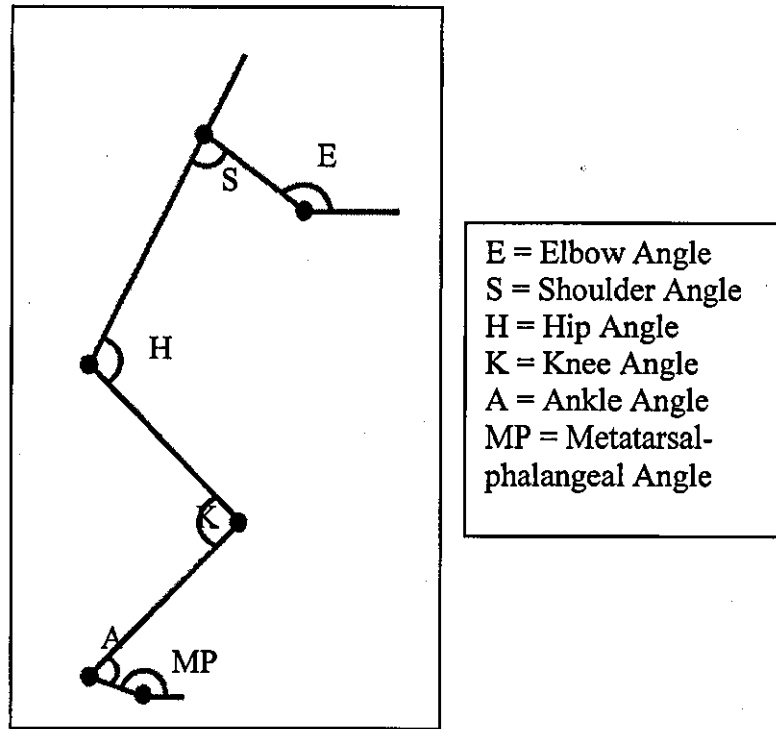


**Figure 4.28** Subject joint angles.

Initial joint angular velocities were calculated by averaging the joint angular velocity over the last 0.08 s prior to mat contact. A positive joint angular velocity indicated that the joint was extending and a negative angular velocity indicated that the joint was flexing (Table 4.20).

**Table 4.20** Initial Joint Angular Velocities

Trial	Shoulder Angular Velocity ( $^{\circ}/s$ )	Hip Angular Velocity ( $^{\circ}/s$ )	Knee Angular Velocity ( $^{\circ}/s$ )	Ankle Angular Velocity ( $^{\circ}/s$ )
1	+150	+75	-50	-50
2	-100	-100	+25	+25
3	-150	-50	-100	+50
4	+250	-50	-150	+100

Figure 4.29 shows an example of the joint angle time histories for each joint during the landing phase of a standing backward somersault (Trial 1).

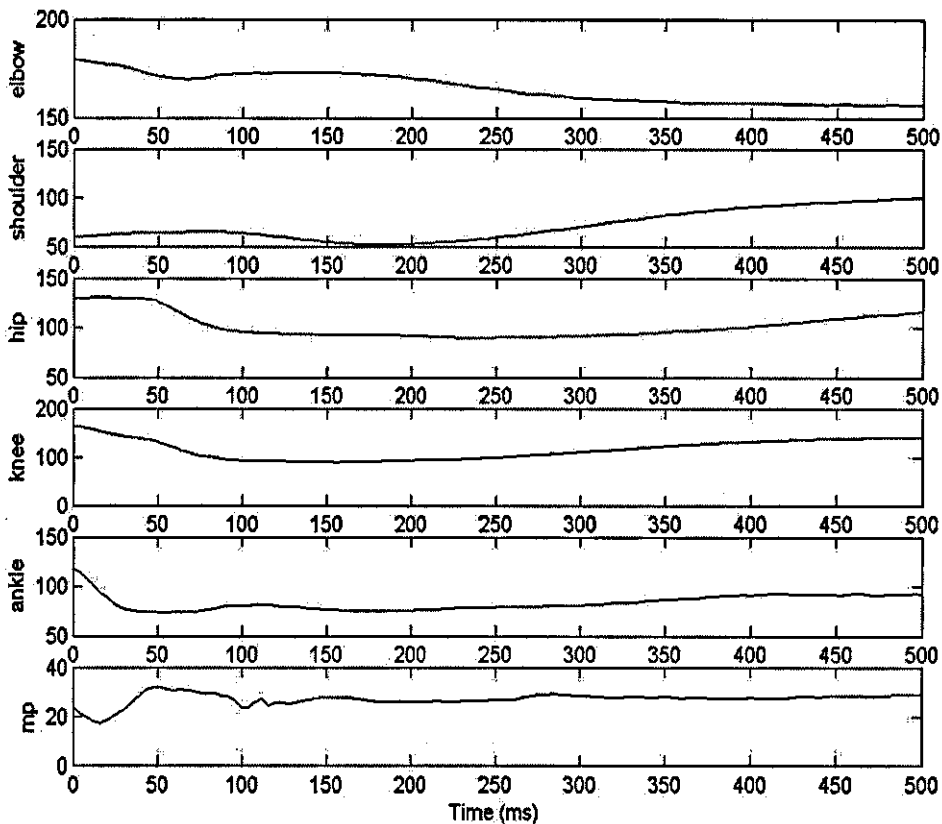


**Figure 4.29** Joint angle time histories (backward somersault).

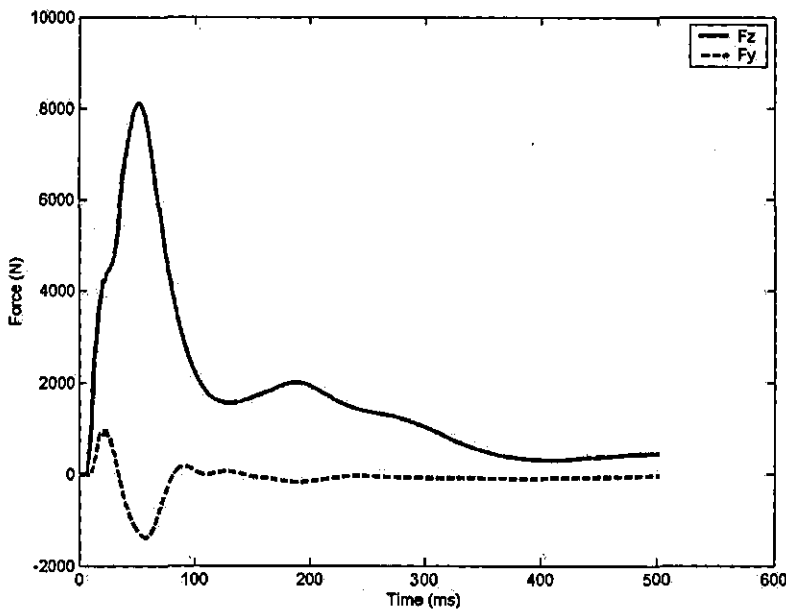
The BioAnalysis software supplied with the AMTI force plate was used to analyse the ground reaction forces associated with each trial. The forces from 6 ms prior to force detection up until 0.5 s into the landing phase were processed for each trial. The 6 ms refers to the average time taken for the shock transmission wave to pass through the mat and register on the force plate (Chapter 3).

Table 4.21 shows the key characteristics of the force time history associated with the landing during each trial.

**Table 4.21** Key Characteristics of the Landing Phase

Trial	Peak Vertical Force (N)	Time to peak (s)	Peak Horizontal Force (N)	Time to peak (s)
1	8107	52	-1395	58
2	8276	53	-1212	57
3	10873	40	-1818	47
4	10903	54	-2590	59

Figure 4.30 shows an example of the force time history for a standing backward somersault (Trial 1).

**Figure 4.30** Force time history of landing during trial 1.

The kinematic and kinetic results show that a greater impact velocity does not necessarily produce a greater peak vertical ground reaction force. For example trial 1 has an impact velocity of 6.4 m/s compared to 5.2 m/s in trial 2 however trial 2 has the greater peak vertical impact force. Chapter 3 has shown that increased impact velocity produces greater impact force when using a rigid body. This suggests that the gymnast's initial body configuration and landing strategy has an influence on the impact force, as the landing mat was the same for all trials. Although the mass centre velocity has been reported it is possible that due to rotation of the legs the actual leg impact velocity could be faster or slower

depending also upon whether the legs are extending or flexing and whether they are rotating with or against the linear momentum of the body.

The Plab software was used with the Biovision EMG system to record the electrical activity in the muscles prior to and during landing. The trigger signal used to activate the force plate produced a square pulse on channel one of the EMG system allowing synchronisation of the force and EMG data. Data prior to impact was used to determine muscle activation levels prior to impact. Data from 50 ms prior to initial mat impact until 0.5 s after impact was processed for each trial. The EMG results could be used to estimate the muscle activation level prior to landing, the ramp up time (time from initial activation level to maximum activation level) and the ramp down times. Figure 4.31 shows a raw full wave rectified EMG signal from the standing backward somersault (Trial 1). The raw EMG signal was processed using a second order Butterworth filter, the cut off frequency was set at 6 Hz. Only the envelope of the EMG was required for the temporal timing. Filtering above this level allowed too much of the raw signal through making it difficult to use for the muscle activation history. Filtering below 6 Hz caused some loss of the underlying signal. Figure 4.32 shows the same EMG data from Trial 1 but filtered at 6 Hz.

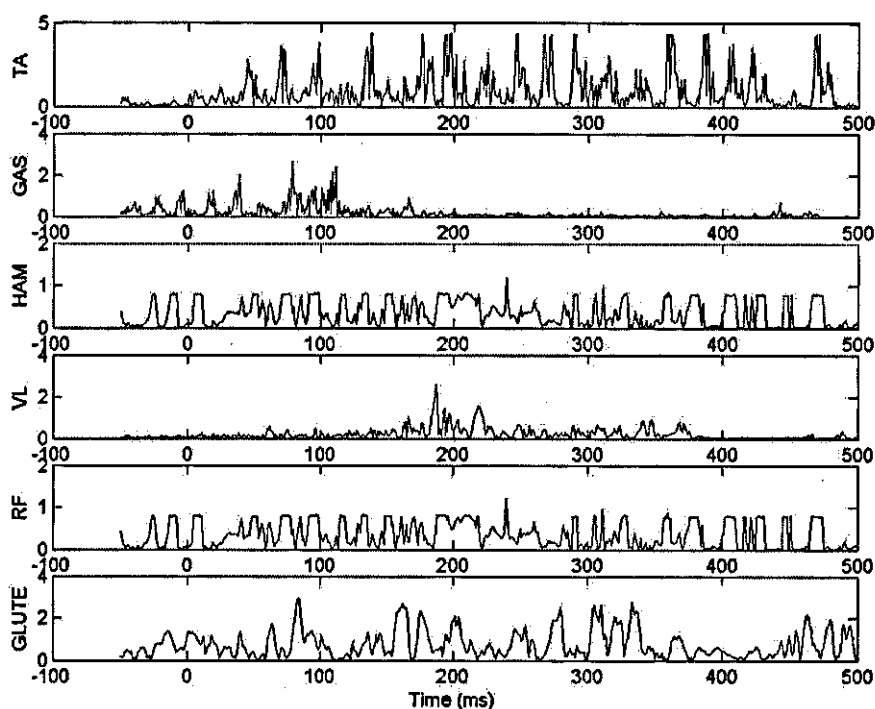
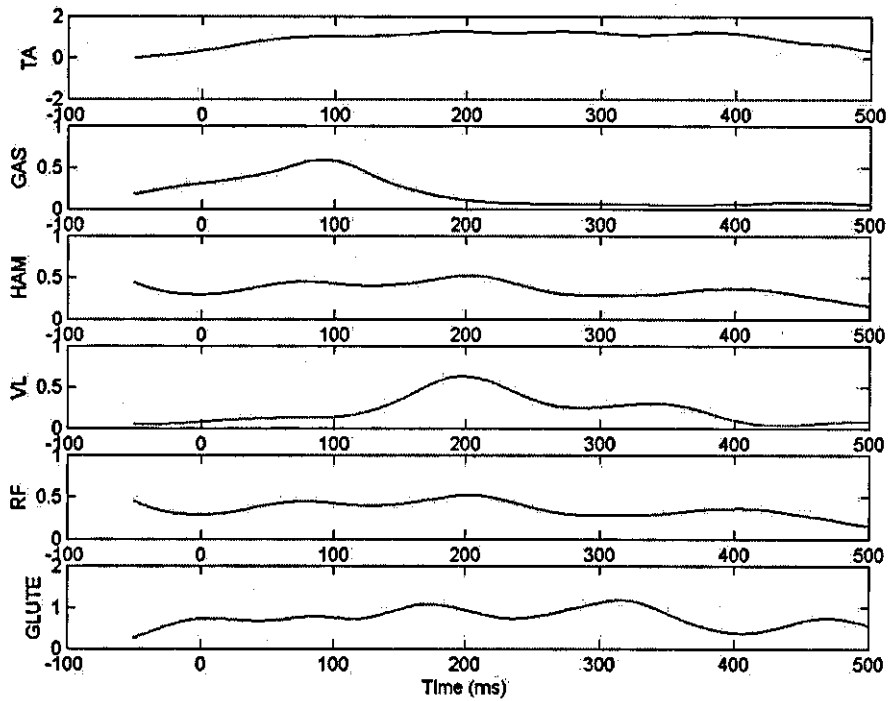
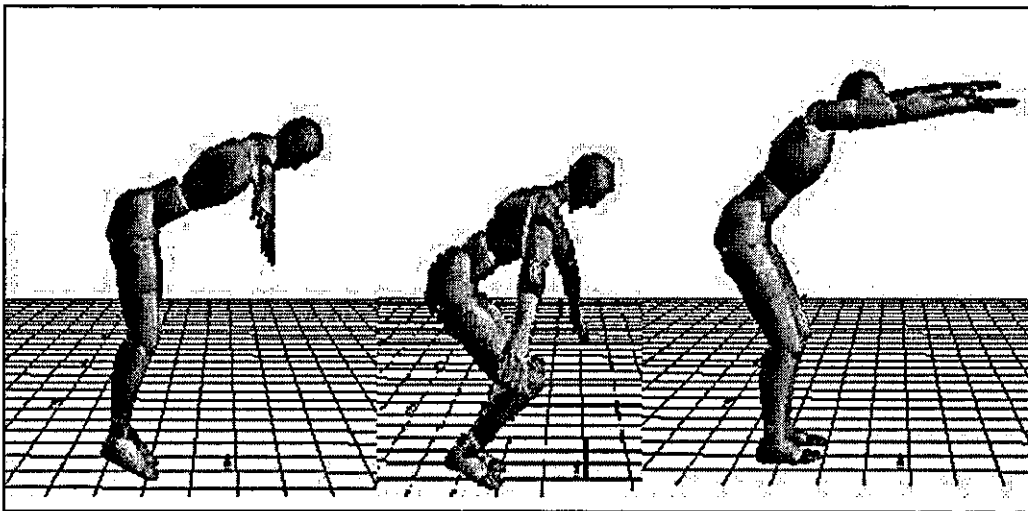


Figure 4.31 EMG time history for the landing of a backward somersault (Trial 1).



**Figure 4.32** EMG time history (filtered) for a backward somersault (Trial 1).

A graphical representation of the key phases of the landing during trial 1 is shown in Figure 4.33. These are: initial mat contact, 100 ms after contact and 0.5 s after initial contact.



**Figure 4.33** Landing strategy during trial 1.

The joint angle time histories, ground reaction force time histories and EMG time histories for all the trials can be found in Appendix I plus the remaining skills graphical representations.

#### 4.2.24 Kinematic and Kinetic Data Analysis - Summary

The methods used to record and analyse four gymnastic skills have been described. The data obtained from this analysis can be used as initial inputs for the simulation models developed earlier in Chapter 4. The data can also be used to evaluate the model's performance when attempting to match a simulation to an actual trial. The initial joint angles and velocities, the initial impact velocity of the mass centre and initial muscle activation level can be input into the model to ensure the model have the same initial conditions as the subject during the trial. The joint time histories, force time histories and muscle activation time histories can all be combined in an attempt to match the model's landing to that of the subject trial.

#### 4.3 *Modelling the Gymnast – Summary*

This chapter has described the structure of the four models of the gymnast in detail. Data has been collected to determine the strength, anthropometric and skill based parameter values. The literature has been reviewed to determine wobbling mass, bone and foot parameter values. Each component has been evaluated in turn and can be used in all of the four gymnast models. The models of the gymnast can be combined with the landing mat model (Chapter 3) and evaluated against actual skills performed by the gymnast.

## CHAPTER 5

### MODEL EVALUATION

The simulation models developed in Chapter 4 must be evaluated before they can be used for any applications. This chapter explains how the models were evaluated by comparing simulation with actual performance. This chapter also compares the results of the estimated joint reaction forces and bone deformations for selected models.

#### *5.1 Description of the Models*

Each model of the gymnast was planar with seven segments comprising of the head + trunk, upper arm, lower arm + hand, thigh, shank and a two-segment foot. Each segment was subject-specific in terms of mass, length, location of the mass centre and moment of inertia, and parameters were determined using anthropometric measurements and the inertia model developed by Yeadon (1990). The segments were linked via pin joints, which constrained the joints to rotate in the sagittal plane. Wobbling masses were included within the trunk, thigh and shank segments to represent soft tissue movement. Each of these body segments were divided into a fixed element and a wobbling element which was attached to the fixed element via two non-linear spring-dampers. One spring-damper system was located at the proximal end of the segment and the other at the distal end of the segment. The elbow joint was fixed as little joint angle change occurred at the elbow. The metatarsal-phalangeal joint was modelled as a torsional spring using the parameters from Gilchrist & Winter (1996). The landing mat was based upon the material testing results.

In models One, Two and Three the fixed elements comprised two parts joined by a rigid joint to allow the bone bending moments at the mid-point of the segment to be calculated. Model Four contained a linear finite element model of bone in the lower extremities.

Models One and Two included torque generators at the shoulder, hip, knee and ankle joints. The maximum torque produced by the torque generators was based upon the isovelocity dynamometer data. Model One's torque generators were based

upon the contractile component of the muscle tendon complex. Model Two's torque generators included the same contractile component and an additional series elastic component.

Models Three and Four used lumped muscle models instead of torque generators, except at the shoulder joint. The joint torques were calculated in the same way as models One and Two but the torque was divided by the joint's moment arm to give the muscle force. The muscle force was used in the model to produce joint rotation.

### *5.2 Model Refinement*

The following section describes the changes to the model that were implemented during the model development and evaluation stage.

#### *5.2.1 Horizontal Mat Component*

After attempting to match the simulated mat model's behaviour to that of the actual landing mat during the subject landing it was found that the model of the mat was not performing correctly in the horizontal direction. Upon further examination of the high-speed video of the material mat testing and the subject landing it was found that the mat behaved differently. During material testing the mat did not deform much initially but then due to the mat 'folding' the deformation increased dramatically (Figure 5.1).

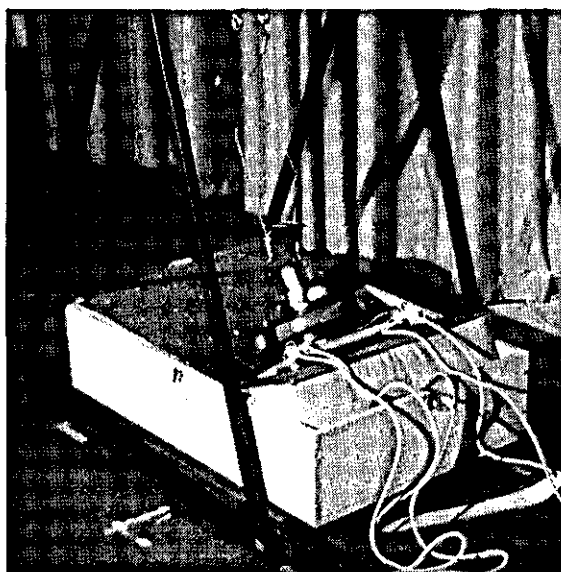


**Figure 5.1** The 'folding' of the landing mat.



This 'folding' did not happen during the subject landings. To ensure the mat behaved in a manner similar to when a gymnast landed on it, the horizontal spring parameters were re-optimised. The impactor in the mat model was given the displacement time history of the M-P joint from a back somersault trial. The horizontal force from a back somersault trial was used in the score and a new horizontal spring equation and parameters were determined. The new horizontal spring equation was:

$$F = -kx - rvx$$

The result of the optimisation gave a RMS difference score of 231 N using the following parameters:

$$k = 15417 \text{ Nm}$$

$$r = 557 \text{ Ns/m}$$

Figure 5.2 shows the match of the model data to the experimental data from a back somersault trial. This match was thought to be adequate as the model force time history follows the general shape of the experimental force time history. The latter half of the simulation does not perform as well but this may be due to the effect the gymnast has on the mat after the initial contact as the mass of the impactor is only the passive part of the gymnast's landing mass. Since the model used the impactor to model the impact it was possible that the difference between the model and the experimental data was due to the influence of the gymnast. This match was not sensitive to the parameter values and was used in gymnast mat model.

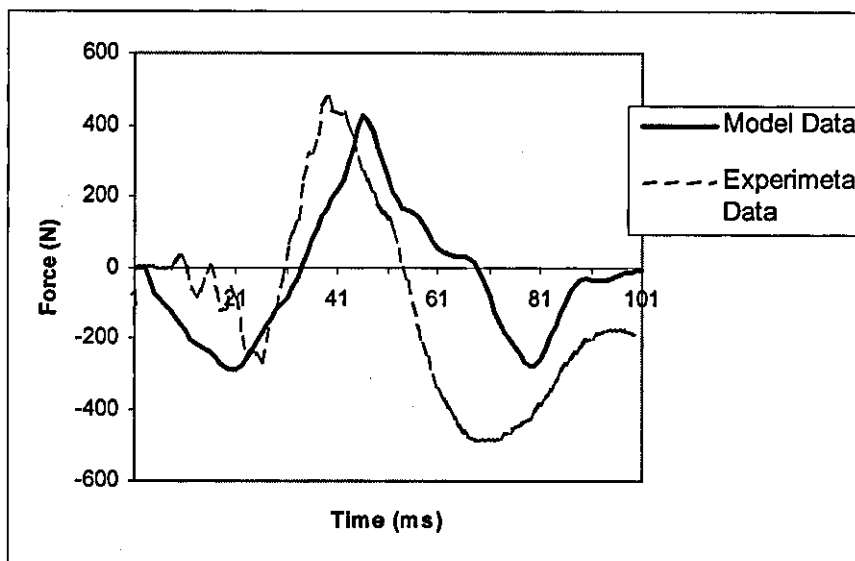


Figure 5.2 Horizontal ground reaction force using re-optimised spring parameters.

### 5.2.2 Ankle Strength

After many attempts of simulating the landing from each skill it seemed that the ankle was not sufficiently strong enough to allow the gymnast model to reproduce the landing. The subject was measured isometrically on a force plate with the ankle in a better position to produce maximum torque than in the isokinetic dynamometer test. The ankle strap supplied with the isokinetic dynamometer was insufficient in preventing any movement of the foot in relation to the crank arm foot plate. The subject had reported not being able to produce maximal effort at the ankle due to the restraining straps. Results showed an increase in  $T_0$  from 138 Nm measured on the isokinetic dynamometer to 255 Nm measured on the force plate. This new value was used to re-optimize the 9 parameter function and then used in the model evaluation as it was thought that it more accurately represented the maximum isometric torque produced at the ankle.

### 5.2.3 The Angle Fit Range of Knee Extension, Ankle Dorsi and Plantar Flexion

When the angle parameters were optimized to fit to the isokinetic dynamometer results the parameters produced a tight angle fit to the data. However it was found that the subject's joint range of motion during landing was greater than that used during the isokinetic dynamometer measurements. This led to negative torques being produced at the extremes of the range of motion. The subject was measured isometrically on a force plate at the extreme ranges of motion to determine the actual torque that could be produced. This was used as a guide when adjusting the angle fit to ensure that the correct subject torque was produced at the ends of the range of motion.

### 5.3 Evaluating the Models by Optimising Muscle Activation Profiles

During landing the strength and inertia parameters of the gymnast are set as a result of training and the landing mat is pre-selected based upon the competition requirements. The only parameters controlled by the gymnast during landing are the muscle activation timings. To simulate the landing from different skills the muscle activation histories of each model were optimized in an attempt to match the simulations to the performances. Four parameters were required to define the activation time histories of the extensor muscles using a quintic function (Chapter 4) which ramped up from a low activation to a high activation (Figure 5.3).

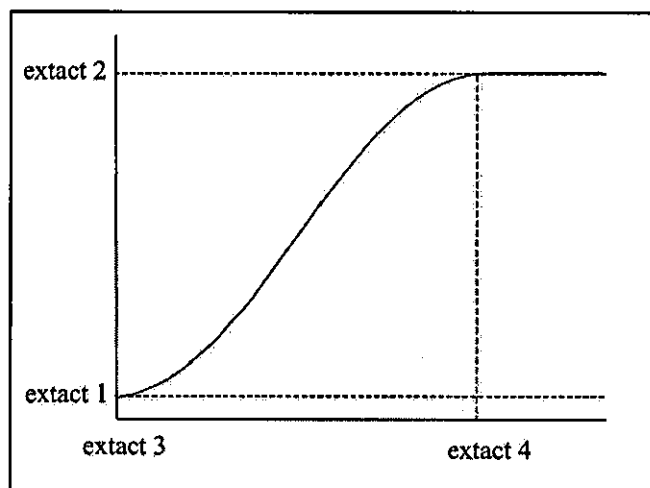


**Figure 5.3** Extensor activation history.

Extact1 corresponds to the initial activation state of the muscle (this corresponds to the amount of pre-activation prior to landing). Extact2 corresponds to the maximum activation level of the muscle during the landing. Extact3 refers to the time the extensors start to ramp up and was set to zero at the start of the simulation (one less parameter to optimise). Extact4 refers to the time taken to reach full muscle activation. Table 5.1 shows the lower and upper limits of the four parameters used to define the muscle activation history. Model One does not contain a SEC therefore the limits of extact4 are different to that of models Two and Three.

**Table 5.1** Lower and upper limits for the extensor activation parameters

Parameter	Lower Limit	Upper Limit
extact1	0.10	0.75
extact2	0.25	1.00
extact3	0	0
extact4	0.06 s / 0.01 s *	0.50 s

\* 0.06 s refers to model One and 0.01 s refers to models Two and Three.

The minimum activation level (extact1) was set at 0.10 as it was thought that the muscles would have some level of activation prior to landing to stiffen the joint; this was supported by the EMG results. The maximum activation level (extact2) that a muscle can have prior to contact was harder to determine from the EMG. The

extensor muscles could not be fully activated as little joint motion occurred prior to impact, hence the extensor muscles could only be activated at a level corresponding to the maximum torque produced by the flexors. A muscle pre-activation level as high as 80% has been reported by Arampatzis et al., (2003) during drop landings; however Kovacs et al. (1999) reported a level of 50%. Santello (2005) reported that EMG amplitudes prior to touchdown do increase with greater drop heights. This could explain the results from Arampatzis et al. (2003) and Kovacs et al. (1999) because greater drop heights were used by Arampatzis et al. (2003). These findings were used to determine the maximum activation level prior to landing in this study. The drop heights in this study were similar to that of Arampatzis et al. (2003) and slightly more conservative level of 75% was chosen.

The parameter `extact3` was set to zero so that ramping up started at the instant of touchdown. Ramping up could possibly start earlier (as visible motion of the limb may be delayed by the muscle mechanics) or later than this; however to reduce the number of parameters required for the optimisation this remained constant. Additionally `extact4` could be shorter as a trade-off.

The ramp up time (`extact4`) depended upon the model. Models Two and Three contained a SEC within the model and therefore ramp up times in these models represented the time interval between the application of the stimulus to the change in electrical activity in the muscle. This time can be as low as 9 or 10 ms (Corcos et al. 1992; Grabiner, 1986). A limit of 10 ms was set as the lower bound for the optimisations in models Two and Three. Model One did not include a SEC and therefore the ramp up time in the model must also include the stretching of any SEC, increasing the ramp up time to 50 ms (Winter & Brookes, 1991) or 71 ms (Grabiner, 1986). These times act as a lower limit for the ramp up time, therefore 60 ms was set as the lower bound in the optimisations in model One.

The activation history for the flexor muscles was very similar to that of the extensors except that the flexors ramped down from a high level to a lower level. The same form of quintic function was used (Figure 5.4).

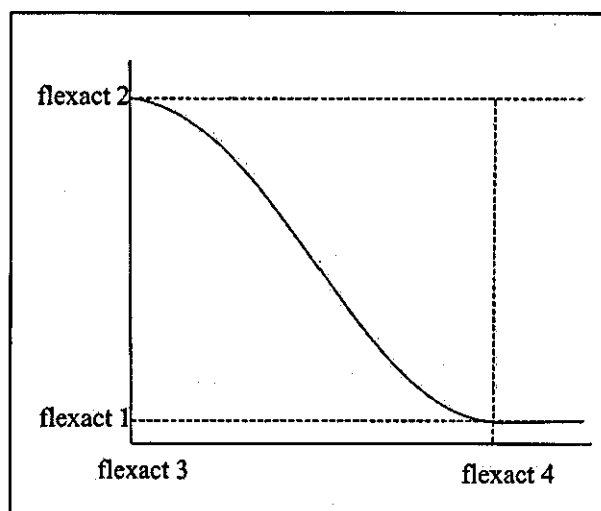


**Figure 5.4** Flexor activation history.

Similar bounds were used for the flexors as for the extensors. Table 5.2 shows the lower and upper bounds for the flexor activation histories.

**Table 5.2** Lower and upper bounds for the flexor activation histories

Parameter	Lower Limit	Upper Limit
flexact1	0.05	0.25
flexact2	0.2	0.75
flexact3	0	0
flexact4	0.06 s	0.50 s

The starting activation level (flexact2) was constrained to be between 0.2 and 0.75. The lower bound was imposed to ensure some level of co-contraction at the joint was present at impact. This co-contraction at landing is supported by Kovacs et al. (1999); Arampatzis et al. (2003) and Santello (2005). The activation was allowed to ramp down to a lower level of between 0.05 and 0.25 (flexact1) to ensure a small amount of co-contraction was still present during the landing (Santello, 2005). The time the flexors started to ramp down (flexact3) was set to zero in order to reduce the number of parameters optimised. The ramp down time (flexact4) was constrained to 60 ms although Santello (2005) suggested that this time could be as low as 50 ms.

### 5.3.1 Criteria for Evaluating the Models

Models One, Two and Three were evaluated based upon four criteria:

1. Vertical force time history
2. Horizontal force time history
3. Joint angle time histories
4. Trunk orientation time history

For each vault the vertical force time history from the force plate was used to evaluate the model's vertical force time history. The RMS difference between the two force time histories was divided by the peak force and converted to a percentage. This approach was also used for the horizontal force. The sum of the RMS differences of all four joint angle time histories were divided by their respective joint ranges and were converted to percentages. The percentages were used to evaluate the joint angle changes during the simulation. Finally the trunk orientation angle was used to compare the body orientation in the simulation to that of the actual skills.

### 5.3.2 Objective Function and Weightings

A total score was calculated for each simulation as a measure of how well the simulation matched the actual performance. The four criteria were weighted within the total score, as presented in equation 5.1. One percent of RMS difference in force was thought to be equivalent to one percent RMS difference in the joint angles. Curvature of the spine made the trunk orientation angle less accurate than the other criteria therefore the trunk orientation was not weighted as heavily. The following equation shows the score used in the optimisations:

$$Score = \frac{\%VGRF + \%HGRF + \left( \frac{\sum \%Joint\ Angles}{4} \right) + \circ Trunk}{4} \quad (5.1)$$

$$\%VGRF = (VGRF_{RMS}/pFz) \times 100$$

$$\%HGRF = (HGRF_{RMS}/pFy) \times 100$$

$$\%Joint\ Angles = (\sum (Joint\ Angle_{RMS}/Joint\ Range) \times 100) / 4$$

$$\circ Trunk = Trunk_{RMS}$$

pFz = experimental peak vertical force

pFy = experimental peak horizontal force

Variations on the score were tried in order to improve the match to the GRF, one method was to include the peak force in the score as it is of interest when attempting to estimate internal forces and bending moments in bone and therefore to assess injury potential.

$$\%VGRF = (VGRF_{RMS}/pFz) + (abs(pFz - spFz) / pFz) \times 100$$

$$\%HGRF = (HGRF_{RMS}/pFy) + (abs(pFy - spFy) / pFy) \times 100$$

spFz = simulated peak vertical force

spFy = simulated peak horizontal force

However the use of peak forces in the score caused a problem when the optimisation routine attempted to find a solution. The solution tended to match the peak forces but at a cost of increasing the overall RMS difference with the peak forces not matching in time. An example of the problem is highlighted in the horizontal force during a handspring (Figure 5.5). The optimisation has successfully matched the peak force but has increased the RMS difference by shifting it in time to achieve this. Not only was the peak force important but also the time at which it occurred. This problem occurred in several of the force time histories for different skills if the peak forces were included in the score. The decision was made not to include the peak forces in the score.

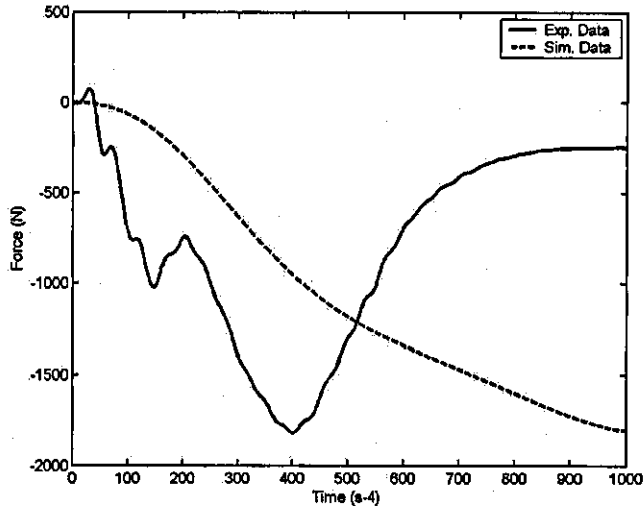


**Figure 5.5** Horizontal force time history illustrating problem with objective function.

After the peak forces were removed from the score the decision was made to try to increase the weighting of the VGRF in the score to ensure a better force time history match. The weighting was increased by a factor of three. This also caused a problem, this new score successfully reduced the RMS score but it did so by reducing the peak force. However this weighting reduced the RMS difference during the latter half of the force time history (Figure 5.6). The original score was more successful in matching the peak force and the decision was made not to include the weighting in the score. The final score used to evaluate models 1, 2 and 3 was the original score (equation 5.1).

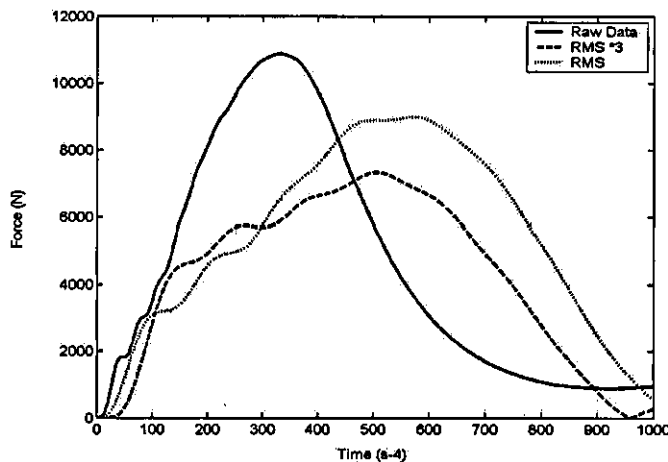


**Figure 5.6** Vertical force time history illustrating the problem with the modified weighting of the objective function.



### 5.3.3 Penalties

Penalties were also introduced into the calculation of the score if certain elements of the models' behaviour exceeded certain limits. The first penalty was introduced to ensure the vertical deformation of the landing mat did not exceed the depth of the landing mat. The second penalty ensured that the horizontal deformation of the landing mat did not exceed 0.12 m as this would represent a 20% larger horizontal mat deformation than found in the experimental data. Other penalties would stop the current simulation if the vertical or horizontal force exceeded a pre-set value (15% greater than the peak vertical or horizontal force within that skill) and would return a high score. This was to ensure as little time as possible was spent running simulations that were not close to an optimal solution.

### 5.3.4 Results

The optimisations were run using the Simplex optimisation algorithm within MatLab until the closest possible match between the actual performances and the simulations was achieved. The main problem was the time required for one simulation (21m 30s) and hence the optimisation for a single trial took several days. It was important to provide the optimisation routine with a 'good' starting position. It was also important to minimise the number of variables optimised at one time. The extensors and flexors were only allowed to ramp in one direction and the simulation length was kept to the passive impact phase of the landing (approx. 0.1s). The lowest objective function scores are shown in Table 5.3.

**Table 5.3** Objective function scores for models One to Three and all four skills

Skill	Model 1	Model 2	Model 3
Front Somersault	11.9%	13.9%	10.1%
Back Somersault	18.2%	17.6%	16.2%
Handspring	17.1%	22.1%	17.2%
Tsukahara	20.6%	23.9%	23.6%

Model Three achieved the lowest score in both the front and back somersault skills. Model One achieved the lowest score for the handspring and Tsukahara skills. Details of each component of the score, simulation results, muscle activation

parameters for each skill using model Three are shown in Figures 5.7 to 5.14 and Table 5.5. Model Three's results are reported in this chapter as model Three was used during the optimisation stage to answer the research questions. A complete set of results for models One and Two can be found in Appendix K. Later in this chapter the results of model One's joint reaction forces and bone deformations are compared with those of model Three.

No markers were used on the mat during testing so the actual amount of mat deformation is not known. To estimate the landing mat deformation the amount of vertical and horizontal displacement of the M-P joint after initial contact was measured. The subject landed successfully (no movement of the feet on the mat after initial contact) during the front and back somersault skills and the handspring skill. The subject took a step on the Tsukahara skill making the estimate of the landing mat deformation more difficult. Table 5.4 shows the estimated vertical and horizontal mat deformation using the M-P displacement method.

**Table 5.4** Estimated maximum landing mat deformations during all four skills

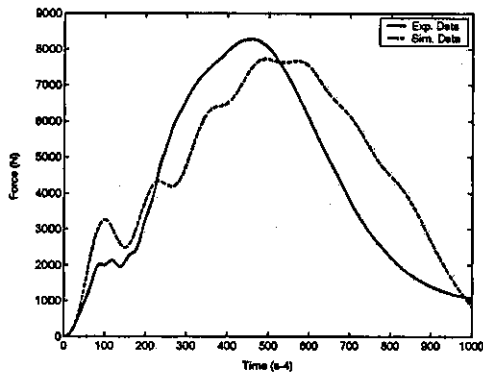
<b>Gymnastic Skill</b>	<b>Vertical deformation (m)</b>	<b>Horizontal deformation (m)</b>
Front Somersault	0.08	0.02
Back Somersault	0.15	0.06
Handspring	0.16	0.03
Tsukahara	0.14	0.10

For the front somersault skill model Three performed better than models One or Two, with an overall score of 10.1%. Model Three was able to match the vertical peak force very well (6.7%). The RMS difference was the second lowest of all the models at 16.8%. The horizontal force time history of model Three also matched the complex force time history from the actual skill better than models One and Two, with an RMS difference of 12.3% and a difference in peak force of only 25.9%. The score breakdown can be found in Table 5.5.

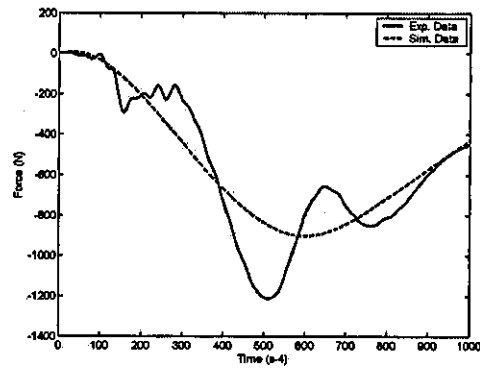
**Table 5.5** Model Three overall score breakdown

<b>Gymnastic Skill</b>	<b>Overall Score %</b>	<b>All joints</b>	<b>Trunk orientation</b>	<b>VGRF</b>	<b>HGRF</b>
Front Somersault	10.1	3.6° (6.6%)	4.6°	16.8%	12.3%
Back Somersault	16.2	6.9° (15.7%)	0.8°	12.1%	36.1%
Handspring	17.2	11.7° (15.7%)	1.1°	22.4%	29.6%
Tsukahara	23.6	15.1° (34.3%)	9.1°	25.8%	25.4%

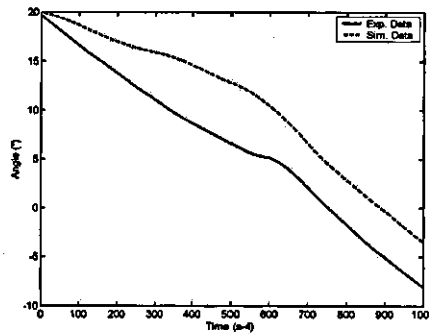
Figure 5.7 compares the results of the simulation with the results from the actual front somersault skill. There was good agreement between the joint angles, the orientation angle followed the same trend as the skill but was approximately 5° greater in the simulation. The VGRF and HGRF start and finish at the same point as the skill and follow the same general trend.



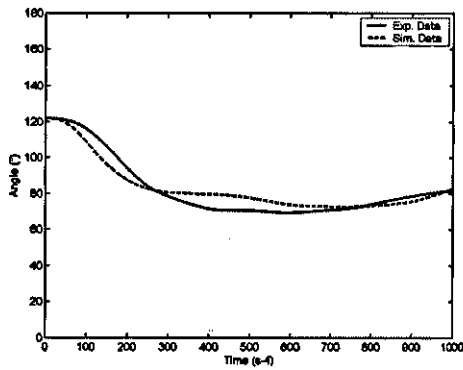
(a)



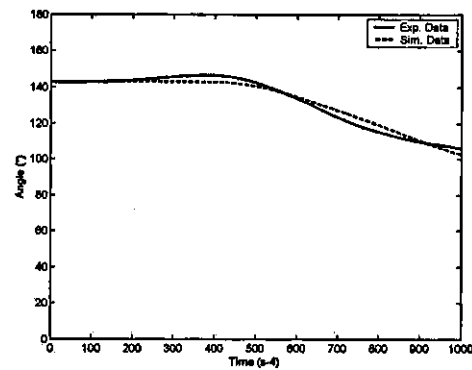
(b)



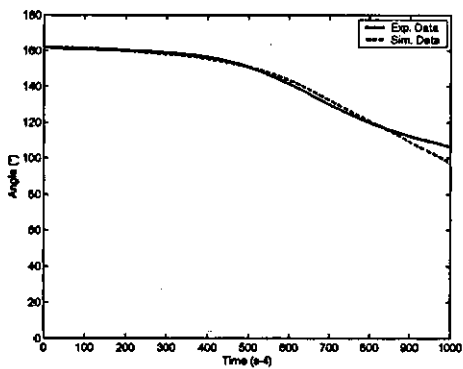
(c)



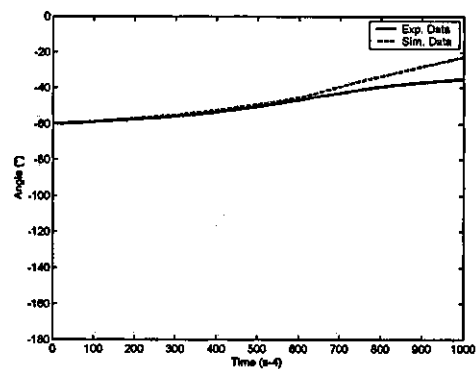
(d)



(e)



(f)



(g)

**Figure 5.7** Comparison of Model Three simulation and performance for the front somersault in terms of (a) VGRF (b) HGRF (c) trunk orientation (d) ankle angle (e) knee angle (f) hip angle (g) shoulder angle.

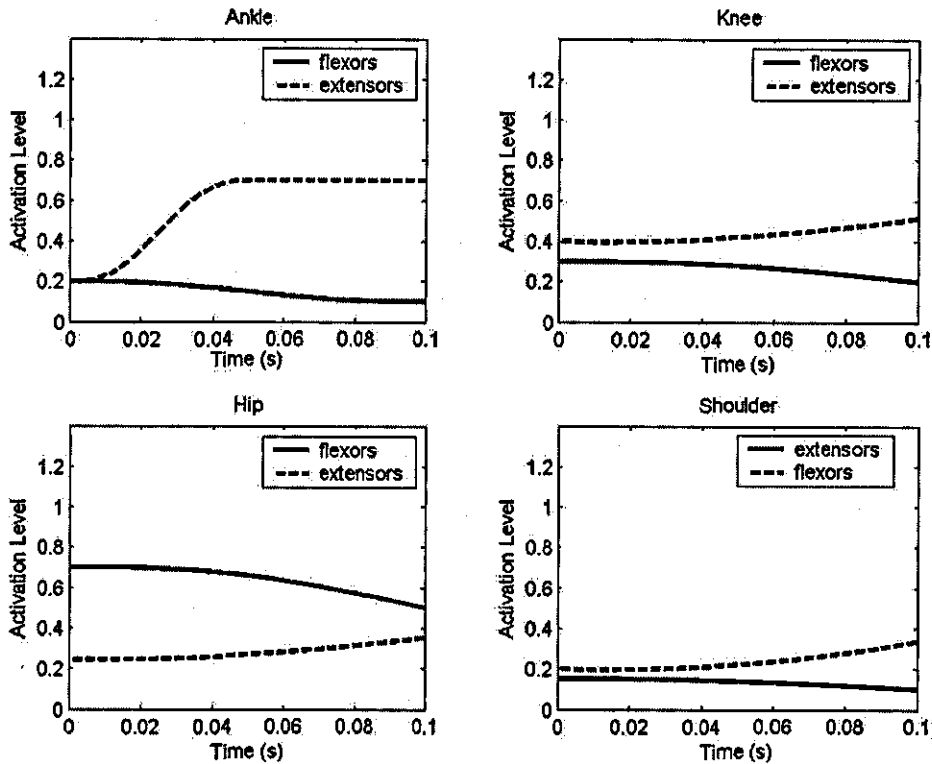


Figure 5.8 Activation time histories for model Three front somersault simulation.

The torque activation histories used to achieve the simulated angle changes are shown in Figure 5.8. During the simulation there was co-contraction at touch-down in each joint as both flexors and extensors were activated. This supports EMG results and the literature findings that muscles are activated prior to landing.

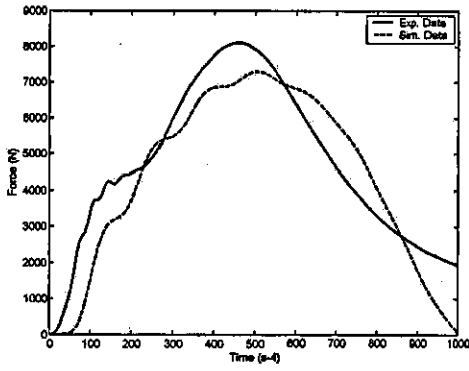
The landing mat in the simulation deformed a maximum of 0.15 m vertically and 0.05 m horizontally. This indicated that the model of the landing mat during the simulation deformed more than the estimated mat deformation during the skill (Table 5.4).

The simulated mass centre velocity was similar to that of the actual mass centre velocity of the front somersault skill at 0.1 s. A vertical velocity of  $-5.2$  m/s at the start of the simulation resulted in a simulated vertical velocity of  $-0.6$  m/s at the end of the simulation compared to  $-0.3$  m/s at the same time during the actual skill. A simulated horizontal velocity of  $-0.4$  m/s compared to that actual  $-0.5$  m/s at the same time during the front somersault skill.

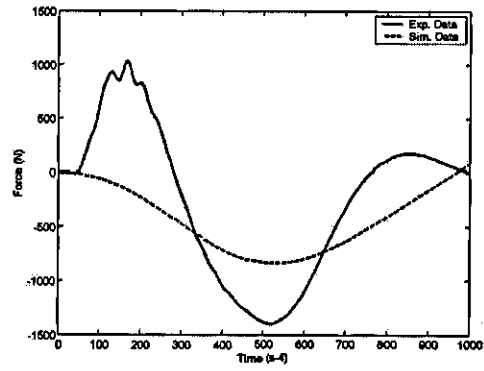
Overall model Three reproduced the key characteristics of the front somersault skill and the results obtained for joint reaction forces and bone deformations are thought to be relatively accurate.

For the back somersault skill model Three performed better than models One or Two, with an overall score of 16.2%. Model Three was able to match the vertical peak force to within 9.9%. The vertical force RMS difference was the lowest of all the skills at 12.1%. The horizontal force time history of the simulation matched the force time history from the actual skill with an RMS difference of 36.1% and a difference in peak force of 40.4%. The score breakdown can be found in Table 5.5.

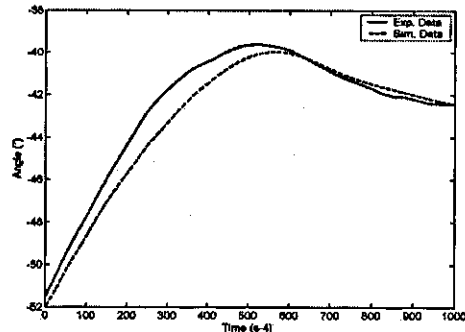
Figure 5.9 compares the results of the simulation with the results from the actual back somersault skill. Again there was good agreement between the joint angles and the trunk orientation angle followed the same trend as the skill and was within 1° of the simulation. The VGRF achieved a good RMS difference score but did not finish at the same point as the actual skill. The HGRF started and finished at the same point as the skill but did not follow as good general trend. (This is discussed later in this chapter).



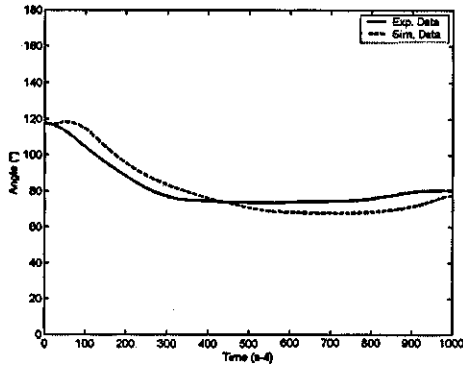
(a)



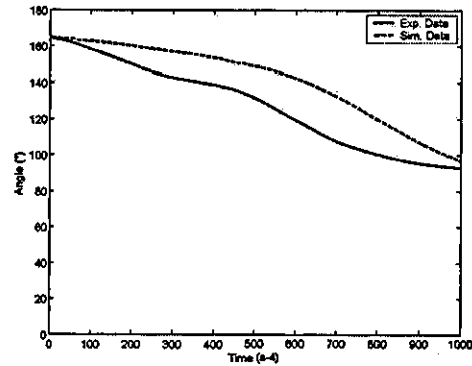
(b)



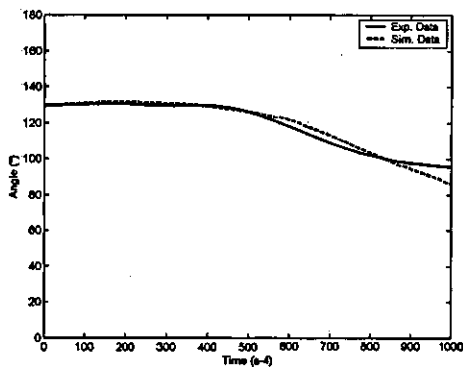
(c)



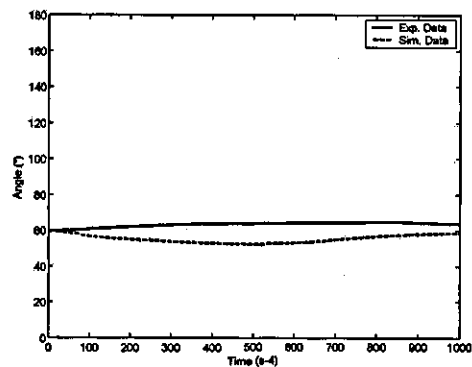
(d)



(e)



(f)



(g)

**Figure 5.9** Comparison of Model Three simulation and performance for the back somersault in terms of (a) VGRF (b) HGRF (c) trunk orientation (d) ankle angle (e) knee angle (f) hip angle (g) shoulder angle.

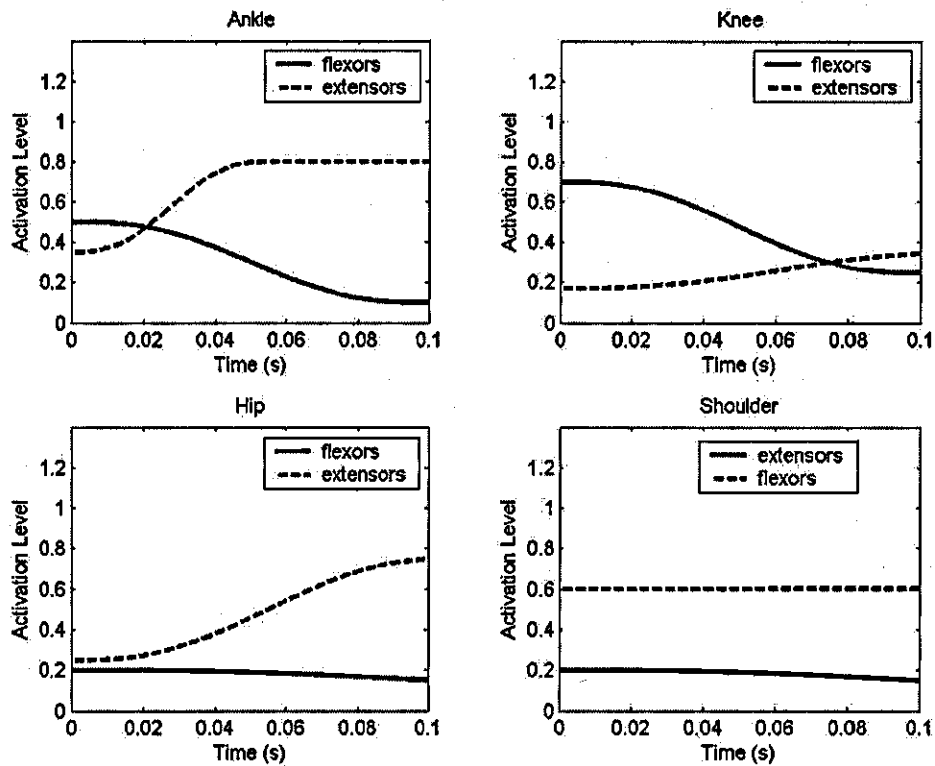


**Figure 5.10** Activation time histories for model Three back somersault simulation.

The torque activation histories used to achieve the simulated angle changes for the back somersault are shown in Figure 5.10. Again during the simulation there was co-contraction at touch-down in each joint as both flexors and extensors were activated. The landing mat in the simulation deformed a maximum of 0.15 m vertically and 0.05 m horizontally. This indicated that the model of the landing mat during the simulation deformed to a similar amount as estimated during the skill (Table 5.4).

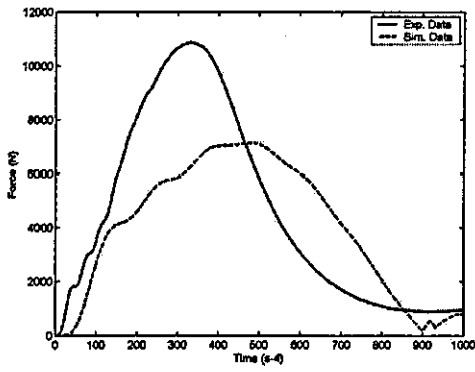
The vertical simulated mass centre velocity was similar to that of the actual mass centre velocity at the end of simulation (0.1 s) during the back somersault skill. A vertical velocity of  $-6.4$  m/s at the start of the simulation resulted in a simulated vertical velocity of  $-0.3$  m/s at the end of the simulation compared to  $+0.2$  m/s during the actual skill. The simulated horizontal velocity of  $-0.9$  m/s was half that of the actual back somersault skill ( $-1.8$  m/s).



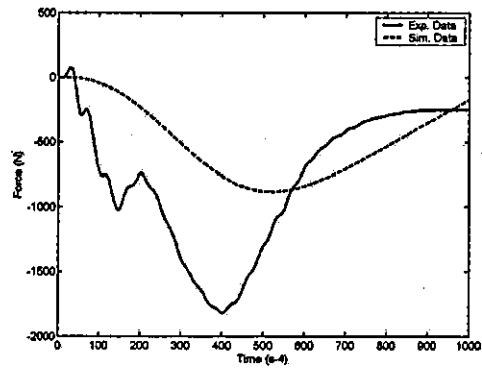
Overall the simulation using model Three reproduced the key characteristics of the back somersault skill and produced the second best score. The results can be used to estimate joint reaction forces and bone deformations.

For the handspring skill model Three performed better than model Two and very similarly to model One, with an overall score of 17.2%. Model Three was able to match the vertical peak force to within 34.3%; this was the worst of all the skills. The vertical RMS difference was 22.4%. Peak vertical GRF occurred at 35 ms in the handspring vault, yet in the remaining skills peak vertical force occurred between 50 and 60 ms. This may be why the simulation struggled to match the force time history, although it is not known why the peak force was earlier during the handspring. The horizontal force time history of the simulation matched the force time history from the actual skill with an RMS difference of 29.6% and a difference in peak force of 51.6%. The score breakdown can be found in Table 5.5.

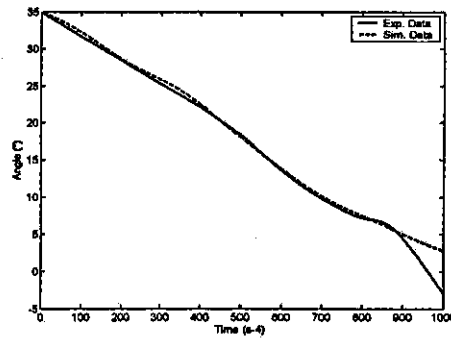
Figure 5.11 compares the results of the simulation with the results from the actual handspring skill. Again there was good agreement between the joint angles. The simulation trunk orientation angle was a very close match to the actual skill and was within  $1.5^{\circ}$ . The VGRF did not follow the general trend of the force time history but achieved a reasonable RMS difference score. The HGRF starts and finishes at the same point as the skill but lacks the magnitude to improve the RMS difference.



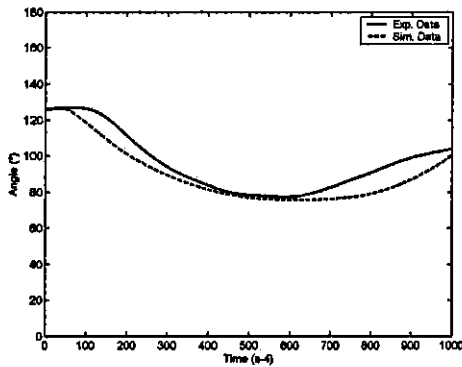
(a)



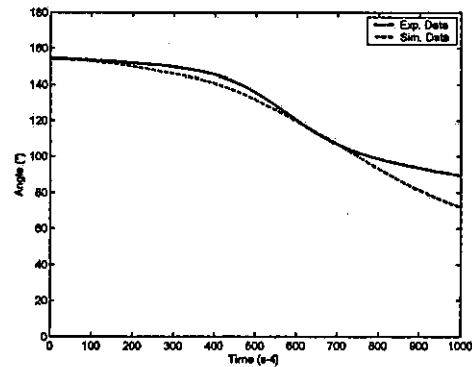
(b)



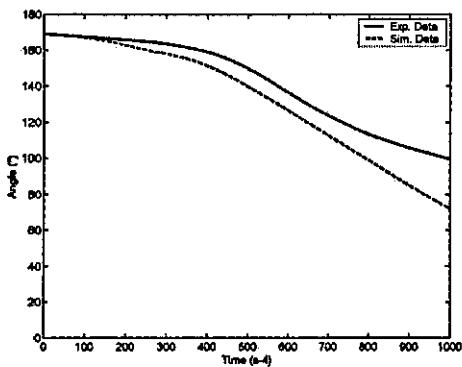
(c)



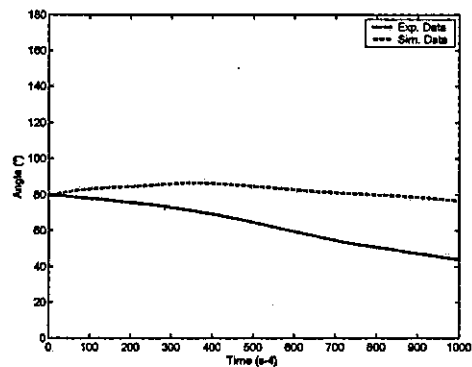
(d)



(e)



(f)



(g)

Figure 5.11 Comparison of Model Three simulation and performance for the handspring in terms of (a) VGRF (b) HGRF (c) trunk orientation (d) ankle angle (e) knee angle (f) hip angle (g) shoulder angle.

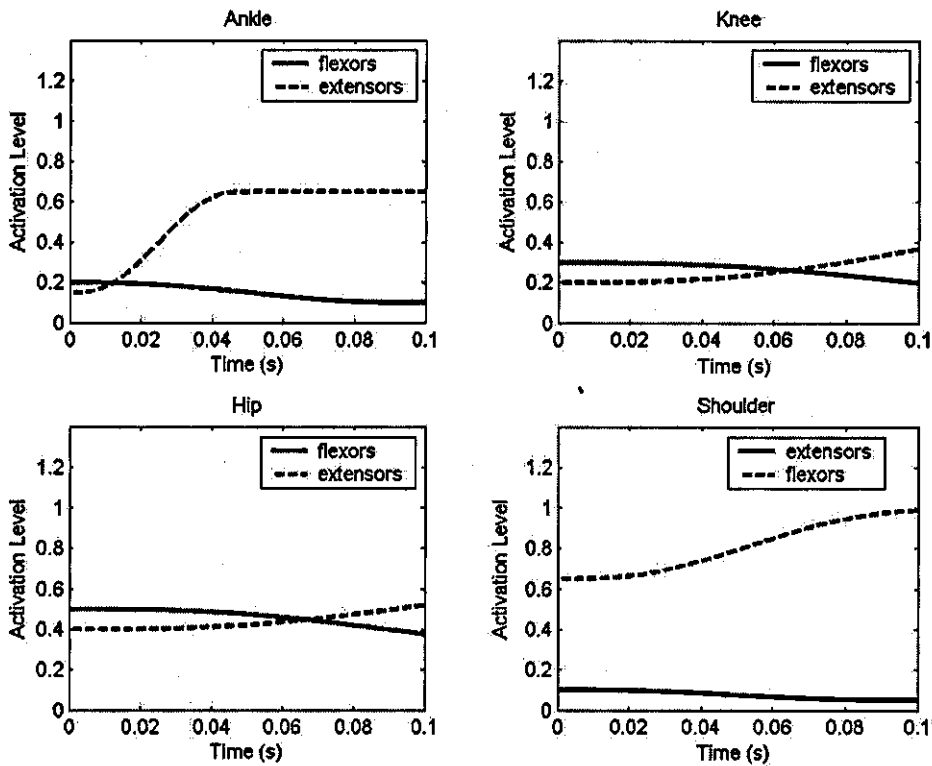


**Figure 5.12** Activation time histories for model Three handspring simulation.

The torque activation histories used to achieve the simulated angle changes for the handspring are shown in Figure 5.12. Again during the simulation there was co-contraction at touchdown in each joint as both flexors and extensors were activated. The landing mat in the simulation deformed a maximum of 0.16 m vertically and 0.05 m horizontally. This indicated that the model of the landing mat during the simulation deformed to a similar amount as the estimated mat deformation during the skill (Table 5.4).

The vertical simulated mass centre velocity was a little higher than that of the actual mass centre velocity at the end of simulation (0.1 s) during the handspring skill. A vertical velocity of  $-6.2$  m/s at the start of the simulation resulted in a simulated vertical velocity of  $-1.7$  m/s at the end of the simulation compared to  $-1.1$  m/s during the actual skill. The simulated horizontal velocity of  $-1.8$  m/s was higher than that of the actual handspring skill ( $-1.1$  m/s).

Overall the handspring simulation using model Three reproduced some of the key characteristics of the handspring skill and produced score comparable to the best score for model One despite the unusual timing of the peak vertical GRF.

For the Tsukahara skill model Three performed better than model Two but not as good as model One, with an overall score of 23.6%. Model Three was able to match the vertical peak force to within 3.4%, the best of all the skills. The vertical force RMS difference was 25.8%. The horizontal force time history of the simulation matched the force time history from the actual skill with an RMS difference of 25.4%, a better score than the back somersault and handspring. The difference in peak force was 33.5%, this again was better than the back somersault and handspring skills. The score breakdown can be found in Table 5.5.

Figure 5.13 compares the results of the simulation with the results from the actual Tsukahara skill. There was good agreement between the joint angles except for the ankle joint (this is discussed in detail later in this chapter). The simulation orientation angle was not a very close match to the actual skill and was only within an RMS of  $9.1^\circ$ . The VGRF did follow the general trend of the force time history but it appeared that the simulated force time history was shifted in time. This produced a relatively bad RMS difference score but matched the peak force very well. The HGRF started and finished at the same force as the skill but did not follow the general trend of the force time history (discussed later in this chapter).

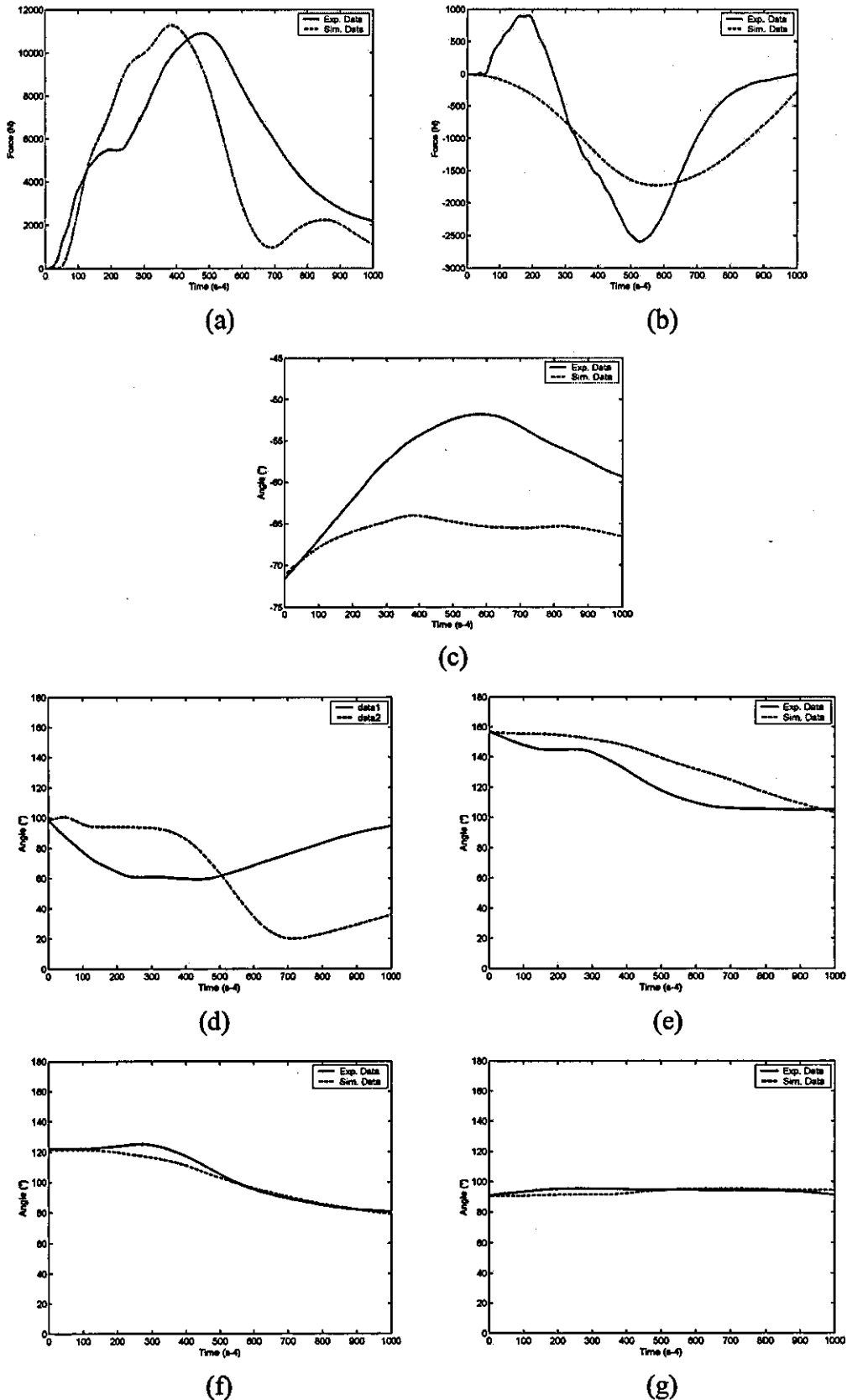


**Figure 5.13** Comparison of Model Three simulation and performance for the Tsukahara in terms of (a) VGRF (b) HGRF (c) trunk orientation (d) ankle angle (e) knee angle (f) hip angle (g) shoulder angle.

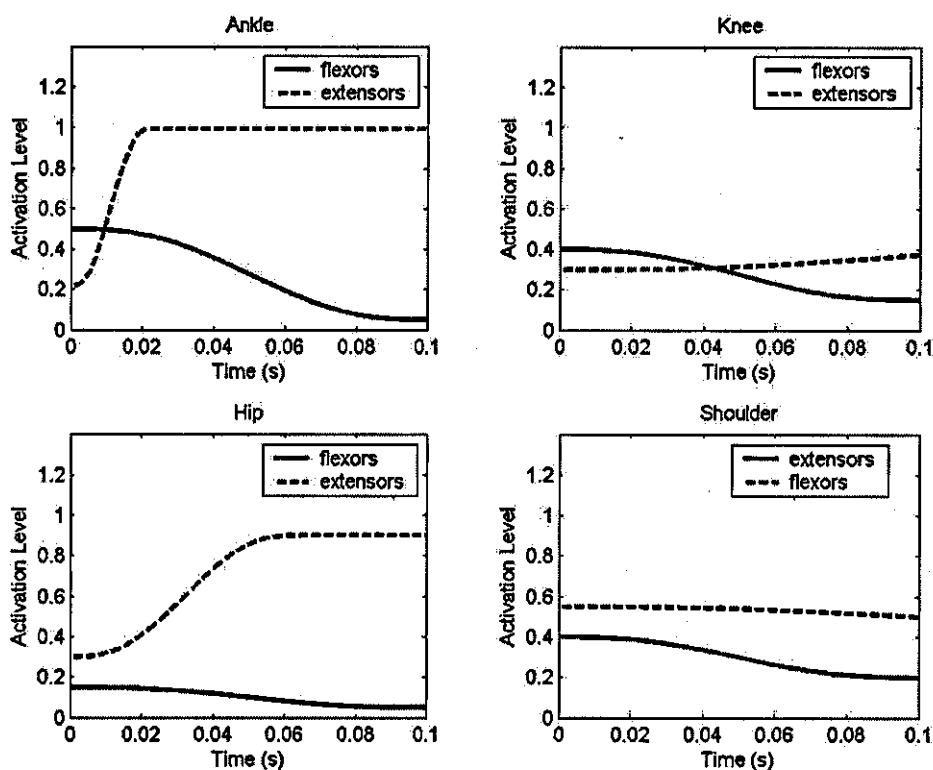


**Figure 5.14** Activation time histories for model Three Tsukahara simulation.

The torque activation histories used to achieve the simulated angle changes for the Tsukahara skill are shown in Figure 5.14. Again during the simulation there was co-contraction at touchdown in each joint as both flexors and extensors were activated. It was noted that the ankle extensors ramped up to maximum in the minimum time possible; this may indicate that they are not strong enough to perform this skill (this is discussed later in this chapter). The landing mat in the simulation deformed a maximum of 0.17 m vertically and 0.10 m horizontally. This indicated that the model of the landing mat during the simulation deformed to a similar amount as the estimated mat deformation during the skill (Table 5.4).

The vertical simulated mass centre velocity was similar to that of the actual mass centre velocity at the end of simulation (0.1 s) during the Tsukahara skill. A vertical velocity of  $-7.5$  m/s at the start of the simulation resulted in a simulated vertical velocity of  $-0.5$  m/s at the end of the simulation compared to  $-0.7$  m/s during the actual skill. The simulation may have struggled to match this as during the actual skill the gymnast took a step during landing, the simulation being unable

to do this. The simulated horizontal velocity of  $-1.6$  m/s was a little higher than that of the actual Tsukahara skill ( $-1.4$  m/s).

Overall the Tsukahara simulation using model Three reproduced some of the key characteristics of the Tsukahara skill and produced a score comparable to the other models. An improved match may be obtained by increasing the ankle strength but since the gymnast took a step during landing the simulation may still struggle to match the joint angle changes.

### 5.3.5 Analysis and Discussion of Selected Results

A few specific results are analysed in greater depth. The first area for discussion relates to the initial increase in HGRF during backward rotating skills (Figure 5.15).

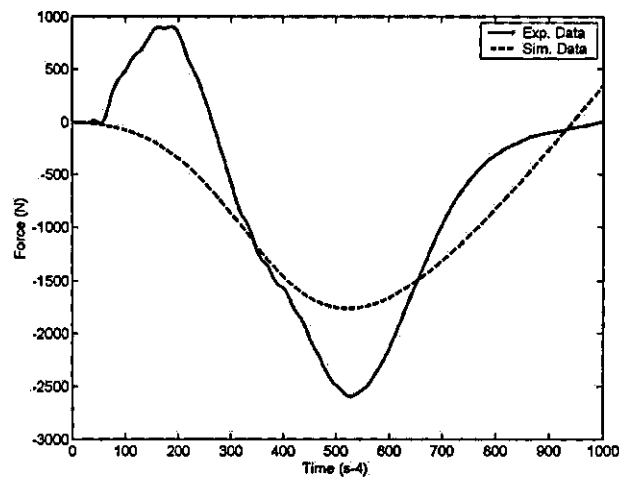


**Figure 5.15** HGRF from Tsukahara vault and model One.

A positive initial peak force in the backward rotating vaults suggests that the gymnast's feet had a velocity towards the vault horse at initial contact. Analysis of the displacement data from Vicon does not show any movement in the direction of the vault horse prior to landing, therefore the simulation model does not reproduce this initial peak either. Examining the material test results for the oblique drops does not show any positive peak followed by a negative peak. So the question arises why does it occur in the experimental data? A possible suggestion is that it may be something to do with the way the gymnast interacts with the mat at initial contact. Maybe the way the gymnast deforms the mat is different to the material tests. During backward rotating vaults the gymnast tended to land near the edge of the

mat, this may have caused some movement of the bottom layer of the mat when the air was forced out and the mat compressed. The horizontal displacement data of the toe showed that after impact the toe moved slightly towards the vault horse before it moved back. It can be seen from the high-speed video that the gymnast landed near the edge of the mat. After initial contact the feet of the gymnast moved slightly towards the vault horse for a few frames then moved away from the vault horse for the remainder of the impact. So as the toes initially contacts the mat's surface the mat begins to deform but as the point of impact was near the edge of the mat, the mat initially deformed at the edge of the mat as well as the point of contact. This caused the feet to move slightly towards the vaulting table. A few milliseconds later the heel contacts and the centre of pressure moved further back and the mat behaved like the impact tests where the impact site was further from the edge of the mat. Since the horizontal model of the mat is far simpler the model cannot account for this 'local' deformation near the edge of the mat and so the model does not reproduce the initial positive peak force found in the backward rotating vaults. This positive peak force was evident on the sample mat but it is unlikely to appear during landings on a full size competition mat as the gymnast is less likely to land near the edge of the mat.

The second area for discussion relates to the ankle strength during the Tsukahara vault using model Three. The activation history for the ankle extensors ramps up as quickly as possible to its maximum (Figure 5.16) but the muscle is unable to reduce the amount ankle dorsi flexion in the model. The model's ankle range far exceeds the ankle range during the actual skill (Figure 5.17).



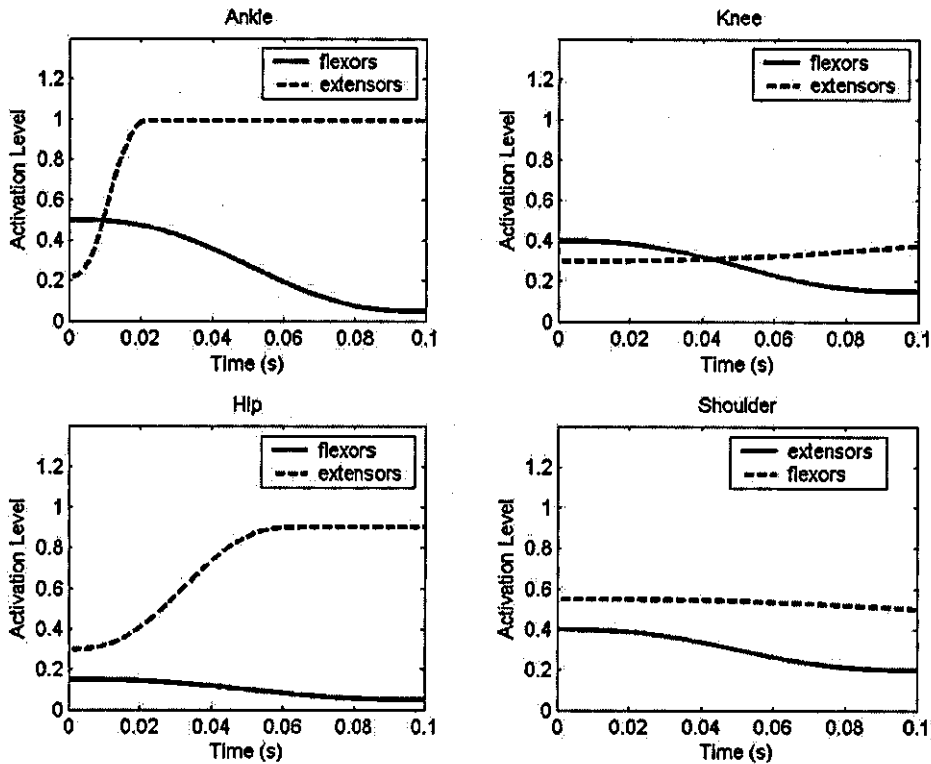


Figure 5.16 Model Three activation history during Tsukahara vault.

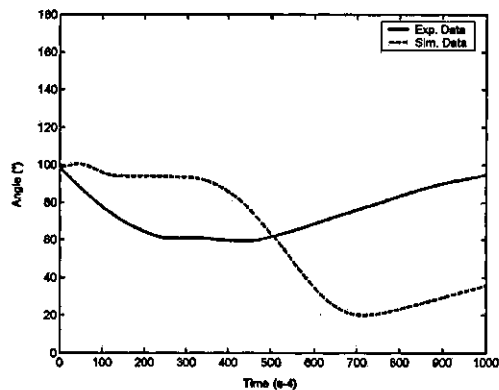
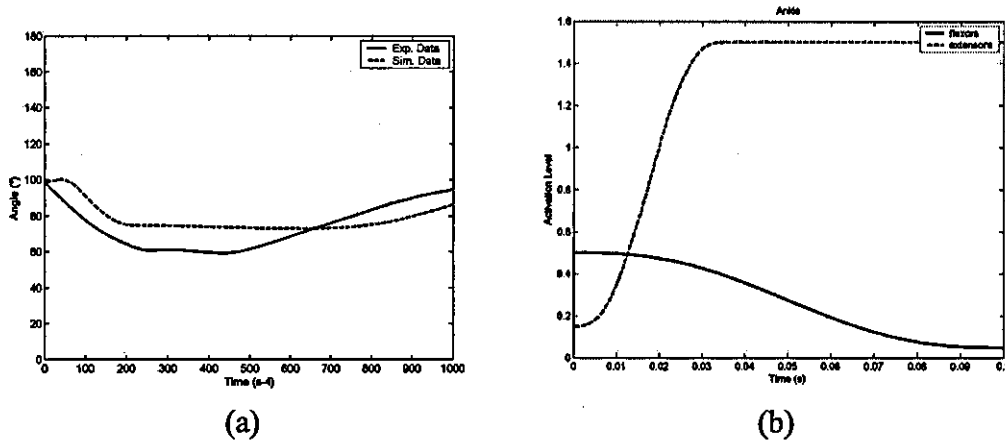


Figure 5.17 Joint angle time history for the ankle joint during a Tsukahara vault (model Three).

Possible reasons for the increased joint range in the model was that the ankle extensors were not strong enough or that there was some passive resistance to excessive dorsi flexion. This may have been due to a number of reasons. Although the ankle extensors of the subject were re-measured using the force plate (subsection 5.2.3) it was felt that the ankle of the subject was still stronger than the parameters obtained from earlier measurements. Due to the design of the muscle tendon constraint in VN4D the ankle caused a problem during simulations. The

problem was that the ankle rotated over a range that the constraint could not cope within VN4D, this was also due to the body configuration at the start, making it difficult to attach the muscle in the correct place. Since the linear actuator could pivot at both ends it was possible that at certain body configurations and joint angles that the force from the muscle could pass through the joint hence decreasing the effective moment arm. Within the normal working range the moment arm was kept constant due to the circular body that the muscle and SEC were attached to. Beyond this range the muscle could pass through the circular body decreasing the moment arm (see Figure 4.4). This problem meant that as the simulation ran the moment arm at the ankle decreased beyond unrealistic values. Therefore the muscle force was not sufficient to produce enough torque to match the joint angle changes in the actual skill. To see if this was the case the ankle strength in the model was increased by 50% to account for any decrease in moment arm. Re-optimisation improved the overall score from 23.6% to 18.6%. This also improved the ankle time history match (Figure 5.18 (a)).



**Figure 5.18** Joint angle (a) and activation histories (b) for the ankle joint during a Tsukahara vault.

The simulated ankle joint rotation was able to match the actual joint change in the skill (Figure 5.18a) if the muscle strength was increased to account for the decrease in moment arm. The activation history (Figure 5.18b) also shows that the muscle no longer needs to ramp up as quickly as possible as the ankle plantar flexors can produce a greater force later to account for the change in moment arm. The longer ramp up time but to a higher level dramatically improved the ankle joint

angle time history which in turn decreased the overall score to a level comparable to that of the back somersault.

### 5.3.6 Summary

Using the landing mat model parameters determined from the material testing and the gymnast parameters determined from experimental data collection and the literature it was possible to optimise the muscle activation timings of the models to match the four gymnastic skills. The forward and backward somersault skills were matched the best and will be used in future optimisations. Although the gymnast-mat models matched the other skills reasonably well some elements such as peak vertical GRF in the Handspring skill were not so well represented therefore the Handspring and Tsukahara skills will not be used for future optimisations. It can be concluded that all the models are a realistic representation of the landing phase during gymnastic vaults. The models can be used for further analysis and various applications and optimisations.

### *5.4 Analysis of Joint Reaction Forces*

The research questions in Chapter 1 refer to reducing the joint reaction forces during different gymnastic vaults. The internal joint reaction forces cannot be evaluated directly as it is impossible to measure these forces in a gymnast performing a vault. However the models have been evaluated and have been shown to match the ground reaction forces and joint kinematics during landings. Based upon the evaluations of the models it is possible to investigate the effects of a torque driven model (model One) and a lumped muscle model (model Three) on joint reaction forces during gymnastic vaults. Model One was chosen instead of model Two as it consistently produced a better score for all the vault skills.

The results from model Three's front somersault skill are shown in Figure 5.19; these results reflect the general trend of results from all the skills. A complete set of results for all the skills can be found in Appendix I.

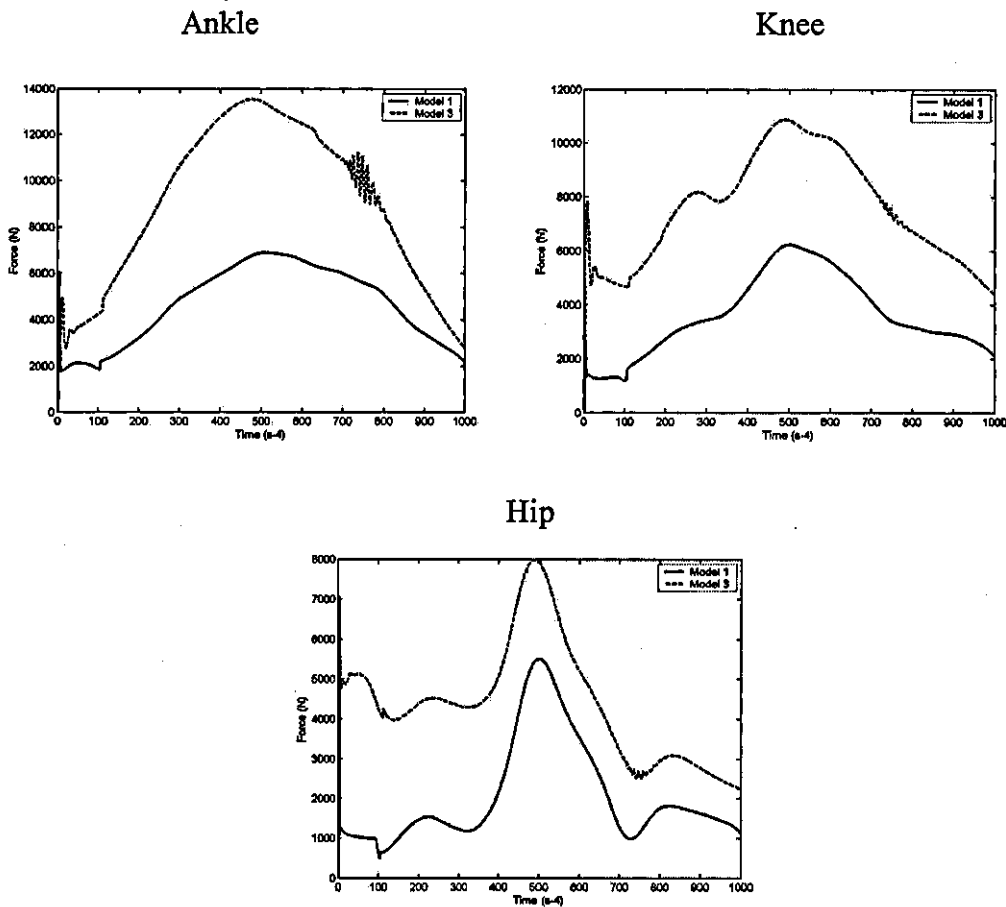


**Figure 5.19** Joint reaction forces for the front somersault skill (models One and Three).

For all the gymnastic skills and all the lower extremity joints model Three exhibited higher joint reaction forces than model One. The general shape of the force time history for each joint was comparable between models that used a similar activation history for the joint but the magnitude of the forces were greater in model Three (Figure 5.19). Models that used a different activation history for a joint (hip joint, back somersault skill) resulted in slightly different shapes of the force time histories but again the magnitude of the force in model Three was greater than model One. These results suggest that the lumped muscle models are required if the risk of bone injury is to be assessed.

The peak joint reaction forces (Table 5.6) do not appear to increase with the skill complexity or increased ground reaction force during landing. It is possible that as the skill complexity increases the joint reaction forces experienced by the gymnast remain relatively constant by the modification of the landing strategy until a certain point. Once this point is exceeded the modifications to the landing strategy

are unable to maintain a relatively constant joint reaction force and therefore the joint reaction forces begin to increase.

**Table 5.6** Estimated peak joint reaction force during all four vault landings

<b>Skill</b>	<b>Joint</b>	<b>Peak JRF (N)</b>	<b>Peak GRF (vert) (N)</b>
<b>Front Somersault</b>	Ankle	13550	8276
	Knee	10978	
	Hip	7998	
<b>Back Somersault</b>	Ankle	13107	8107
	Knee	8452	
	Hip	9486	
<b>Handspring</b>	Ankle	12234	10873
	Knee	7489	
	Hip	6490	
<b>Tsukahara</b>	Ankle	18237	10903
	Knee	10809	
	Hip	11605	

### *5.5 Analysis of Bone Torques and Deformation*

The following sub-sections describe the effects of internal and external landing forces on bone deformation.

#### **5.5.1 Bone Torque and Deformation Results**

The torque measured at the centre of the lower extremity bones (shank and thigh) were greater in model Three than model One. An example from the backward somersault skill is shown in Figure 5.20. The complete set of results for all skills can be found in Appendix I.

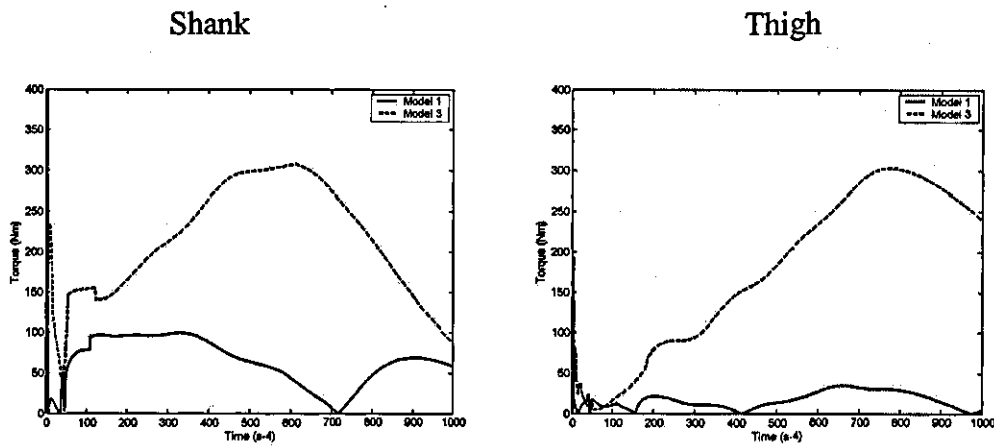


**Figure 5.20** Bone torques during the landing of a backward somersault skill (Model Three).

The bone torque results are consistent with the results from the joint reaction forces. The greater joint reaction forces present in model three also produced greater bone torques than in model one during the landing of each skill (Table 5.7). The peak bone torques do not increase with the increase in skill complexity and ground reaction force. These results are consistent with the joint reaction forces. The magnitudes of the torques do suggest that some deformation does occur in the bone during landing. These results may be useful when assessing the risk of bone injury during landing.

**Table 5.7** Maximum bone torques during each skill using models One and Three

Skill	Bone	Maximum bending torque (model 1) (Nm)	Maximum bending torque (model 3) (Nm)
Front Somersault	Shank	191	363
	Thigh	224	260
Back Somersault	Shank	102	310
	Thigh	42	290
Handspring	Shank	81	252
	Thigh	109	241
Tsukahara	Shank	184	432
	Thigh	158	369

The amount of bone deformation was estimated assuming a linear relationship between load and strain within the elastic strain region of the bone (Turner & Burr, 1993). The estimated bone deformation of the shank was based upon the deformation behaviour of the femur and scaled according to bone size.

The maximum bone deformation for the lower extremity bones are reported in Table 5.8. The simulated bone deformations are thought to represent values higher than the actual bone deformation present in a gymnast's bone during landing because the simulated deformations are close to the fracture limit for the bone. The vaults performed during this study are not the highest tariff vaults possible in gymnastics. More complex vaults require greater post flight height, this extra height increases the landing velocity and the forces associated with landing. However few bone fractures occur during highly complex vaults therefore less bone deformation than simulated is thought to occur at the lower velocity landings. The amount of bone deformation is difficult to evaluate.

**Table 5.8** Maximum bone deformations during each skill using models One and Three

<b>Skill</b>	<b>Bone</b>	<b>Maximum bone deformation (model 1) (cm)</b>	<b>Maximum bone deformation (model 3) (cm)</b>
Front Somersault	Shank	0.73	1.38
	Thigh	0.85	0.99
Back Somersault	Shank	0.39	1.18
	Thigh	0.16	1.10
Handspring	Shank	0.31	0.96
	Thigh	0.41	0.92
Tsukahara	Shank	0.70	1.64
	Thigh	0.60	1.40

### 5.5.2 Analysis of Bone Torque and Deformation Results

All the bone torques were below the fracture threshold reported in Martens et al. (1986) except for the shank bone in the Tsukahara vault using model Three. The bone torque in the shank exceeded the experimental fracture torque (Martens et al.,

1986) by approximately 60 Nm. However this was within one standard deviation of the mean reported in the study. There may be two possible reasons why the bone torque exceeded the reported fracture threshold. Firstly the gymnast during testing did not land with a single foot placement and hence took a step. As the simulation model cannot do this it may be possible that the forces in the simulation are unrealistically high. Secondly the experimental study (Martens et al., 1986) was performed using human bones in vitro. Human bones are naturally curved to allow for predictable bending direction. The muscles surrounding the bone are structured to support the bone bending in one direction. This curvature in the bones reduces the strength but increases the load predictability (Bertram & Biewener, 1988). When a bone is loaded in vivo, simultaneous contraction of the surrounding muscles act to oppose the loads, so the bone can withstand higher loads (Kaastad et al., 2000). This suggests that in reality the co-contraction of the surrounding muscles reduce the bending bone torque and hence the bone deformation. The likelihood that the gymnast has denser bones than the 'normal' population as a result of training must be considered. This may increase the strength of the bones may increase the fracture threshold.

The 'lumped' muscle model does not support the bones in the same way as in a human subject. Although the lumped muscle model may produce a realistic estimate of the joint reaction forces, the bones in the model may appear to experience more torque than in reality. The results from Table 5.7 and 5.8 should be viewed with caution as they may reflect higher bone torques and deformations than may actually be present during gymnastic vault landings. The results are useful in themselves as the values can be used later to determine if the bending torque and deformation has decreased as a result of the optimisation of landing mat properties or landing strategy adopted by the gymnast.

### 5.5.3 The FEM of Bone

Implementing the FEM of bone into the model of the gymnast (model Four) proved difficult. Although the FEM of bone was able to reproduce the results of the three point bending test, once the FEM was placed in the gymnast model a problem occurred. This problem related to the way the forces at the joints were applied to the FEM. The joint reaction forces could only be uniformly distributed on the contact surface of each end of the bone. Although the estimated bone bending torque should



have produced approximately 1 cm of bone deformation (Table 5.8) the FEM bone only bent 0.02 mm. The software restricted the application of the forces and little torque was produced in the bone and therefore the bending forces appeared to cancel. To improve this a computer aided design (CAD) model of the bone may have helped since importing a CAD model allows more control over how the forces are applied to the FE CAD model.

The FEM of the bone was modified to account for the natural curvature of human bone. This meant the bone had effectively bent a small amount before the simulation started. Running the simulation with this initial condition improved the maximum bone deformation to 2 mm. However this changed the geometry of the model making it difficult to compare any results of the model as a whole to model Three. The decision was made not to use any results from model Four due to the problems described earlier.

### *5.6 Summary*

This chapter has evaluated all four of the simulation models. It has been demonstrated in the evaluation that each model successfully simulated the landing from four gymnastic vaults. The best agreement between the simulation and the performance was Model Three for the front and back somersault vaults. Models One and Three performed similarly when attempting to match the performance of the handspring and Tsukahara vaults. The forward and backward somersault skills were matched the best and will be used in future optimisations. Although the gymnast-mat models matched the other skills reasonably well some elements such as peak vertical GRF in the Handspring skill were not so well represented therefore the Handspring and Tsukahara skills will not be used for future optimisations. Analysis of the simulated joint reaction forces and bone deformations showed that a lumped muscle model (model Three) increased these forces above the levels seen using a torque driven model. Model Three is ready for use when investigating landing techniques and different landing mat properties.

## CHAPTER 6

### MODEL OPTIMISATION AND APPLICATION

This chapter uses the models evaluated in Chapters 3 and 5 to investigate the mechanics of landing and answer two research questions. The extensor activation histories of the lumped muscle model (gymnast-mat model Three) were optimised to determine whether changes to the landing mat or strategy of the gymnast can reduce the ground and joint reaction forces experienced by the gymnast.

#### *6.1 Optimising the Landing Strategy*

What adjustments can be made to the landing strategy to reduce GRF's, internal forces and minimize the chances of injury?

In Chapter 5 it was shown that the gymnast tended to modify his landing strategy (muscle activation timings) to produce the same internal loading characteristics independent of the skill. This meant that as ground reaction forces increased with skill complexity the joint reaction forces did not. A gymnast will have a landing goal; this may be to minimise the forces experienced by the gymnast at landing or to 'stick' the landing regardless of the forces. A balance is selected between the two goals. A gymnast may have a preferred landing technique (joint orientation) that he applies to most landing skills. The landing technique may not minimise the internal joint forces experienced by the gymnast but may incorporate the most adaptable landing strategy (McNitt-Gray, 2000). Since the gymnast can voluntarily modulate the external loading experienced during impact, it may be possible for the gymnast to minimise the internal forces by altering the muscle recruitment / activation patterns (McNitt-Gray et al., 1990).

Gymnast-mat model Three was used to investigate whether it is possible to reduce the ground and joint reaction forces during landing through adjustments in muscle activation. The extensor muscle activation time histories were optimised in order to reduce the internal and external forces experienced by the gymnast.

Firstly the Simplex optimisation algorithm was used to vary 12 extensor muscle activation parameters (the flexor activation histories remained the same as in

the evaluation) and minimise score one ( $S_1$ ). Score one consisted of the maximum vertical and horizontal ground reaction force plus penalties. The score was defined by the equation:

$$S_1 = (F_z + F_y) + \text{penalties}$$

$F_z$  = peak vertical GRF

$F_y$  = peak horizontal GRF

Secondly the Simplex optimisation algorithm was used to vary the muscle activation parameters and minimise score two ( $S_2$ ). Score two consisted of the maximum torque in the shank and thigh bones plus penalties. The score was defined by the equation:

$$S_2 = (T_s + T_t) + \text{penalties}$$

$T_s$  = peak shank bone torque

$T_t$  = peak thigh bone torque

Several constraints were placed upon the simulations during the optimisation to minimise the computational time and ensure a result that was within the limits of the human body. Each constraint was written as a penalty and when the simulation exceeded any of the constraints a penalty was added to the score. The penalties were weighted so that approximately 100 N of force was equivalent to  $1^\circ$  in joint angle and 0.1 m/s in centre of mass velocity. However this was finely adjusted depending upon the joint. Each penalty contained an exponent and multiplier that was adjusted depending upon how much each penalty would ramp up and what the initial step would be. The ankle ramped up the steepest as any angle below the limit could cause problems with the ankle's construction (as discussed in chapter five). The 'force at the end' of the simulation penalty did not ramp up as quickly as it was thought that a few Newtons of force either side of the bounds was less severe. The exact number for the multiplier or exponent was determined partly by calculating what the output of the parameter had to be multiplied by to achieve a score of one, but mainly by trial and error.

The first constraint (endforce) was based on the vertical GRF at the end of the simulation. If this force was between 500 N and 2000 N at the end of the simulation no penalty was added. This range was chosen as it was similar to the

range found during model evaluation for the matching of the four skills. The penalty (pen1) due to the force at the end of the simulation was defined by the MatLab syntax:

```
if endforce > 2000
pen1 = (endforce - 2000)^1.3;
end
if endforce < 500
pen1 = (abs(500 - endforce))^1.3;
end
```

The ankle constraint (anklemin) was based on the minimum ankle joint angle during the simulation. The ankle was limited so that if the ankle joint angle was less than 60° a penalty was added to the total score. This minimum limit of 60° was chosen for two reasons. Firstly, as discussed in chapter five, if this ankle range is exceeded it causes problem with the construction of the muscles surrounding the ankle joint. Secondly, this value was the approximate minimum in the evaluation trials of all four skills. The ankle penalty (pen2) was defined by the MatLab syntax:

```
if anklemin < 60
pen2 = (60 - anklemin)^2 x 500;
end
```

The knee constraint (kneemin) was similar to the ankle constraint but was based on the minimum knee angle during the simulation. The minimum knee angle during the simulation was set at 80°. This was chosen for two reasons. Firstly it was just below the minimum knee angle during the evaluation trials. Secondly a knee angle below this was deemed by an experienced F.I.G. gymnastics judge to be excessive and may incur a landing deduction. The knee penalty (pen3) was defined by the MatLab syntax:

```
if kneemin < 80
pen3 = (80 - kneemin)^1.5 x 250;
end
```

The hip constraint (hipmin) was similar to the knee constraint but was based on the minimum hip angle during the simulation. For the same reasons as the knee constraint the minimum hip angle was set at  $80^\circ$ . The hip penalty (pen4) was defined by the MatLab syntax:

```
if hipmin < 80
pen4 = (80 - hipmin)^1.5 x 250;
end
```

The vertical velocity constraint (cofmvertvel) was based on the vertical velocity of the mass centre at the end of the simulation. The limits were based upon the evaluation trials in Chapter 5. It was thought that if the gymnast could complete the landing by standing up when their vertical mass centre velocity was within  $\pm 1.0$  m/s at the end of the simulation it was best to keep these limits for the optimisation. The vertical velocity penalty (pen5) was defined by the MatLab syntax:

```
if cofmvertvel < -1.0
    pen5 = ((abs(cofmvertvel))-1.0) x 10000;
end
if cofmvertvel > 1.0
    pen5 = ((abs(cofmvertvel))-1.0) x 10000;
end
```

The horizontal velocity constraint (cofmhorvel) was similar to the vertical velocity constraint but it defined the limits of the mass centre in the horizontal direction. The limits were  $\pm 2.0$  m/s for the same reason as discussed in the vertical velocity constraint. The horizontal velocity penalty (pen6) was defined by the MatLab syntax:

```
if cofmhorvel < -2.0
    pen6 = ((abs(cofmhorvel))-2.0) x 10000;
end
if cofmhorvel > 2.0
```

```
pen6 = ((abs(cofmhorvel))-2.0) x 10000;
end
```

## 6.2 Optimising the Landing Mat

What adjustments can be made to the landing mat to reduce GRF's and internal forces to minimize the chances of injury?

It has been shown that the landing mat can influence the ground reaction force during impacts (McNitt-Gray et al., 1993, 1994; Dixon et al., 2000). The landing mat has been reported as one of the factors that may contribute to the frequency and severity of injuries (Dufek & Bates, 1991).

Model Three was used to investigate whether it is possible to reduce the ground and joint reaction forces experienced by the gymnast during landing by modifying the landing mat. Six landing mat spring parameters (spring stiffness and damping coefficient for each layer) were optimised in order to reduce the external forces (score one) experienced by the gymnast and to determine what the effects were on the internal forces. The muscle activation timings remained the same as in the model evaluation. Since the muscle activation histories remained unchanged any decrease in external GRF's may also result in decreased internal forces.

The Simplex optimisation algorithm was used to vary the landing mat spring parameters and minimise score one. Score one ( $S_1$ ) consisted of the maximum vertical and horizontal ground reaction force plus penalties. The score was defined by the equation:

$$S_1 = (F_z + F_y) + \text{penalties}$$

$F_z$  = peak vertical GRF

$F_y$  = peak horizontal GRF

The same constraints used when optimising the landing strategy were also used during the optimisation of the landing mat. However additional constraints were required to ensure the landing mat behaved within acceptable limits. The first additional constraint (peakmatdefvert) was based on the maximum vertical mat deformation during the simulation. If the landing mat's maximum deformation was between 0.08 m and 0.18 m no penalty was added. This range was chosen as it was

similar to the minimum and maximum depression found during model evaluation for the matching of the four skills. The exponent of 1.5 or 2 was required to ensure the penalty ramped up quickly so that the mat depression could not exceed the maximum depth of the mat (0.20 m). The multiplier ensured that 1 cm of mat deformation was approximately equivalent to 1000 N of GRF. The penalty (pen7) due to the vertical mat deformation was defined by the MatLab syntax:

```
peakmatdefvert = max(matvertdef);
if peakmatdefvert < 0.08
    pen7 = abs(0.08 - peakmatdefvert)^1.5 x 10000000;
end
if peakmatdefvert > 0.18
    pen7 = abs(peakmatdefvert - 0.18)^2 x 10000000;
end
```

The second additional constraint (peakmatdefhor) was based on the maximum horizontal mat deformation during the simulation. If the landing mat deformed horizontally between 0.01 m and 0.10 m no penalty was incurred. This range was chosen as it was similar to the minimum and maximum horizontal mat deformations during model evaluation. The penalty (pen8) due to the horizontal mat deformation was defined by the MatLab syntax:

```
peakmatdefhor = max(mathordef);
if peakmatdefhor < 0.01
    pen8 = abs(0.02 - peakmatdefhor)^1.5 x 10000000;
end
if peakmatdefhor > 0.10
    pen8 = abs(peakmatdefhor - 0.10)^2 x 10000000;
end
```

The upper and lower bounds were set at  $\pm 20\%$  of the landing mat parameters determined in chapter three. These were chosen to ensure the optimised landing mat parameters were within the construction capabilities of the manufacturer, as the optimised landing mat may not be too dis-similar to the current F.I.G. landing mat.

### 6.3 Optimisation Results

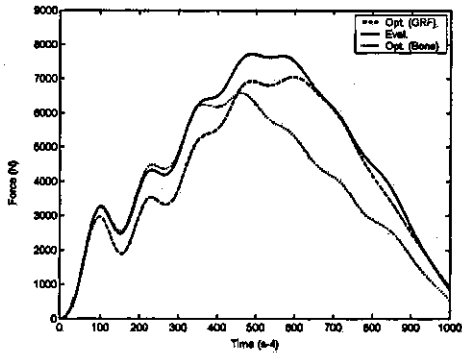
The following sub-sections report the results of the optimisations. The results reflect the general trend and less emphasis should be placed on the actual numbers when reading through this section. The muscle activation timings and landing mat spring parameters were optimised using gymnast-mat model Three for the front and back somersault skills. Only the front and back somersault skills were chosen for optimisation since they performed the best during the evaluation. The problems associated with the handspring and Tsukahara skills discussed in chapter five meant they were not used for subsequent optimisations.

#### 6.3.1 Optimisation of the Landing Strategy – Front Somersault

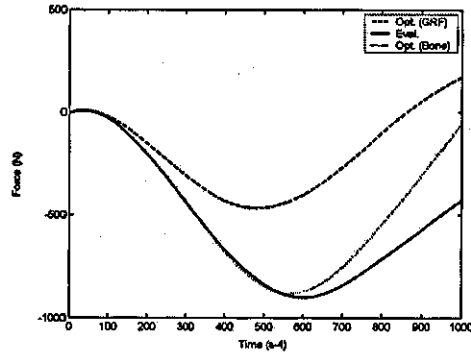
The optimisation of the landing strategy (using score one) successfully reduced both the peak vertical and horizontal ground reaction forces to yield a score of 7522 N with no penalties. The peak vertical GRF decreased from 7725 N in the evaluation to 7057 N in the optimised landing. The peak horizontal GRF decreased from 900 N in the evaluation to 465 N in the optimised landing. This decrease in GRF appeared to result from greater joint motion (Figure 6.1).

The optimisation of the landing strategy (using score two) also decreased the peak vertical and horizontal GRF's to produce a score of 473 Nm with no penalties. The optimised score is lower than the evaluation score of 643 Nm. The peak vertical GRF decreased from 7725 N in the evaluation to 6582 N in the optimised landing. Using score two during the optimisation resulted in a lower peak vertical GRF than when attempting to minimise the GRF's (score one). The peak horizontal GRF decreased from 900 N in the evaluation to 882 N in the optimised landing. The peak horizontal GRF using score two produced a greater peak force than when using score one (Figure 6.1).

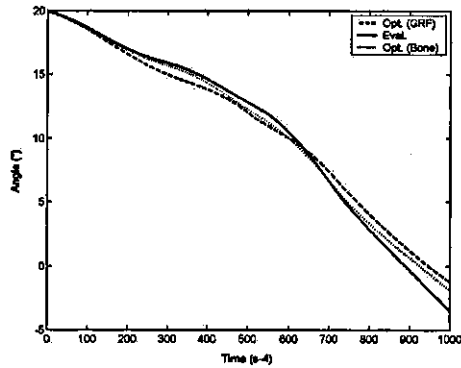




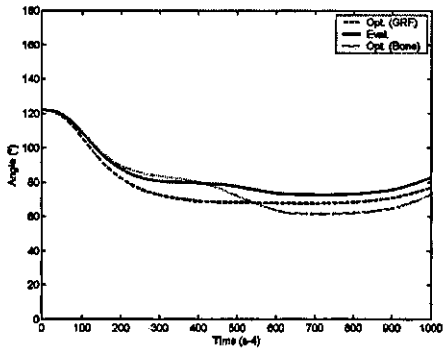
(a)



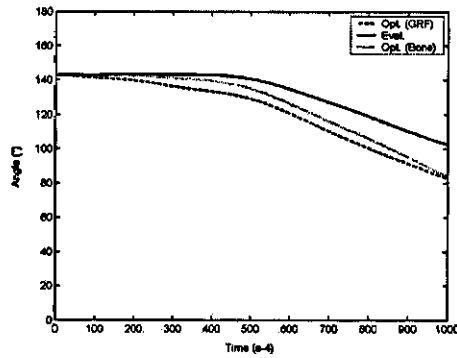
(b)



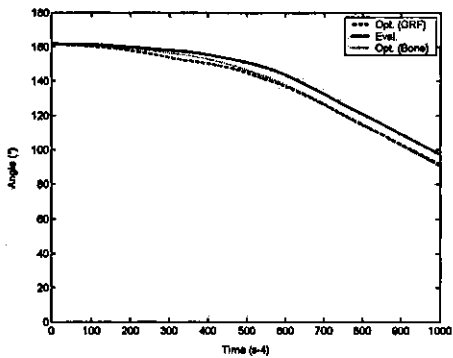
(c)



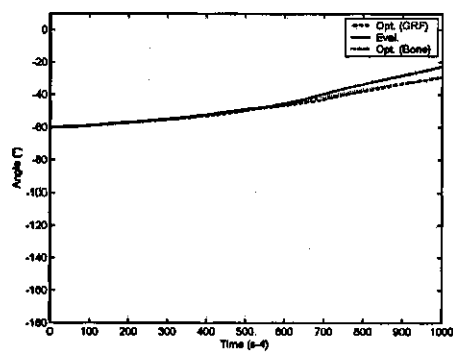
(d)



(e)



(f)



(g)

**Figure 6.1** Optimisation of landing strategies for the front somersault skill (a) VGRF (b) HGRF (c) trunk orientation (d) ankle angle (e) knee angle (f) hip angle (g) shoulder angle.

The changes in joint angle timings were due to the changes in the muscle activation timings. When minimising the GRF's (score one) these changes were characterised by a later ramp up time at the ankle and earlier ramp up times at the remaining joints (Figure 6.2). The magnitudes of the optimised activation levels were greater than the evaluation activation levels.

When minimising the bone torques (score two) the activation level at the ankle ramped up earlier than either the evaluation or score one (GRF's) but did not ramp up to such a high level. This depressed activation using score two was present at the remaining joints (Figure 6.2).

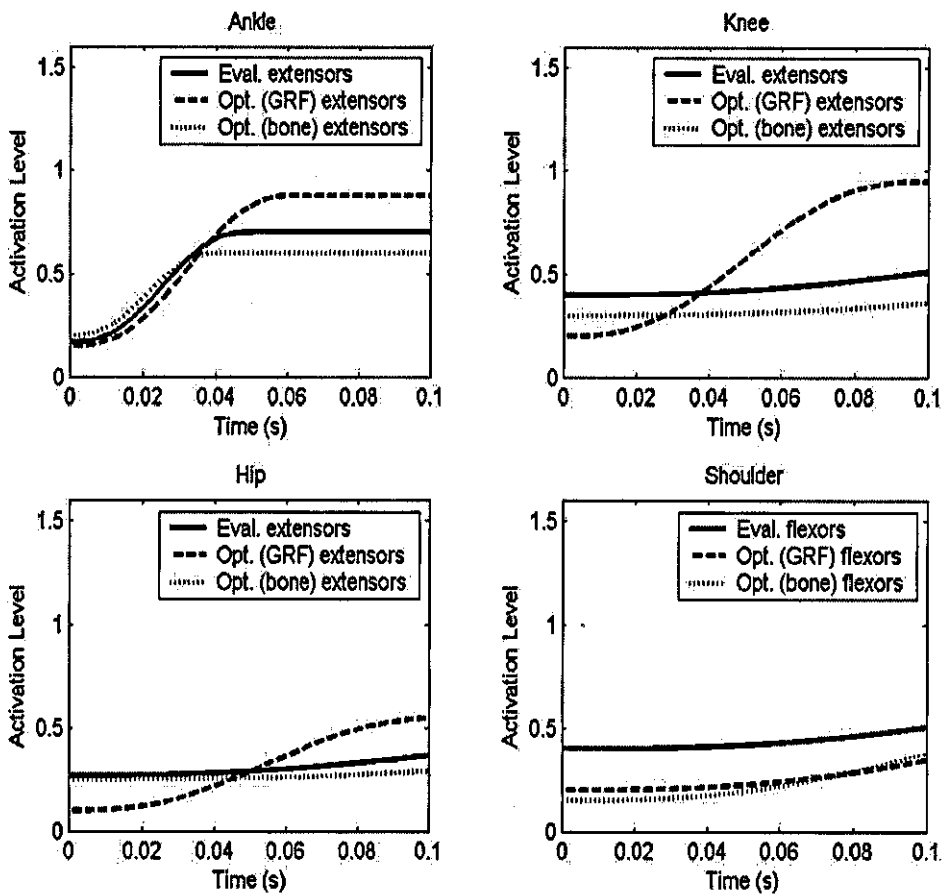


**Figure 6.2** Comparison of the muscle activation histories for the front somersault skill: model evaluation and optimisation results.

The changes in muscle activation caused changes to the joint reaction forces (JRF's). All of the JRF's in the optimised landing (using score one) exhibited a later peak force than the evaluation. The magnitude of the force was decreased at the ankle and the hip but was increased at the knee (Figure 6.3).

All the JRF's in the optimised landing (using score two) exhibited an earlier peak JRF and all the peak JRF's were lower than both the evaluation and the forces using score one (Figure 6.3).

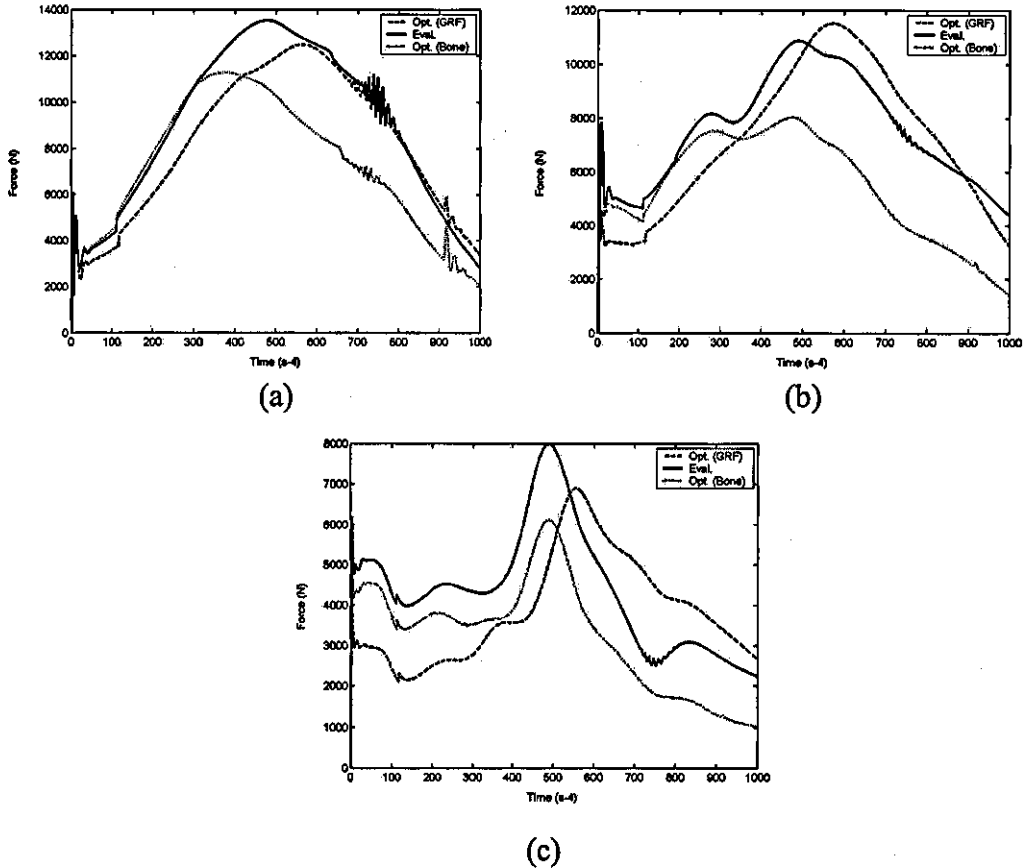


**Figure 6.3** Joint reaction forces during the optimised landing strategies for the front somersault (a) Ankle, (b) Knee, (c) Hip.

When optimising the muscle activation timings using score one the reduced ground reaction forces resulted in increased bending moments in the lower extremity bones when compared to the evaluation. The peak torque in the shank bone increased by approximately 100 Nm and the peak torque in the thigh bone increased by approximately 130 Nm (Figure 6.4).

However when optimising the muscle activation timings using score two the reduction in bone bending moments within the lower extremity also caused a decrease in GRF's when compared to the evaluation. The peak torque in the shank bone decreased by approximately 86 Nm and the peak torque in the thigh bone decreased by approximately 84 Nm (Figure 6.4).

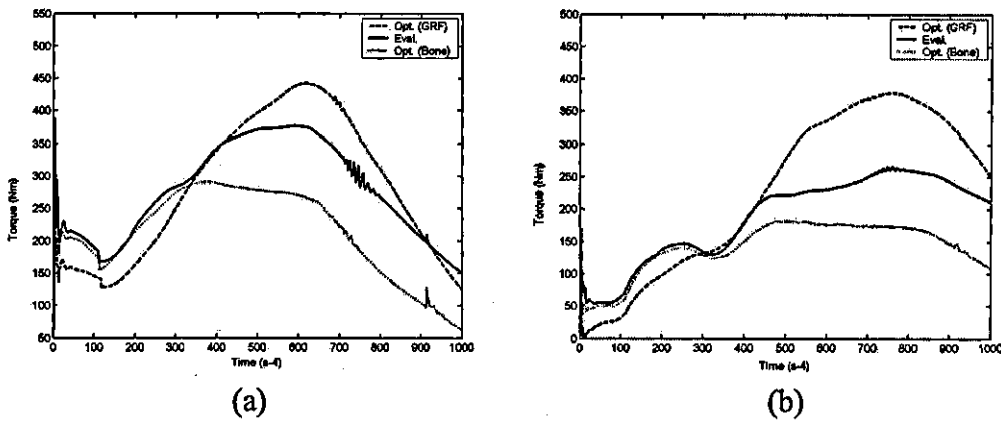


**Figure 6.4** Lower extremity bone bending torques during the front somersault skill (a) shank, (b) thigh.

Another result of optimising the landing strategy using score one was that although the JRF's were reduced at some joints this was at a cost of increasing the peak muscle forces required to land successfully (Figure 6.5).

However when optimising the landing strategy to minimise the bone torques (score two) the muscle forces decreased. The muscle forces were lower than both the evaluation and the muscle force when using score one (Figure 6.5).

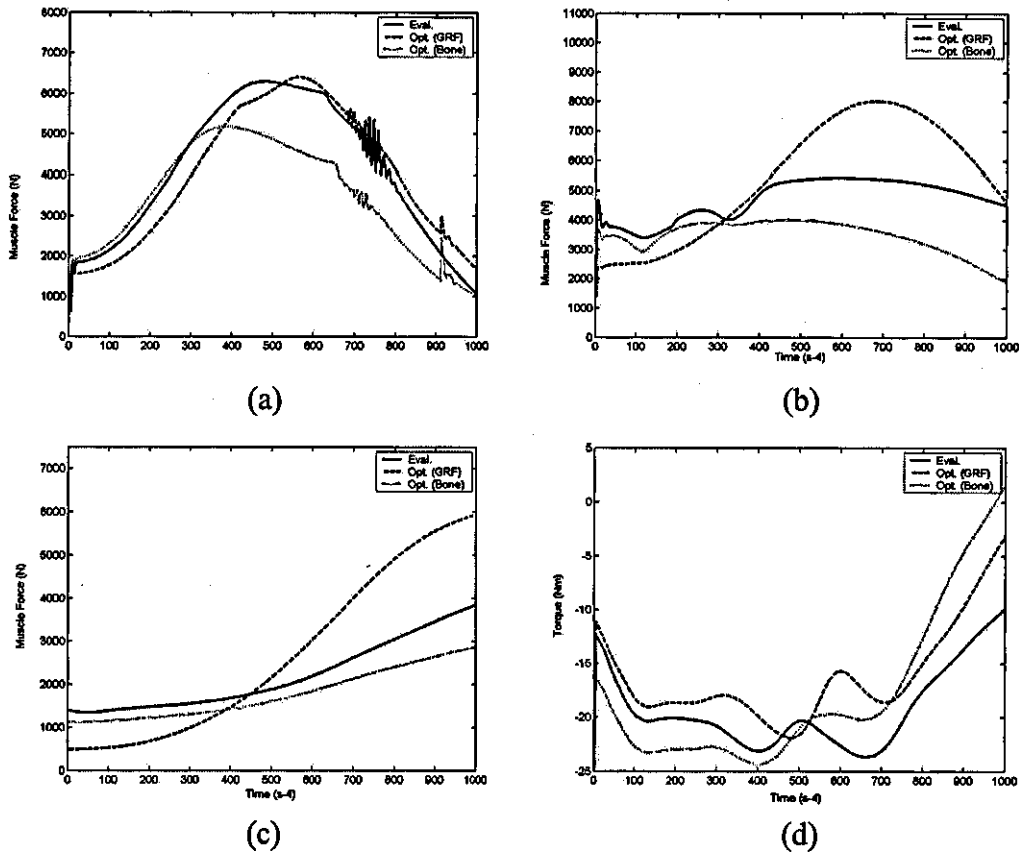


**Figure 6.5** Extensor muscle forces and shoulder torque during the front somersault skill (a) Ankle, (b) Knee, (c) Hip, (d) Shoulder.

A summary of the peak ground and joint reaction forces, peak bone torques and muscle forces are reported in Table 6.1. It has been shown that when the landing strategy was optimised using score one (minimising GRF's) the GRF's in the solution are lower than the evaluation but this results in greater bone torques during the landing. When the landing strategy was optimised using score two (minimising bone torques) the bone torques were lower than the evaluation and that of score one. Using score two also reduces the peak vertical GRF to a force lower than both the evaluation and that of score one.

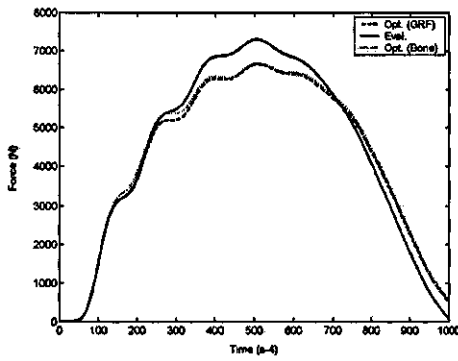
**Table 6.1.** Comparison of peak forces and torques during model evaluation and optimisation for the front somersault skill

Parameter (peaks)	Evaluation	Opt. (GRF)	Opt. (Bone)
VGRF	7725 N	7075 N	6582 N
HGRF	900 N	465 N	882 N
Ankle JRF	13543 N	12499 N	11294 N
Knee JRF	10870 N	11519 N	8051 N
Hip JRF	7990 N	6900 N	6117 N
Shank torque	377 Nm	442 Nm	291 Nm
Thigh torque	266 Nm	379 Nm	182 Nm
Ankle extensors	6294 N	6406 N	5188 N
Knee extensors	5442 N	8022 N	4011 N
Hip extensors	3848 N	5936 N	2875 N

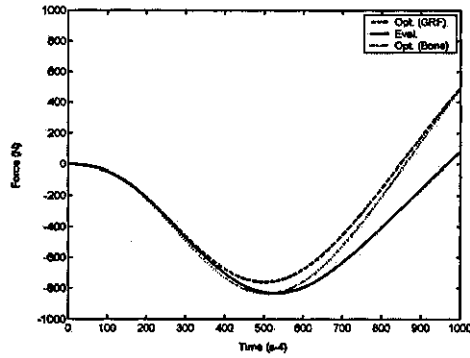
### 6.3.2 Optimisation of the Landing Strategy – Back Somersault

The optimisation of the landing strategy (using score one) successfully decreased both the peak vertical and horizontal ground reaction forces to yield a score of 7450 N with two penalties. The peak vertical GRF decreased from 7304 N in the evaluation to 6667 N in the optimised landing. The peak horizontal GRF decreased from 831 N in the evaluation to 759 N in the optimised landing. The optimised landing incurred two penalties, the first penalty of 0.15 was equivalent to 0.33 N below the minimum limit set by the vertical force at the end of the simulation constraint. The second penalty was 23.07 and was equivalent to 0.21° below the minimum limit set by the ankle constraint. Despite these small penalties the optimised landing was still able to improve upon the evaluation. Again this reduction in GRF's appeared to result from greater joint motion especially at the ankle joint (Figure 6.6).

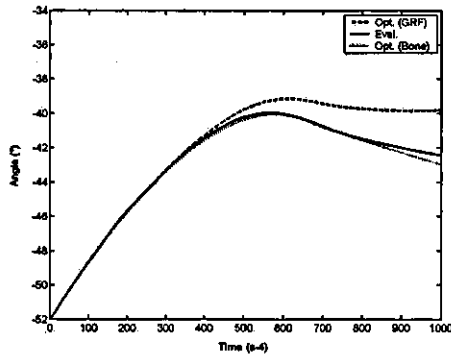
The optimisation of the landing strategy (using score two) resulted in a lower peak vertical force and the same horizontal force as in the evaluation and produced a score of 595 Nm with one penalty, compared to a score of 608 Nm in the evaluation. The peak vertical GRF decreased from 7450 N in the evaluation to 6667 N in the optimised landing (the same as score one). The peak horizontal GRF was 831 N in the evaluation and was also 831 N in the optimised landing. The peak horizontal GRF using score two produced a higher peak force than when using score one (Figure 6.6). The optimised landing incurred one penalty, the penalty of 2.12 was equivalent to a force of 1.0 N below the limit set by the vertical force at the end of the simulation constraint (endforce).



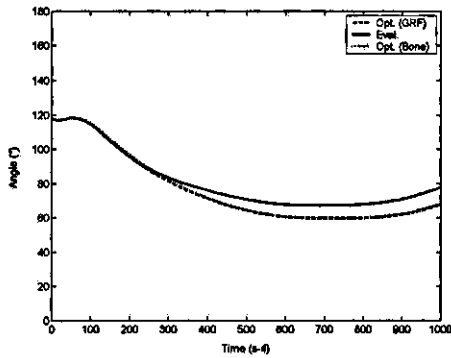
(a)



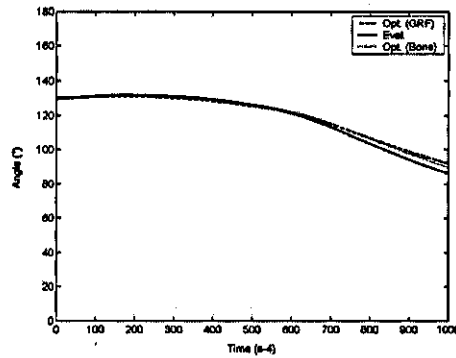
(b)



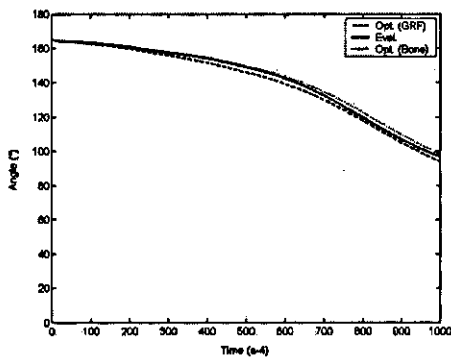
(c)



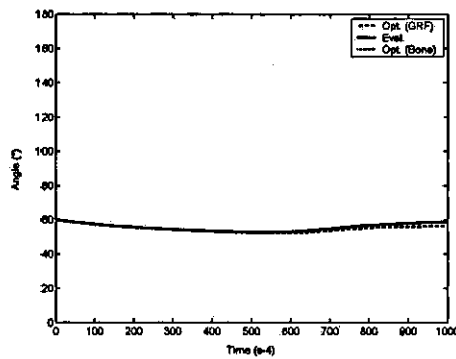
(d)



(e)



(f)



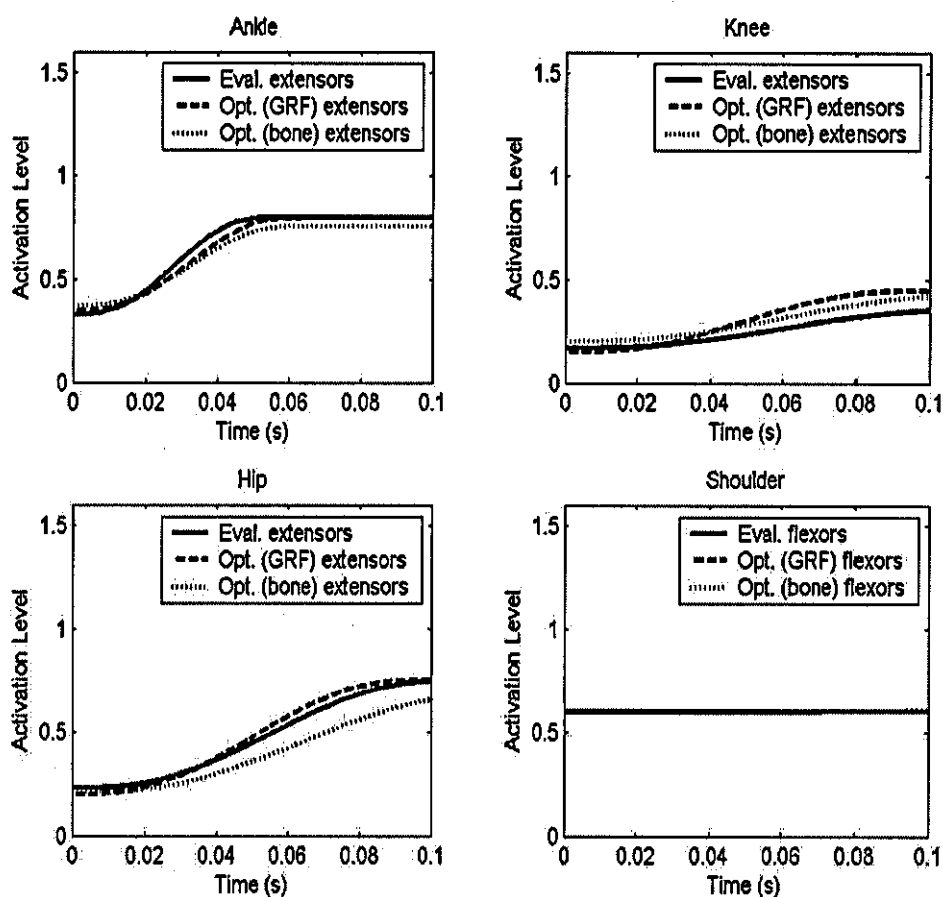
(g)

Figure 6.6 Optimisation of landing strategies for the back somersault skill (a) VGRF (b) HGRF (c) trunk orientation (d) ankle angle (e) knee angle (f) hip angle (g) shoulder angle.



The changes in joint angle timings were due to the small changes in the muscle activation timings. These changes (using score one) were characterised by a later ramp up time at the ankle and earlier ramp up times at the remaining joints (Figure 6.7). The magnitudes of the optimised activation levels were very similar to the evaluation activation levels except at the knee where the optimised activation level was a little higher.

The changes to the muscle activation timings using score two were characterised by slightly later ramp up times than score one and lower magnitudes of activation at the ankle and hip when compared to the evaluation and score one (Figure 6.7).



**Figure 6.7** Comparison of the muscle activation histories for the back somersault skill: model evaluation and optimisation results.

The changes in muscle activation caused changes to the JRF's. All of the JRF's in the optimised landing (using score one) exhibited a later peak force than the evaluation except at the hip where the peaks were similar. The magnitudes of the

forces were reduced at the ankle, increased at the knee and were approximately the same at the hip (Figure 6.8).

The JRF's at the ankle and hip (using score two) were lower in the optimised landing than the evaluation and score one. The knee JRF using score two was lower than score one but not as low as in the evaluation (Figure 6.8).

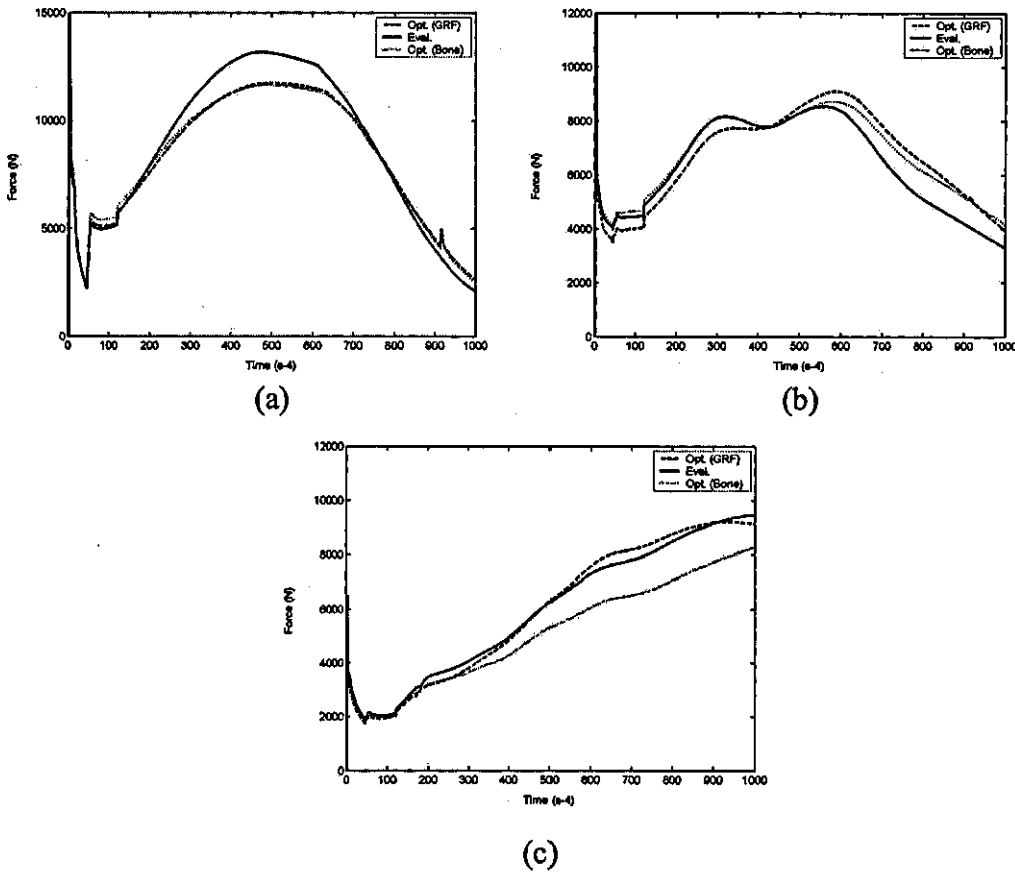


**Figure 6.8** Joint reaction forces during the optimised landing strategies for the back somersault (a) Ankle, (b) Knee, (c) Hip.

The changes in muscle activation and therefore ground and joint reaction forces (using score one) resulted in increased bending moments in the lower extremity bones. These results are consistent with the results from the front somersault skill. The peak torque in the shank bone increased by approximately 25 Nm and the peak torque in the thigh bone increased by approximately 50 Nm (Figure 6.9).

When using score two the optimised landing strategy resulted in small decreases in bone bending moments compared to the evaluation. The peak torque in

the shank bone decreased by 1 Nm compared to the evaluation and the peak torque in the thigh bone decreased by 12 Nm. (Figure 6.9).

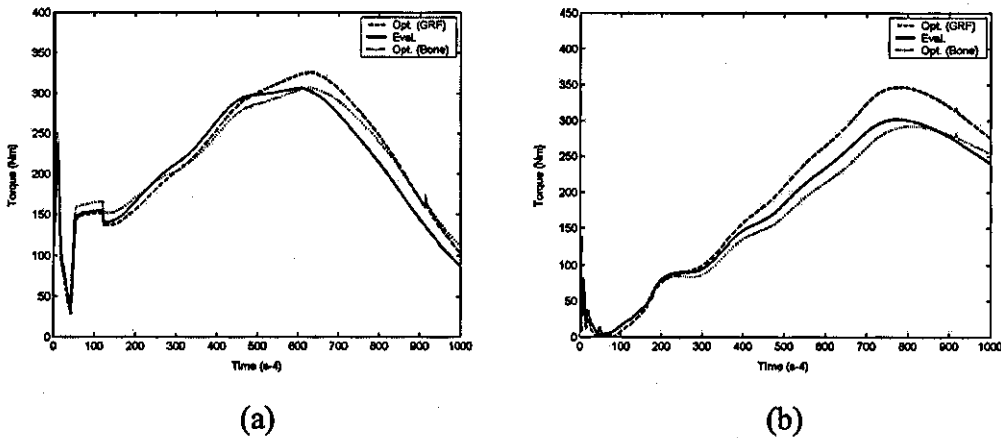


**Figure 6.9** Lower extremity bone bending torques during the back somersault skill (a) shank, (b) thigh.

At the ankle the peak muscle forces were less in the optimised landing than the evaluation using score one. However at the knee the peak muscle forces were greater in the optimised landing than in the evaluation. The greater muscle force at the knee in the optimised landing was consistent with the front somersault skill. The peak muscle force at the hip and the shoulder torque during the optimised landing was very similar to that of the evaluation (Figure 6.10).

The peak muscle forces using score two were consistently lower than score one and the evaluation except at the knee joint where the muscle force was only lower than the optimised landing of score one. Peak muscle forces using score two occurred slightly later than score one and the evaluation (Figure 6.10).

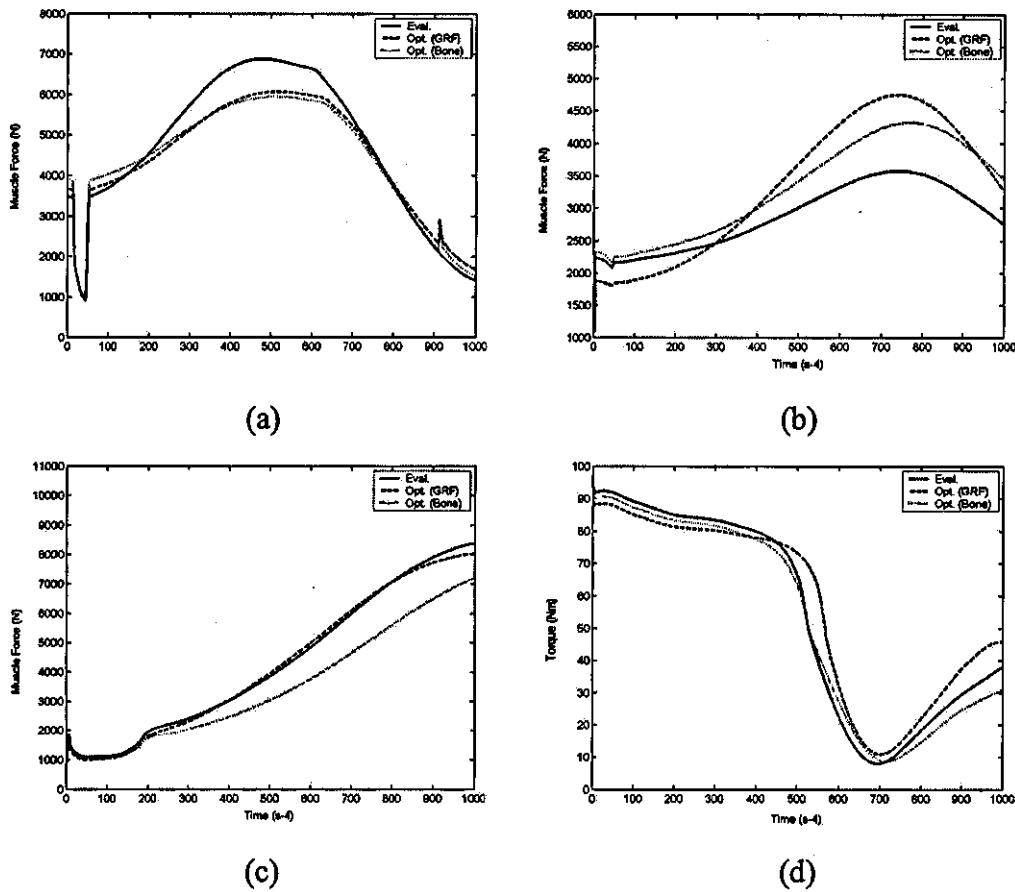


**Figure 6.10** Extensor muscle forces and shoulder torque during the back somersault skill (a) Ankle, (b) Knee, (c) Hip, (d) Shoulder.

A summary of the peak ground and joint reaction forces, peak bone torques and muscle forces for the back somersault skill are reported in Table 6.2. The back somersault results are consistent with the results from the front somersault skill. It has been shown that when the landing strategy was optimised using score one (minimising GRF's) the GRF's in the solution are lower than the evaluation but this results in greater bone torques during the landing. When the landing strategy was optimised using score two (minimising bone torques) the bone torques were lower than the evaluation and that of score one. Using score two also reduces the peak vertical GRF to a force lower than the evaluation.

**Table 6.2.** Comparison of peak forces and torques during model evaluation and optimisation for the back somersault skill

Parameter (peaks)	Evaluation	Opt. (GRF)	Opt. (Bone)
VGRF	7304 N	6667 N	6667 N
HGRF	831 N	759 N	831 N
Ankle JRF	13172 N	11740 N	11648 N
Knee JRF	8548 N	9099 N	8726 N
Hip JRF	9460 N	9138 N	8293 N
Shank torque	306 Nm	326 Nm	305 Nm
Thigh torque	302 Nm	347 Nm	290 Nm
Ankle extensors	6882 N	6070 N	5954 N
Knee extensors	3580 N	4756 N	4332 N
Hip extensors	8388 N	8050 N	7203 N

### 6.3.3 Optimising the Landing Mat – Front Somersault

The optimisation of the six landing mat parameters resulted in a decreased peak vertical and horizontal ground reaction force with a score of 8494 N and no penalties, compared to a score of 8625 N in the evaluation. The peak vertical ground reaction force was reduced from 7725 N in the evaluation to 7642 N using the optimised landing mat. The peak horizontal force decreased from 900 N in the evaluation to 852 N using the optimised landing mat (Figure 6.11). This reduction in peak GRF's also resulted in a slight decrease in peak shank and thigh bone torques. The shank bone torque decreased from 377 Nm in the evaluation to 374 Nm using the optimised landing mat. The peak thigh bone torque decreased from 266 Nm in the evaluation to 264 Nm using the optimised landing mat (Figure 6.12).

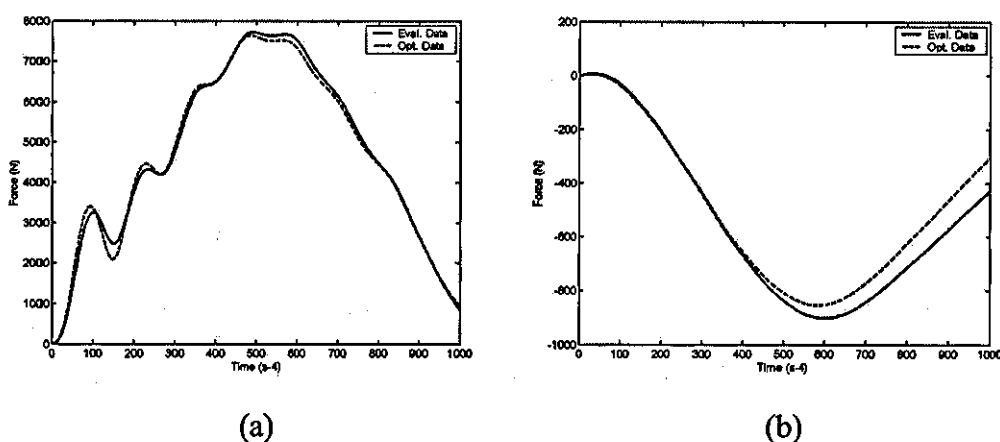


**Figure 6.11** Optimisation of landing mat properties for the front somersault skill (a) VGRF (b) HGRF.

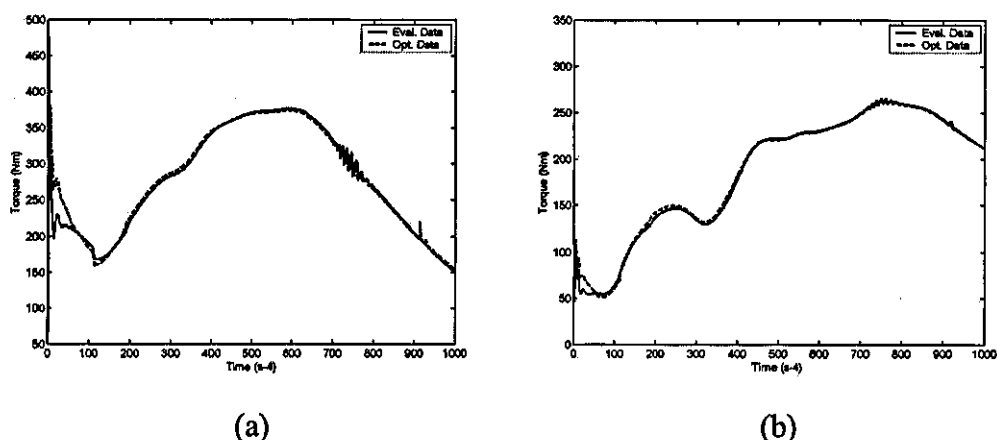


**Figure 6.12** Lower extremity bone bending torques during the front somersault skill (a) shank, (b) thigh.

The changes in the VGRF and HGRF were due to the changes in the landing mat parameters. The optimisation did not change the stiffness values for any layer by much, less than 0.5%. However, the optimisation selected damping parameters that hit the upper bounds for each layer of the mat. Therefore the results suggest that a landing mat that has its damping increased by 20% reduces the internal and external forces on the gymnast. Increasing the damping further may reduce the forces on the gymnast even more.

Increasing the damping of each layer means that the landing mat does not deform as much in the optimised landing when compared to the evaluation, 0.12 m to 0.15 m respectively. A further result of increased damping means that the initial

force between the foot and the top layer of the mat is greater using the optimised landing mat compared to the evaluation (Figure 6.13).

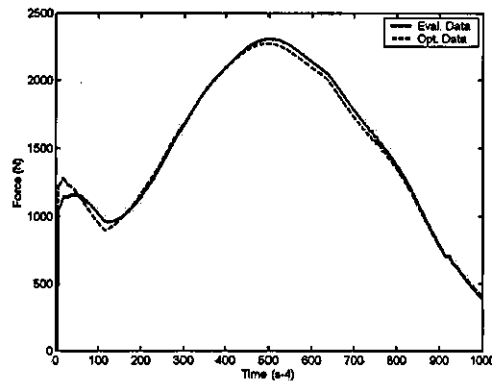


**Figure 6.13** Toe to top mat layer force during the front somersault skill.

The optimised mat parameters are presented in Table 6.3 and are compared to the evaluation landing mat parameters.

**Table 6.3.** Optimised landing mat parameters for the front somersault skill

Parameter	Optimised Landing Mat	Evaluation Landing Mat
Score	8494 N	8625 N
Penalties	0	0
Top layer stiffness (N/m)	61197	61080
Middle layer stiffness (N/m)	57591	57530
Bottom layer stiffness (N/m)	928340	928120
Top layer damping (Ns/m)	420 *	350
Middle layer damping (Ns/m)	516 *	430
Bottom layer damping (Ns/m)	348 *	290

\* = upper bound reached

### 6.3.4 Optimising the Landing Mat – Back Somersault

The optimisation of the landing mat parameters resulted in a decreased peak vertical and horizontal ground reaction force with a score of 10880 N and one penalty, compared to a score of 10994 N in the evaluation. The peak vertical ground reaction force was reduced from 7304 N in the evaluation to 7219 N using the optimised landing mat. The peak horizontal force decreased from 831 N in the evaluation to 801 N using the optimised landing mat (Figure 6.14). The one penalty of 2859 was for the force at the end of the simulation being below the 500 N limit. The reduction in peak GRF's also resulted in slight decrease in peak shank and thigh bone torques. The shank bone torque decreased from 306 Nm in the evaluation to 305 Nm using the optimised landing mat. The thigh bone torque decreased from 302 Nm in the evaluation to 300 Nm using the optimised landing mat (Figure 6.15).

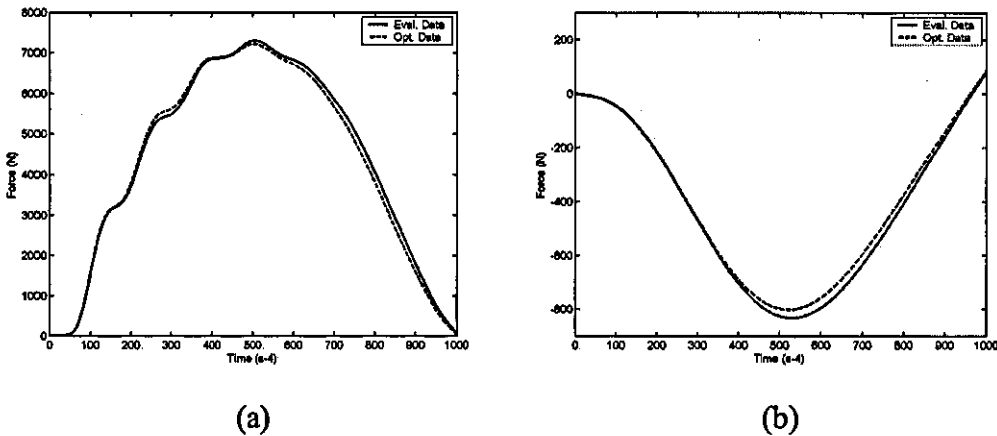


**Figure 6.14** Optimisation of landing mat properties for the back somersault skill (a) VGRF (b) HGRF.

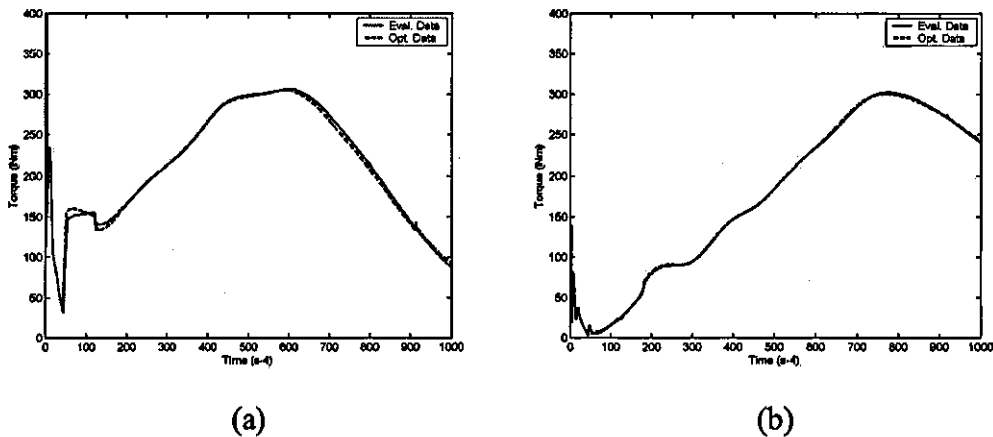


**Figure 6.15** Lower extremity bone bending torques during the back somersault skill (a) shank, (b) thigh.



The changes in the VGRF and HGRF were due to the changes in the landing mat parameters. The optimisation did not change the stiffness values for any layer by much, less than 0.1%. However, the optimisation selected damping parameters that hit two out of three of the upper bounds for each layer of the mat. Therefore the results suggest that a landing mat that has its damping increased by 20% reduces the internal and external forces on the gymnast, yet increasing the damping further may reduce the forces on the gymnast even more. These results are consistent with the front somersault results.

Increasing the damping of each layer means that the landing mat does not deform as much in the optimised landing when compared to the evaluation, 0.15 m to 0.13 m respectively. Again a further result of increased damping meant that the initial force between the foot and the top layer of the mat was greater using the optimised landing mat compared to the evaluation (Figure 6.16).

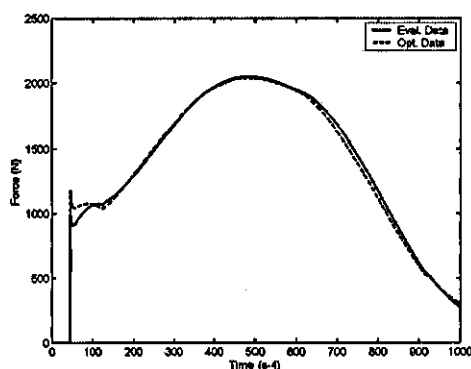


**Figure 6.16** Toe to top mat layer force during the back somersault skill.

The optimised mat parameters are presented in Table 6.4 and are compared to the evaluation landing mat parameters.

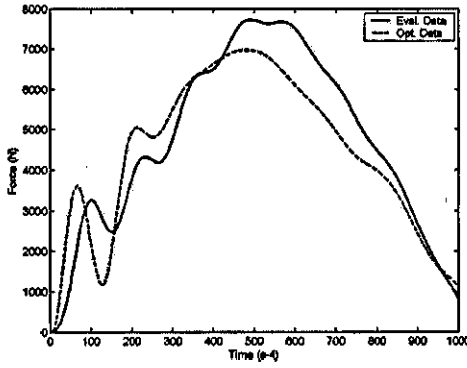
**Table 6.4.** Optimised landing mat parameters for the back somersault skill

<b>Parameter</b>	<b>Optimised Landing Mat</b>	<b>Evaluation Landing Mat</b>
Score	10880 N	10994
Penalties	2859	2859
Top layer stiffness (N/m)	61089	61080
Middle layer stiffness (N/m)	57534	57530
Bottom layer stiffness (N/m)	928210	928120
Top layer damping (Ns/m)	420 *	350
Middle layer damping (Ns/m)	395	430
Bottom layer damping (Ns/m)	348 *	290

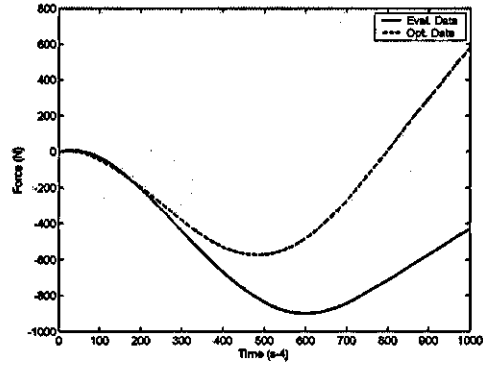
\* = upper bound reached

### 6.3.5 Optimising the Landing Mat – Front Somersault (increased upper bound)

The upper bound for the damping parameters in the optimisation were increased by 1000%, since the upper bounds were hit during earlier optimisations. This was also to determine that a further decrease in GRF's resulted in a further decrease in the internal force experienced by the gymnast. The optimisation of the landing mat parameters resulted in a decreased peak vertical and horizontal ground reaction force with a score of 7559 N and no penalties. The peak vertical ground reaction force was decreased from 7725 N in the evaluation to 6979 N using the optimised landing mat. The peak horizontal force decreased from 900 N in the evaluation to 580 N using the optimised landing mat (Figure 6.17). This reduction in peak GRF's also resulted in a decrease in peak shank and thigh bone torques. The shank bone torque decreased from 377 Nm in the evaluation to 356 Nm using the optimised landing mat. The thigh bone torque decreased from 266 Nm in the evaluation to 249 Nm using the optimised landing mat (Figure 6.18).

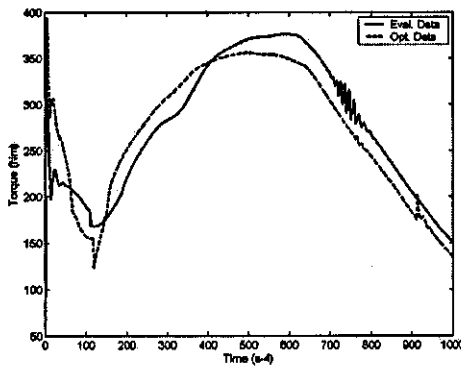


(a)

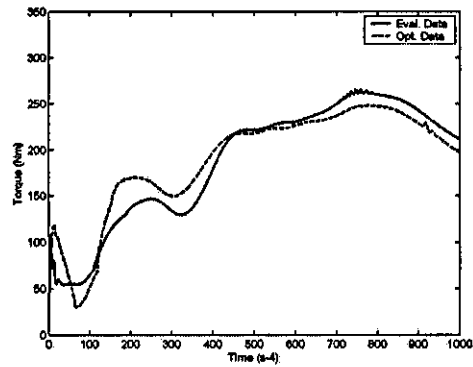


(b)

**Figure 6.17** Optimisation of landing mat properties for the front somersault skill (a) VGRF (b) HGRF.



(a)



(b)

**Figure 6.18** Lower extremity bone bending torques during the front somersault skill (a) shank, (b) thigh.

The optimisation did not change the stiffness values for any layer by much, less than 0.5%. However, the optimisation selected damping parameters higher than the previous optimisation (Table 6.5).

**Table 6.5.** Optimised landing mat parameters for the front somersault skill (increased upper bounds)

Parameter	Optimised Landing Mat (1000%)	Optimised Landing Mat (20%)	Evaluation Landing
Score	7559 N	8494 N	10994
Penalties	0	0	2859
Top layer stiffness (N/m)	61063	61197	61080
Middle layer stiffness (N/m)	57529	57591	57530
Bottom layer stiffness (N/m)	928215	928340	928120
Top layer damping (Ns/m)	940	420 *	350
Middle layer damping (Ns/m)	916	516 *	430
Bottom layer damping (Ns/m)	1079	348 *	290

Note: upper bounds for damping changed by (a) 1000% and (b) 20%

\* = upper bound reached

Again this increase in damping increased the initial peak force between the foot and top layer of the mat (Figure 6.19).

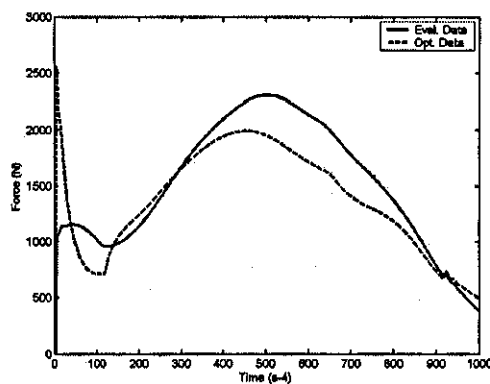


**Figure 6.19** Toe to top mat layer force during the front somersault skill.

An additional optimisation using score two was not performed as minimising score one resulted in decreased GRF's which also caused a decrease in the internal forces experienced by the gymnast during landing. Since the landing strategy of the gymnast remained unchanged during optimisation the joint reaction forces caused by the muscles compressing the joints also remained unchanged. Therefore any decrease in external forces also caused the decrease in the internal forces. It is likely that similar changes in the mat's spring parameters would be required to minimise the internal forces as used to decrease the external forces.

#### *6.4 Discussion*

Optimising the landing strategy to minimise the ground reaction forces (using score one) resulted in decreased peak vertical and horizontal ground reaction forces when compared to the model evaluation results for both the front and back somersault skills. The optimisation of the extensor activation histories was characterised by a later time to peak activation at the ankle and earlier times to peak activation at the knee and hip. The muscle forces at the knee were larger than those during the evaluations. Joint reaction forces at the ankle and hip were lower than in the evaluations but the joint reaction force at the knee was greater than in the model evaluations. A combination of all these factors resulted in an increase in the peak bone bending torque at the shank and thigh. Model Three has sufficient complexity to show that if the peak ground reaction forces are minimised in an optimisation the peak bone bending torques can actually increase. A model of the gymnast that does not have this level of model complexity would not have determined that this type of optimisation actually increases the internal loading on the structures of the human body. Minimising the ground reaction forces does not necessarily minimise the internal forces on the human body.

Optimising the landing strategy to minimise the peak bone bending torques (using score two) resulted in decreased peak bone bending torques within the shank and thigh when compared to the evaluation results for both the front and back somersault skills. The optimisation of the extensor activation histories was characterised by lower activation levels than in the evaluations. Muscle forces generally appeared to ramp up earlier than in the evaluations but not to the same magnitude. The decreased peak muscle forces also reduced the peak joint reaction forces at all joints. The combination of these factors resulted in decreased peak bone

bending torques at the shank and thigh. Optimising the peak bone bending torques also resulted in decreased peak ground reaction forces. The peak vertical ground reaction force decreased to a level below that of the evaluations and score one. The peak horizontal ground reaction force also decreased to a level below that of the evaluation but did not achieve a level that improved upon the results from score one.

The evaluation results appear to be closer to the optimised landing using the bone torques (score two). This may suggest that the landing goal may have been towards landing with minimal internal forces as opposed to minimising F.I.G. deductions. This is particularly apparent during the first 40 ms of the landing where the evaluation and bone optimisation were similar. After the first 40 ms the GRF's and bone bending torques in the bone optimisation differ from that of the evaluation. This may be due to the gymnast using a more complex muscle activation pattern than was available in the model. It is possible that as skill complexity increases and hence landing velocity, the gymnast may continue to shift the landing goal towards landing with minimal internal forces and the second half of the evaluation may begin to resemble that of an optimised bone result.

Model Three contained a SEC within the model and therefore the minimum time interval between the stimulus and the change in electrical activity in the muscle was set to 10 ms (Corcos et al. 1992; Grabiner, 1986). This limit was never reached by model Three during the optimisations, the lowest ramp up time being 42 ms. The choice of ramp up time was set as a minimum limit for the optimisations although it is possible that the gymnast may not have been able to achieve this. However, the model of the gymnast does not allow for more complex activation patterns, it is possible that the gymnast cannot ramp up as quickly as the model but may be able to modify the landing strategy in a more complex way than the model. The results suggest that there is a landing strategy that could be adopted by the gymnast to minimise internal loading. It is also possible that as landing velocity increases, the complexity of the muscle activation patterns decrease because there are less possible patterns available to land safely. The gymnast may have to attempt to activate maximally prior to landing due to the high landing velocity. A lower landing velocity may give the gymnast more options when executing the individual landing strategy.

The rotational direction of the gymnast prior to landing may also affect the landing technique and strategy selected for the landing goal. A 'blind' landing

during forward rotating skills may mean that the gymnast chooses to increase the amount of muscle pre-activation during the flight phase to give more room for error whilst landing (McNitt-Gray, 2000). A backward rotating skill allows the gymnast to 'spot' the landing prior to touchdown and select a more refined landing strategy. This is supported by the results of the optimisations that show that during a front somersault it is possible to land safely with less knee and hip muscle pre-activation than was actually used whilst minimising internal forces during landing.

To minimise the internal and external forces on the human body during landing through the optimisation of the gymnast's landing strategy a model must be sufficient in complexity so that the bone bending moments can be estimated. The approach used in this study has been effective but is unlikely to be the only way of achieving this goal. Using the ground reaction forces as a basis for reducing the internal forces in a gymnast may lead to the internal forces actually being increased.

Optimising the landing mat properties to minimise the peak ground reaction forces resulted in decreased peak vertical and horizontal ground reaction forces when compared to the model evaluation results for both the front and back somersault skills. The optimisation of the landing mat parameters were characterised by minimal changes to the landing mat's stiffness (<0.5%) but increased damping. The upper bound of +20% (this means 20% more damping than in the F.I.G. mat) was reached during the optimisation of both the front and back somersault skills. A more damped landing mat seems to decrease the external and internal forces experienced by the gymnast during landing.

However increasing the amount of damping in the landing mat had a problem. This problem related to the initial force between the foot and top layer of the mat during initial touchdown. More damping in the mat increased the initial force on the foot, this may have felt uncomfortable to the gymnast yet the peak VGRF experienced by the gymnast was reduced. The gymnast in this study has reported in the past a pain in the feet during 'stiffer' landings. Increasing the upper bound in the optimisation to 1000% that of the evaluation allowed more damping to be selected for the optimised solution. The extra damping in the landing mat resulted in reduced peak vertical and horizontal GRF's and reduced peak shank and thigh bone bending torques. However the initial force between the foot and the top layer of the mat was increased from 1253 N in the evaluation to 2580 N in the optimised

mat. This again may make the landing feel uncomfortable to the gymnast with the possibility of injury to the foot.

The results of the optimisation of the landing mat properties suggest that a landing mat with increased damping may help to reduce the peak external forces experienced by the gymnast and the peak bending moments in the shank and thigh bones during landing. However the increased damping may increase forces in the foot causing pain and possibly injury.

### *6.5 Summary*

The results of the optimised landing strategy showed that it was possible for the gymnast to modify his muscle activation patterns to minimise the external and internal forces experienced by the gymnast during landing.

Optimisation of the landing mat parameters has shown that when the gymnast's landing strategy remains the same different material properties for the landing mat can reduce the external and internal forces experienced by the gymnast during landing.

If the landing parameters can only be changed by 20% due to the material construction, this is not as effective as the gymnast adjusting his landing strategy to reduce the internal and external forces during landing.



## CHAPTER 7

### SUMMARY AND CONCLUSIONS

This chapter summarises the main findings of the present study and the research questions are answered. The limitations of this study are discussed and suggestions for improvements in the future are outlined. Finally, the potential uses of the model in this study for further investigations of landing in gymnastics are highlighted.

#### *7.1 Summary of Main Findings*

A computer simulation model of a gymnast and landing mat was developed to investigate vault landings in gymnastics. The landing mat model was evaluated using drop test results and successfully reproduced the landing mat's deformation behaviour with a mean RMS difference error of 1014 N for the middle velocity trial. The unloading phase of the impact produced the most of the error. The gymnast-mat model was evaluated successfully using four actual vault landings and the results showed good agreement between the simulations and the actual performances with difference scores between 10.1% and 23.6%. The landing strategy and landing mat were optimised to minimise the ground reaction forces, internal joint reaction forces and hence bone bending moments. Optimised landing strategy results suggest that modifications to the gymnast's landing strategy could reduce the peak ground reaction forces and the peak internal joint forces. Optimised landing mat parameter results suggest that a landing mat with 20% more damping could reduce the peak ground reaction forces and internal joint forces but this may increase the initial impact force between the foot and the mat's surface.

#### *7.2 Answering the Research Questions*

Q.1. How do ground reaction forces and internal forces acting on a gymnast change in response to different impact velocities?

The results from the four vaults show that as landing velocity increases vertical ground reaction force (GRF) does not. However the highest impact velocity

did result in the greatest vertical GRF. These results are in conflict with the results from McNitt-Gray et al. (1993) and Dufek & Bates (1990) who found that as drop height increased so did vertical GRF. The reason for this discrepancy may be due to the fact that the gymnast must perform a skill during the flight phase therefore the direction of rotation during the vault and the ability of the gymnast to spot the landing may produce different results to that of simple drop landings. It may be unfair to compare the results of actual vault landings to those of drop landings from McNitt-Gray et al. (1993). During a drop landing the subjects are more likely to have a similar body configuration prior to landing since no complex skill is required to be performed prior to landing. In the present study, however, what happened in flight seemed to effect the landing technique and strategy adopted by the gymnast during landing therefore greater impact velocity did not necessarily result in greater vertical GRF.

The joint reaction forces (JRF) follow a similar pattern to that of the vertical GRF. The results do not seem to suggest that as impact velocity increases so do the internal JRF's. However, the greatest impact velocity did result in the greatest internal JRF's. The results have highlighted one important point. The results suggest that the gymnast was able to modify his landing strategy at all the impact velocities to produce a similar JRF. However, once the impact velocity had reached that of the Tsukahara vault the adjustments to the landing strategy were unable to maintain similar JRF's and the JRF's increased by approximately 30%.

Q.2. What adjustments can be made to the landing strategy to reduce GRF's, internal forces and minimize the chances of injury?

Optimising the landing strategy to minimise the external forces experienced by the gymnast during landing has shown that it is possible for the gymnast to select a landing strategy that could reduce these forces. The optimisation of the extensor activation histories were characterised by a later time to peak activation at the ankle and earlier times to peak activation at the knee and hip than in the evaluations. The changes to the activation histories reduced the peak vertical GRF by up to 8.6% but increased the internal bone bending moments by up to 23%.

Optimising the landing strategy to minimise the internal forces experienced by the gymnast during landing has shown that it is possible for the gymnast to select

a landing strategy that could reduce these forces. The optimisation of the extensor activation histories were characterised by lower activation levels than in the evaluations. The changes to the activation histories reduced the peak vertical GRF by up to 15% and also decreased the internal bone bending moments by up to 25%. It has been shown that using optimisation to minimise the external forces on the gymnast may in fact increase the internal forces within the gymnast. Minimising the internal forces during an optimisation reduces the internal and external forces experienced by the gymnast during landing.

A reduction in the internal forces may help to reduce the risk of bone fracture injury associated with a single landing as the bone is stressed well below its fracture threshold. Furthermore Burr (1997) and Nordin & Frankel (1989) have stated that although repetitive lower loads can increase the risk of chronic bone injuries such as stress fractures, if the load is kept below a certain level, theoretically, the bone will remain intact, no matter how many repetitions. Although the 'level' is individual due to many factors including age, sex, density and geometry, generally the lower the load experienced by the bone the lower the risk of a chronic injury such as a stress fracture.

Q.3. What adjustments can be made to the landing mat to reduce GRF's and internal forces to minimize the chances of injury?

Optimising the landing mat spring parameters to minimise the external forces experienced by the gymnast during landing has shown that an optimal landing mat may exist. These spring parameters also resulted in a reduction of internal forces. The optimal landing mat parameters were characterised by minimal changes to the landing mat's stiffness (<0.5%) but increased damping. The upper bound of +20% (this means 20% more damping than in the F.I.G. mat) was reached during the optimisation but a more damped landing mat seems to decrease the external and internal forces experienced by the gymnast during landing.

Increasing the amount of damping in the landing mat does have a problem. This problem relates to the initial force between the feet and top layer of the mat during initial touchdown. More damping in the mat increased the initial force on the feet, this may cause an uncomfortable feeling on the feet of the gymnast yet the peak GRF's experienced by the gymnast were reduced. In the past gymnasts have

reported pain in the feet during 'stiffer' landings. Increasing the upper bound in the optimisation to 1000% of the evaluation allowed more damping to be selected for the optimised solution. The extra damping (approximately 272% more than the F.I.G. mat) in the landing mat resulted in reduced peak vertical and horizontal GRF's combined with reduced peak shank and thigh bone bending torques. However the initial force between the foot and the top layer of the mat was increased from 1253 N in the evaluation to 2580 N in the optimised mat. This again may make the landing feel uncomfortable to the gymnast.

Again the reduction in the internal and external forces may help to reduce the risk of bone fracture injury associated with a single landing and reduce the risk of a chronic injury such as a stress fracture.

It is noted that the optimum for the three layer mat model construction may not be the optimum mat construction. It is possible that a two layer mat or a single layer non-linear mat may produce better results. This can be a direction investigated in future work.

#### Q.4. How much bone deformation occurs during landing?

The results from the model evaluation of the four vaults suggested that either the shank or thigh bones can bend approximately 0.99 cm to 1.64 cm (lateral displacement) during a vault landing. All the bone deformations were within one standard deviation of the mean reported in Martens et al. (1986). However, the amount of bone deformation did appear to be closer than expected to the fracture limit. A possible reason for this may be because the experimental study (Martens et al., 1986) was performed using human bones in vitro. Human bones are naturally curved to allow for predictable bending direction. The muscles surrounding the bone are structured to support the bone bending in one direction. This curvature in the bones reduces the strength but increases the load predictability (Bertram & Biewener, 1988). When a bone is loaded in vivo, simultaneous contraction of the surrounding muscles act to oppose the loads, so the bone can withstand higher loads (Kaastad et al., 2000). This suggests that in reality the co-contraction of the surrounding muscles reduces the bone deformation. The bones were modelled as cylinders which works well for the three and four point bending tests but they do not perform as well during longitudinal axial loading. An additional consideration is that

the gymnast may have denser, stronger bones than the normal population and the bones tested by Martens et al. (1986). Therefore the bending moments and deformation within the gymnast's bones during landing may be well below the fracture limit.

Unfortunately the FEM of bone did not work as hoped therefore a more accurate estimate of bone deformation was not possible. Although the FEM of bone was able to reproduce the results of the three point bending test, once the FEM was placed in the gymnast model a problem occurred. This problem related to the way the forces at the joints were applied to the FEM. The joint reaction forces could only be uniformly distributed on the contact surface at each end of the bone. This limitation within VN4D resulted in less bone deformation for the same load. Yet, since bone deformation does occur during vault landings this level of model detail may be required in the future to assess the effects of different landing mats or strategies on the internal structures of the human body.

### *7.3 Discussion*

The following sub-sections will discuss the problems and limitations associated with the experimental data collections and the model construction.

#### *7.3.1 Landing Mat Data Collection*

The landing mat's surface was covered by an array of 28 passive markers and was recorded at 1000 Hz using two high-speed video cameras. Each marker was manually digitised which proved very time consuming. During the impact the impactor tended to cover four of the markers in the centre of the mat making it more difficult to identify the markers' locations. The points were estimated during digitisation which would have increased the error in the displacement data. This error was approximately 1 cm at maximum vertical landing mat deformation during the highest velocity vertical trial.

The oblique trials proved more difficult than the vertical trials because the impactor did not always land flat because the impactor swung back and forth whilst travelling down the guide rail. Multiple trials were required at each drop angle and height to ensure at least one flat impactor landing. Visual inspection of the high-speed film allowed a trial to be selected or rejected. Again this proved very time consuming and the impactor did not land exactly the same in any of the oblique

trials. This may have introduced some error into the data but this was difficult to quantify.

### 7.3.2 Gymnast Data Collection

Overall the data collection session that involved the collection of force, video and EMG data during four vault landings went well. One problem was with the portable EMG data logger that tended to be a little temperamental especially during the Tsukahara vault. The EMG data logger sometimes did not record properly or did not receive the trigger signal making it impossible to synchronise the EMG data with the other data for that trial. There did not seem to be any obvious reason for this and after a series of trials one was successful.

The use of more high-speed cameras at various angles may have helped to qualitatively understand the mat's surface deformation and its interaction with the local foot deformation during landing.

A full size landing mat or range of mat sizes could be used in the future during vault landings. Although it is possible for force to be dissipated by the landing mat over a larger area than that measured by the force plate it may help to reduce the problems (discussed in Chapter 5) associated with the horizontal GRF when landing near the edge of the sample landing mat.

### 7.3.3 Landing Mat Model

The final model of the landing mat was designed to incorporate most of the physical characteristics of the sample landing mat, such as the respective masses of each layer, each layer's stiffness and damping. The models of the landing mat using MatLab did not produce any problems however the model of the landing mat using VN4D did have a limitation when optimising the landing mat parameters. The limitation related to the amount of time required to perform one simulation (approximately 30 seconds). The optimisation algorithm required many thousands of simulations to be run until an optimum was found.

Modelling the landing mat vertically did not prove too much of a problem but once the horizontal component was introduced, the actual physical structure of the model in VN4D was harder to implement. A simple force applied to each mat layer caused problems with the inputs and outputs to and from Simulink and increased the simulation time. A number of different methods were used to

implement the horizontal part of the mat but the final design seemed to minimise simulation time and reduced the chances of the mat model becoming unstable during the simulation. The horizontal force time history match during the actual vaults was not as good as hoped due to problems discussed in section 5.3.5. Further work is required in this area of mat modelling to further understand these problems.

The masses of each component layer of the landing mat were obtained from the actual mass of each layer of the sample mat. These masses were not optimised during the spring parameter determination, but one optimisation was carried out in which the total mat mass was kept constant but the relative masses of the three layers were allowed to vary. The results showed that the optimised mat masses were within 0.01 kg of the actual mat masses used in the gymnast-mat model.

It might be argued that the mat mass layers should be distributed differently. For example, since the mass of the whole layer is distributed throughout the layer. The mass of that layer in the model could be split so that half is above the spring-damper system and half below. An additional re-optimisation of the spring parameters with redistributed mat masses ( $m_1 = 3.06$  kg,  $m_2 = 1.22$  kg,  $m_3 = 24$  kg) showed a worse RMS of 1266 N. The redistribution of mat mass failed to match the first 30 ms of the impact accurately (Figure 7.1). The optimised spring parameters also show a softer top layer for the landing mat which we know is not the case. Although this redistribution of mass in the mat layers improves the unloading phase match it fails to reproduce either of the impact peaks. Although the original mat layer mass distribution over estimates the momentum in the impact towards the end of the simulation it does accurately match the first two force impact peaks.

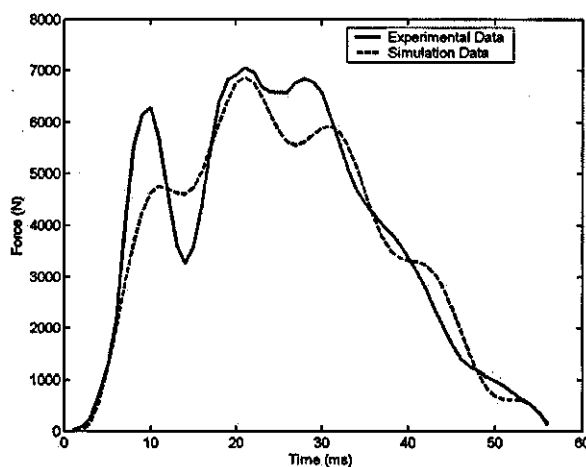


Figure 7.1 Mat model four with redistributed mat mass.

The force time histories for actual vault landings suggest that a one degree of freedom model may be complex enough to successfully model the mat especially if the gymnast lands normally and a fast simulation is required. However if the aim is to assess injury risk a three degree of freedom model may be required because injuries are more likely to occur during unsuccessful landings. Different body and limb orientations may result in a different dynamic response in the mat.

Subsequent research (Pain et al., 2005) has shown that the effective mass of the mat layers could have been used instead. This would have been difficult to implement as the model required three separate masses to be used. However, this may be something that will be considered in the future. Additional measurements of the stiffness in both the vertical and horizontal directions, possibly using static measures, of the independent layers in the landing mat may help to select the appropriate mass for each layer of the mat.

#### 7.3.4 Gymnast Models

Gymnast-mat models One and Two were relatively simple to construct using VN4D and the torque generators could be easily implemented. Model Three proved far more difficult. The actual physical construction of the muscles and their attachments was very time consuming and complex. The overlaying of the bodies that defined the moment arm proved extremely complex and the attachment of the muscles and SEC to the correct points was difficult. This structure also had the problem that it would only successfully work over a limited joint range as the rotation of the moment arm body could not always account for the joint range. Therefore it was possible that the effective moment arm could be reduced to near zero if the joint range for the muscle set up was exceeded. This was a particular problem at the ankle during the Tsukahara vault. This is particularly important as in the human body the actual ankle moment arm increases during muscle contraction and ankle plantar flexion. The initial choice regarding the construction of the muscle and moment arm could not be implemented due to a fundamental problem with VN4D that the manufacturer refused to fix. Model Three also had to be built four times, once for each skill, as the initial angles could not just be changed to match the new skill. This was primarily a problem with VN4D that could not be overcome.

A further problem was the order of the inputs and outputs from VN4D to Simulink and back. With up to 62 inputs and outputs it was difficult to determine



which inputs controlled which element within VN4D and the order the relevant outputs were input into Simulink. This problem again proved very time consuming as the inputs and outputs did not follow their unique identification number or the order in which they were selected from the menu.

The last problem related to the simulation time for the gymnast-mat model: typically 21 minutes. The optimisation algorithm required many simulations to be run to find a local optimum. A good initial guess was required to ensure that a solution was found. The optimisation algorithm may have only found the local optimum closest to the initial guess. A better global optimum may exist but was not found. The ability to determine the global optimum has been compromised by the simulation time. A shorter simulation would have allowed multiple optimisations to have been run from different starting positions that may have all converged upon the same optimum. If this was the case more confidence could have been placed upon the optimisation algorithm finding a global solution.

### 7.3.5 Strength Parameters and Data Collection

The subject performed well during the strength measurements but the ankle joint proved difficult to measure accurately. The problem arose from the positioning of the foot in relation to the crank arm. This seems to be a problem with the isokinetic dynamometer itself: the attachments are not conducive to maximal ankle plantar and dorsi flexion. The subject was re-tested using a force plate to determine the isometric ankle strength and this increase by approximately 85%. It was still felt that the subject could exhibit greater torques at the ankle during landing but the force plate ankle data was used in the gymnast-mat model. Whilst evaluating gymnast-mat model Three performing the Tsukahara vault the ankle did not appear to be strong enough and this may have been due to the decreased moment arm during the simulation or a low strength measurement of the subject.

The use of an automated tracking system to determine the joint angular velocity during testing may have helped to increase the accuracy of the estimate of the actual joint angular velocity.

The isokinetic dynamometer was used to determine the joint torque that could be exerted by the subject at different joint angles and angular velocities. However some of the muscle groups contained bi-articular muscles and when using torque generators in the gymnast-mat models the effect of these could not be

represented. Although model Three contained lumped muscle models these were not bi-articular either. This is a consideration for future torque driven or muscle driven models but it may be difficult to establish the contribution of each muscle to the relevant joint.

A limitation of the torque generator and lumped muscle model approach was that the moment arms and cross-sectional areas of muscles were scaled from the reported values in the literature in order to determine SEC stiffness. Subject-specific muscle parameters can be measured directly using MRI scans but this is costly, time consuming and requires access to MRI equipment although it would provide subject-specific data.

#### 7.3.6 Segmental Inertia Parameters

The bone to soft tissue ratio was calculated from the estimate of the percentage body fat of the subject and the literature and then scaled to the subject. It may have been possible to use an MRI scan to determine a more accurate measure of the bone and soft tissue masses. The body segmental inertias were calculated using the model of Yeadon (1990). This is suitable when using rigid body models but little is known about inertia properties of the soft tissue within a segment. Pain & Challis (2001a) have shown that the inertia properties of soft tissue do change in response to muscular contraction. This is another potential improvement to the gymnast-mat models in the future.

#### 7.3.7 Model Limitations

Several assumptions were made during the development of the gymnast-mat model and the determination of the parameters. Some assumptions have already been discussed earlier in this chapter but another limitation of this study was that the human body had no intrinsic damping. Although soft tissue motion, bone deformation and some series elastic components of the muscle tendon complexes were included other internal structures in the human body, that can distribute force through viscoelastic deformation were not present in the model. These include cartilage, ligaments and other tendons that are not already modelled (Nigg & Herzog, 1999). Additionally the trunk and head segment in the gymnast-mat model was a single rigid segment. In reality the trunk is comprised of many segments that allow the trunk to bend and flex. The gymnast-mat model could not do this therefore

any energy dissipated within the trunk during landing would have to have been transferred to the elongation of muscles or displacement of the soft tissue or bone deformation. Many rigid body models include an optimised ground to foot spring (Alexander, 1990; Wilson et al., 2005; King & Yeadon, 2004). This optimised spring seems to account for the surface, heel pad and intrinsic damping in the human body. The gymnast-mat model does not have this optimised ground to foot spring therefore the results do not match as well as they might if an optimised spring in the trunk or foot segment was implemented into the model. However this gymnast-mat model set up was necessary so that the model of the landing mat could be replaced with another experimentally tested landing mat. An optimised ground to foot spring approach would not allow this to happen as it is not known what the individual contributions from the surface, heel pad and human body are to the optimised spring.

An additional limitation was that the gymnast-mat model was a planar model. However the landings from the more complex vaults were not as symmetrical as expected, especially the Tsukahara. A gymnast-mat model that could replicate 3D movements may have been more relevant for the more complex vaults but the time required to implement this was beyond that of this study.

#### 7.3.8 Optimisation Algorithm

The Simulated Annealing optimisation algorithm (Corana et al., 1987) was used to determine the strength parameters and the simple landing mat model parameters. This has been shown to be robust and able to find a global optimum rather than a local optimum (Goffe et al., 1994). The time required can be substantial due to the number of simulations to be performed to find the global optimal although this was less of a problem when the simulation time was very short. Simulated Annealing could not be used when determining the muscle activation histories for the gymnast-mat model evaluation or optimisation because the simulation time was too long. Therefore the Simplex optimisation algorithm within the MatLab environment was used instead. This required less simulations to be performed but was more likely to find a local optimum.

The starting values were important to ensure the Simplex optimisation would start to look for a solution in a given area. The initial values were determined via the EMG data and trial and error by the user. This proved time consuming but not as

time consuming as the time required for Simulated Annealing to complete an optimisation. The other problem related to the amount of computer memory required to run multiple simulations during an optimisation. The VN4D model seemed to require a fair amount of memory to run a simulation and as the optimisation software would run many simulations, the memory filled up to a point where the computer would crash. This was another reason why Simulated Annealing could not be used for the gymnast-mat model and the Simplex optimisation algorithm had to be used instead.

### 7.3.9 Optimisation Score and Penalties

The optimisation score for the evaluation of the gymnast-mat model was difficult to finalise. The relative weighting and penalties had a marked influence on the solution found (Chapter 5). Many variations on the weighting of the score were attempted but the final score was the one that seemed to produce the closest results to the experimental data despite it not being the score that was expected to do the best. The penalties were selected carefully to ensure they were within sensible ranges. The weightings of the penalties were also important to ensure that the penalties were not so small that any violation of them was ignored.

## 7.4 *Future Research*

Although the latter half of this study has focused upon the lumped muscle driven model, the torque driven models may also be useful in future work. Following are examples of possible future research that either one or both the lumped muscle model and torque driven models could address.

### 7.4.1 The Landing Mat

Since the landing mat properties in this study were determined from experimental data it would be possible in the future to replace the landing mat model in the current gymnast-mat model with another landing mat where the properties have been determined using the same experimental data collection method. This could be used to assess if one mat rather than another is better at reducing the internal and external forces experienced by a gymnast during landing.

A different mat model construction such as a two layer mat or a model with non-linear springs may also be investigated to see if a different mat construction is able to reduce the forces experienced by a gymnast during landing.

A mat model that was not restricted by the total mat thickness of 20 cm may also be an area for future work however the current F.I.G. guidelines restrict the maximum thickness of the landing to 20 cm. Modifying other mat properties such as the density of the component layers may also be an area for future research.

#### 7.4.2 Initial Conditions

It has been shown that greater impact velocities result in greater vertical ground reaction forces (McNitt-Gray et al., 1993). The initial conditions within the gymnast-mat model could be modified to investigate the effects of greater landing velocities. McNitt-Gray (2000) has also reported that the joint and body orientation prior to landing has a marked influence on the landing strategy. Using the gymnast-mat model it may possible to investigate the effects of various landing techniques on the internal and external forces on the gymnast.

#### 7.4.3 Inertial Parameters

The gymnast-mat model can be modified to match different body sizes and inertias. The optimum landing technique or strategy could be determined for a specific body shape which may help coaches to train an improved landing technique to the relevant body shapes and sizes.

#### 7.4.4 Strength Parameters

Similar to the inertia parameters, the strength of an individual gymnast may influence the optimal landing strategy or technique. The gymnast-mat model allows for the strength characteristics of the gymnast model to be easily modified. The model may be able to help to determine whether increases or decreases in strength help to reduce or increase the risk of injury during landing.

#### 7.4.5 Sensitivity Analysis

The sensitivity of the landing mat model to its parameters has been assessed by varying the parameters by  $\pm 10\%$  and investigating its influence on the deformation behaviour of the landing mat. The sensitivity of the gymnast model to

its parameters can be assessed by varying the individual parameters values and seeing how these parameters affect the overall result. The wobbling masses parameters were found to have some influence on the landing if they are varied more than  $\pm 10\%$ . The sensitivity of other model parameters such as the SEC stiffness, moment arm and position of muscle attachment (within VN4D) could also be examined.

### *7.5 Conclusion*

The gymnast-mat model developed in this study has been successfully evaluated and applied to optimise the landing strategy of the gymnast during forward and backward rotating vaults. The model has also been applied to optimise the landing mat used by the gymnast during vault landings. The problems and limitations of the data collection, model construction and parameter determination have been discussed and some suggestions for improvement in the future have been outlined. The model can be used for further investigations of landings in gymnastics to answer questions that cannot be addressed by experimental studies.

## REFERENCES

- Abdel-Aziz, Y. & Karara, H. (1971). Direct linear transformation from comparator coordinates into space coordinates in close range photogrammetry. IN Bartlett, R. (1997). *Introduction to Sports Biomechanics*. Human Kinetics Publishers, Champaign, IL.
- Alexander, R. (1990). Optimum take off techniques for high and long jumps. *Philosophical Transactions of the Royal Society*, B329, 3-10.
- Allard, P., Stokes, I. & Blanchi, J-P. (1995). *Three-Dimensional Analysis of Human Movement*. Human Kinetics, Champaign, IL.
- Andrish, J. (1985). Knee injuries in gymnastics. *Clinics in Sports Medicine*, 4 (1), 111-121.
- Arampatzis, A., Bruggemann, G., Morey-Klapsing, G. & Wiehn, M. (2002). A three-dimensional shank-foot model to determine the foot motion during landings. *Medicine and Science in Sports and Exercise*, 34, 130-138.
- Arampatzis, A., Morey-Klapsing, G., & Bruggemann, G. (2003). The effect of falling height on muscle activity and foot motion during landings. *Journal of Electromyography and Kinesiology*, 13, 533-544.
- Arnold, A., Salinas, S., Asakawa, D. & Delp, S. (2000). Accuracy of muscle moment arms estimated from MRI-based musculoskeletal models of the lower extremity. *Computer Aided Surgery*, 5, 108-119.
- Baker, J. (1994). An evaluation of the effectiveness of a variety of data smoothing techniques to criterion force platform generated data. *Journal of Human Movement Studies*, 26, 75-86.

Baltzopoulos, V. (1997). Isokinetic dynamometry. IN Bartlett, R. (1997). *Biomechanical Analysis of Movement in Sports and Exercise*. British Association of Sport and Exercise Science, England.

Bartlett, R. (1997). *Introduction to Sports Biomechanics*. E & FN Spon, London.

Bartlett, R., Messenger, N. & Lindsay, M. (1997). Force platform. IN Bartlett, R. (1997). *Biomechanical Analysis of Movement in Sports and Exercise*. British Association of Sport and Exercise Science, England.

Bertram, J. & Biewener, A. (1988). Bone curvature: sacrificing strength for load predictability. *Journal of Theoretical Biology*, **131**, 75-92.

Bobbert, M., Yeadon, M. R. & Nigg, B. (1992). Mechanical analysis of the landing phase in heel-toe running. *Journal of Biomechanics*, **25**(3), 223-234.

Burden, A. & Bartlett, R. (1997). Electromyography. IN Bartlett, R. (1997). *Biomechanical Analysis of Movement in Sports and Exercise*. British Association of Sport and Exercise Science, England.

Burr, D. (1997). Bone, exercise and stress fractures. *Exercise and Sport Sciences Reviews*, **25**, 171-194.

Challis, J. (1999). A procedure for the automatic determination of filter cut-off frequency for the processing of biomechanical data. *Journal of Applied Biomechanics*, **15**, 303-317.

Challis, J., Bartlett, R. & Yeadon, M. (1997). Image based analysis. IN Bartlett, R. (1997). *Biomechanical Analysis of Movement in Sports and Exercise*. British Association of Sport and Exercise Science, England.

Challis, J. & Kerwin, D. (1987). An evaluation of splines in biomechanical data analysis. *ISB XI-B*, edited by Groot, G., Hollander, A. & Huijing, P. Free University Press, Amsterdam.



Challis, J. & Kerwin, D. (1992). Calculating upper limb inertia parameters. *Journal of Sports Sciences*, **10**, 275-284.

Chandler, R.F., Clauser, C. E., McConville, J. T., Reynolds, H. M. and Young, J. W. (1975). Investigation of inertial properties of the human body. AMRL-TR-74-137, AD-A016-484, DOT-HS-801-430. Aerospace Medical Research Laboratories, Wright-Patterson Air Force Base, OH.

Clarys, J.P. & Marfell-Jones, M.J. (1986). Anthropometric prediction of component tissue masses in the minor limbs of the human body. *Human Biology*, **58**, 761-769.

Cole, G., Nigg, B. & van den Bogert, A. (1996). Lower extremity joint loading during impact in running. *Clinical Biomechanics*, **11** (4), 181-193.

Corana, A., Marchesi, M., Martini, C. and Ridella, S. (1987). Minimising multimodal functions of continuous variables with the 'simulated annealing' algorithm. *ACM Transactions on Mathematical Software*, **13** (3), 262-280.

Corcos, D., Gottlieb, G., Latash, M. Almeida, G. & Ararwal, G. (1992). Electromechanical delay: an experimental artefact. *Journal of Electromyography and Kinesiology*, **2** (2), 59-68.

Dainty, D. & Norman, R. (1987). *Standardising Biomechanical Testing in Sport*. Human Kinetics Publishers, Champaign, IL.

Delp, S., Ringwelski, D. & Carroll, N. (1994). Transfer of the rectus femoris: effects of transfer site on moment arms about the knee and hip. *Journal of Biomechanics*, **27** (10), 1201-1211.

Du Luca, C. (1997). The use of electromyography in biomechanics. *Journal of Applied Biomechanics*, **13**, 135-163.

Dempster, W. (1955). *Space requirements of the seated operator*. Wright-Paterson Air Force Base, Ohio WADC-TR, 55-159.

- Denoth, J. (1985). The dynamic behaviour of a three-link model of the human body during impact with the ground. *Biomechanics IX-A, International Series on Biomechanics, Volume 5A*, Human Kinetics Publishers, Champaign, Illinois.
- Devita, P. & Skelly, W. (1992). Effect of landing stiffness on joint kinetics and energetics in the lower extremity. *Medicine and Science in Sports and Exercise*, **24** (1), 108-115.
- Dixon, S., Collop, A. & Batt, M. (2000). Surface effects on ground reaction forces and lower extremity kinematics in running. *Medicine and Science in Sports and Exercise*, **32** (11), 1919-1926.
- Duda, G., Brand, D., Freitag, S., Lierse, W. & Schneider, E. (1996). Variability of femoral muscle attachments. *Journal of Biomechanics*, **29** (9), 1185-1190.
- Dufek, J. & Bates, B. (1990). The evaluation and prediction of impact forces during landings. *Medicine and Science in Sports and Exercise*, **22** (2), 370-377.
- Dufek, J. & Bates, B. (1991). Biomechanical factors associated with injury during landing in jump sports. *Sports Medicine*, **12** (5), 326-337.
- Dufek, J. & Zhang, S. (1996). Landing models for volleyball players: a longitudinal evaluation. *Journal of Sports Medicine and Physical Fitness*, **36**, 35-42.
- Federation Internationale de Gymnastique – F.I.G. (2000/2001). Apparatus Norms. F.I.G., Switzerland.
- Federation Internationale de Gymnastique – F.I.G. (2001). Code of Points – men's artistic gymnastics. F.I.G., Switzerland.
- Finni, T. & Komi, P. V. (2002). Two methods of estimating tendinous tissue elongation during human movement. *Journal of Applied Biomechanics*, **18**, 180-188.

Forwood, M., Neal, R. & Wilson, B. (1985). Scaling segmental moments of inertia for individual subjects. *Journal of Biomechanics*, **18** (10), 755-761.

Fritz, M. & Peikenkamp, K. (2003). Simulation of the influence of sports surfaces on vertical ground reaction forces during landing. *Medical and Biological Engineering & Computing*, **41**, 11-17.

Fukuda, H., Miyashita, M. & Fukuoka, M. (1987). Unconscious control of impact force during landing. *Biomechanics X-A. International Series on Biomechanics*, **6A**, 301-305.

Fuller, N. J., Laskey, M. A. and Elia, M. (1992). Assessment of the composition of major body regions by dual-energy x-ray absorptiometry (DEXA), with special reference to limb muscle mass. *Clinical Physiology*, **12**, 253-266.

Fung, Y. (1981). *Biomechanics: Mechanical Properties of Living Tissue*. Springer-Verlag, New York.

Gilchrist, L. & Winter, D. (1996). A two part, viscoelastic foot model for use in gait simulations. *Journal of Biomechanics*, **29** (6), 795-798.

Goffe, W., Ferrier, G. & Rogers, J. (1994). Global optimisation of statistical functions with simulated annealing. *Journal of Econometrics*, **60**, 65-99.

Gross, T. & Nelson, R. (1988). The shock attenuation role of the ankle during landing from a vertical jump. *Medicine and Science in Sports and Exercise*, **20** (5), 506-514.

Grabner, M. (1986). Bioelectric characteristics of the electromechanical delay preceding concentric contraction. *Medicine and Science in Sports and Exercise*, **18** (1), 37-43.

Gruber, K., Ruder, H., Denoth, J. & Schneider, K. (1998). A comparative study of impact dynamics: wobbling mass model versus rigid body models. *Journal of Biomechanics*, **31**, 439-444.

Harry, J. D., Ward, A. W., Heglund, N. C., Morgan, D. L. and McMahon, T. A. (1990). Cross-bridge cycling theories cannot explain high-speed lengthening behaviour in frog muscle. *Biophysical Journal*, **57**, 201-208.

Hatze, H. (1980). A mathematical model for the computational determination of parameter values of anthropomorphic segments. *Journal of Biomechanics*, **13**, 833-843.

Hatze, H. (1998). Biomechanics of sports – selected examples of successful applications and future perspectives.

<http://www.isbs98.uni-konstanz.de/fullpaper/isb98-hatze.pdf>

Henley, J., Weddock, K., Masiello, G. & Nogi, J. (2002). A new three-segment foot model for gait analysis in children and adults. *Clinical Gait*.

Herzog, W. (1988). The relationship between the resultant moments at a joint and the moments measured by an isokinetic dynamometer. *Journal of Biomechanics*, **21** (1), 5-12.

Hiley, M., Yeadon, M. R. (2005). Maximal dismounts from high bar. *Journal of Biomechanics*, **38**, 2221-2227.

Hinrichs, R. N. (1975). Regression equations to predict segmental moments of inertia from anthropometric measurements: An extension of the data of Chandler et al. *Journal of Biomechanics*, **18** (8), 621-624.

Hume, P. (2001). Minimising injuries in gymnastics activities.

<http://www.education.ed.ac.uk/gym/papers/ph.html>

- Huxley, A. F. (1957). Muscle structure and theories of contraction. *Progress in Biophysics and Biophysical Chemistry*, 7, 225-318.
- Jacobs, R., Bobbert, M. & van Ingen Schenau, G. (1996). Mechanical output from individual muscles during explosive leg extensions: the role of biarticular muscles. *Journal of Biomechanics*, 29 (4), 513-523.
- Jensen, R. (1978). Estimation of the biomechanical properties of three body types using a photogrammetric method. *Journal of Biomechanics*, 11, 349-358.
- Jensen, J. (1998). Stress fracture in a world-class athlete: a case study. *Medicine and Science in Sports and Exercise*, 30 (6), 783-787.
- Jessop, D. M. & Pain, M. (2005). Strategies for maximum velocity movements in relation to reaction time and performance outcome. *Journal of Sports Sciences*, 23, 93-223.
- Kaastad, T., Huiskes, R., Reikeras, O. & Nordsletten, L. (2000). Effects of hormonal conditions and drugs on both muscle and bone strength can be assessed in a single rat test. *Bone Vol.*, 26 (4), 355-360.
- King, M. & Yeadon, M.R. (2002). Determining subject-specific torque parameters for use in a torque-driven simulation model of dynamic jumping. *Journal of Applied Biomechanics*, 18, 207-217.
- King, M. & Yeadon, M.R. (2004). Maximising somersault rotation in tumbling. *Journal of Biomechanics*, 37, 471-477.
- King, M., Yeadon, M. & Kerwin, D. (1999). A two-segment simulation model of long horse vaulting. *Journal of Sports Sciences*, 17, 313-324.
- Knoll, K. & Krug, J. (2000). The vaulting table – a new vaulting apparatus in artistic gymnastics. <http://www.education.ed.ac.uk/gym/papers/kk.html>.

- Kovacs, I., Tihanyi, J., Devita, P., Racz, L., Barrier, J. & Hortobagyi, T. (1999). Foot placement modifies kinematics and kinetics during drop jumping. *Medicine and Science in Sports and Exercise*, **31** (5), 708-716.
- Lafortune, M., Lambert, C., Lake, M. (1992). Skin marker displacement at the knee joint. In *Proceedings of the Second North American Congress on Biomechanics*, Chicago.
- Lees, A. (1981). Methods of impact absorption when landing from a jump. *Engineering in Medicine*, **10** (4), 207-211.
- Luchetti, L., Cappozzo, A., Capello, A. & Della Croce, U. (1998). Skin movement artefact assessment and compensation in the estimation of knee-joint kinematics. *Journal of Biomechanics*, **31**, 977-984.
- Lyn, G. & Mills, N. (2002). Design of foam crash mats for head impact protection. *The Engineering of Sport* **4**, 1-6.
- Maganaris, C. N., Baltzopoulos, V. & Sargeant, A. J. (1998). Changes in achilles tendon moment arm from rest to maximum isometric plantar flexion: in vivo observations in man. *Journal of Physiology*, **510.3**, 977-985.
- Martens, M., van Audekercke, R., Meester, P. & Mulier, J. (1986). Mechanical behaviour of femoral bones in bending loading. *Journal of Biomechanics*, **19** (6), 443-454.
- Martin, R., Burr, D. and Sharkey, N. (1998). *Skeletal Tissue Mechanics*, Springer, NY.
- Martin, R., Liptai, L., Yerby, S. & Williams, K. (1994). The relationship between mass and acceleration for impacts on padded surfaces. *Journal of Biomechanics*, **27** (3), 361-364.

- McAuley, E., Hudash, G., Shields, K., Albright, J., Garrick, J., Requa, R. & Wallace, R. (1987). Injuries in women's gymnastics. *The American Journal of Sports Medicine*, 15 (6), 558-566.
- McNitt-Gray, J. (2000). *Musculoskeletal Loading During Landing*. The Encyclopaedia of Sports Medicine: Biomechanics in Sport. edited by Zatsiorsky, V. (2000). IOC, Blackwell Science.
- McNitt-Gray, J., Anderson, D., Barbieri, C & Cvengos, K. (1990). Adjustments in kinematics and kinetics during modified landings. In: *Proceedings of XIVth ASB Meeting*, 75-76.
- McNitt-Gray, J., Hester, D., Mathiyakom, W. & Munkasy, B. (2001). Mechanical demand and multijoint control during landing depend on orientation of the body segments relative to the reaction force. *Journal of Biomechanics*, 34, 1471-1482.
- McNitt-Gray, J., Requejo, P., Costa, K., Mathiyakom, W. (2000). Landing success rate during artistic gymnastics competition of the 2000 Olympic games: Implications for improved gymnast / mat interaction.  
<http://www.education.ed.ac.uk/gym/papers/jm2.html>.
- McNitt-Gray, J., Yokoi, T., Millward, C. (1993). Landing strategy adjustments made by female gymnasts in response to drop height and mat composition. *Journal of Applied Biomechanics*, 9, 173-190.
- McNitt-Gray, J., Yokoi, T., Millward, C. (1994). Landing strategies used by gymnasts on different surfaces. *Journal of Applied Biomechanics*, 10, 237-252.
- Meeusen, R. & Borms, J. (1992). Gymnastic injuries. *Sports Medicine*, 13 (5), 337-356.
- Miller, D. & Nissinen, M. (1987). Critical examination of ground reaction force in the running forward somersault. *International Journal of Sports Biomechanics*, 3, 189-206.

- Miller, S. & Bartlett, R. (1997). Other motion analysis techniques. IN Bartlett, R. (1997). *Biomechanical Analysis of Movement in Sports and Exercise*. British Association of Sport and Exercise Science, England.
- Mizrahi, J. & Susak, Z. (1982). In vivo elastic and damping response of human leg to impact forces. *Journal of Biomechanical Engineering*, 104, 63-65.
- Muramatsu, T., Muraoka, T., Takeshita, D., Kawakami, Y., Hirano, Y. & Fukunaga, T. (2001). Mechanical properties of tendon and aponeurosis of human gastrocnemius muscle in vivo. *Journal of Applied Physiology*, 90, 1671-1678.
- Nigg, B. (1990). The validity and relevance of tests used for the assessment of sports surfaces. *Medicine and Science in Sports and Exercise*, 22 (1), 131-139.
- Nigg, B. (1999). Mathematically determinate systems. IN Nigg, B. & Herzog, W. (1999). *Biomechanics of the musculo-skeletal system*. John Wiley & Sons inc., Toronto, USA.
- Nigg, B. & Anton, M. (1995). Energy aspects for elastic and viscous shoe soles and playing surfaces. *Medicine and Science in Sports and Exercise*, 27 (1), 92-97.
- Nigg, B. & Herzog, W. (1999). *Biomechanics of the musculo-skeletal system*. John Wiley & Sons inc., Toronto, USA.
- Nigg, B. & Lui, W. (1999). The effect of muscle stiffness and damping on simulated impact force peaks during running. *Journal of Biomechanics*, 32, 849-856.
- Nordin, M. & Frankel, V. (1989). *Basic biomechanics of the musculo-skeletal system*. Lea & Febiger, USA.
- Ozguven, H. & Berme, N. (1988). An experimental and analytical study of impact forces during human jumping. *Journal of Biomechanics*, 21 (12), 1061-1066.



- Pain, M. and Challis, J.H. (2001a). A high resolution technique for determining body segment inertial parameters and their variation due to soft tissue motion. *Journal of Applied Biomechanics*, 17(4), 326-334.
- Pain, M. & Challis, J. (2001b). The role of the heel pad and shank soft tissue during impacts: a further resolution of a paradox. *Journal of Biomechanics*, 34, 327-333.
- Pain, M. & Challis, J. (2001c). Whole body force distributions in landing from a drop. *ISB Congress of International Society of Biomechanics XVIII*, edited by Muller, Gerber & Stacoff, Zurich, Switzerland.
- Pain, M. & Challis, J. (2004). Wobbling mass influence on impact ground reaction forces: A simulation model sensitivity analysis. *Journal of Applied Biomechanics*, 20, 309-316.
- Pain, M. & Challis, J. (2005). The influence of soft tissue movement on ground reaction forces, joint torques and joint reaction forces in drop landings. *Journal of Biomechanics*, (in press).
- Pain, M., Mills, C. and Yeadon, M.R. (2005). Video analysis of the deformation and effective mass of gymnastics landing mats. *Medicine and Science in Sports and Exercise* (in press).
- Peikenkamp, K., Fritz, M. & Nicol, K. (2002). Simulation of the vertical ground reaction force on sport surfaces during landing. *Journal of Applied Biomechanics*, 18, 122-134.
- Pettrone, F. & Ricciardelli, E. (1987). Gymnastic injuries: the Virginia experience 1982-1983. *The American Journal of Sports Medicine*, 15 (1), 59-62.
- Pierrynowski, M. R. (1995). In Allard, P., Stokes, I. A. F. and Blanche, J. (Eds.), *Three-dimensional analysis of human movement*. Champaign: Human Kinetics.

Reinschmidt, C. and van den Bogert, T. (1997). A MATLAB Toolbox for Three Dimensional Kinematic Analyses.

<http://www.isbweb.org/software/movanal/kinemat/index.html>

Requejo, P., McNitt-Gray, J. & Flashner, H. (2004). Modification of landing conditions at contact via flight phase control. *Biological Cybernetics*, **90**, 327-336.

Rolf, C., Westblad, P., Ekenman, I., Lunberg, A., Murphy, N., Lamontage, M. & Halvorsen, K. (1997). An experimental in vivo method for analysis of local deformation on tibia, with simultaneous measures of ground reaction forces, lower extremity muscle activity and joint motion. *Scandinavian Journal of Medicine and Science in Sports*, **7**, 144-151.

Rugg, S., Gregor, R., Mandelbaum, B. & Chiu, L. (1990). In vivo moment arm calculations at the ankle using magnetic resonance imaging (MRI). *Journal of Biomechanics*, **23** (5), 495-501.

Salathe, E., Arangio, G., Salathe, E. (1990). The foot as a shock absorber. *Journal of Biomechanics*, **23** (7), 655-659.

Santello, M. (2005). Review of motor control mechanisms underlying impact absorption from falls. *Gait and Posture*, **21**, 85-94.

Sapega, A., Nicholas, J., Sokolow, D. & Saraniti, A. (1982). The nature of torque overshoot in Cybex isokinetic dynamometry. *Medicine and Science in Sports and Exercise*, **14** (5), 368-375.

Scott, S. & Winter, D.A. (1993). Biomechanical model of the human foot: kinematics and kinetics during the stance phase of walking. *Journal of Biomechanics*, **26** (9), 1091-1104.

Shapiro, R. (1978). Direct linear transformation method for three-dimensional cinematography. *Research Quarterly*, **49** (2), 197-205.

- Skelly, W., Barby, L. & Phillips, K. (2003). Physiological and biomechanical responses to three different landing surfaces during step aerobics. *Journal of Exercise Physiology*, 6(2), 70-79.
- Smith, A.J. (1975). Photographic analysis of movement. *Techniques for Analysis of Human Movement*. Lepus Books, London.
- Snook, G. (1979). Injuries in women's gymnastics. *The American Journal of Sports Medicine*, 7 (4), 242-244.
- Spagale, T. Kistner, A. & Gollhofer, A. (1999). Modelling, simulation and optimisation of a human vertical jump. *Journal of Biomechanics*, 32, 521-530.
- Takei, Y. (1988). Techniques used in performing handspring and salto forward tucked in gymnastics vaulting. *International Journal of Sports Biomechanics*, 4, 260-281.
- Takei, Y. (1998). Three-dimensional analysis of handspring with full turn vault: deterministic model, coach's beliefs and judges' scores. *Journal of Applied Biomechanics*, 14 (2), 190-211.
- Turner, C. & Burr, D. (1993). Basic biomechanical measurements of bone: a tutorial. *Bone*, 14, 595-606.
- van den Bogert, A. & Nigg, B. (1999). Simulation. IN Nigg, B. & Herzog, W. (1999). *Biomechanics of the musculo-skeletal system*. John Wiley & Sons inc., Toronto, USA.
- Walters, Parker, Morgan & Deming. (1991). *Sequential Simplex Optimisation. A technique for improving quality and productivity in research, development and manufacturing*. CRC Press.

Wieners, A., Michael, F., Stallkamp, K., Nicol, K. (1995). Decrease of cushioning properties of sports mats. *XVth Congress of the International Society of Biomechanics*, Jyväskylä, Finland.

Wilson, C., King, M. & Yeadon, M. (2005). Determination of subject-specific model parameters for visco-elastic elements. *Journal of Biomechanics* (in press).

Wilson, C., Yeadon, M.R. & King, M. (2001). The use of simple models in high jumping. *Computer Simulation in Biomechanics*. 19-22.

Winter, D. (1990). *Biomechanics and Motor Control of Human Movement*. John Wiley & Sons inc., Toronto, USA.

Winter, E. M. & Brookes, F. B. C. (1991). Electromechanical response times and muscle elasticity in men and women. *European Journal of Applied Physiology*, **63**, 124-128.

Winter, D., Wells, R. & Orr, G. (1981). Errors in the use of isokinetic dynamometers. *European Journal of Applied Physiology*, **46**, 397-408.

Yeadon, M.R., Hiley, M.J. (2000). The mechanics of the backward giant circle on the high bar. *Human Movement Science* **19**, 153-173.

Yeadon, M. (1990). The simulation of aerial movement – II. A mathematical inertia model of the human body. *Journal of Biomechanics*, **23** (1), 67-74.

Yeadon, M. & Challis, J. (1994). The future of performance-related sports biomechanics research. *Journal of Sports Sciences*, **12**, 3-32.

Yeadon, M., King, M. & Wilson, C. (2005). Modelling the maximum voluntary joint/angular velocity relationship in human movement. *Journal of Biomechanics*, (in press).

Yeadon, M. & Morlock, M. (1989). The appropriate use of regression equations for the estimation of segmental inertia parameters. *Journal of Biomechanics*, **22**, 683-689.

Yeadon, M. & Nigg, B. (1988). A method for the assessment of area elastic surfaces. *Medicine and Science in Sports and Exercise*, **20** (4), 403-407.

Zatsiorsky, V. (2002). *Kinetics of Human Motion*. Human Kinetics Publishers, Champaign, Illinois.

Zatsiorsky, V. & Prilutsky, B. (1987). Soft and stiff landings. *Biomechanics X-B. International Series on Biomechanics*, **63**, edited by Jonsson, B. Human Kinetics, Champaign, IL.

Zatsiorsky, V. & Seluyanov, V. (1983). The mass and inertia characteristics of the main segments of the human body. In Matsui, H. and Kobayashi, K. (Eds.), *Biomechanics VIII-B* (pp. 1152-1159). Human Kinetics, Champaign, IL.

Zatsiorsky, V. & Seluyanov, V. and Chugunova, L. G. (1990). Methods of determining mass-inertial characteristics of human body segments. In *Contemporary problems of biomechanics*, Ed. Chernyi, G. G. and Regirer, S. A. CRC Press, Moscow.

## **Appendix A**

### **Raw Anthropometric Data For Gymnast**

## Appendix A Raw Anthropometric Data For Gymnast

ANTHROPOMETRIC MEASUREMENTS FOR SEGMENTAL INERTIA PARAMETERSNAME AGE DATE 

All measurements in millimetres

TORSO

Level	hip	umbilicus	ribcage	nipple	shoulder	neck	→	nose	ear	top
Length	0	172	198	424	530	616	0	92	150	255
Perimeter	912	764	766	1002		396		495	593	
Width	284	227	231	282	313					
Depth					183					

LEFT ARM

Level	shoulder	midarm	elbow	forearm	wrist	→	thumb	knuckle	nails
Length	0		270	329	535	0	78	119	199
Perimeter	414	343	279	291	187		266	212	127
Width					68		103	85	59

RIGHT ARM

Level	shoulder	midarm	elbow	forearm	wrist	→	thumb	knuckle	nails
Length	0		273	330	531	0	79	120	197
Perimeter	421	340	273	293	193		260	216	121
Width					69		103	89	53

LEFT LEG

Level	hip	crotch	midthigh	knee	calf	ankle	→	heel	arch	ball	nails
Length	0	88		398	578	840	0	22		154	215
Perimeter		540	512	366	361	256		333	262	258	159
Width										106	71
Depth								126			

RIGHT LEG

Level	hip	crotch	midthigh	knee	calf	ankle	→	heel	arch	ball	nails
Length	0	93		396	575	838	0	22		148	213
Perimeter		549	516	353	369	269		340	260	265	155
Width										112	69
Depth								129			

Height Mass

**Appendix B**

**Gymnast Inertia Data**



## Appendix B Gymnast Inertia Data

Results using anthropometric data of gymnast and inertia model (Yeadon, 1990).

### SEGMENTAL INERTIA PARAMETER VALUES

UNITS: MASS IN KG  
 DISTANCE IN METRES  
 MOMENT OF INERTIA IN  $KG \cdot M^2$

#### FORMAT AND SEQUENCE OF DATA PRESENTATION

SEGMENT NAME  
 MASS, DISTANCE OF MASS CENTRE FROM PROXIMAL JOINT,  
 SEGMENT LENGTH  
 PRINCIPAL MOMENTS OF INERTIA

SUBJECT: sam1

HEAD H			
	5.683	.128	.255
	.032	.032	.019
TRUNK PTC			
	31.880	.293	.616
	1.047	1.035	.305
HEAD-TRUNK PTCH			
	37.562	.361	.871
	2.058	2.046	.324
UPPER ARM 1A			
	2.599	.105	.270
	.015	.015	.004
UPPER ARM 1B			
	2.942	.117	.273
	.020	.020	.005
FOREARM 2A			
	1.423	.122	.265
	.007	.007	.001
FOREARM 2B			
	1.552	.112	.258
	.008	.008	.001
HAND 3A			
	.577	.079	.199
	.002	.001	.000
HAND 3B			
	.569	.078	.197
	.002	.001	.000
STRAIGHT ARM A			
	4.599	.257	.734
	.183	.183	.006
STRAIGHT ARM B			
	5.063	.254	.728
	.183	.183	.006
FOREARM + HAND 23A			
	2.000	.186	.464
	.029	.029	.001
FOREARM + HAND 23B			
	2.121	.172	.455
	.031	.031	.002

THIGH 1J			
9.520	.170		.398
.135	.135		.034
THIGH 1K			
9.623	.167		.396
.133	.133		.035
CALF 2J			
4.723	.196		.442
.074	.074		.007
CALF 2K			
4.854	.201		.442
.075	.075		.007
FOOT 3J			
1.251	.081		.215
.004	.004		.001
FOOT 3K			
1.305	.082		.213
.005	.004		.001
ankle/ball 4J			
1.128	.071		.154
.003	.003		.001
ankle/ball 4K			
1.147	.069		.148
.003	.003		.001
ball/toes 5J			
.123	.024		.061
.000093	.000093		.000061
ball/toes 5K			
.158	.026		.065
.000139	.000139		.000094
SHANK + FOOT 23J			
5.975	.264		.657
.184	.184		.008
SHANK + FOOT 23K			
6.159	.270		.655
.187	.187		.009
TOTAL MASS =	78.50 KG	DENSITY =	1.073

## **Appendix C**

### **Wobbling Mass Parameter Determination**

### Appendix C Wobbling Mass Parameter Determination

Mass of each leg or arm is added (ie) total mass is for both legs and arms.

Segment	Total mass	Wobble (kg)	Bone (kg)	% Bone	Comments
Lower Foot	0.28	-	-	-	
Upper Foot	2.27	-	-	-	
Lower Leg (shank)	9.54	6.63	2.91	30.5	Using Clarys & Jones (1986)
Upper Leg (thigh)	19.07	16.08	2.99	15.7	(Accounting for fat)
Trunk (and head)	37.42	30.41	7.01	18.7	
Upper Arm	5.52	-	-	-	
Lower Arm	4.10	-	-	-	

Total mass = 78.2 kg (fat = 7 % ~ 5.47 kg)

#### How the amount of wobble to bone was calculated

Using % body fat to re-calculate the bone to soft tissue ratio.

Subject = 7% fat

Clarys et al (1984, p.468) subject = 34.6 % fat

Using the SHANK as the first example:

In Clarys & Jones (1986):

Fat ratio = % fat in shank / whole body % fat  
 = 28.95 / 34.6 = 0.837

Subject = 7% (whole body fat) \* 0.837 = 5.859 %

Fat in Clarys & Jones (1986) = 1.237 kg \* 5.859 % = 0.07 kg (in subject shank)

Now use this fat (in kg) in Clarys & Jones (1986) to re-calculate % of bone to soft tissue.

New shank mass = 3.043 kg

Mass of bone (Clarys & Jones, 1986) = 0.9269 kg

$(0.9269 / 3.043) * 100 = 30.5 \%$  (bone) therefore 69.5 % soft tissue

Subject SHANK mass = 9.54 kg

Therefore bone = 2.91 kg and soft tissue = 6.63 kg

The thigh ratio is calculated using the same method.

The TRUNK ratio:

From Clarys et al (1984)

Whole body mass = 64.3 kg  
 Whole body fat = 34.6 %  
 Whole body fat = 22.25 kg

Sum of all limbs mass = 26.85 kg  
 Trunk mass = whole body mass – sum of all limbs = 37.45 kg

Sum of all limbs fat = 10.05 kg  
 Trunk fat mass = 22.25 – 10.05 = 12.2 kg

Fat in trunk =  $(12.2 / 37.45) * 100 = 32.58 \%$

Fat ratio = % fat in trunk / whole body fat % =  $32.58 / 34.6 = 0.942$

Subject =  $7\%(\text{whole body fat}) * 0.942 = 6.594 \%$  (fat in trunk)

Fat in trunk (Clarys et al 1984) =  $12.2 * 6.594\% = 0.804 \text{ kg}$

Now use fat (in kg) to re-calculate % bone and soft tissue.

New trunk mass =  $(37.45 - 12.2) + 0.804 = 26.05 \text{ kg}$

Whole body fat % = 13.4 % (Clarys et al, 1984)  
 Whole body bone =  $64.3 * 13.4\% = 8.616 \text{ kg}$   
 Sum of bones in limbs (Clarys & Jones, 1986) = 3.736 kg

Therefore bone in trunk =  $8.616 - 3.736 = 4.88 \text{ kg}$

Mass of bone in trunk / mass of trunk (subject) =  $(4.88 / 26.05) * 100\%$

= 18.7 % bone in TRUNK

= 81.3 % soft tissue in TRUNK

Therefore

Subject trunk mass = 37.42 kg

Bone =  $37.42 \text{ kg} * 18.7\% = 7.01 \text{ kg}$   
 Soft tissue =  $37.42 * 81.3\% = 30.41 \text{ kg}$

## **Appendix D**

### **Segment Moment Of Inertia And Radius Calculation**

### Appendix D Segment Moment Of Inertia And Radius Calculation

Both arms and legs are averaged to give segment lengths and MofI and CofM

Segment		Length of Segment (m)	Distance to CofM from proximal end (m)	Moment of Inertia (kg/m <sup>2</sup> )		
				X	Y	Z
Lower foot	Bone	0.063	0.025	0.000115	0.000115	0.000077
	Wobble	-	-	-	-	-
Upper foot	Bone	0.151	0.70	0.003	0.003	0.001
	Wobble	-	-	-	-	-
Lower leg	Bone	0.442	0.221	0.048	0.048	0.002
	Wobble	0.440	0.189	0.098	0.098	0.009
Upper leg	Bone	0.397	0.1985	0.04	0.04	0.002
	Wobble	0.395	0.162	0.112	0.112	0.012
Trunk	Bone	0.871	0.436	0.223	0.223	0.03
	Wobble	0.869	0.344	1.804	1.804	0.25
Upper arm	Bone	0.272	0.111	0.0175	0.0175	0.0045
	Wobble	-	-	-	-	-
Lower arm	Bone	0.460	0.171	0.030	0.030	0.0015
	Wobble	-	-	-	-	-

Segment		Estimated radius one leg (m)	Both legs (m)
Lower Leg	Bone	0.0295	0.059
	Wobble	0.048	0.096
Upper Leg	Bone	0.031	0.062
	Wobble	0.079	0.158
Trunk	Bone	0.032	0.064
	Wobble	0.073	0.146

Remember trunk is actually hip girdle, trunk and head.

Proximal refers to closest to hip

Bone in shank, thigh and trunk are uniform

Foot to be modelled as cube – dimensions are:

Lower foot = 0.063 m length  
0.210 m width  
0.028 m height

Upper foot = 0.151 m length  
0.210 m width  
0.070 m height

The ankle joint is approx 0.050 m from the rear of the heel.

X = somersault

Y = cartwheel

Z = twist

### How the radius and MoI was calculated

Assuming the bone is modelled as a cylinder the radius of the cylinder is given by:

$$\pi r^2 L = \frac{M_b}{d} \quad \text{density shank (d) = 1208 kg/m}^3$$

$M_b$  = mass of bone (one leg)

$L$  = length of segment (one leg)

The moment of inertia ( $I_b$ ) of the bone can be determined using:

$$I_b = \frac{1}{12} m_b L^2 + \frac{1}{4} m_b r^2$$

Assuming the bone has uniform density, the distance of the mass centre to the proximal joint is given by:

$$Z_b = 0.5 * L$$

For the wobbling mass component, the distance ( $Z_w$ ) of the mass centre to proximal joint is given by the equation :

$$m_b z_b + m_w z_w = (m_b + m_w) z$$

( $z$  = distance of whole segment mass centre to proximal joint)

The whole segment moment of inertia ( $I_g$ ) was determined using Yeadon's (1990) model. The moment of inertia of the wobbling component ( $I_w$ ) can be calculated using the parallel axis theorem:

$$I_g = I_b + m_b(z_b - z)^2 + I_w + m_w(z_w - z)^2$$



## **Appendix E**

**Informed consent form (Cybex Testing)**

**Appendix E Informed consent form (Cybex Testing)**  
**INFORMED CONSENT FORM**

Purpose

To obtain torque data during isometric and isovelocity trials.

Procedures

Torque data will be obtained using an isokinetic dynamometer (Cybex). Plus a digital camera will be used to obtain a record of the trails and will be used to estimate joint angles.

The joints to be tested isometrically and dynamically are the knee, hip and shoulder. The ankle will be tested isometrically only.

During the testing a minimum of three researchers will be present.

Questions

The researcher will be pleased to answer any questions you may have at any time.

Withdrawal

You are free to withdraw from the study at any stage, without having to give any reasons. An opportunity will be provided in this event for you to discuss privately your wish to withdraw.

Confidentiality

Your identity will remain confidential in any material resulting from this work.

I have read the outline of the procedures that are involved in this study and I understand what will be required of me. I have had the opportunity to ask for further information and for clarification of the demands of the session. I am aware I have the right to withdraw at any time. As far as I am aware I do not have any injuries that would be affected by the testing procedure.

Name ..... (subject)

Signed ..... (subject)

Name ..... (researcher)

Signed ..... (researcher)

Date .....

## **Appendix F**

### **SEC stiffness calculation**

**Appendix F SEC stiffness calculation**Calculating tendon stiffnessAnkle Plantar Flexion

Soleus and gastrocnemius produce ankle plantar flexion

Ratio of cross sectional area from Allard et al (1995):

Soleus:Gast  
11868:6167

Ratio of moment arm = 1:1

Therefore ratio of torque = 11868:6167

Maximum isometric ankle plantar flexion torque (from subject) = 138 Nm.

Soleus torque =  $138 * (11868 / (11868 + 6167)) = 90.7 \text{ Nm}$

Gast torque =  $138 * (6167 / (11868 + 6167)) = 47.2 \text{ Nm}$

Soleus:

SEC length = 271 mm

Moment arm = 42 mm

Change in length =  $0.271\text{m} * 5\% = 0.01355\text{m}$

Change in angle =  $\text{inv tan}(0.01355\text{m} / 0.042\text{m}) = 17.9^\circ$

SEC stiffness =  $90.7 \text{ Nm} / 17.9^\circ = 5.07 \text{ Nm}/^\circ$

Gast:

SEC length = 293 mm

Moment arm = 42 mm

Change in length =  $0.293\text{m} * 5\% = 0.01465\text{m}$

Change in angle =  $\text{inv tan}(0.01465 / 0.042\text{m}) = 19.2^\circ$

SEC stiffness =  $47.2 \text{ Nm} / 19.2^\circ = 2.46 \text{ Nm}/^\circ$

Soleus + Gast =  $7.5 \text{ Nm}/^\circ (*2 \text{ for both legs}) = 15 \text{ Nm}/^\circ$

Total SEC stiffness for the ankle plantar flexors = 15 Nm/°

Linear tendon for muscle models:

$$M = f * d$$

$$138 \text{ Nm} / 0.042\text{m} = 3286 \text{ N}$$

$$F = -kx$$

$$3286 / ((0.01355 + 0.01465) / 2) = 2.3 * 10^5 \text{ N/m}$$

\*2 for both legs

**Total SEC stiffness (linear) for ankle plantar flexors =  $4.6 * 10^5 \text{ N/m}$**

Ankle Dorsi Flexion

Tib Anterior produces ankle dorsi flexion

Maximum isometric ankle plantar flexion torque (from subject) = 36 Nm.

CSA = 2040

SEC length = 315 mm

Moment arm = 42 mm

Change in length =  $0.315\text{m} * 5\% = 0.01575\text{m}$

Change in angle =  $\text{inv tan}(0.01575 / 0.042\text{m}) = 20.6^\circ$

SEC stiffness =  $36 \text{ Nm} / 20.6^\circ = 1.7 \text{ Nm}/^\circ$

\*2 for both legs

SEC stiffness for the ankle dorsi flexors = 3.4 Nm/°

Linear tendon for muscle models:

$M = f * d$

$36 \text{ Nm} / 0.042\text{m} = 857 \text{ N}$

$F = -kx$

$857 / 0.01575 = 5.4 * 10^4 \text{ N/m}$

\*2 for both legs

**SEC stiffness for the ankle dorsi flexors =  $10.8 * 10^4 \text{ N/m}$**

Knee Extension

The rectus femoris, vastus medialis, vastus lateralis and vastus intermedius are the primary muscles used for knee extension.

Ratio of cross sectional area from Allard et al (1995):

3367:4674:6880:5368

sum of csa = 20289

moment arm from Jacobs (1996) = 39 mm

Maximum isometric knee extension torque (from subject) = 242.2

RF torque =  $242.2 * 3367/20289 = 40.2 \text{ Nm}$

VM torque =  $242.2 * 4674/20289 = 55.8 \text{ Nm}$

VL torque =  $242.2 * 6880/20289 = 82.1 \text{ Nm}$

VI torque =  $242.2 * 5368/20289 = 66.5 \text{ Nm}$

RF:

SEC length = 401 mm

Moment arm = 39 mm

Change in length =  $0.401\text{m} * 5\% = 0.02005\text{m}$

Change in angle =  $\text{inv tan}(0.02005\text{m} / 0.039\text{m}) = 27.2^\circ$

SEC stiffness =  $40.2 \text{ Nm} / 27.2^\circ = 1.48 \text{ Nm} / ^\circ$

VM:

SEC length = 299 mm

Moment arm = 39 mm

Change in length =  $0.299\text{m} * 5\% = 0.01495\text{m}$

Change in angle =  $\text{inv tan}(0.01495\text{m} / 0.039\text{m}) = 21.0^\circ$

SEC stiffness =  $55.8 \text{ Nm} / 21.0^\circ = 2.66 \text{ Nm} / ^\circ$

VL:

SEC length = 303 mm

Moment arm = 39 mm

Change in length =  $0.303\text{m} * 5\% = 0.01515\text{m}$

Change in angle =  $\text{inv tan}(0.01515\text{m} / 0.039\text{m}) = 21.2^\circ$

SEC stiffness =  $82.1 \text{ Nm} / 21.2^\circ = 3.87 \text{ Nm} / ^\circ$

VI:

SEC length = 302 mm

Moment arm = 39 mm

Change in length =  $0.302\text{m} * 5\% = 0.0151\text{m}$

Change in angle =  $\text{inv tan}(0.0151\text{m} / 0.039\text{m}) = 21.2^\circ$

SEC stiffness =  $66.5 \text{ Nm} / 21.2^\circ = 3.14 \text{ Nm} / ^\circ$

RF + VM + VL + VI \* 2 (for both legs)

Total SEC stiffness for the knee extensors = 22.3 Nm/°

Linear tendon for muscle models:

$$M = f * d$$

$$242.2 \text{ Nm} / 0.039\text{m} = 6210 \text{ N}$$

$$F = -kx$$

$$6210 / 0.0163 = 3.8 * 10^5 \text{ N/m}$$

\*2 for both legs

$$\underline{\text{Total SEC stiffness for the knee extensors} = 7.6 * 10^5 \text{ N/m}}$$

### Knee Flexion

The biceps femoris and other hamstrings are the primary muscles used for knee flexion.

Ratio of cross sectional area from Allard et al (1995):

$$3905:4926$$

$$\text{sum of csa} = 8831$$

$$\text{moment arm from Jacobs (1996)} = 20 \text{ mm}$$

$$\text{Maximum isometric knee flexion torque (from subject)} = 146.3$$

$$\text{BF torque} = 146.3 * 3905/8831 = 64.7 \text{ Nm}$$

$$\text{HAM torque} = 146.3 * 4926/8831 = 81.6 \text{ Nm}$$

BF:

$$\text{SEC length} = 223 \text{ mm}$$

$$\text{Moment arm} = 20 \text{ mm}$$

$$\text{Change in length} = 0.223\text{m} * 5\% = 0.01115\text{m}$$

$$\text{Change in angle} = \text{inv tan}(0.01115\text{m} / 0.020\text{m}) = 29.1^\circ$$

$$\text{SEC stiffness} = 64.7 \text{ Nm} / 29.1^\circ = 2.22 \text{ Nm}/^\circ$$

HAM:

$$\text{SEC length} = 327 \text{ mm}$$

$$\text{Moment arm} = 20 \text{ mm}$$

$$\text{Change in length} = 0.327\text{m} * 5\% = 0.01635\text{m}$$

$$\text{Change in angle} = \text{inv tan}(0.01635\text{m} / 0.020\text{m}) = 39.3^\circ$$

$$\text{SEC stiffness} = 81.6 \text{ Nm} / 39.3^\circ = 2.08 \text{ Nm}/^\circ$$

\*2 for both legs

$$\underline{\text{Total SEC stiffness for the knee flexors} = 8.6 \text{ Nm}/^\circ}$$

Linear tendon for muscle models:

$$M = f * d$$

$$146.3 \text{ Nm} / 0.020\text{m} = 7315 \text{ N}$$

$$F = -kx$$

$$7315 / 0.014 = 5.2 * 10^5 \text{ N/m}$$

\*2 for both legs

$$\text{Total SEC stiffness for the knee flexors} = 10.4 * 10^5 \text{ N/m}$$

### Hip Flexion

The psoas and rectus femoris is the primary muscle used for hip flexion.

Ratio of cross sectional area from Allard et al (1995):

$$1383:3367$$

$$\text{sum csa} = 4750$$

$$\text{moment arm from Jacobs (1996)} = 33 \text{ mm}$$

$$\text{Maximum isometric hip flexion torque (from subject)} = 131.9 \text{ Nm}$$

$$\text{PS torque} = 131.9 * 1383/4750 = 38.4 \text{ Nm}$$

$$\text{RF torque} = 131.9 * 3367/4750 = 93.5 \text{ Nm}$$

PS:

$$\text{SEC length} = 103 \text{ mm}$$

$$\text{Moment arm} = 33 \text{ mm}$$

$$\text{Change in length} = 0.103\text{m} * 5\% = 0.00515\text{m}$$

$$\text{Change in angle} = \text{inv tan}(0.00515\text{m} / 0.033\text{m}) = 8.9^\circ$$

$$\text{SEC stiffness} = 38.4 \text{ Nm} / 8.9^\circ = 4.31 \text{ Nm} / ^\circ$$

RF:

$$\text{SEC length} = 401 \text{ mm}$$

$$\text{Moment arm} = 33 \text{ mm}$$

$$\text{Change in length} = 0.401\text{m} * 5\% = 0.02005\text{m}$$

$$\text{Change in angle} = \text{inv tan}(0.02005\text{m} / 0.033\text{m}) = 31.3^\circ$$

$$\text{SEC stiffness} = 93.5 \text{ Nm} / 31.3^\circ = 2.99 \text{ Nm} / ^\circ$$

\*2 for both legs

$$\text{Total SEC stiffness for the hip flexors} = 14.6 \text{ Nm} / ^\circ$$

Linear tendon for muscle models:

$$M = f * d$$

$$131.9 \text{ Nm} / 0.033\text{m} = 3997 \text{ N}$$

$$F = -kx$$

$$3997 / 0.0128 = 3.1 * 10^5 \text{ N/m}$$

\*2 for both legs



Total SEC stiffness for the hip flexors =  $6.2 * 10^5$  N/m

### Hip Extension

The glutes are the primary muscles used for hip extension.

Ratio of cross sectional area from Allard et al (1995):

CSA = 11759

moment arm from Jacobs (1996) = 59 mm

Maximum isometric hip flexion torque (from subject) = 239.9 Nm

SEC length = 80 mm

Moment arm = 59 mm

Change in length =  $0.080\text{m} * 5\% = 0.004\text{m}$

Change in angle =  $\text{inv tan}(0.004\text{m} / 0.059\text{m}) = 3.9^\circ$

SEC stiffness =  $239.9 \text{ Nm} / 3.9^\circ = 61.5 \text{ Nm}/^\circ$

\*2 for both legs

Total SEC stiffness for the hip extensors =  $123 \text{ Nm}/^\circ$

Linear tendon for muscle models:

$M = f * d$

$239.9 \text{ Nm} / 0.059\text{m} = 4066 \text{ N}$

$F = -kx$

$4066 / 0.004 = 1 * 10^6 \text{ N/m}$

\*2 for both legs

**Total SEC stiffness for the hip extensors =  $2 * 10^6 \text{ N/m}$**

## **Appendix G**

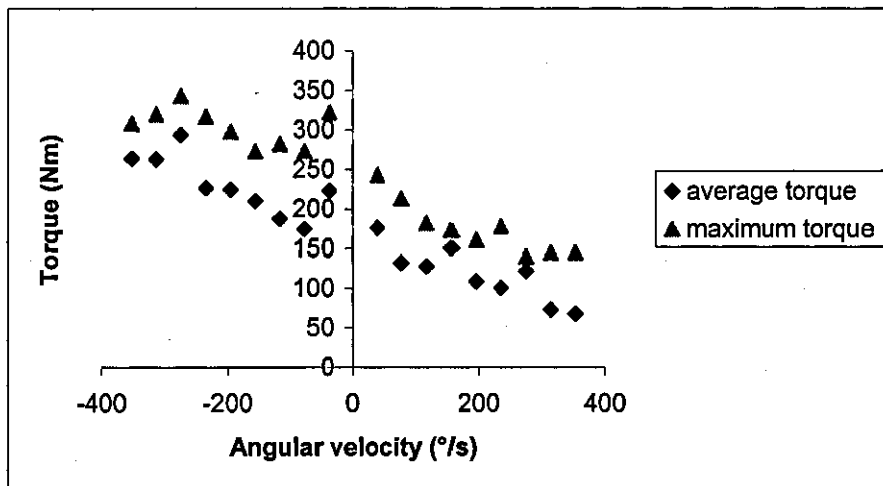
**Isokinetic Dynamometry Raw data and 9 parameter muscle  
function 3D surface plots using muscle angle – all joints**

**Appendix G Isokinetic Dynamometry Raw data and 9 parameter muscle function  
3D surface plots using muscle angle – all joints**

**Knee extension – isovelocity**

Cybox Velocity (°/s)	Cybox Torque (con) (Nm)	Cybox Torque (ecc) (Nm)
50	223	296
100	190	248
150	162	258
200	125	253
250	137	279
300	139	290
350	116	314
400	113	295
450	100	295

Actual Joint Velocity (°/s)	Max Torque (con) (Nm)	Joint Angle at Max Torque (con) (°)	Max Torque (ecc) (Nm)	Joint Angle at Max Torque (ecc) (°)	Av Torque (con) (Nm)	Av Torque (ecc) (Nm)
39	243	124	322	128	176	223
78	213	125	273	128	132	175
118	182	112	282	128	128	188
157	173	105	273	120	151	210
196	161	97	298	120	109	225
235	178	117	317	124	101	227
275	140	113	343	120	122	294
314	145	109	320	131	73	263
353	145	114	308	127	68	264

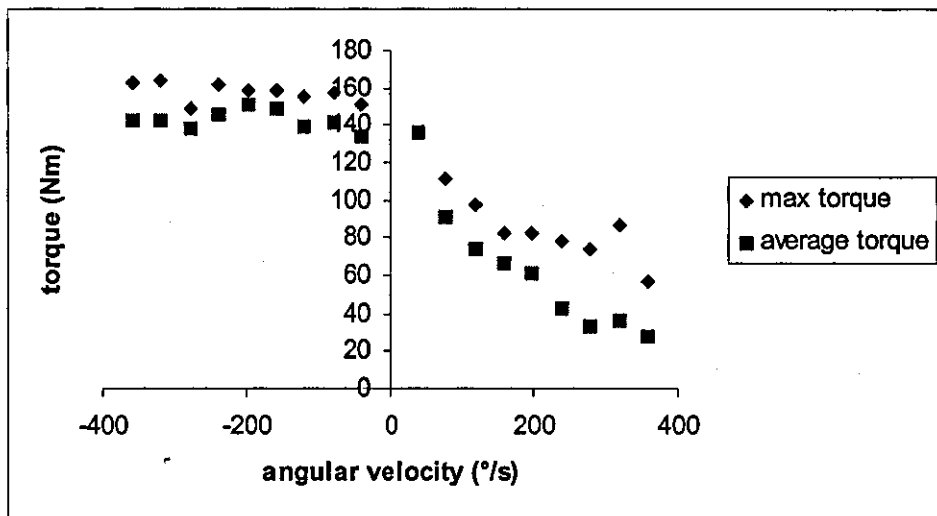


Estimated T<sub>0</sub> from peak torque data was 282.5Nm compared to isometric of 269Nm.

## Knee flexion – isovelocity

Cybox Velocity (°/s)	Cybox Torque (con) (Nm)	Cybox Torque (ecc) (Nm)
50	142	161
100	147	168
150	151	165
200	130	172
250	117	178
300	113	173
350	85	160
400	100	165
450	98	162

Actual Joint Velocity (°/s)	Max Torque (con) (Nm)	Joint Angle at Max Torque (con) (°)	Max Torque (ecc) (Nm)	Joint Angle at Max Torque (ecc) (°)	Av Torque (con) (Nm)	Av Torque (ecc) (Nm)
40	136	152	151	143	136	134
80	111	124	158	152	91	141
120	97	132	155	143	74	139
160	83	119	159	130	66	149
199	83	122	159	153	61	151
239	78	132	162	139	43	146
279	74	119	149	147	33	138
319	87	109	164	129	36	143
359	57	108	163	128	28	142

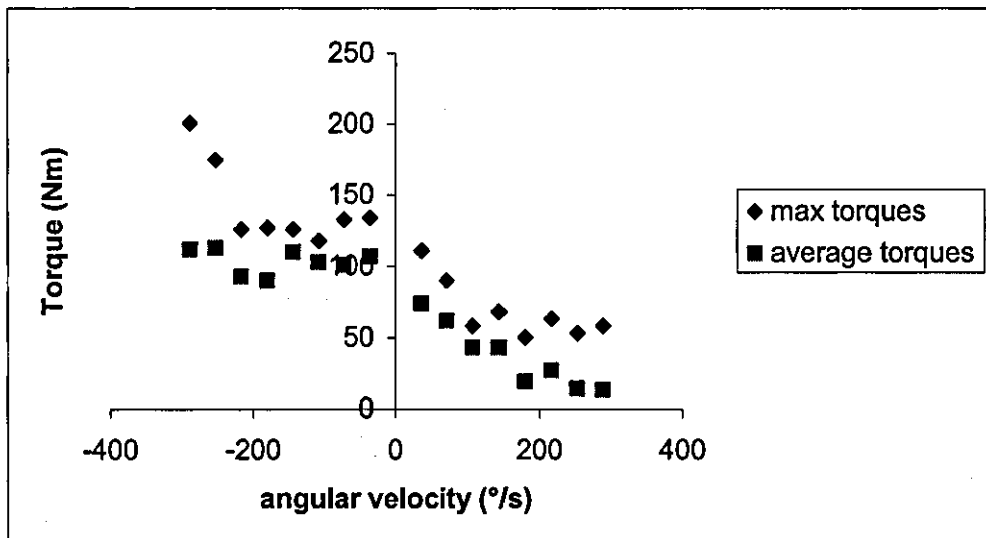


Estimated T0 from peak torque data was 143.5 Nm compared to isometric of 143Nm.

## Hip flexion – isovelocity

Cybox Velocity (°/s)	Cybox Torque (con) (Nm)	Cybox Torque (ecc) (Nm)
50	176	197
100	109	118
150	125	111
200	145	123
250	98	140
300	61	164
350	49	180
400	101	178

Actual Joint Velocity (°/s)	Max Torque (con) (Nm)	Joint Angle at Max Torque (con) (°)	Max Torque (ecc) (Nm)	Joint Angle at Max Torque (ecc) (°)	Av Torque (con) (Nm)	Av Torque (ecc) (Nm)
36	111	55	134	60	74	107
72	90	64	133	56	62	101
108	58	93	118	64	43	103
144	68	76	126	65	43	110
180	50	84	127	50	19	90
217	63	78	126	72	27	93
253	53	93	175	56	14	113
289	58	93	201	41	13	112

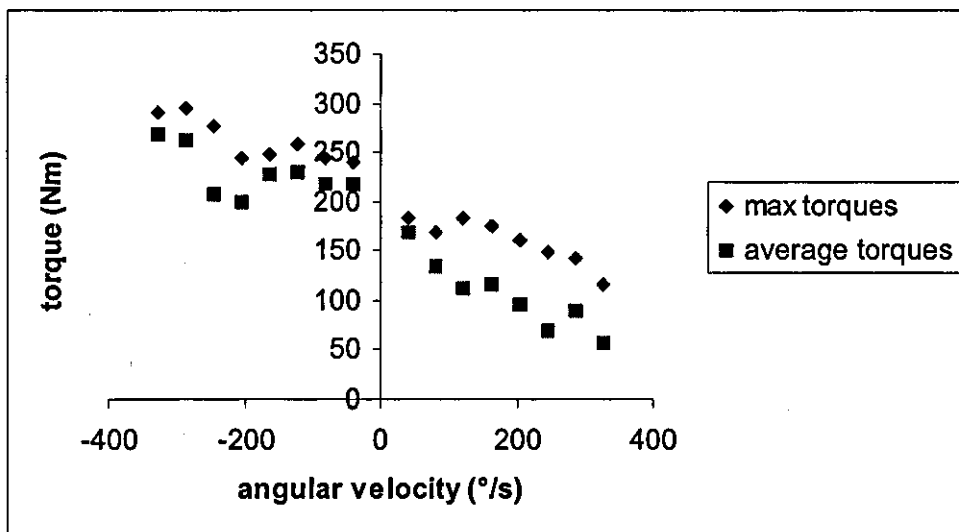


Estimated T0 from peak torque data was 122.5 Nm.

## Hip extension – isovelocity

Cybox Velocity (°/s)	Cybox Torque (con) (Nm)	Cybox Torque (ecc) (Nm)
50	208	232
100	226	243
150	235	254
200	207	246
250	203	243
300	197	267
350	205	298
400	166	307

Actual Joint Velocity (°/s)	Max Torque (con) (Nm)	Joint Angle at Max Torque (con) (°)	Max Torque (ecc) (Nm)	Joint Angle at Max Torque (ecc) (°)	Av Torque (con) (Nm)	Av Torque (ecc) (Nm)
41	183	60	241	86	168	218
82	169	93	244	81	135	217
123	184	85	259	86	111	229
164	176	89	249	86	115	228
204	161	76	245	94	95	199
245	149	51	276	86	69	207
286	142	75	296	61	89	263
327	116	70	291	110	56	268

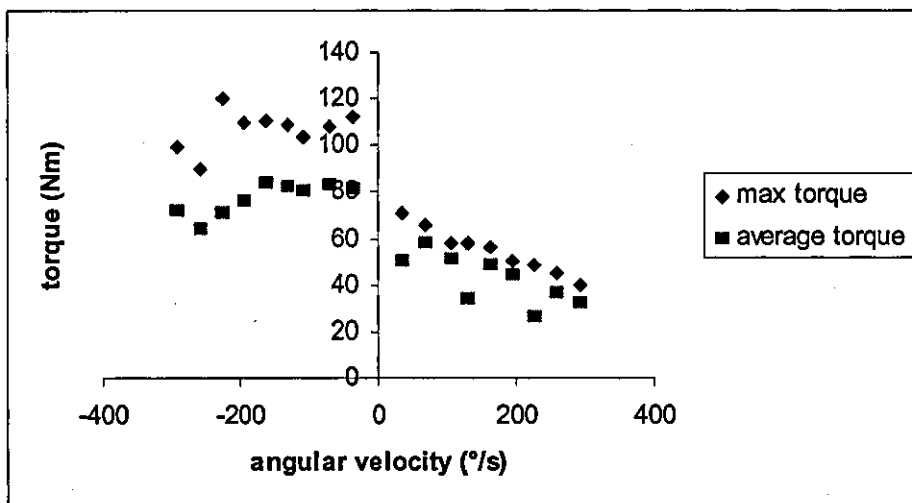


Estimated T0 from peak torque data was 212 Nm.

## Shoulder flexion – isovelocity

Cybox Velocity (°/s)	Cybox Torque (con) (Nm)	Cybox Torque (ecc) (Nm)
50	76	96
100	63	94
150	51	91
200	64	94
250	64	103
300	55	100
350	47	114
400	32	115
450	37	129

Actual Joint Velocity (°/s)	Max Torque (con) (Nm)	Joint Angle at Max Torque (con) (°)	Max Torque (ecc) (Nm)	Joint Angle at Max Torque (ecc) (°)	Av Torque (con) (Nm)	Av Torque (ecc) (Nm)
36	71	130	112	131	50	95
72	66	131	108	117	58	99
108	58	126	104	136	51	94
130	58	116	109	120	56	99
162	56	120	111	111	53	100
194	50	87	110	140	44	88
227	48	96	120	136	26	81
259	45	86	90	92	36	71
292	40	110	99	33	32	79

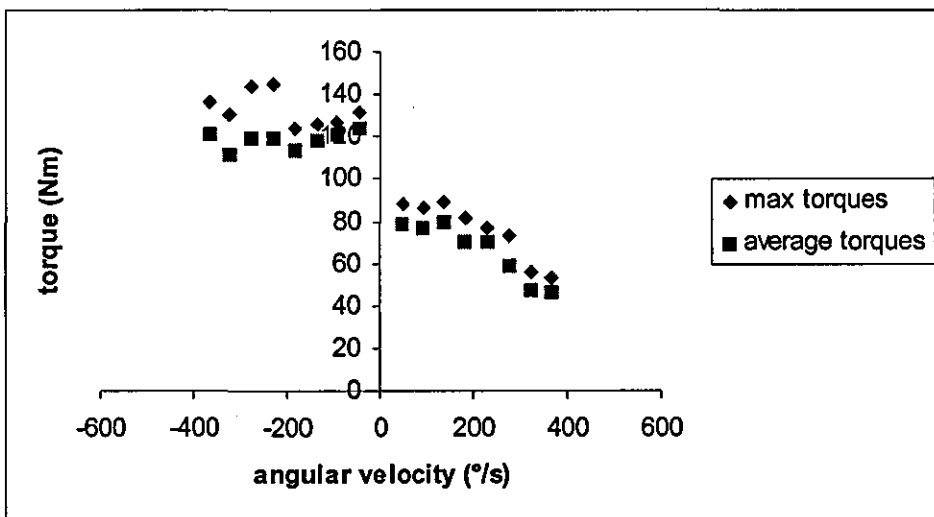


Estimated T0 from peak torque data was 91.5 Nm.

## Shoulder extension – isovelocity

Cybox Velocity (°/s)	Cybox Torque (con) (Nm)	Cybox Torque (ecc) (Nm)
50	120	133
100	107	130
150	109	122
200	104	128
250	88	128
300	81	150
350	74	152
400	60	170

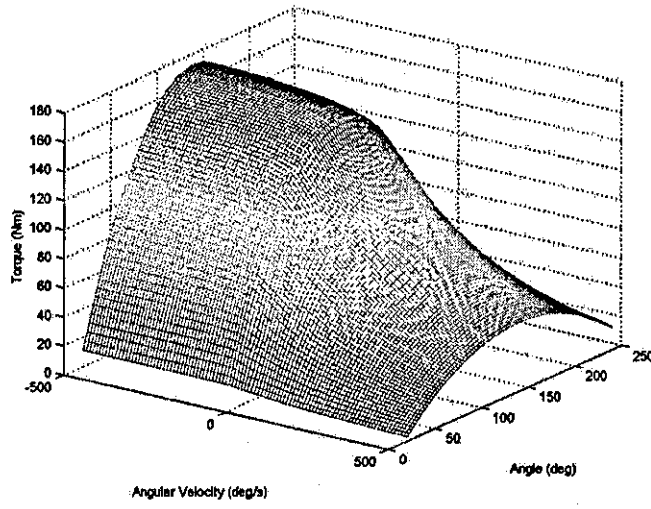
Actual Joint Velocity (°/s)	Max Torque (con) (Nm)	Joint Angle at Max Torque (con) (°)	Max Torque (ecc) (Nm)	Joint Angle at Max Torque (ecc) (°)	Av Torque (con) (Nm)	Av Torque (ecc) (Nm)
46	88	107	132	63	79	124
92	86	112	127	95	77	121
138	89	101	126	74	80	118
184	81	111	124	75	70	114
230	77	89	145	75	70	119
276	73	100	144	69	59	119
322	56	107	131	137	47	112
368	53	87	136	84	46	121



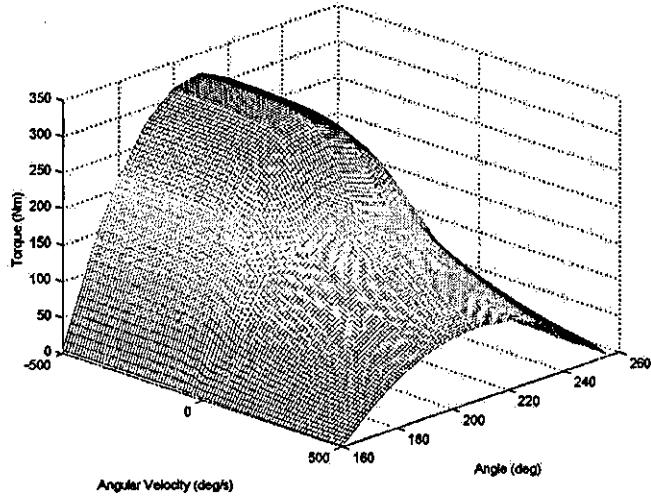
Estimated T<sub>0</sub> from peak torque data was 110 Nm.



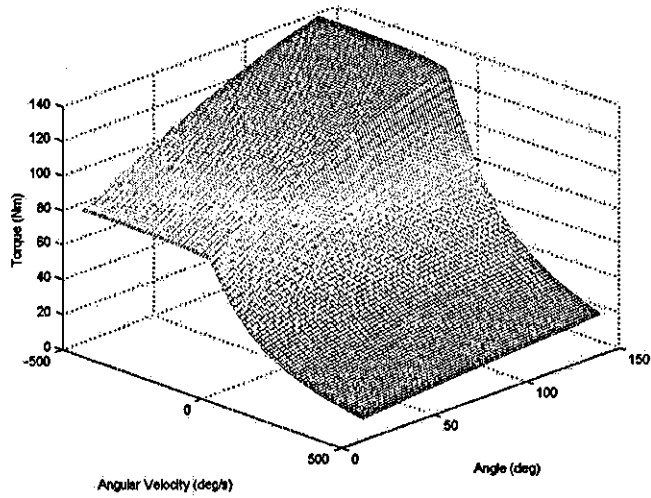
### Knee Flexion



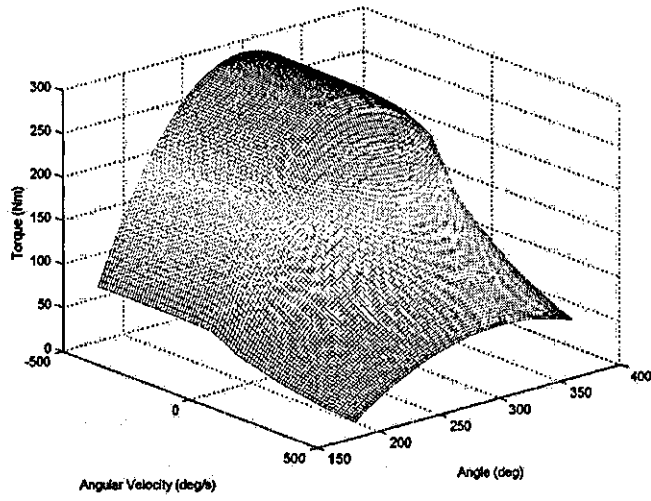
### Knee Extension



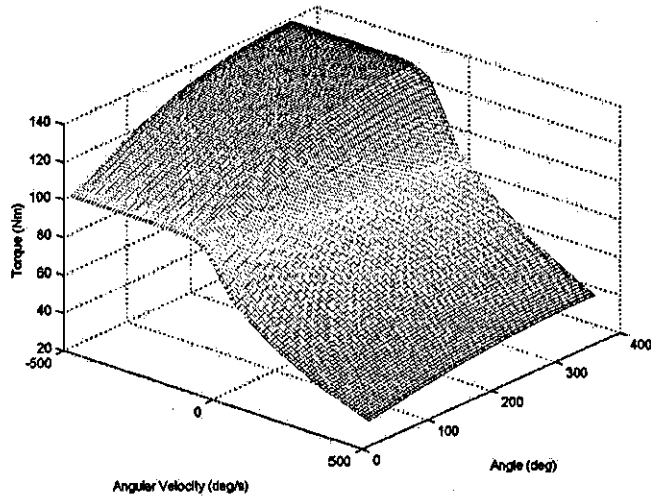
### Hip Flexion



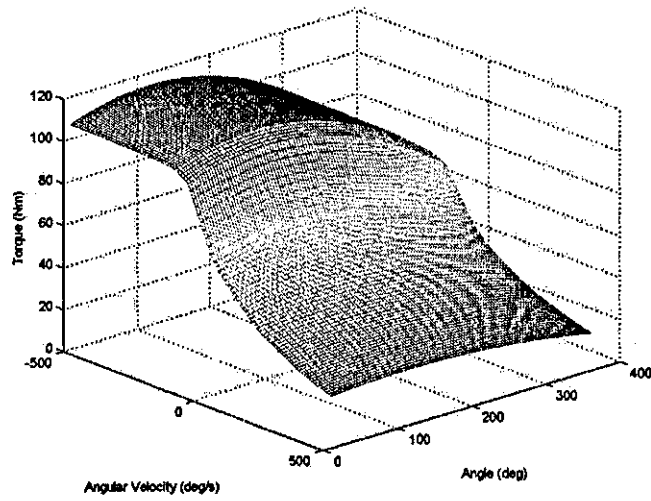
### Hip extension



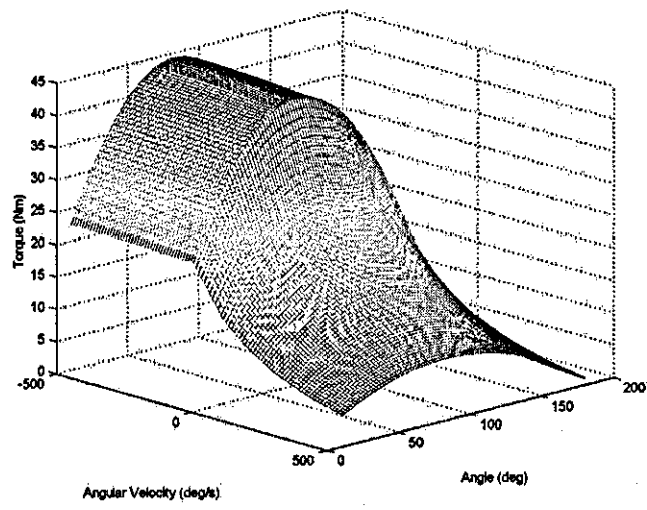
### Shoulder Extension



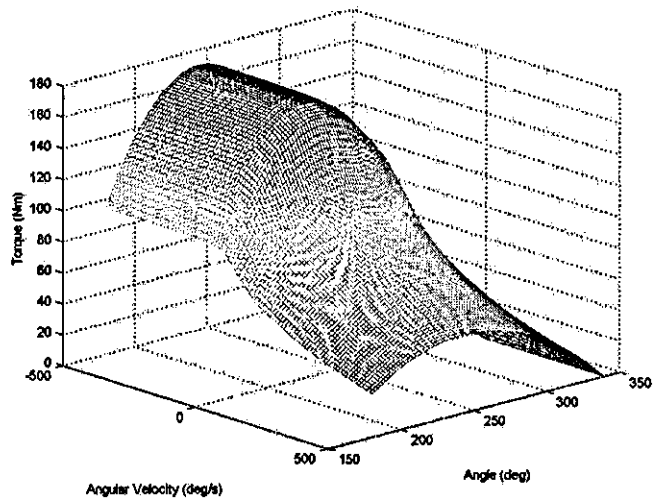
### Shoulder Flexion



## Ankle dorsi flexion



## Ankle plantar flexion



**Appendix H**

Informed consent form (Vault Testing)

**Appendix H Informed consent form (Vault Testing)**

Purpose

To obtain kinematic, kinetic and EMG data during vault landings.

Procedures

Kinematic data will be obtained using the Vicon camera system. Reflective markers attached to the subject will enable the Vicon cameras to capture the data. A force plate beneath the F.I.G. landing mat will be used to obtain kinetic data about the landing. Several EMG electrodes will be placed on key muscles to obtain data on muscle activation during landing.

The subject will be asked to perform both a forward and backward rotating vault of their choice.

During the testing a minimum of three researchers will be present.

Questions

The researcher will be pleased to answer any questions you may have at any time.

Withdrawal

You are free to withdraw from the study at any stage, without having to give any reasons. An opportunity will be provided in this event for you to discuss privately your wish to withdraw.

Confidentiality

Your identity will remain confidential in any material resulting from this work.

I have read the outline of the procedures that are involved in this study and I understand what will be required of me. I have had the opportunity to ask for further information and for clarification of the demands of the session. I am aware I have the right to withdraw at any time. As far as I am aware I do not have any injuries that would be affected by the testing procedure.

Name ..... (subject)

Signed ..... (subject)

Name ..... (researcher)

Signed ..... (researcher)

Date .....

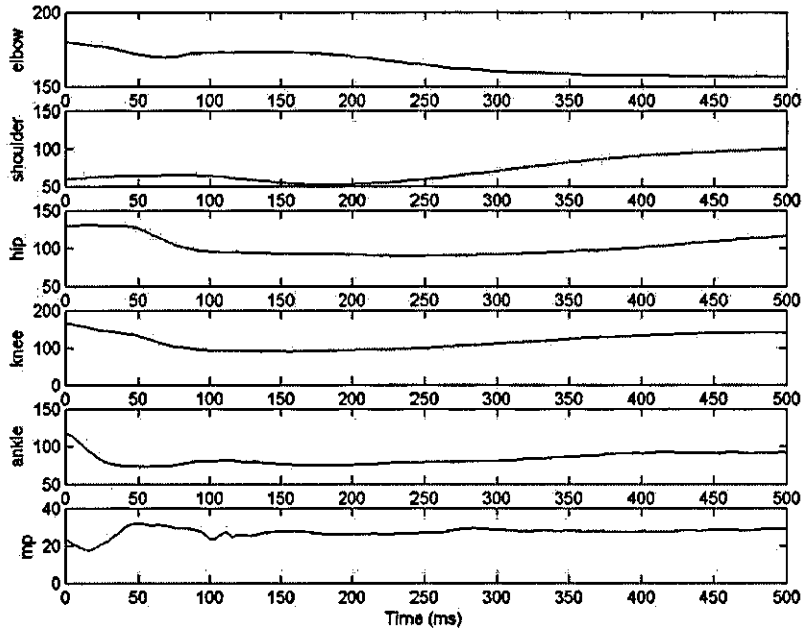
## **Appendix I**

**Processed force, EMG and Vicon data during landing from  
four vault skills**

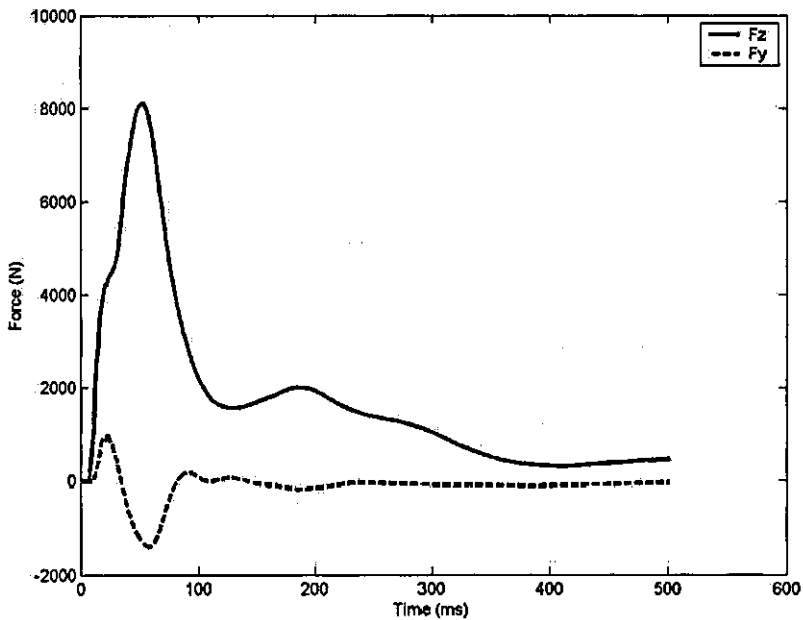
## Appendix I Processed force, EMG and Vicon data during landing from four vault skills

### Backward Somersault

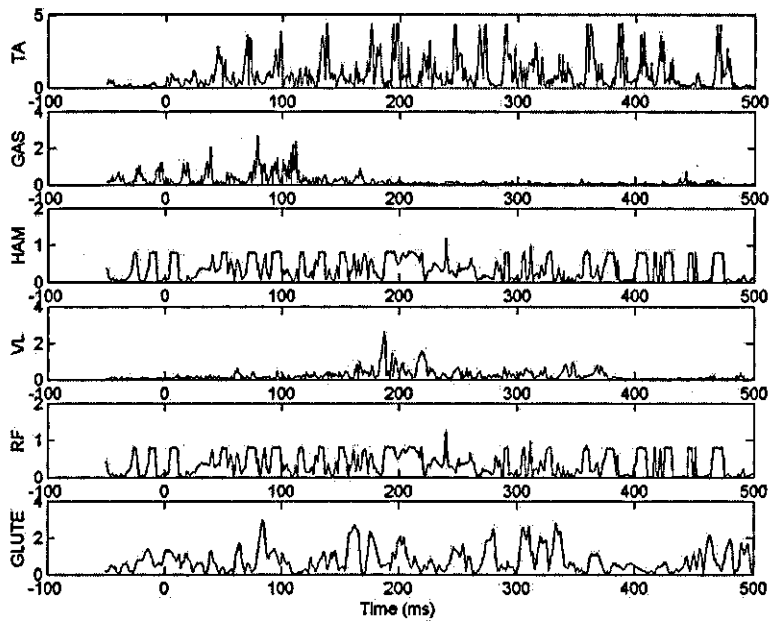
#### Joint angle time history



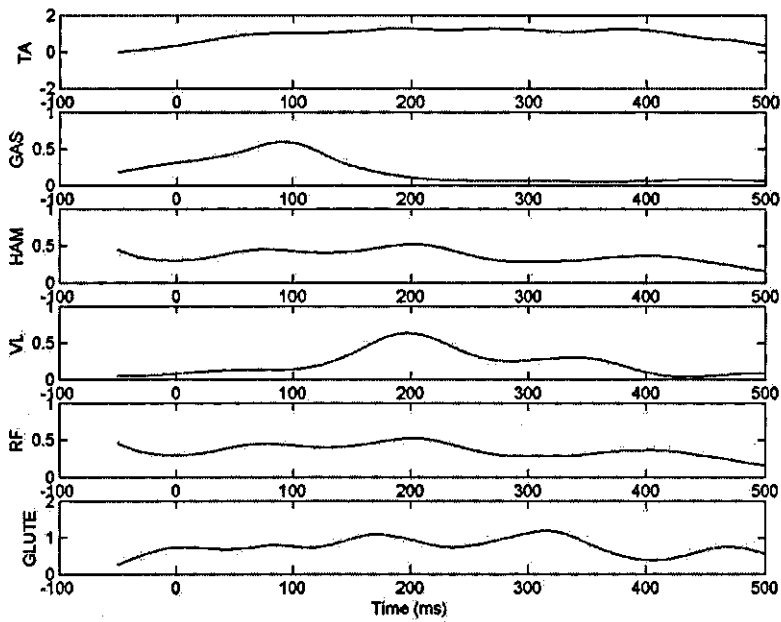
#### Force time history



## EMG time history



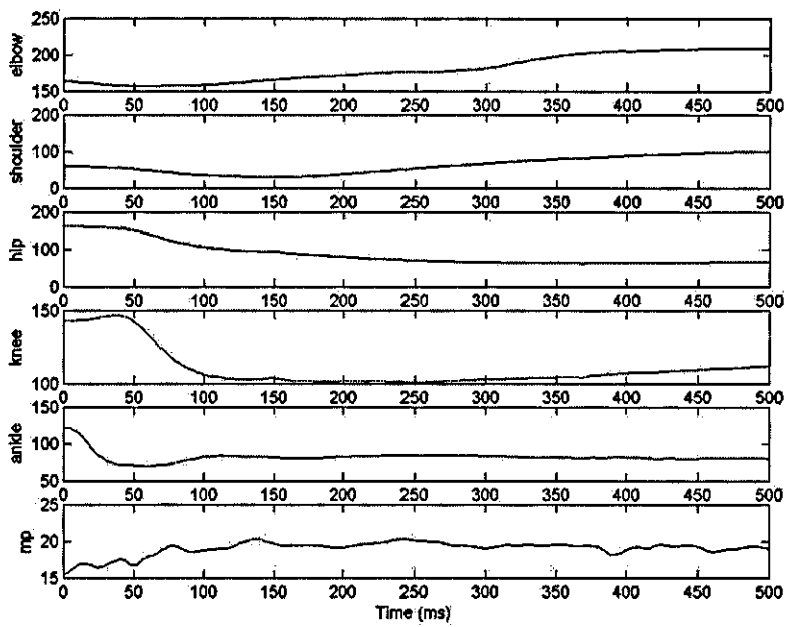
## Processed EMG time history (6 Hz)



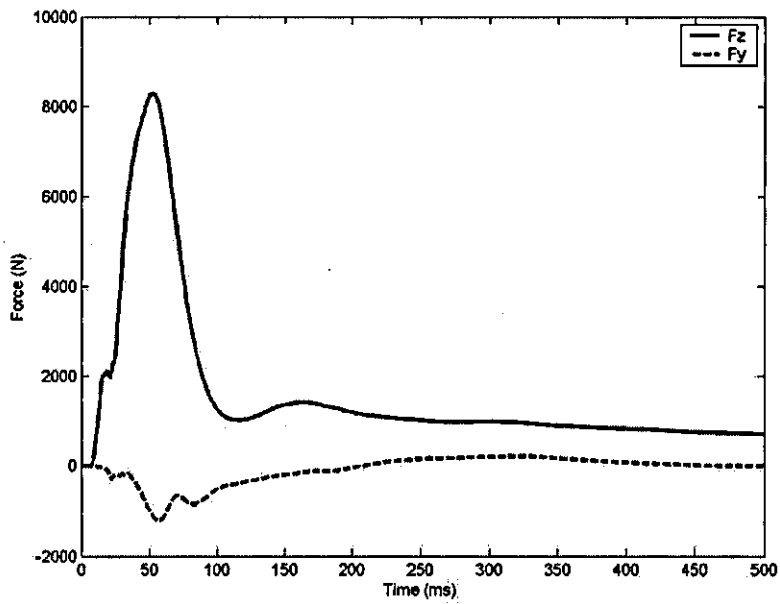


## Forward Somersault

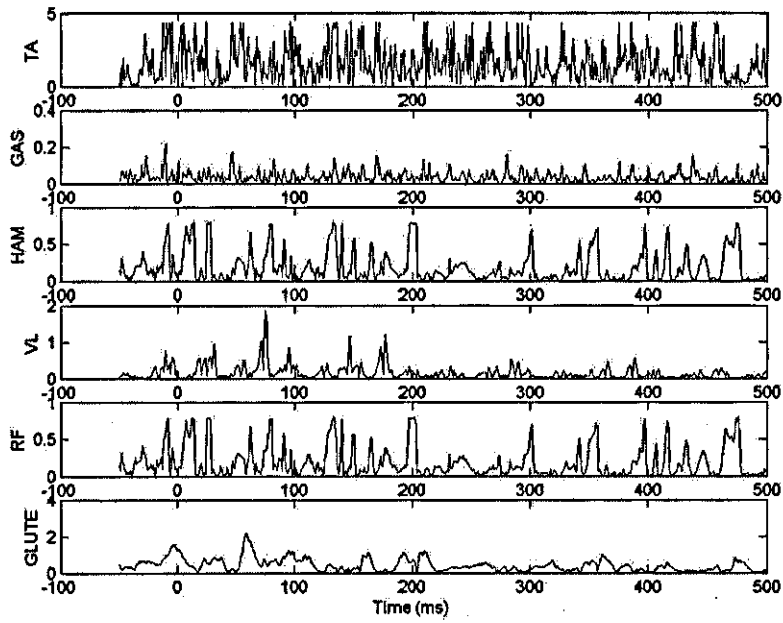
### Joint angle time history



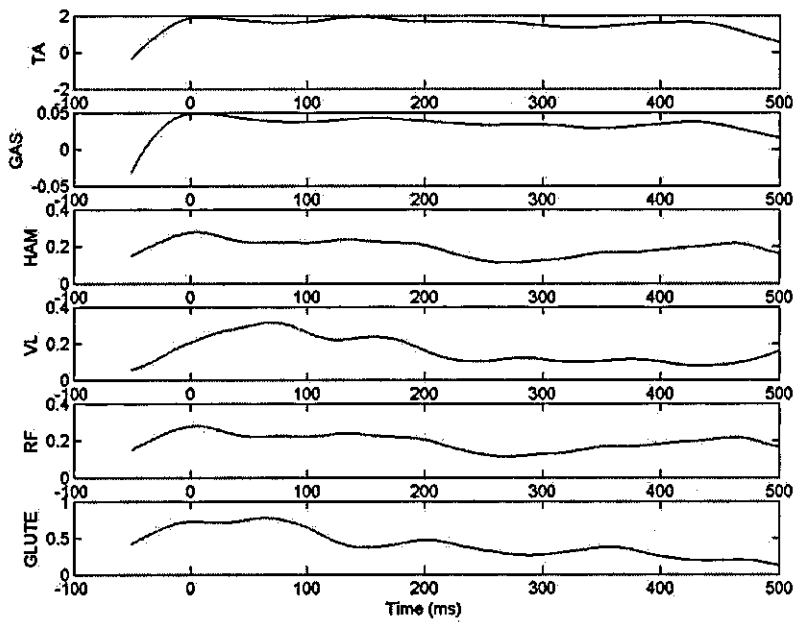
### Force time history



## EMG time history

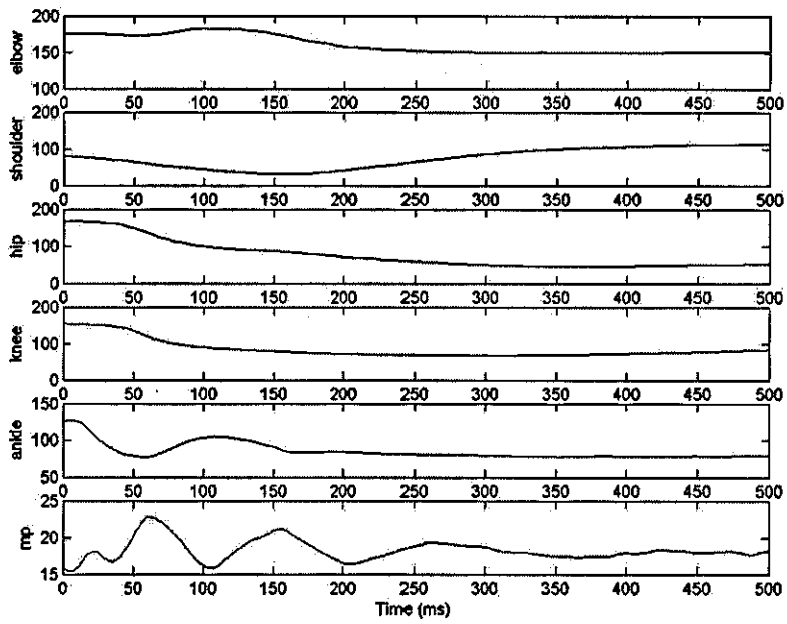


## Processed EMG time history (6 Hz)

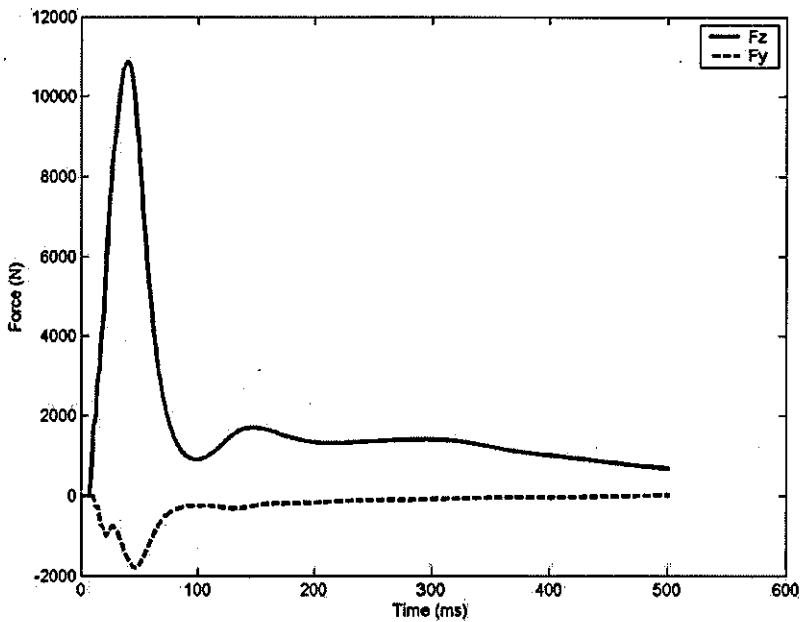


Handspring

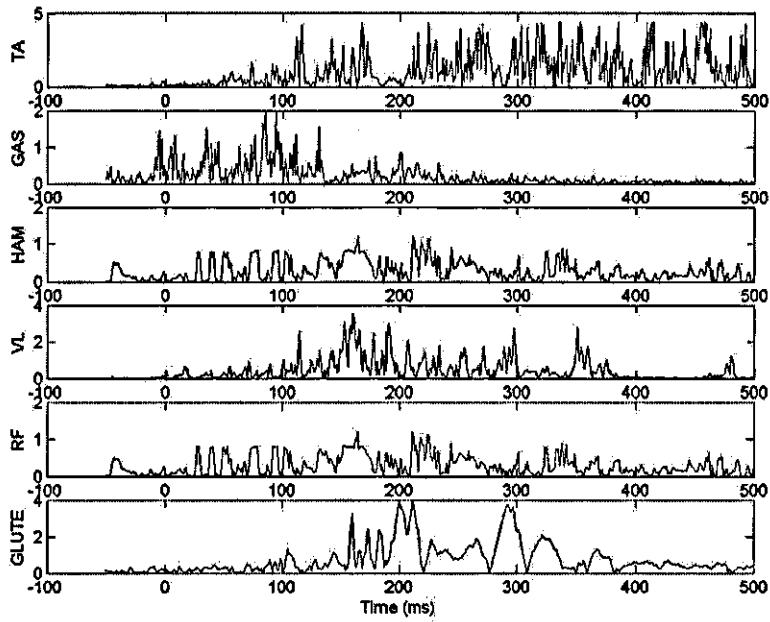
## Joint angle time history



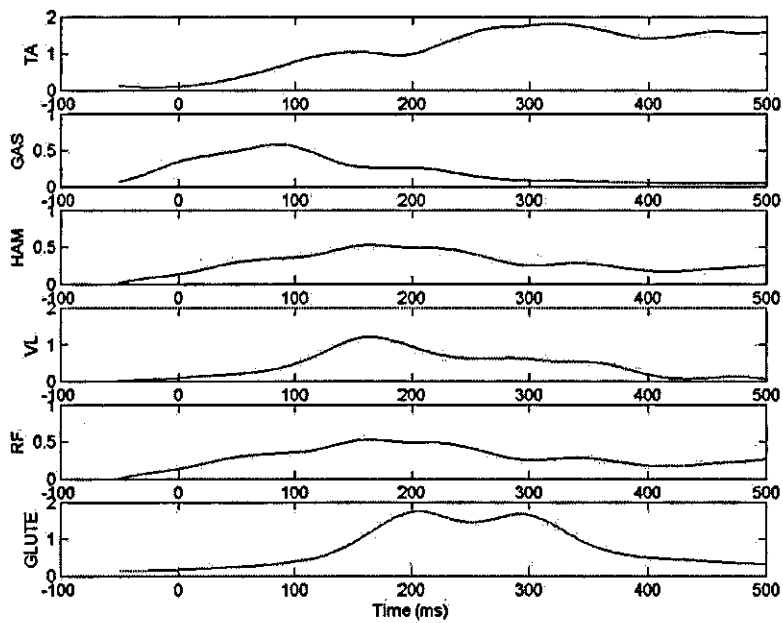
## Force time history



## EMG time history

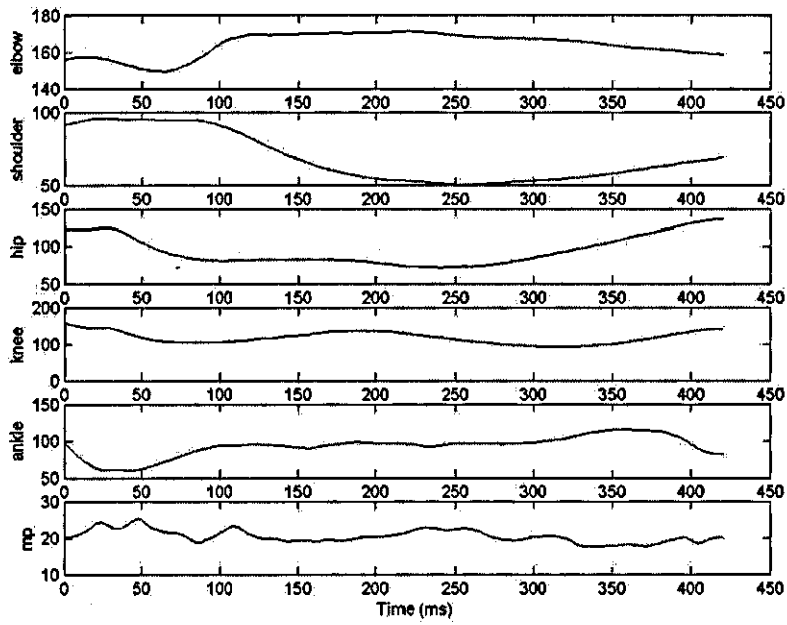


## Processed EMG time history (6 Hz)

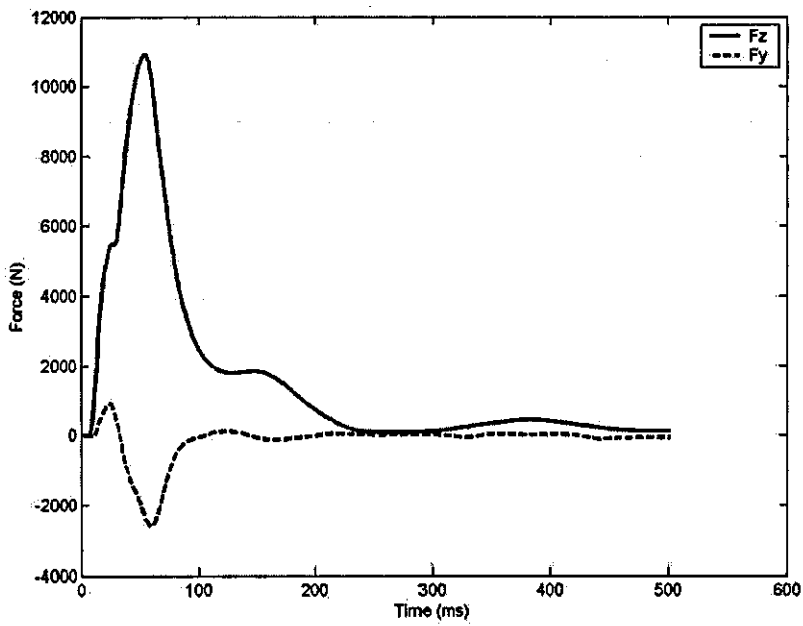


Tsukahara

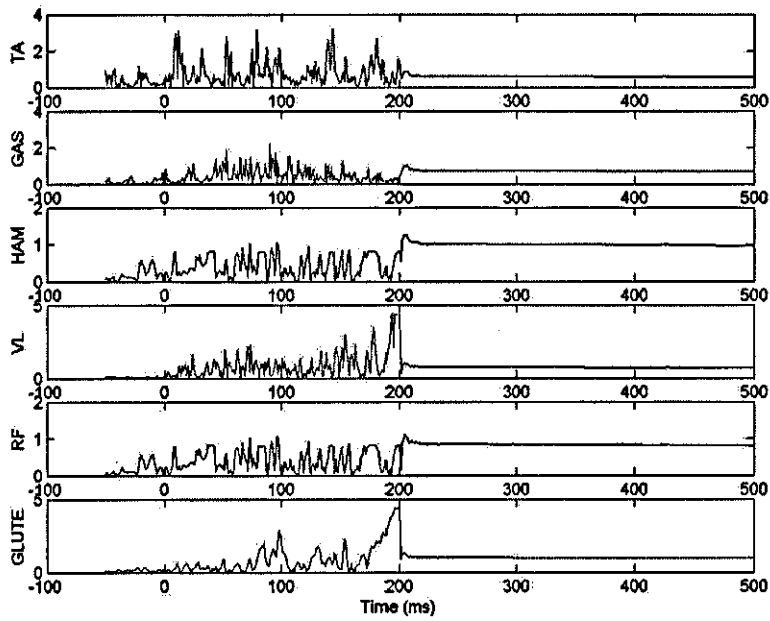
## Joint angle time history



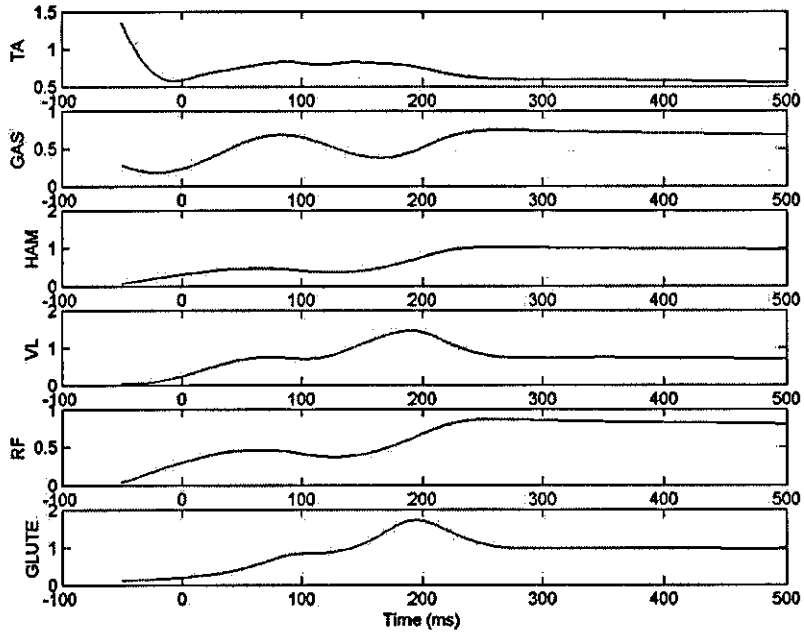
## Force time history



## EMG time history

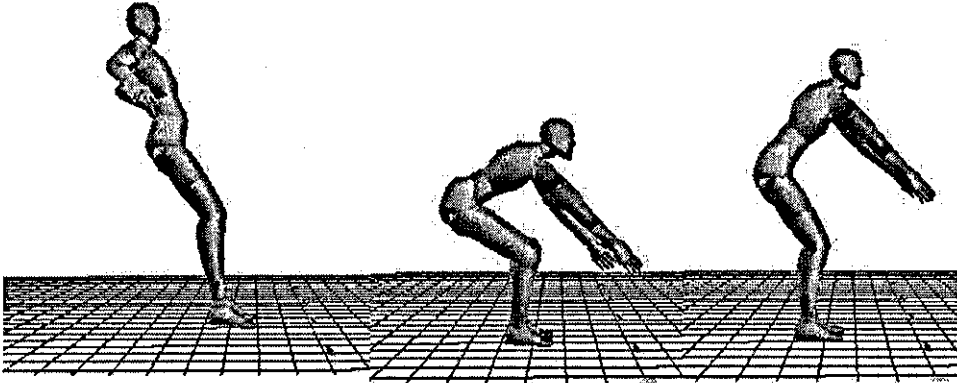


## Processed EMG time history (6 Hz)

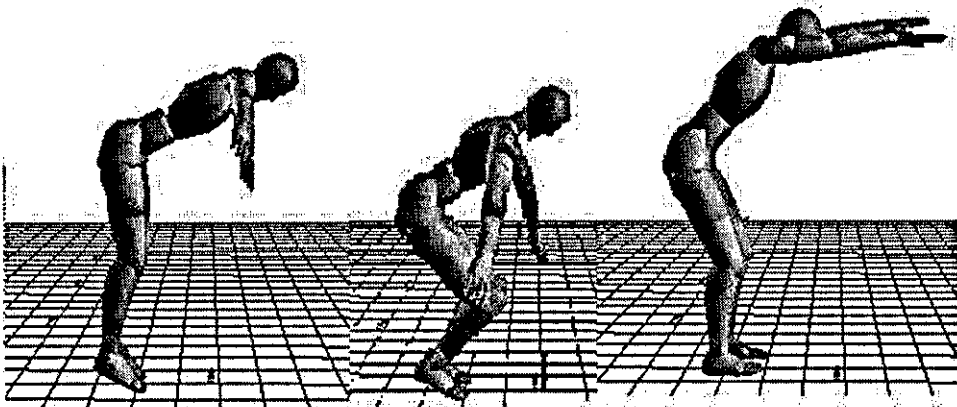


Diagrams of the actual vaults at key stages during the landing

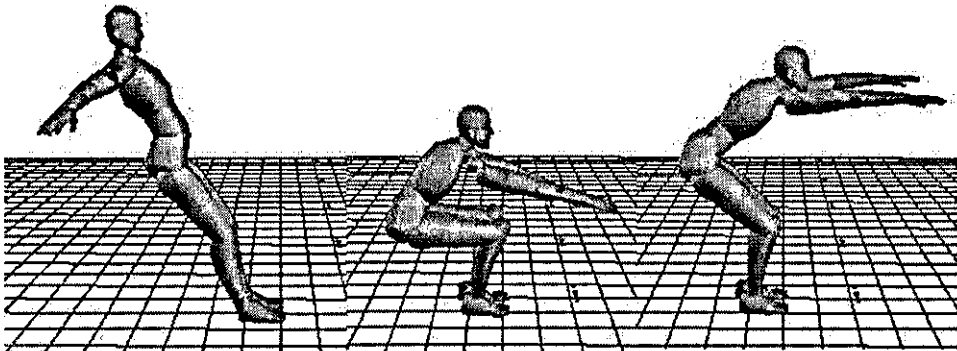
Front Somersault



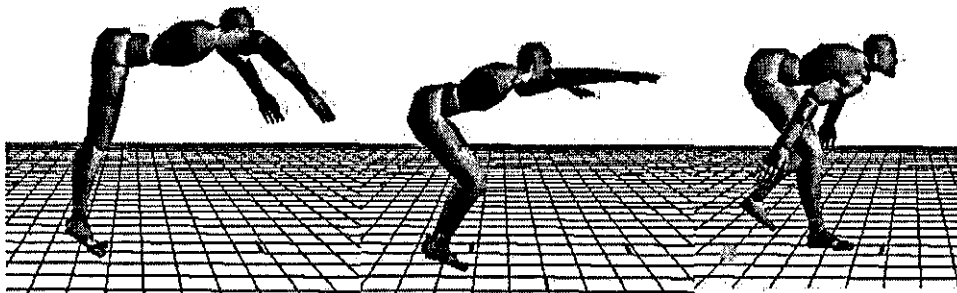
Back Somersault



Handspring

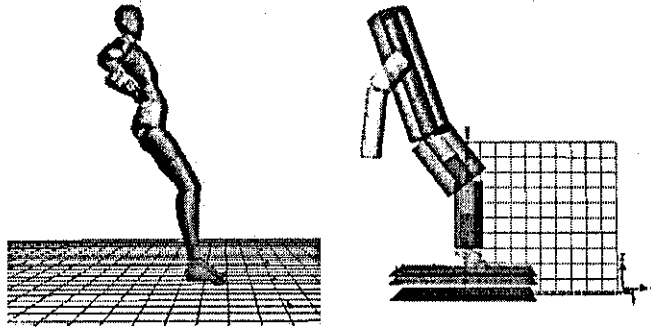


Tsukahara

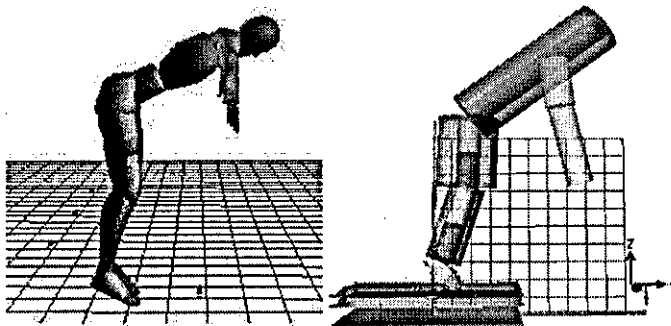


Comparing the model's starting position to subject's initial landing position

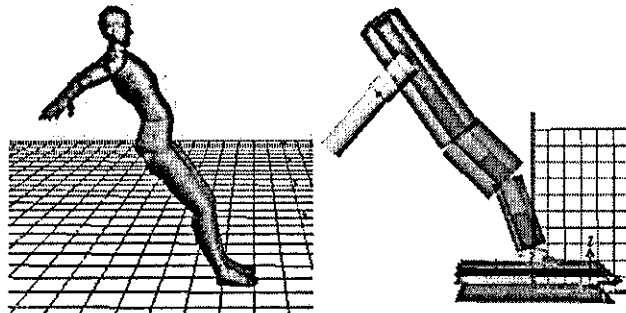
Front Somersault



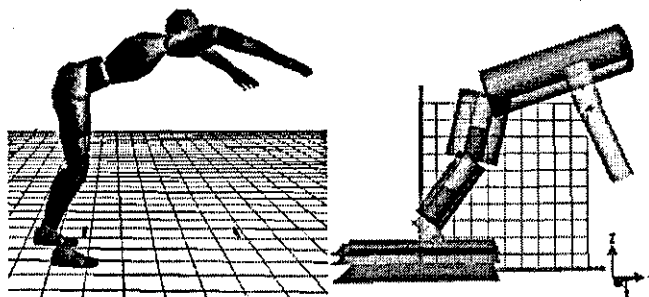
Back Somersault



Handspring



Tsukahara





## **Appendix J**

### **Linear SEC Stiffness Calculations**

## Appendix J Linear SEC Stiffness Calculations

The linear SEC stiffness was calculated in a similar way to that in Appendix F.

The two equations required are :

$$T = F \cdot d$$

$$F = k \cdot x$$

The maximum isometric torque at the joint is known from the Cybex testing and moment arm for each muscle group is estimated using Chapter 4.

The isometric torque divided by the moment arm gives the force in the muscle group. ( $T = F \cdot d$ )

The SEC was allowed to stretch 5% therefore the stretch of the SEC could be calculated from its original length then using  $F = k \cdot x$ . The SEC stiffness could be calculated. The SEC stiffness in the table below is for one leg.

	SEC length (m)	Moment Arm (m)	Force (N)	SEC stretch (5%)	SEC stiffness (Nm-1)
Knee Ext	0.325	0.039	6210	0.01625	382154
Knee Flex	0.275	0.020	7300	0.01375	530909
Hip Ext	0.080	0.059	4068	0.004	1017000
Hip Flex	0.103	0.033	4000	0.00515	776699
Ankle Ext	0.345	0.042	6071	0.01725	3511942
Ankle Flex	0.236	0.042	905	0.0118	76695

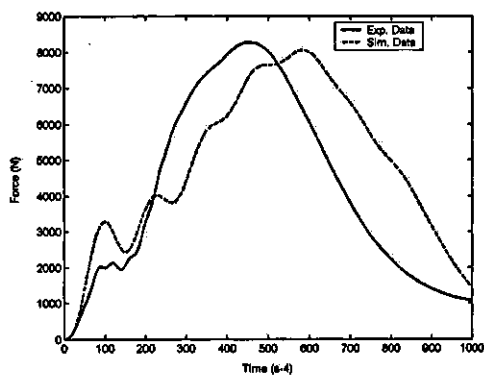
## **Appendix K**

**Evaluation of all four skills using models 1, 2 and 3**

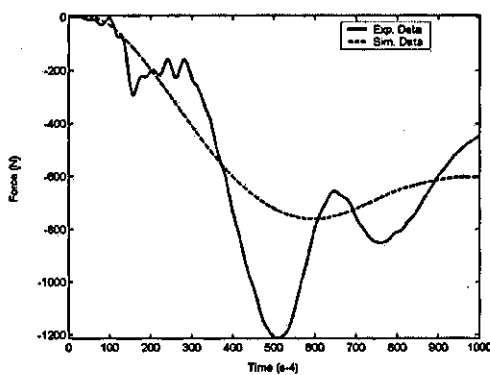
Appendix K Evaluation of all four skills using models 1, 2 and 3

FRONT SOMERSAULT – model one

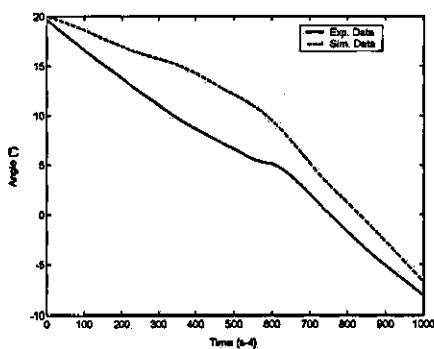
VGRF



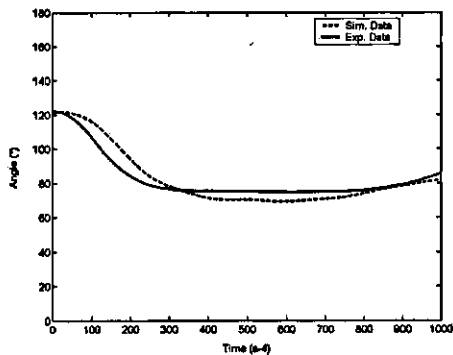
HGRF



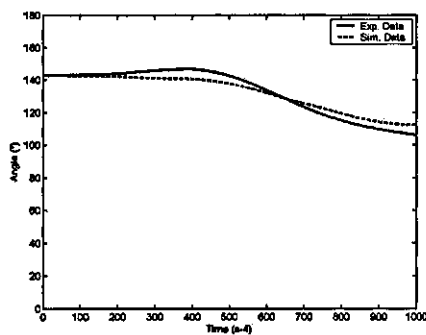
Trunk



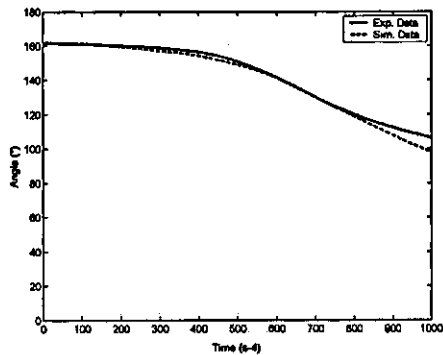
Ankle



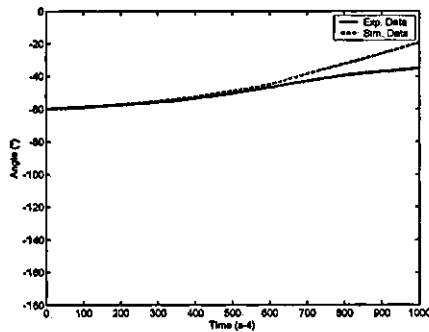
Knee



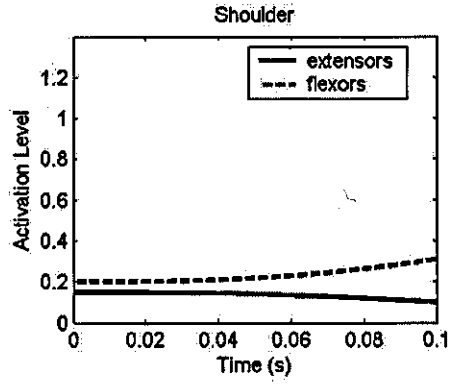
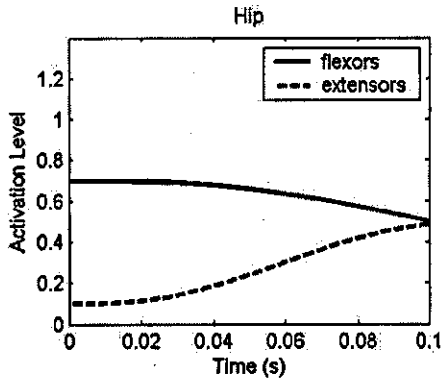
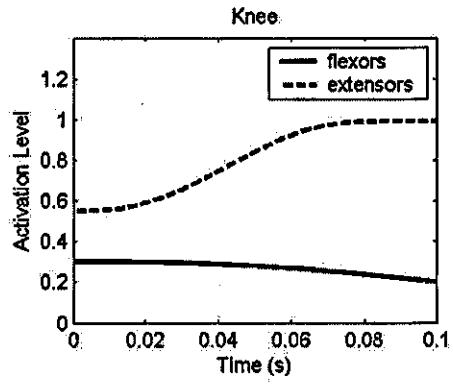
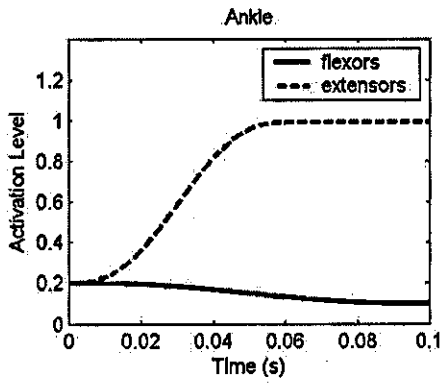
Hip



Shoulder



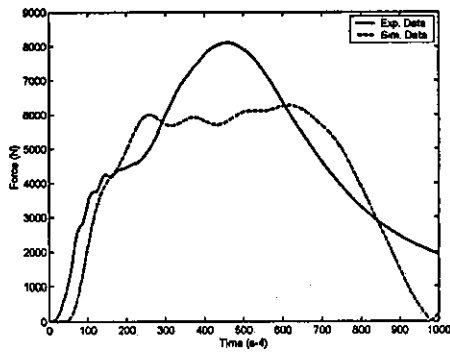
Front somersault model one – activation



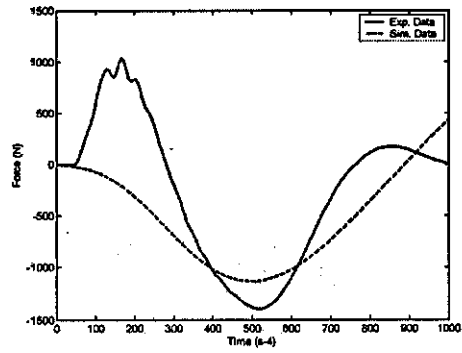


Back Somersault – model one

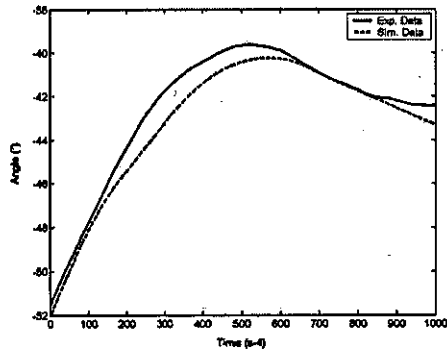
VGRF



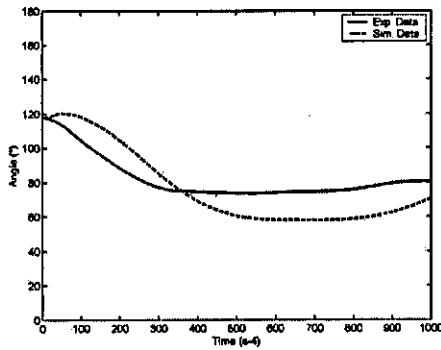
HGRF



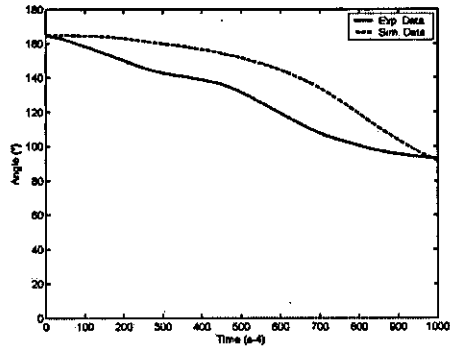
Trunk



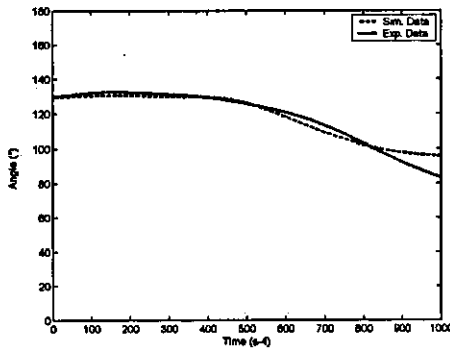
Ankle



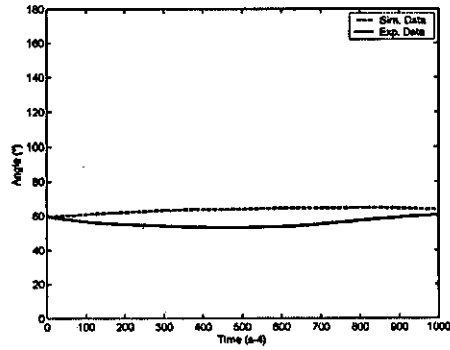
Knee



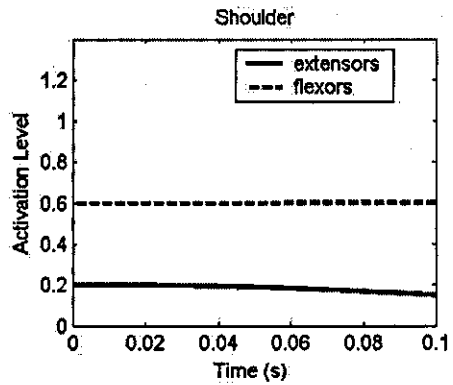
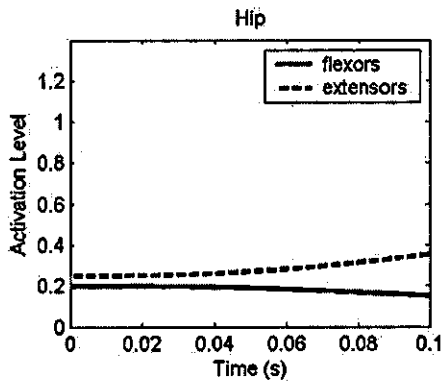
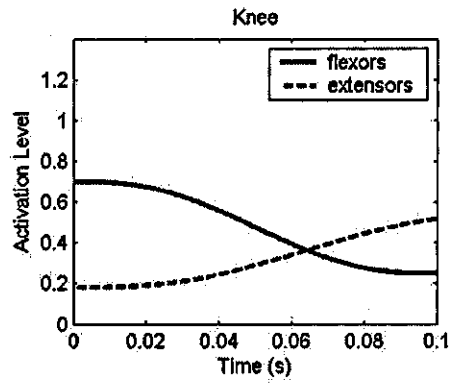
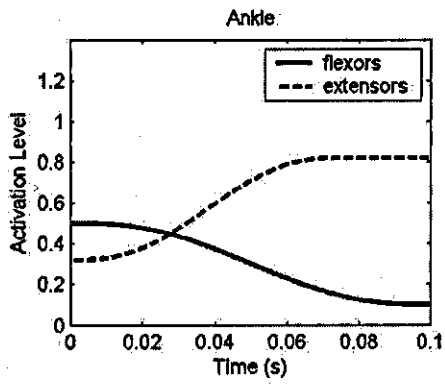
Hip



Shoulder



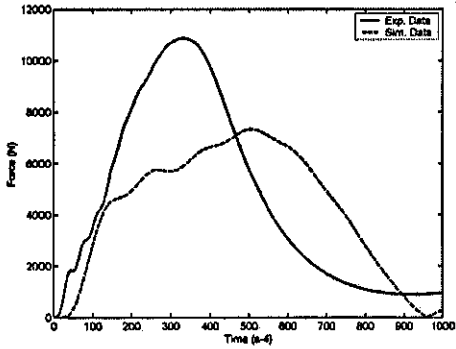
## Back Somersault – model one – activation



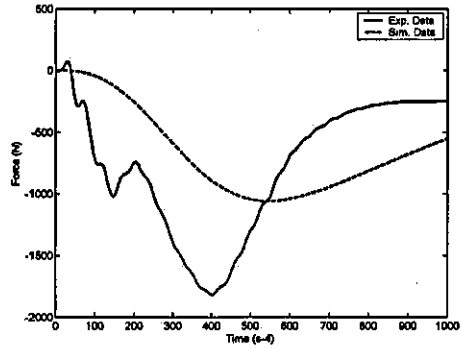




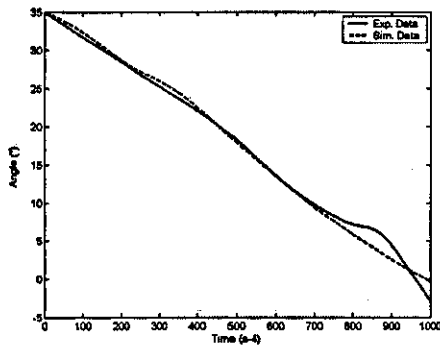
Handspring – model one  
VGRF



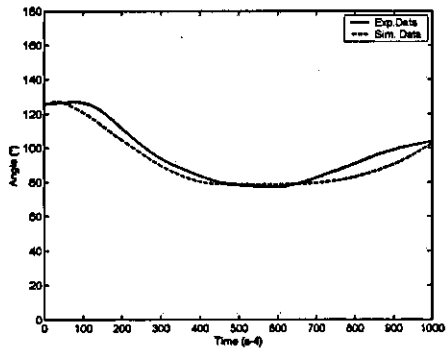
HGRF



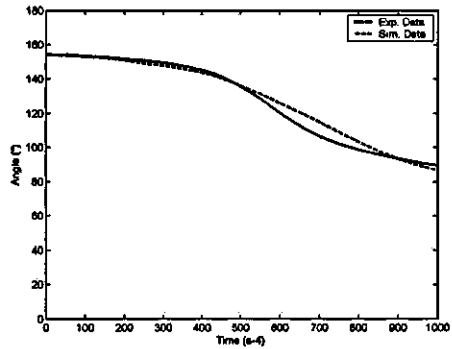
Trunk



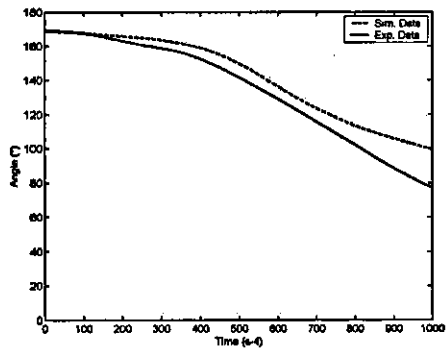
Ankle



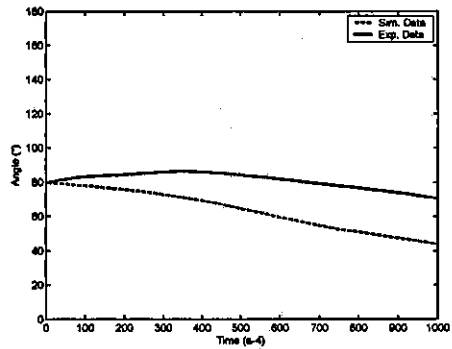
Knee



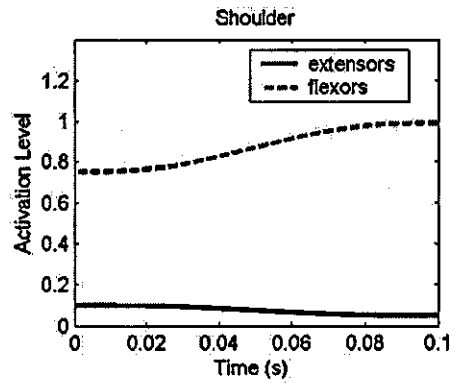
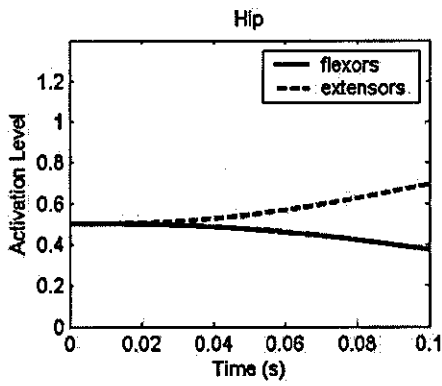
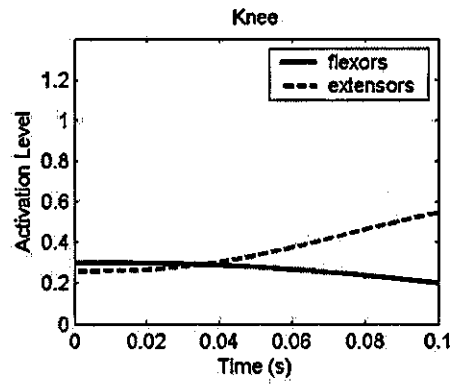
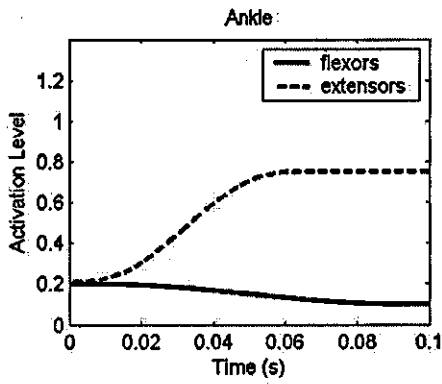
Hip



Shoulder



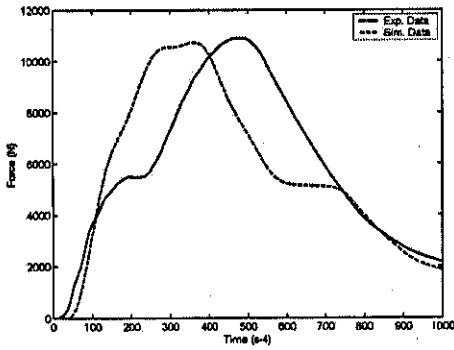
## Handspring – model one – activation



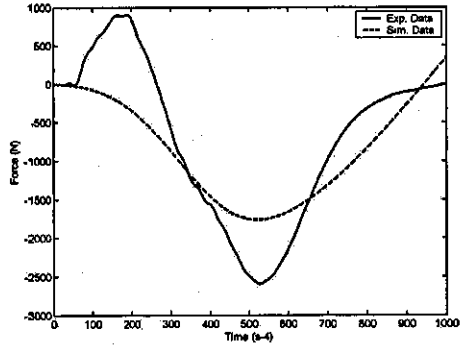


Tsukahara - model one

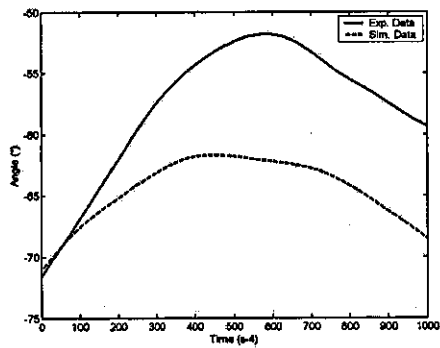
VGRF



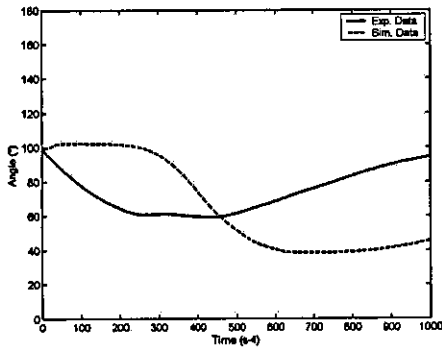
HGRF



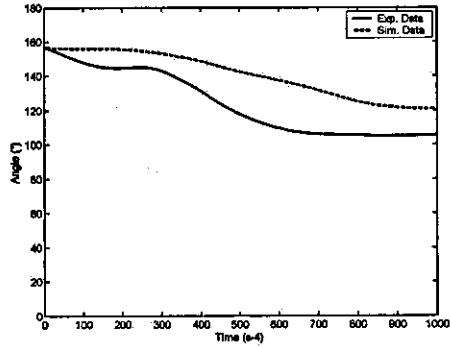
Trunk



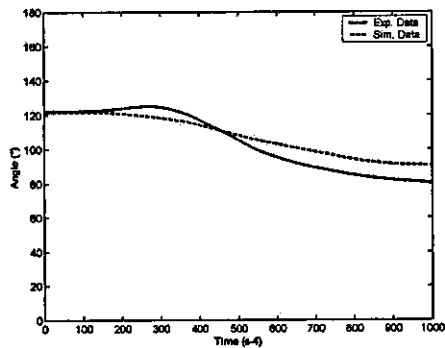
Ankle



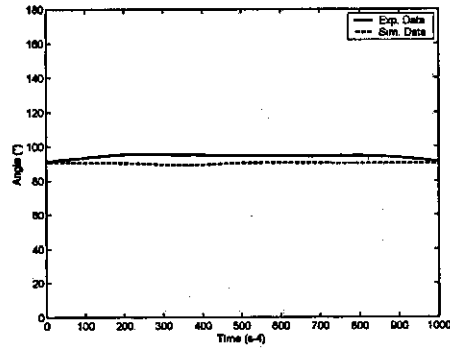
Knee



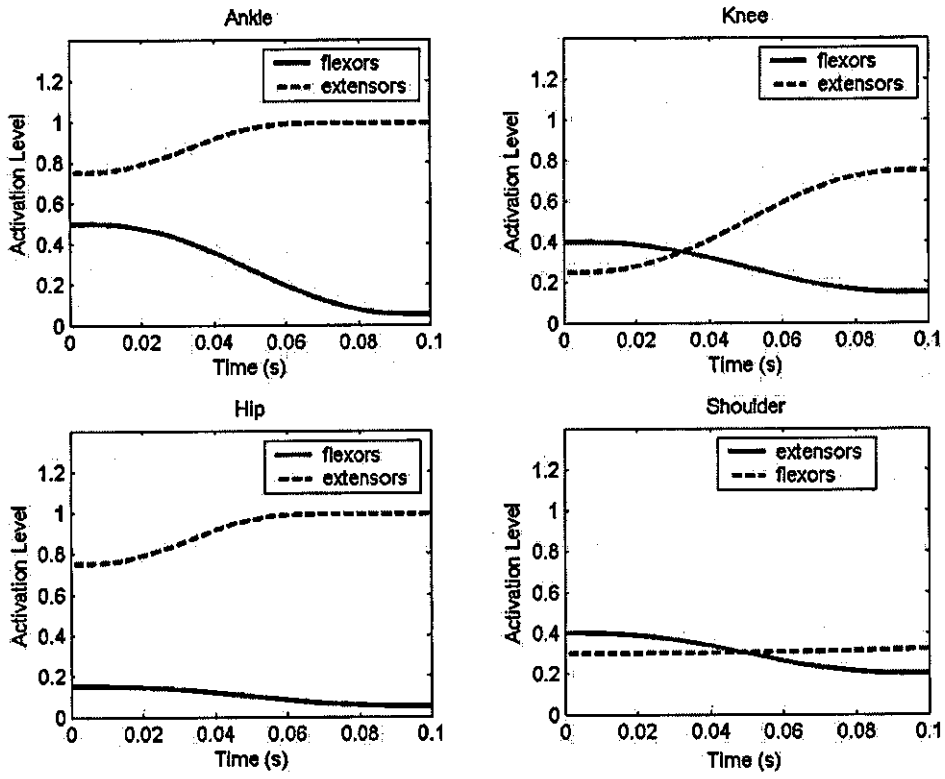
Hip



Shoulder



## Tsukahara – model one – activation





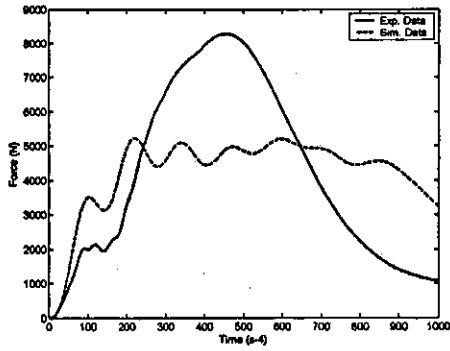
## Model one - Summary

Gymnastic Skill	Overall Score %	RMS (all joints)	RMS (body orientation)	RMS (Vert GRF)	RMS (Hor GRF)
Front Somersault	11.9	8 %	4 %	21 %	15 %
Back Somersault	18.2	15 %	1 %	15 %	36 %
Handspring	17.1	11 %	1 %	25 %	31 %
Tsukahara	20.6	35 %	8 %	20 %	21 %

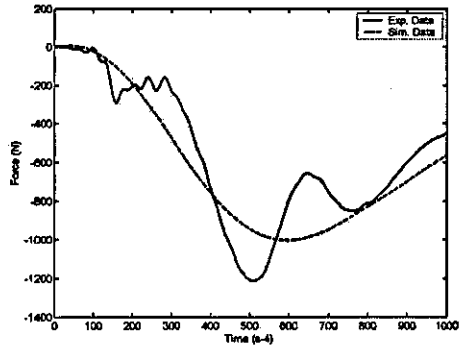
Gymnastic Skill	Peak % (VGRF)	Peak % (HGRF)	Mat deformation (vertical) (m)	Mat deformation (horizontal) (m)
Front Somersault	3	15.1	0.13	0.04
Back Somersault	23	36.3	0.14	0.03
Handspring	33	30.7	0.145	0.05
Tsukahara	2	20.8	0.15	0.09



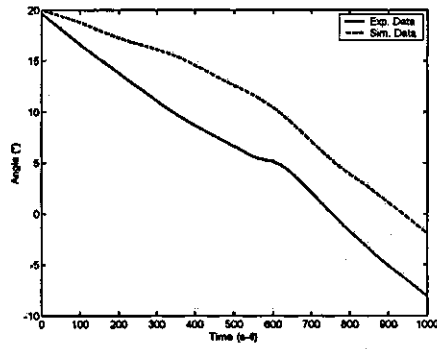
Front Somersault – model two  
VGRF



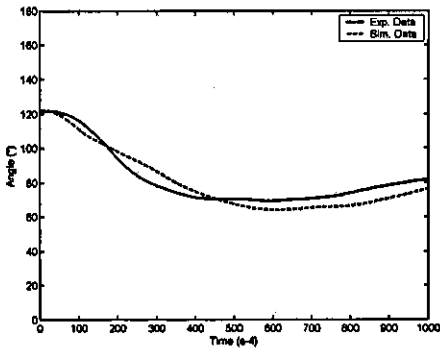
HGRF



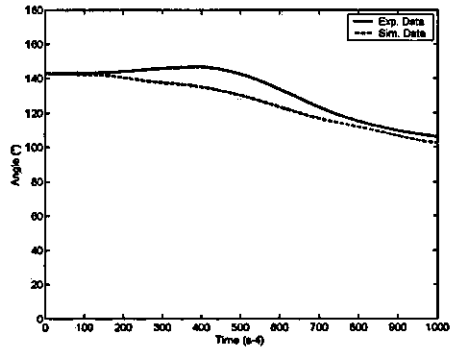
Trunk



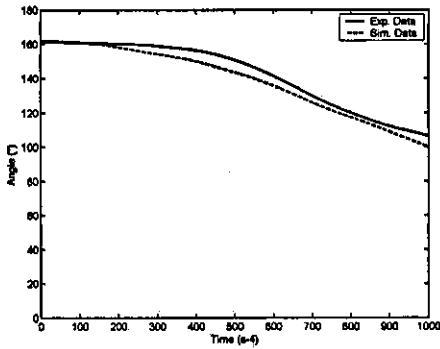
Ankle



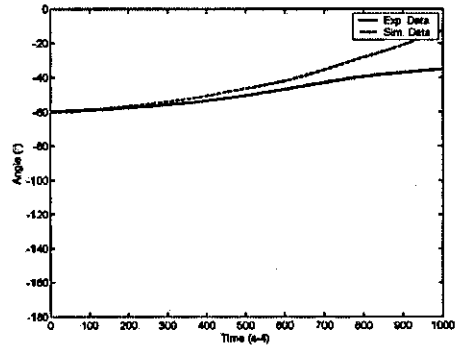
Knee



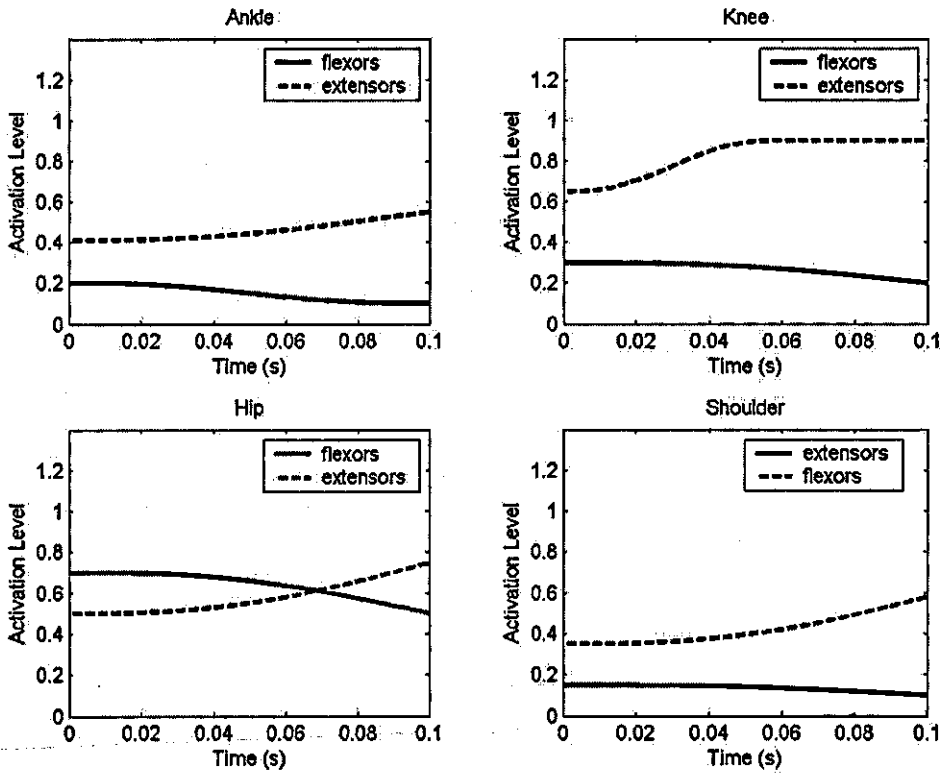
Hip



Shoulder

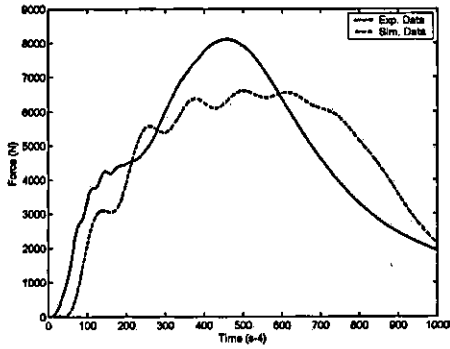


## Front somersault – model two – activation

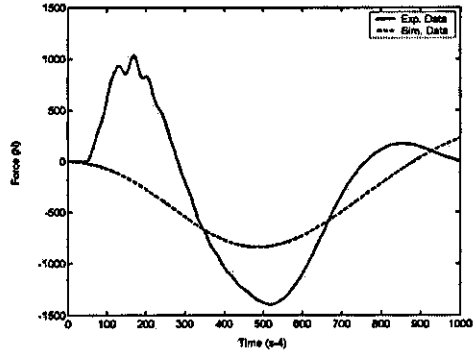




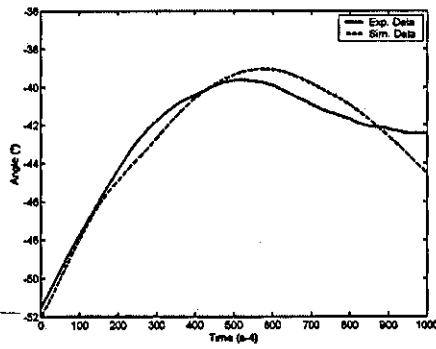
Back Somersault – model two  
VGRF



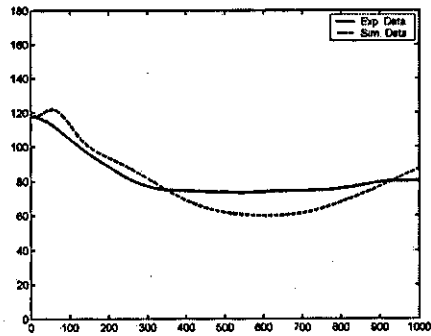
HGRF



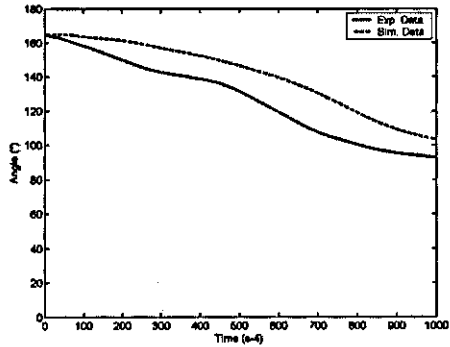
Trunk



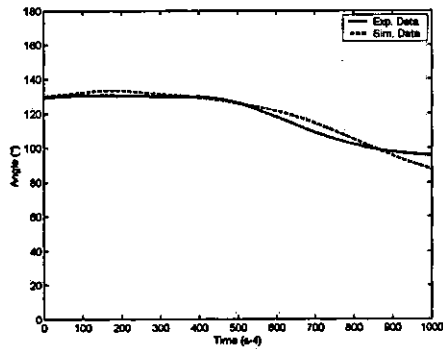
Ankle



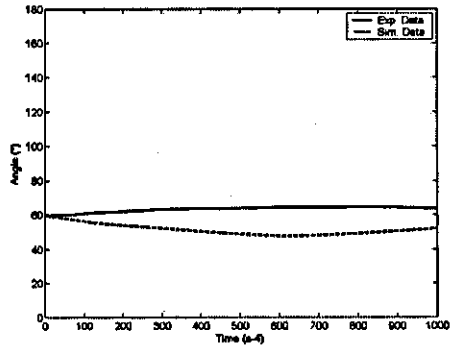
Knee



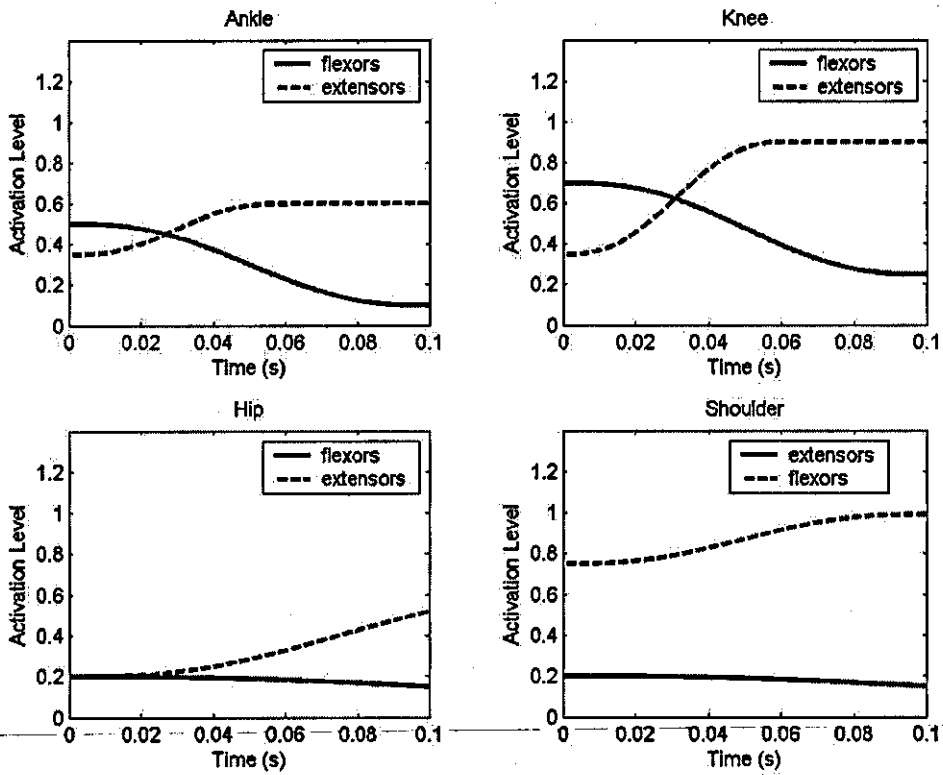
Hip



Shoulder

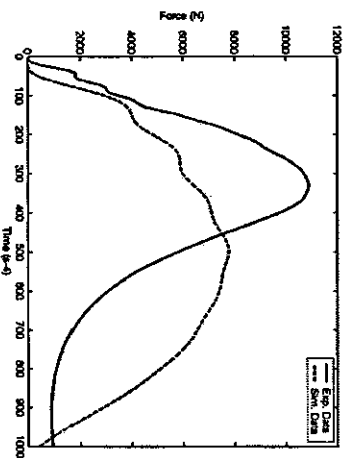


## Back somersault – model two – activation

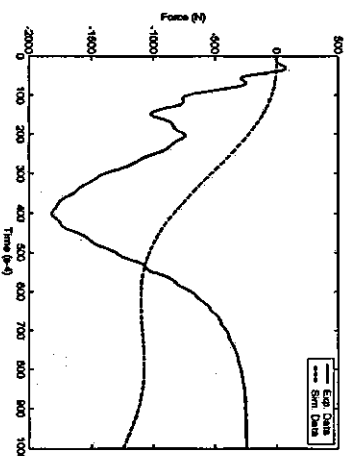




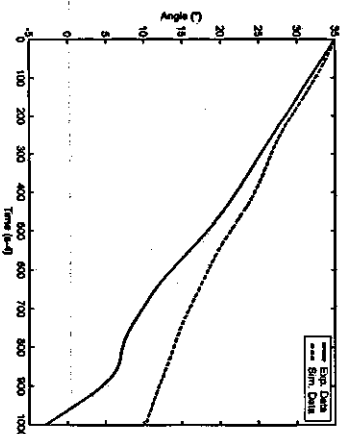
### Handspring - model two VGRF



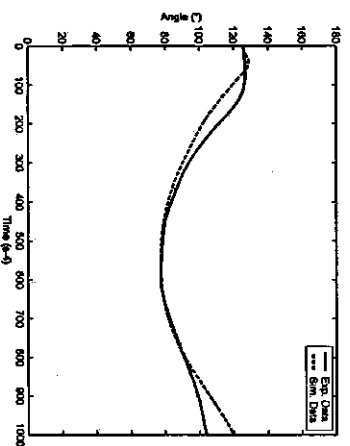
### HGRF



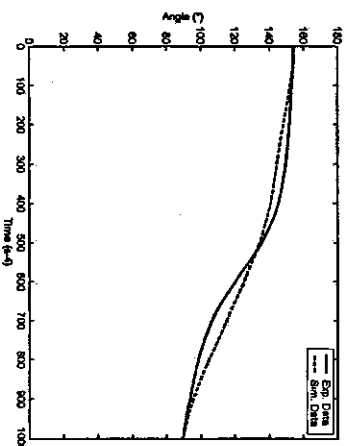
### Trunk



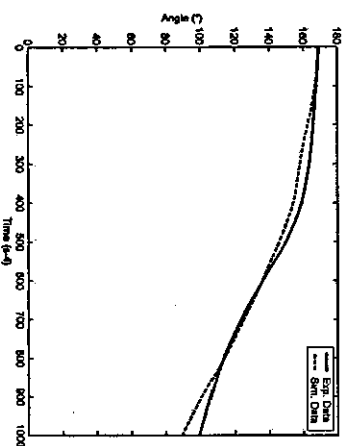
### Ankle



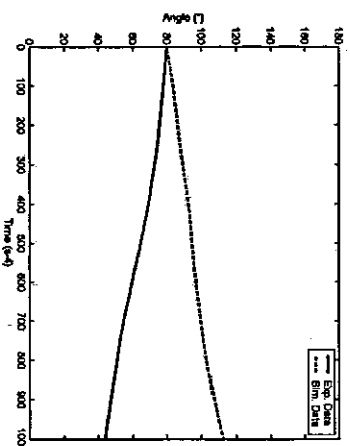
### Knee



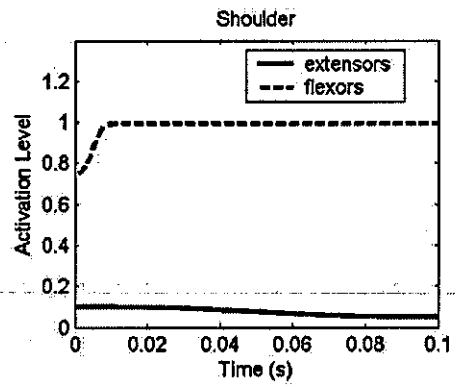
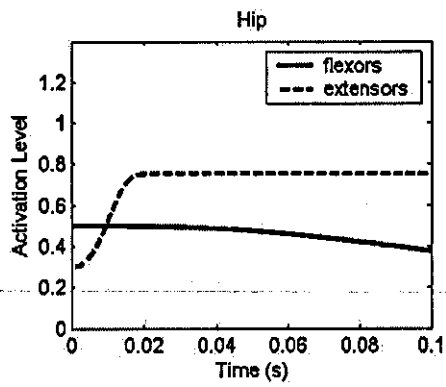
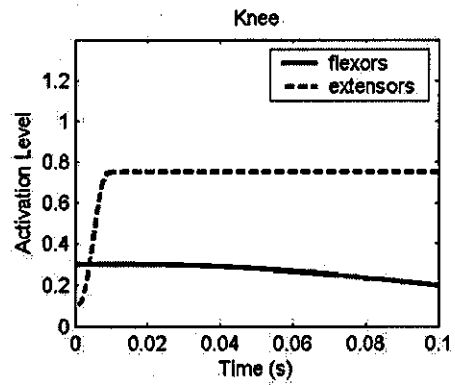
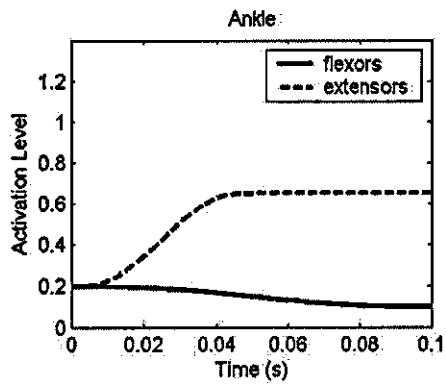
### Hip



### Shoulder



## Handspring – model two – activation

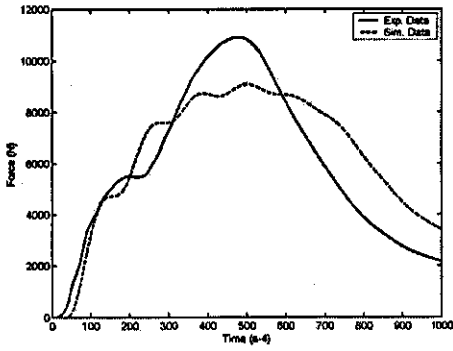




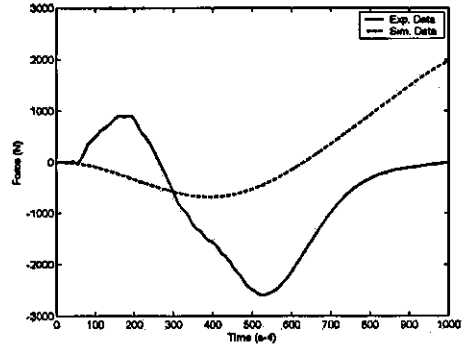


### Tsukahara – model two

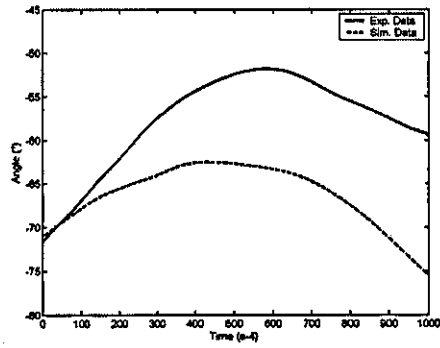
#### VGRF



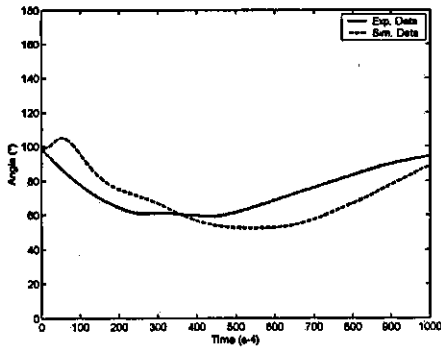
#### HGRF



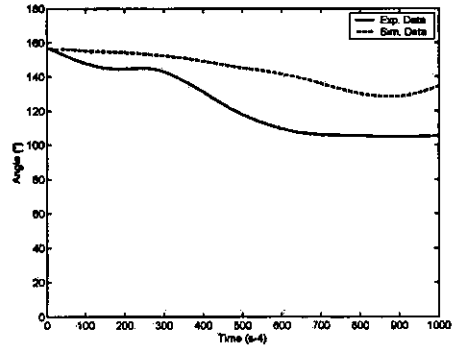
#### Trunk



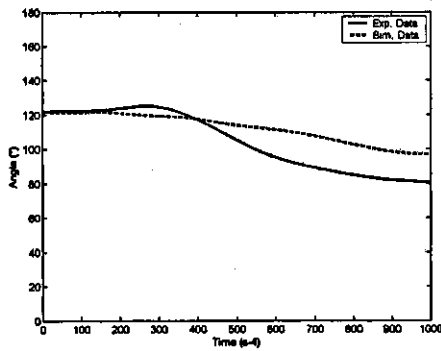
#### Ankle



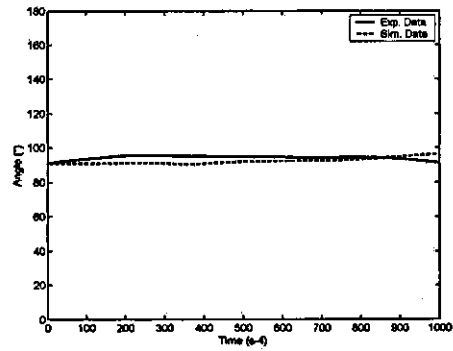
#### Knee



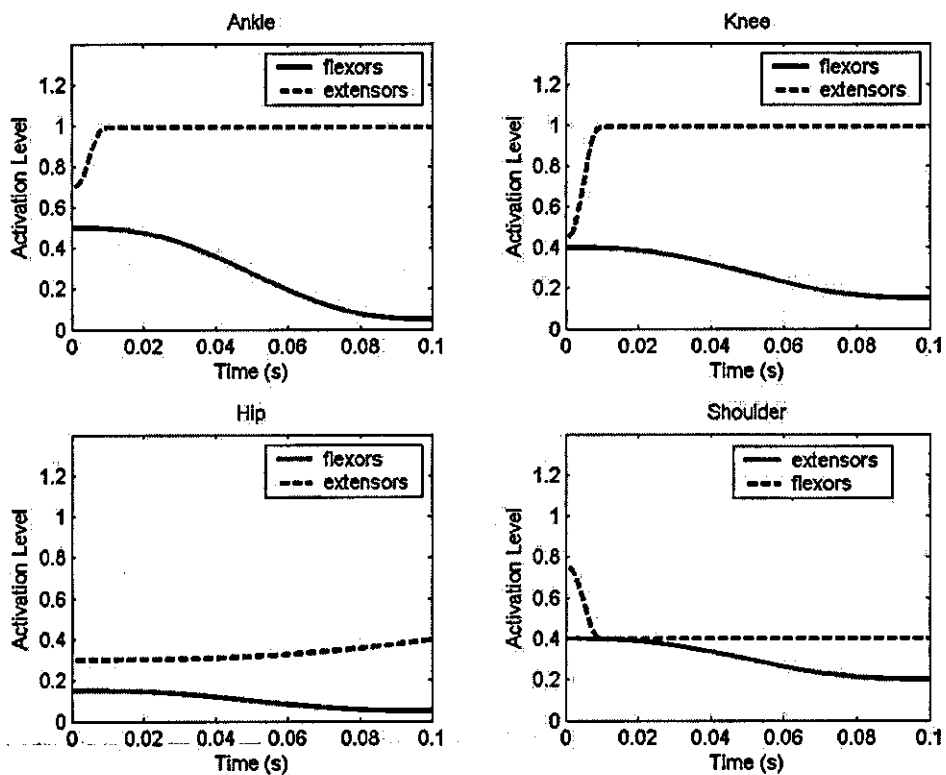
#### Hip



#### Shoulder



## Tsukahara – model two – activation



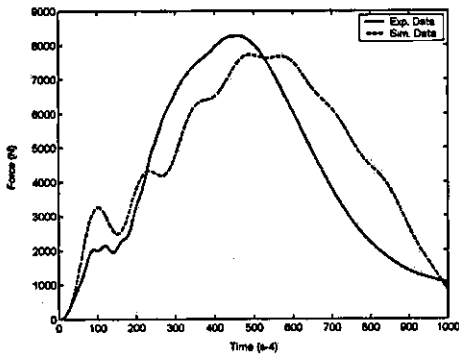


**Model two - Summary**

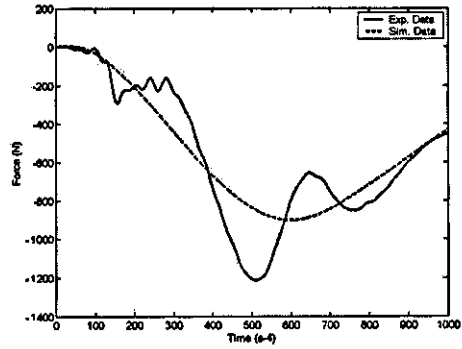
<b>Gymnastic Skill</b>	<b>Overall Score %</b>	<b>RMS (all joints)</b>	<b>RMS (body orientation)</b>	<b>RMS (Vert GRF)</b>	<b>RMS (Hor GRF)</b>
Front Somersault	13.9	12.3	5.1	25.7	12.7
Back Somersault	17.6	19.0	0.8	14.9	35.8
Handspring	22.1	15.1	5.1	29.7	38.6
Tsukahara	23.9	25.5	9.7	13.4	46.8

<b>Gymnastic Skill</b>	<b>Peak % (VGRF)</b>	<b>Peak % (HGRF)</b>	<b>Mat deformation (vertical) (m)</b>	<b>Mat deformation (horizontal) (m)</b>
Front Somersault	36.9	17.5	0.11	0.07
Back Somersault	18.5	40.0	0.13	0.04
Handspring	28.5	32.5	0.15	0.09
Tsukahara	16.8	73.9	0.16	0.05

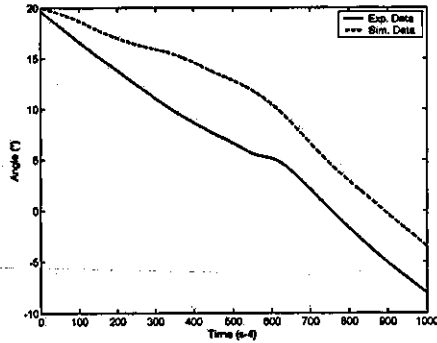
**FRONT SOMERSAULT – model three**  
**VGRF**



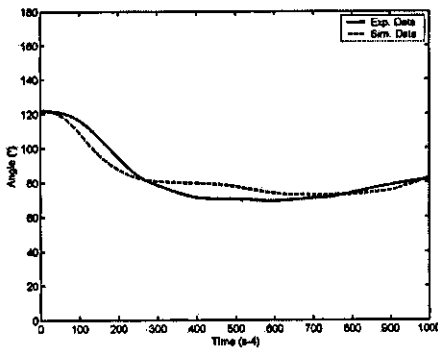
**HGRF**



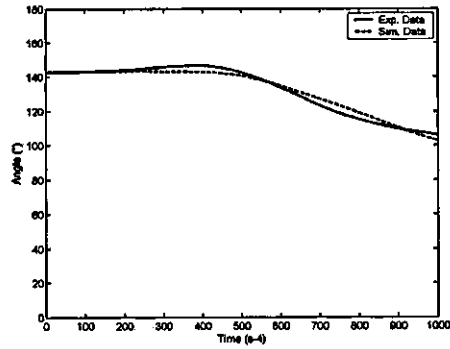
**Trunk**



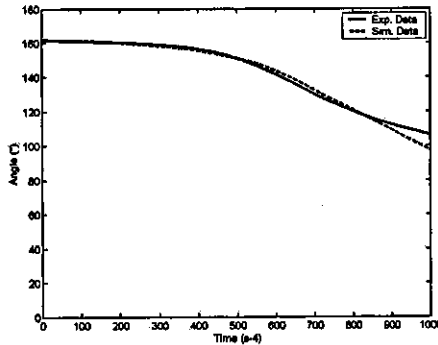
**Ankle**



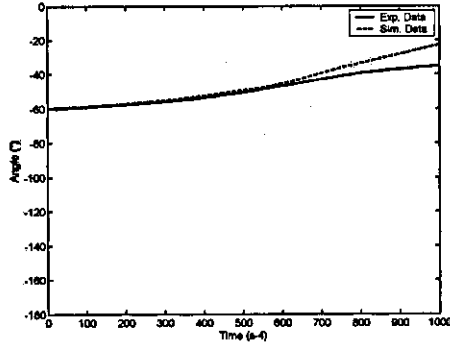
**Knee**



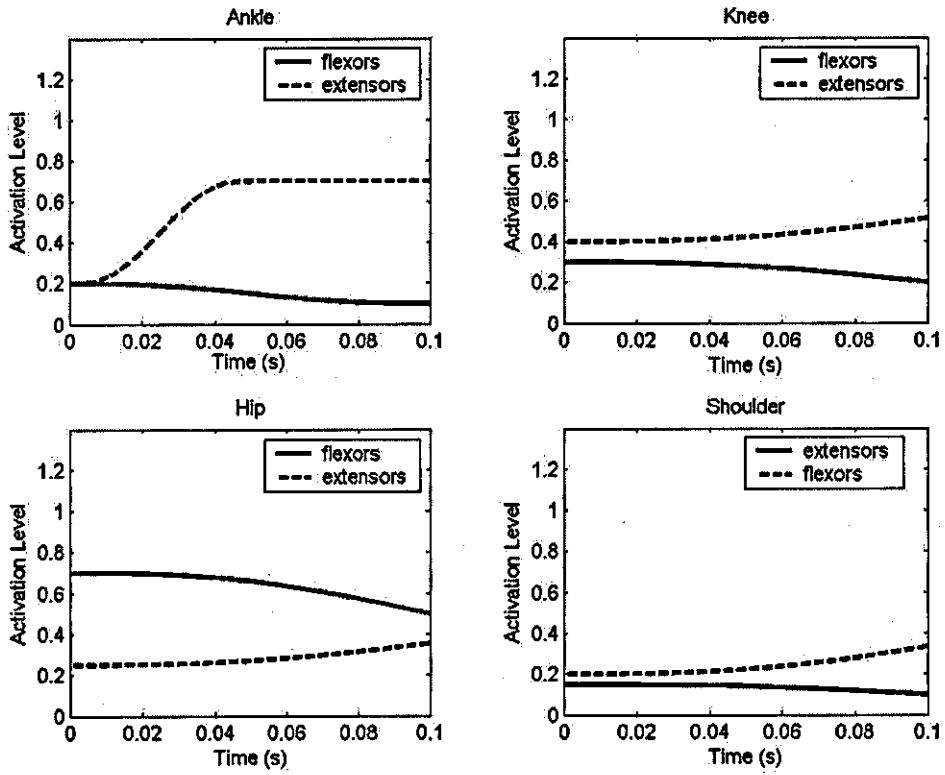
**Hip**



**Shoulder**



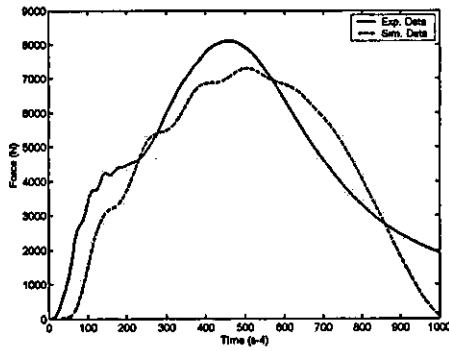
## Front somersault model three – activation



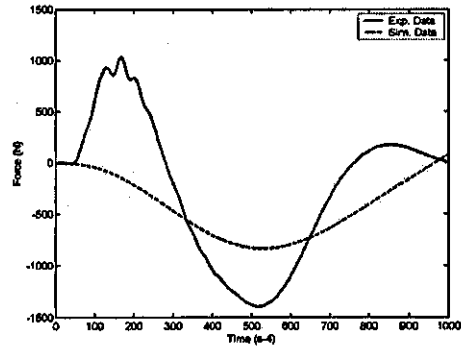




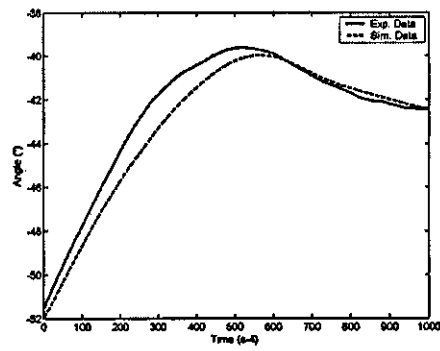
### BACK SOMERSAULT – model three VGRF



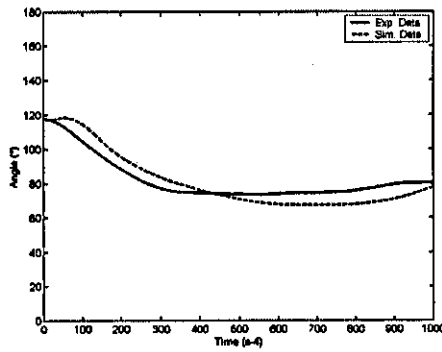
### HGRF



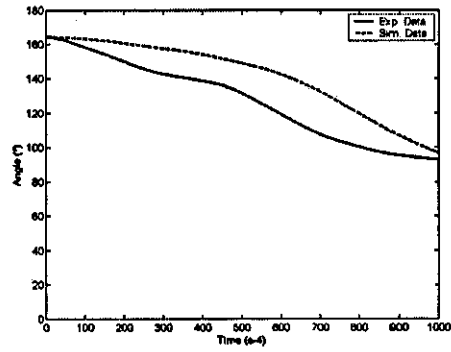
### Trunk



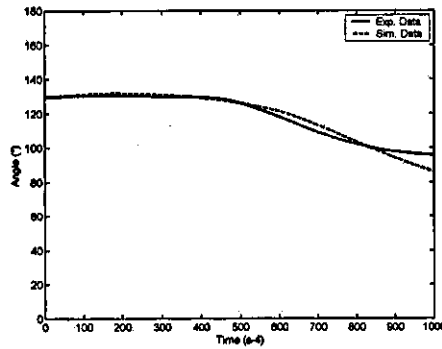
### Ankle



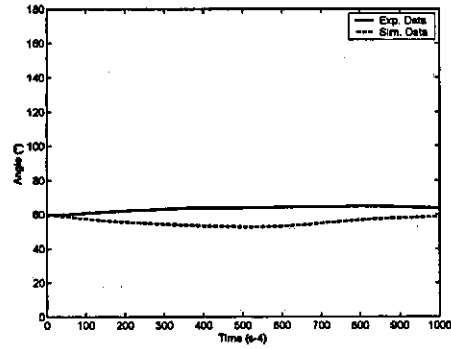
### Knee



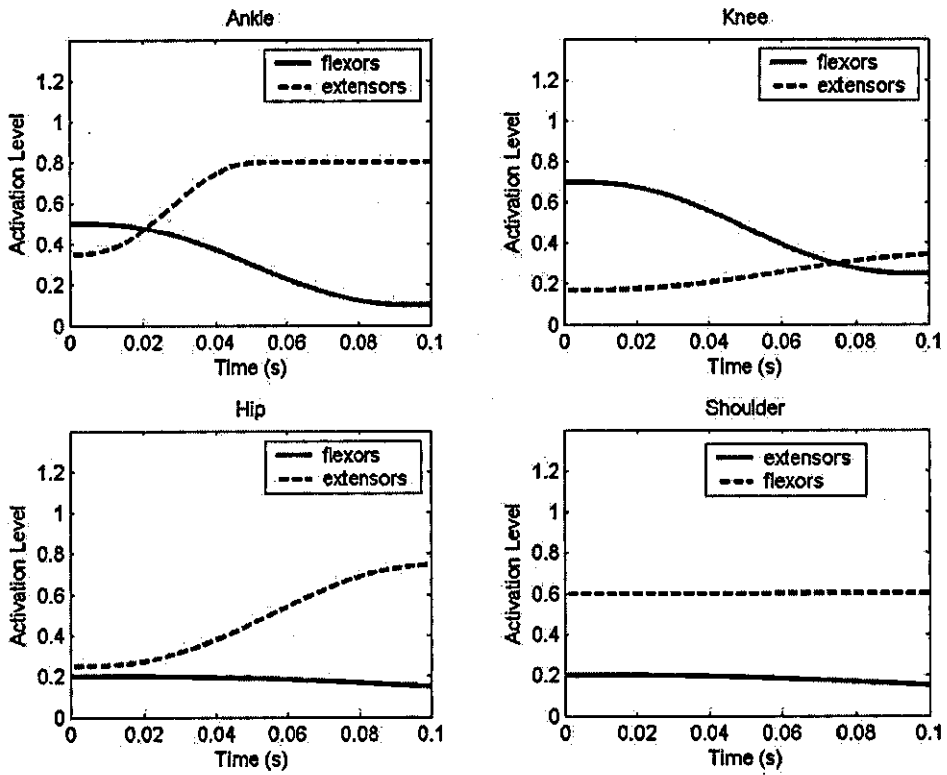
### Hip



### Shoulder

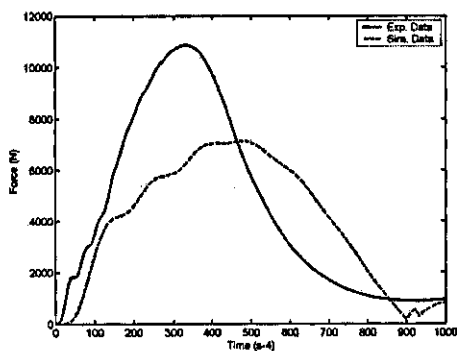


## Back somersault model three – activation

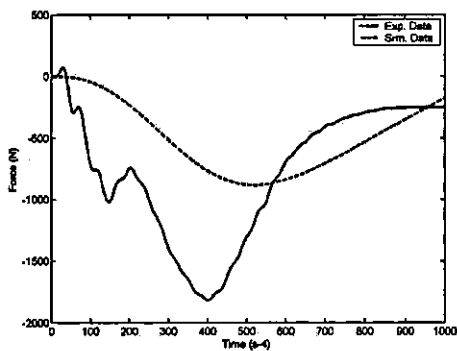




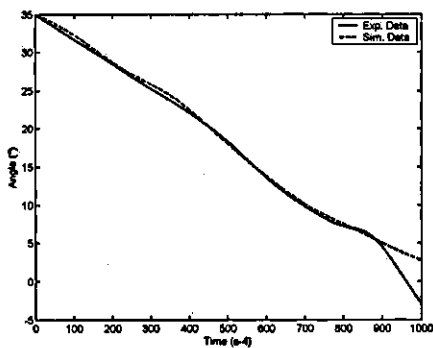
**HANDSPRING – model three**  
**VGRF**



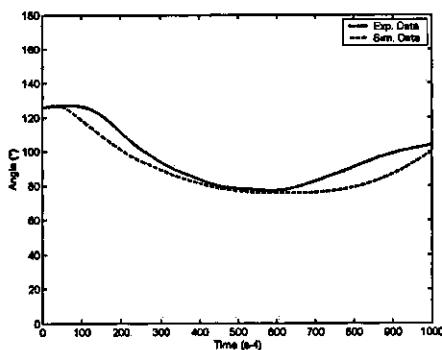
**HGRF**



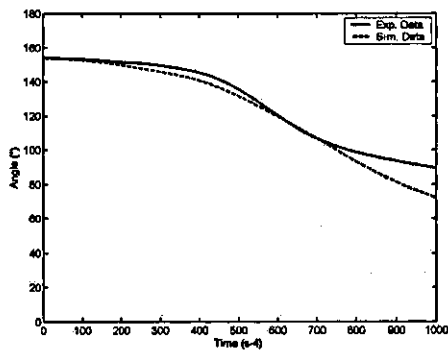
**Trunk**



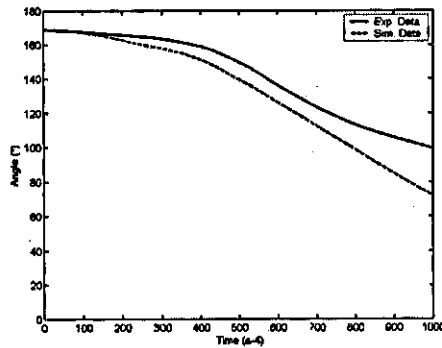
**Ankle**



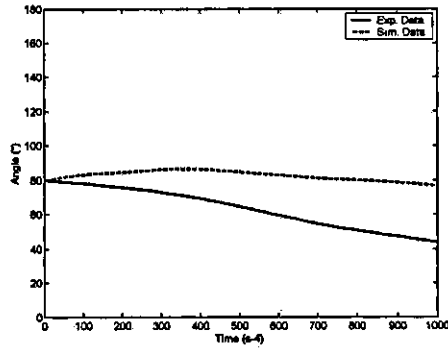
**Knee**



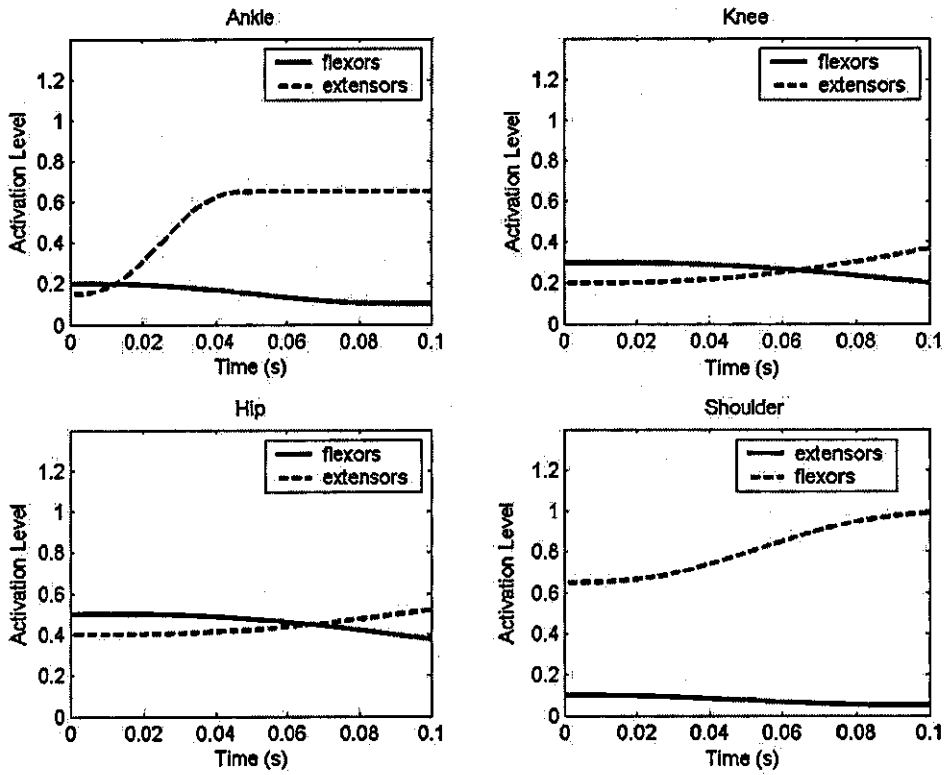
**Hip**



**Shoulder**



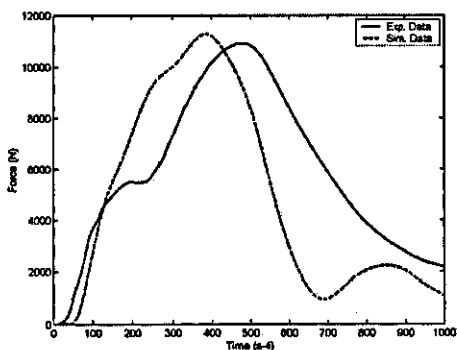
## Handspring model three – activation



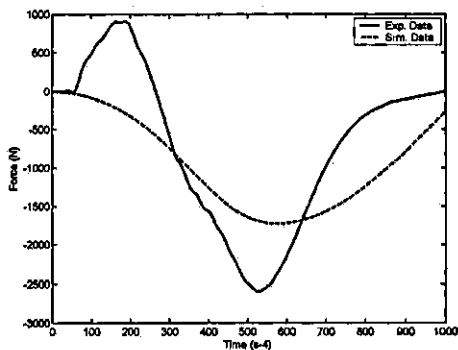


TSUKAHARA - model three

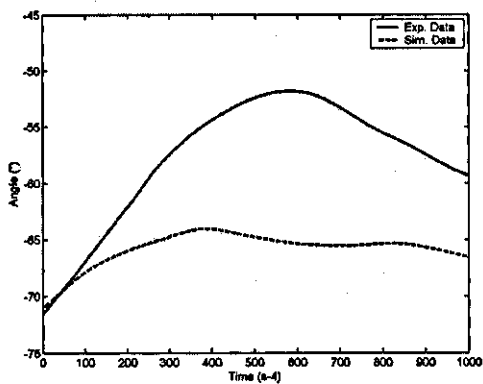
VGRF



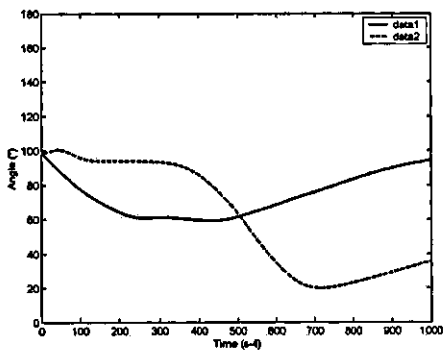
HGRF



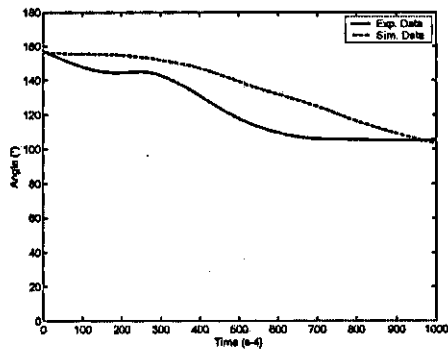
Trunk



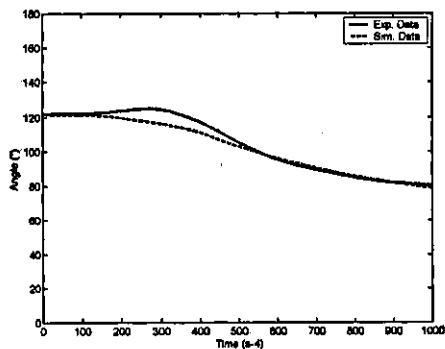
Ankle



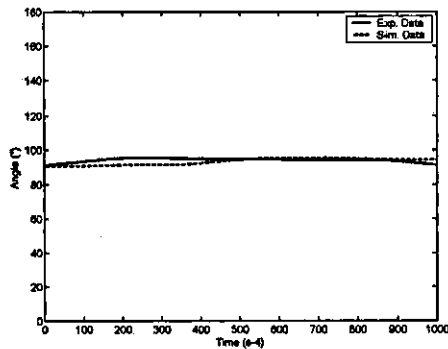
Knee



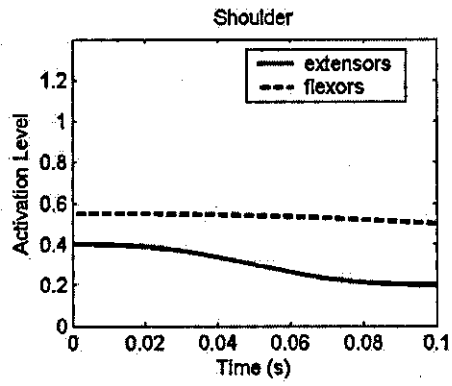
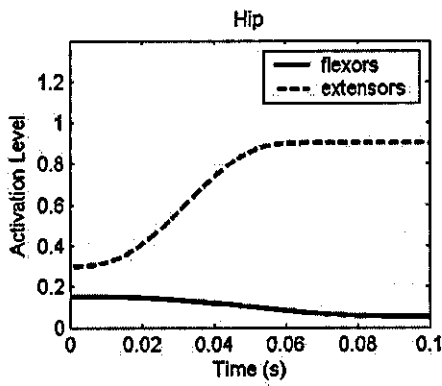
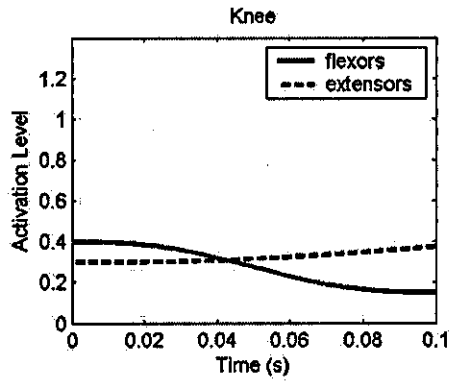
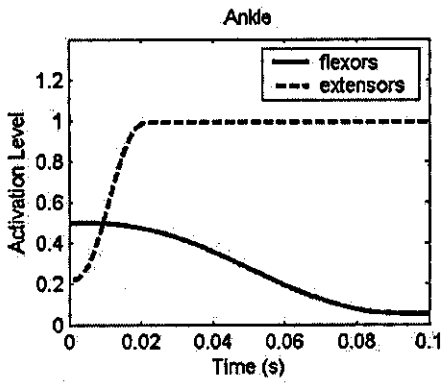
Hip



Shoulder



## Tsukahara model three – activation







**Model three - Summary**

Gymnastic Skill	Overall Score %	RMS (all joints)	RMS (body orientation)	RMS (Vert GRF)	RMS (Hor GRF)
Front Somersault	10.1	6.6	4.6	16.8	12.3
Back Somersault	16.2	15.7	0.8	12.1	36.1
Handspring	17.2	15.7	1.1	22.4	29.6
Tsukahara	23.6	34.3	9.1	25.8	25.4

Gymnastic Skill	Peak % (VGRF)	Peak % (HGRF)	Mat deformation (vertical) (m)	Mat deformation (horizontal) (m)
Front Somersault	6.7	25.9	0.15	0.05
Back Somersault	9.9	40.4	0.15	0.05
Handspring	34.3	51.6	0.155	0.055
Tsukahara	3.4	33.5	0.17	0.10

**Comparison of simulated and estimated landing mat deformations for model 3**

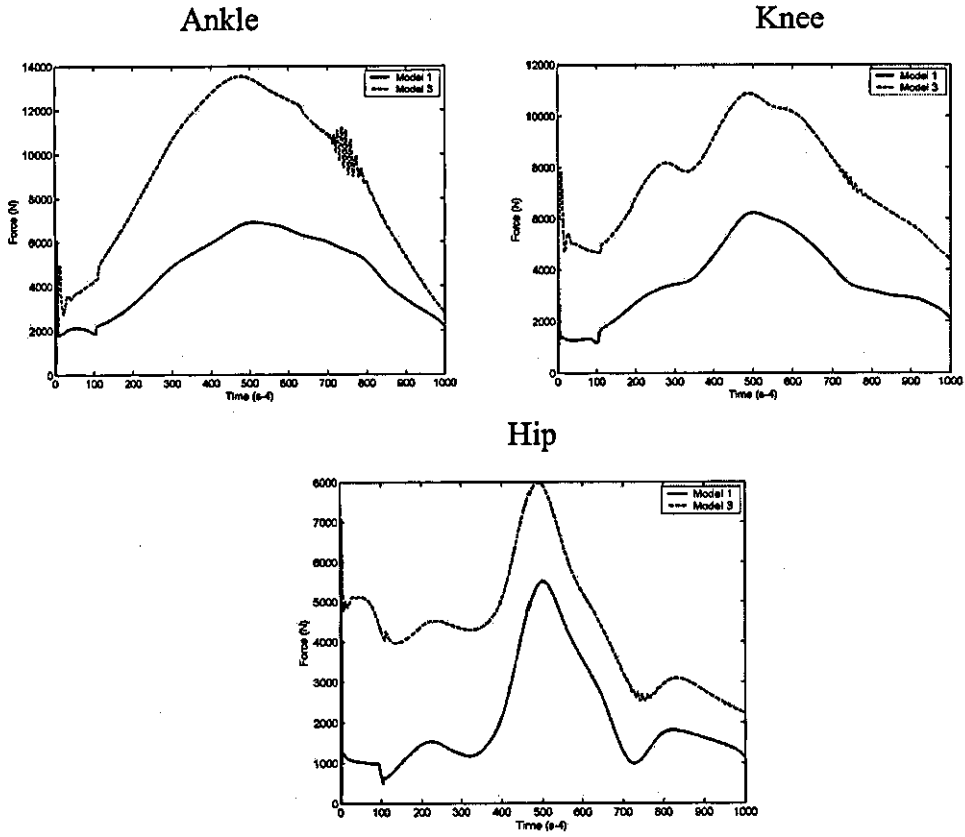
Gymnastic Skill	Estimated vertical (m)*	Simulated vertical (m)	Estimated horizontal (m)*	Simulated horizontal (m)
Front Somersault	0.08	0.15	0.02	0.05
Back Somersault	0.15	0.15	0.06	0.05
Handspring	0.16	0.16	0.03	0.05
Tsukahara	0.14	0.17	0.10	0.10

**Velocity of mass centre at end of simulation (0.1 s) and skill**

Gymnastic Skill	Actual Vert velocity (m/s)	Sim Vertical Velocity (m/s)	Actual Hor velocity (m/s)	Sim Horizontal Velocity (m/s)
Front Somersault	-0.3	-0.6	-0.5	-0.4
Back Somersault	-0.3	+0.2	-0.9	-1.8
Handspring	-1.1	-1.7	-1.1	-1.8
Tsukahara	0.7	-0.5	-1.4	-1.6

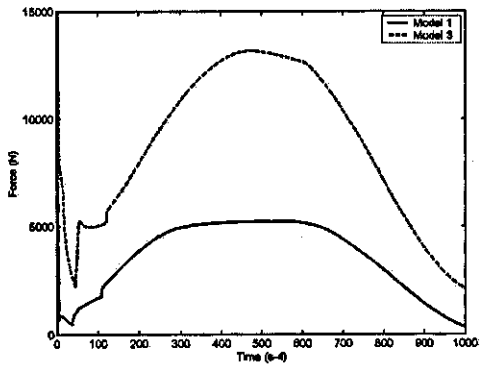
## **Appendix L**

**Joint reaction forces and bone bending moments for all four  
skills**

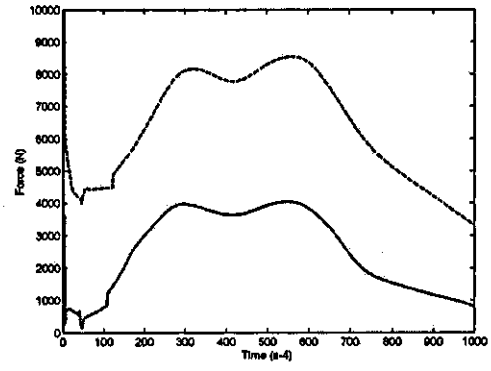
**Appendix L Joint reaction forces and bone bending moments for all four skills****Joint Reaction Forces (model three)****Front Somersault**

## Back Somersault

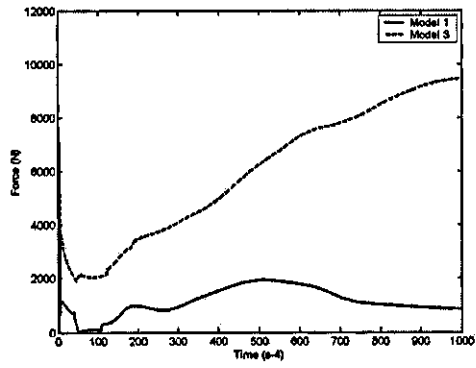
Ankle



Knee

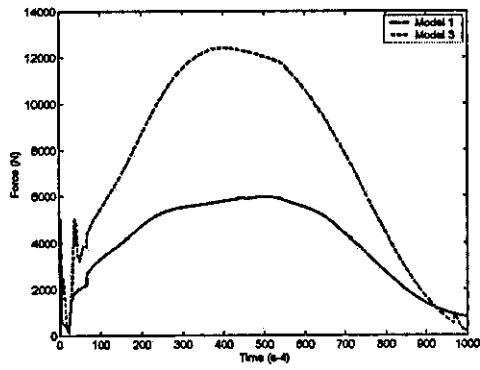


Hip

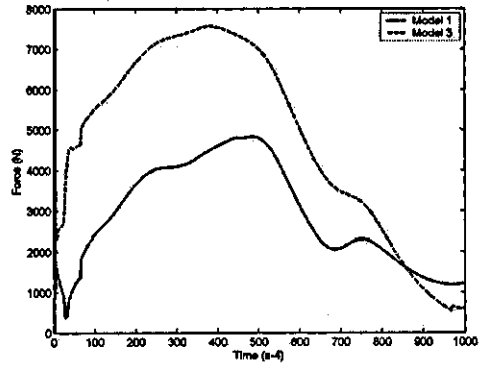


## Handspring

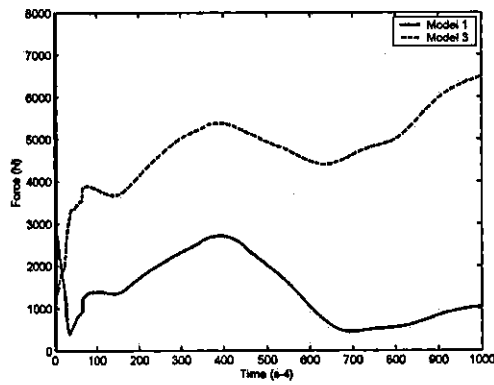
Ankle



Knee

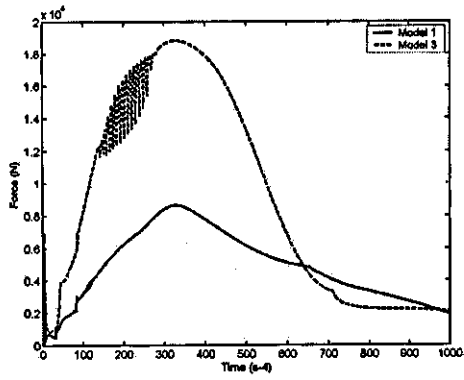


Hip

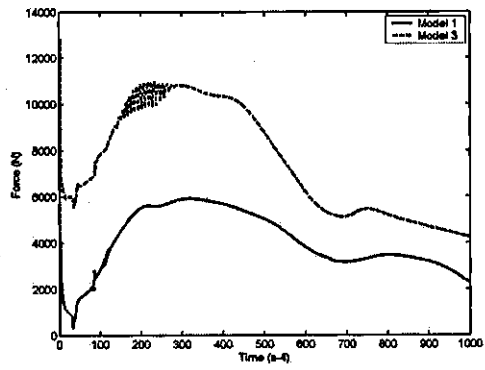


Tsukahara

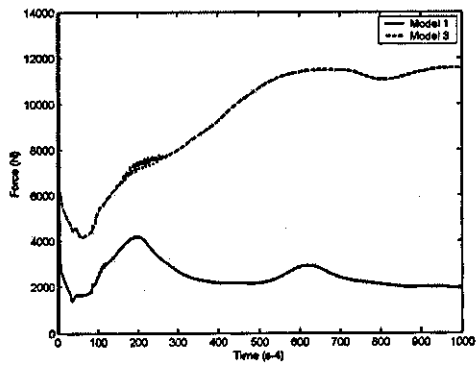
Ankle



Knee



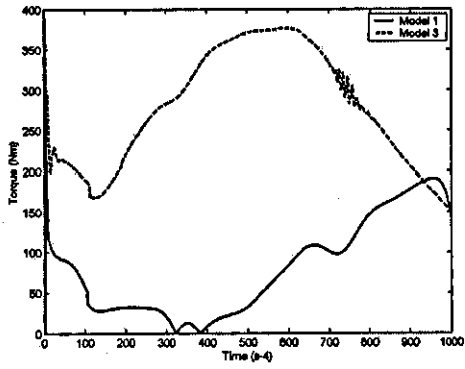
Hip



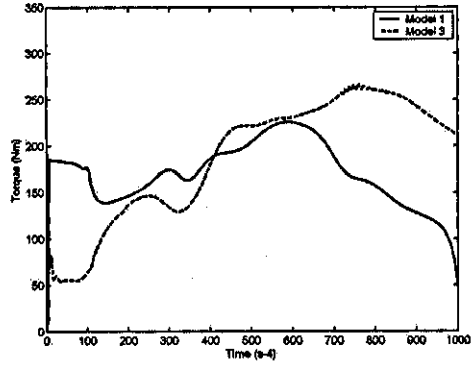
## Bone Torque (model three)

### Front Somersault

#### Shank

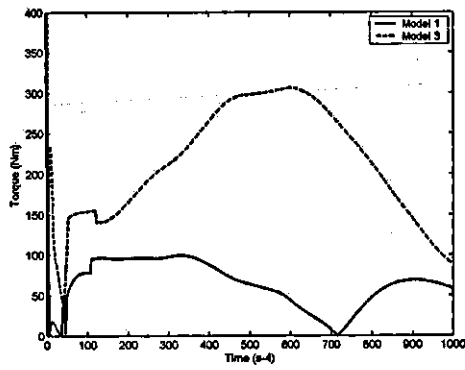


#### Thigh

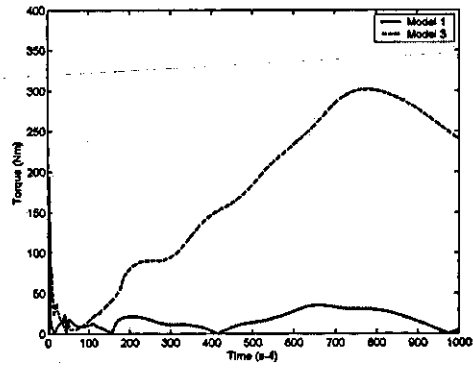


### Back somersault

#### Shank



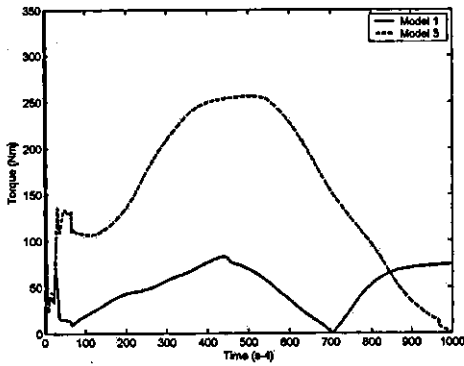
#### Thigh



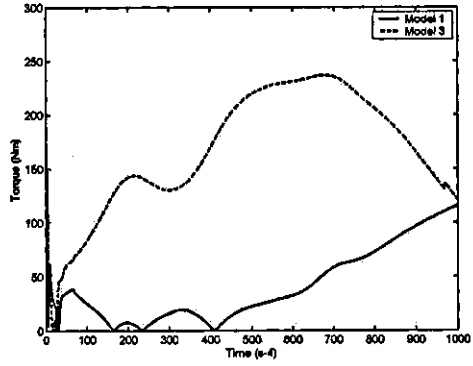


Handspring

Shank

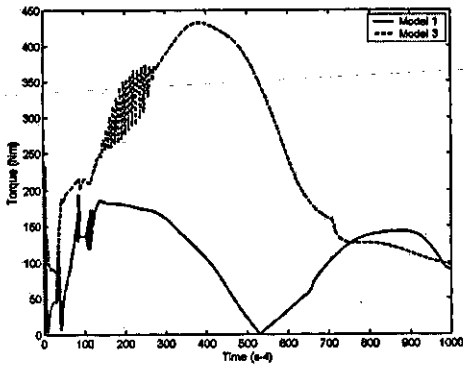


Thigh



Tsukahara

Shank



Thigh

